



National Library
of Canada

Bibliothèque nationale
du Canada

Canadian Theses Service

Services des thèses canadiennes

Ottawa, Canada
K1A 0N4

CANADIAN THESES

THÈSES CANADIENNES

NOTICE

The quality of this microfiche is heavily dependent upon the quality of the original thesis submitted for microfilming. Every effort has been made to ensure the highest quality of reproduction possible.

If pages are missing, contact the university which granted the degree.

Some pages may have indistinct print especially if the original pages were typed with a poor typewriter ribbon or if the university sent us an inferior photocopy.

Previously copyrighted materials (journal articles, published tests, etc.) are not filmed.

Reproduction in full or in part of this film is governed by the Canadian Copyright Act, R.S.C. 1970, c. C-30.

**THIS DISSERTATION
HAS BEEN MICROFILMED
EXACTLY AS RECEIVED**

AVIS

La qualité de cette microfiche dépend grandement de la qualité de la thèse soumise au microfilmage. Nous avons tout fait pour assurer une qualité supérieure de reproduction.

S'il manque des pages, veuillez communiquer avec l'université qui a conféré le grade.

La qualité d'impression de certaines pages peut laisser à désirer, surtout si les pages originales ont été dactylographiées à l'aide d'un ruban usé ou si l'université nous a fait parvenir une photocopie de qualité inférieure.

Les documents qui font déjà l'objet d'un droit d'auteur (articles de revue, examens publiés, etc.) ne sont pas microfilmés.

La reproduction, même partielle, de ce microfilm est soumise à la Loi canadienne sur le droit d'auteur, SRC 1970, c. C-30.

**LA THÈSE A ÉTÉ
MICROFILMÉE TELLE QUE
NOUS L'AVONS REÇUE**

THE UNIVERSITY OF ALBERTA

NUMERICAL AND EXPERIMENTAL STUDIES OF RIME ICE ACCRETION ON
CYLINDERS AND AIRFOILS

by



KAREN JOAN FINSTAD

A THESIS

SUBMITTED TO THE FACULTY OF GRADUATE STUDIES AND RESEARCH
IN PARTIAL FULFILMENT OF THE REQUIREMENTS FOR THE DEGREE
OF DOCTOR OF PHILOSOPHY

IN

METEOROLOGY

DEPARTMENT OF GEOGRAPHY

EDMONTON, ALBERTA

Fall, 1986

Permission has been granted to the National Library of Canada to microfilm this thesis and to lend or sell copies of the film.

The author (copyright owner) has reserved other publication rights, and neither the thesis nor extensive extracts from it may be printed or otherwise reproduced without his/her written permission.

L'autorisation a été accordée à la Bibliothèque nationale du Canada de microfilmer cette thèse et de prêter ou de vendre des exemplaires du film.

L'auteur (titulaire du droit d'auteur) se réserve les autres droits de publication; ni la thèse ni de longs extraits de celle-ci ne doivent être imprimés ou autrement reproduits sans son autorisation écrite.

ISBN 0-315-32478-3

THE UNIVERSITY OF ALBERTA

RELEASE FORM

NAME OF AUTHOR

KAREN JOAN FINSTAD

TITLE OF THESIS

NUMERICAL AND EXPERIMENTAL STUDIES
OF RIME ICE ACCRETION ON CYLINDERS
AND AIRFOILS

DEGREE FOR WHICH THESIS WAS PRESENTED DOCTOR OF PHILOSOPHY

YEAR THIS DEGREE GRANTED Fall, 1986

Permission is hereby granted to THE UNIVERSITY OF ALBERTA LIBRARY to reproduce single copies of this thesis and to lend or sell such copies for private, scholarly or scientific research purposes only.

The author reserves other publication rights, and neither the thesis nor extensive extracts from it may be printed or otherwise reproduced without the author's written permission.

(SIGNED) *Karen J. Finstad*

PERMANENT ADDRESS:

#901 - 10149 Saskatchewan Drive

Edmonton, Alberta

T6E 6B6

DATED .. July 9..... 1986

THE UNIVERSITY OF ALBERTA
FACULTY OF GRADUATE STUDIES AND RESEARCH

The undersigned certify that they have read, and recommend to the Faculty of Graduate Studies and Research, for acceptance, a thesis entitled NUMERICAL AND EXPERIMENTAL STUDIES OF RIME ICE ACCRETION ON CYLINDERS AND AIRFOILS submitted by KAREN JOAN FINSTAD in partial fulfilment of the requirements for the degree of DOCTOR OF PHILOSOPHY in METEOROLOGY. -

Edward Weasen
.....

Supervisor

R. J. ...
.....

P. R. ...
.....

EM ...
.....

Sam ...
.....

External Examiner

Date..... July 9, 1986

Abstract

Four separate studies describe improvements to numerical techniques used in the modelling of ice accretion on circular cylinders and on airfoils.

1. For collision efficiencies, accretion limits and impact velocities on circular cylinders, tables of numerical data and analytical approximating functions are presented. These data replace those of Langmuir and Blodgett (1946).
2. Parameterizations of the local collision efficiency distribution on circular cylinders are derived from numerical data, and applied in an 'operational' style computer model of rime ice accretion. The model's performance is compared with experimental accretions grown in the University of Alberta FROST tunnel.
3. The distribution of local ice density in rime ice is investigated in experimental wind-tunnel accretions made on circular cylinders. A form of the distribution is derived for application to the numerical model described in the previous study.
4. A second model, for rime ice accretion on airfoils or other arbitrary shapes, combines droplet trajectory integrations and parameterizations for local collision efficiency and density distribution. By use of these parameterizations, and of simple numerical methods throughout, the model is made significantly faster than previous models have been. Verification of the model is

provided by comparisons with several wind-tunnel experiments.

Acknowledgements

A most sincere thank-you is due to my thesis supervisor, Professor Edward Lozowski, for his expert guidance and perceptive advice, given throughout the course of my studies, and also for arranging generous research and conference travel funds. Professor [redacted] [redacted], as co-leader of the Icing Group, was an equally valuable source and expertise. To both of them, many thanks for always lending the time, and a good-natured ear, to my questions.

I would also like to express my appreciation to the members of my examination committee for their careful reading of the manuscript, and pertinent comments: Professor Erhard Reinelt, Assistant Professor John Wilson, and especially to Professor Gordon Rostoker for taking time from his busy schedule to serve as Chairman, and External Examiner Dr. Lasse Makkonen, for overcoming the difficulties presented by some 15,000 km and a Finnish postal strike.

Thanks also, to the other student members of the Icing Group, and to the students and staff of the Meteorology Division, for support and friendship.

Financial support in the form of Postgraduate Fellowships from the Atmospheric Environment Service, Canada, and a Graduate Faculty Fellowship from The University of Alberta, is gratefully acknowledged.

Finally, to J.A.H., my chief editor, programming advisor, and billiards marker - thanks for everything.

Table of Contents

Chapter	Page
I. Introduction	1
A. The Icing Problem	3
References	9
II. Cloud Droplet Trajectories Updated	13
A. Introduction	13
B. Impingement Parameters and Droplet Trajectories	14
C. Results	20
D. Curve Fitting	23
E. Limitations of LB Theory	38
F. Summary	43
References	45
III. An Operational Model for Rime Ice Accretion	48
A. Introduction	48
B. Parameterization for Local Collision Efficiency	50
C. Variation of Local Density	55
D. Rotation	59
E. Model Applications	60
References	63
IV. Local Densities of Circular Cylinder Rime Accretions	65
A. Introduction	65
B. Rotating Cylinder Densities Applied to the Non-rotating Case	69
C. Profile-Derived Density Distribution	74
D. Laboratory Measurements of Local Density	77
E. Local Density at the Stagnation Line	86

P. Summary	88
References	90
V. Rime Icing on Airfoils	92
A. Introduction	92
B. Model Outline	93
C. Specifying the Airfoil Shape	95
D. Local Collision Efficiency	99
E. Integration of Droplet Trajectories	110
F. Local Density Variations	115
G. Model Results	116
References	125
VI. Concluding Remarks	128
Appendix I	131
Appendix II	146
Appendix III	170
References	174
Appendix IV	175
Appendix V	178
Appendix VI	215
References	228

List of Tables

<u>Table</u>	<u>Page</u>
II.1 - $\beta_0(K)$ for $\phi = 10^3$.	21
II.2 - Numerically calculated values of β_0 , α_{\max} and E as a function of K and ϕ .	24
II.3 - Numerically calculated values of V_0 as a function of K and ϕ .	26
II.4 - Approximations to the numerical data of Langmuir and Blodgett derived by various authors.	31
II.5 - Comparison of some original E values calculated by Langmuir and Blodgett, and those derived from the approximations of Table II.4.	33
II.6 - Coefficients for approximating impingement parameters by Equation II.11.	37
II.7 - Comparisons between a selection of numerically calculated values, and approximated values calculated according to Table II.6.	39
IV.1 - Local densities as a function of surface slope derived from thickness measurements of shallow ice layers.	78
IV.2 - Experimentally measured local densities as a function of surface slope.	82

V.1 - Sensitivity of the integration results to the time step size and the initial x ² position.	112
A.1 - Droplet size spectra from many different sources.	216
A.2 - Overall and stagnation line collision efficiencies as plotted in Figures A.2 and A.3.	221
A.3 - Overall and stagnation line collision efficiencies as plotted in Figures A.4 and A.5.	224

List of Figures

Figure	Page
II.1 - Droplet trajectories impinging on a circular cylinder.	18
II.2 - Comparison of β_0 vs. K^* for one value of $\phi = 10^3$.	22
II.3 - Smooth curves drawn for the numerical data of β_0 vs. K and ϕ .	27
II.4 - Smooth curves drawn for the numerical data of μ_{max} vs. K and ϕ .	28
II.5 - Smooth curves drawn for the numerical data of E vs. K and ϕ .	29
II.6 - Smooth curves drawn for the numerical data of V_0 vs. K and ϕ .	30
II.7 - The dependence of $(K_{0,\beta} / K)$ on Reynolds Number Re .	36
II.8 - Potential flow streamlines about a cylinder. Viscous flow streamlines about a cylinder at a Reynolds number of 10,000.	40
III.1 - Parameterized $\beta(\alpha)$ values from Equations III.1 and III.2.	53.
III.2 - Parameterized $\beta(\alpha)$ values from Equations III.3 and III.4.	56
III.3 - Comparisons between modelled and experimental profiles and masses per unit length.	58

III.4 - An example of the model output for a rotating cylinder.	61
IV.1 - A 1.5 cm thick cross-section of a circular cylinder rime accretion, viewed in transmitted light.	66
IV.2 - A typical circular cylinder rime accretion showing rime feathers.	68
IV.3 - Experimental and three model accretions, showing the effects of three different density distributions.	72
IV.4 - A circular cylinder rime deposit in profile, with paint layers marking the surface at five minute intervals.	75
IV.5 - Local densities derived from thickness measurements of shallow ice layers.	79
IV.6 - An accretion section of about 1.5 cm thickness, showing the holes drilled for local density measurements.	81
IV.7 - Local density vs. surface angle; experimental measurements and parameterized curves.	84
IV.8 - Local density vs. surface angle; experimental measurements and parameterized curves.	85

IV.9 - Stagnation line density measurements vs. R' , and the rotating cylinder density correlation of Makkonen and Stallabrass vs. R.	89
V.1 - Determination of collision efficiency on an airfoil.	97
V.2 - Comparison of Oleskiw's numerical results with Equation V.3.	101
V.3 - Comparison of Oleskiw's numerical results with Equation V.3.	102
V.4 - Comparison of Oleskiw's numerical results with Equation V.3.	103
V.5 - Comparison of spectrum-weighted collision efficiencies and Equation V.5.	105
V.6 - Comparison of spectrum-weighted collision efficiencies and Equation V.5.	106
V.7 - Comparison of Oleskiw's numerical results with Equation V.7.	108
V.8 - Comparison of Oleskiw's numerical results with Equation V.7.	109
V.9 - Determination of droplet impact point on the surface.	114
V.10 - Comparison of present model results with those of Oleskiw.	118
V.11 - Comparison of present model results with an experimental accretion grown in the NASA/Lewis tunnel.	119

V.12 - Comparison of present model results with experimental profiles from Stallabrass and Stallabrass and Lozowski.	121
V.13 - Comparison of present model results with experimental profiles and masses grown in <u>The University of Alberta FROST tunnel</u> .	123
A.1 - Droplet trajectories impinging on an airfoil.	176
A.2 - Overall collision efficiencies calculated for many different drop size spectra vs. E 's calculated for the mvd and d_{42} of each spectrum.	222
A.3 - Stagnation line collision efficiencies calculated for many different drop size spectra vs. β_0 's calculated for the mvd and d_{42} of each spectrum.	223
A.4 - Overall collision efficiencies calculated for a single drop size spectrum vs. E 's calculated for the mvd and d_{42} of the same spectrum.	225
A.5 - Stagnation line collision efficiencies calculated for a single drop size spectrum vs. β_0 's calculated for the mvd and d_{42} of the same spectrum.	226

List of Symbols

<u>Symbol</u>	<u>Definition</u>
C_d	- droplet drag coefficient
$C_{X,n}$	- constant coefficients for Equation II.11
D_c	- circular cylinder diameter
D_d	- droplet diameter
d_{42}	- diameter of droplet at the 42nd volume percentile of the droplet spectrum
E	- overall collision efficiency
h_0	- airfoil width as a fraction of chord length
K	- Langmuir non-dimensional mass parameter
K_0	- a function of K and Re , used in analytical fits to the data of Langmuir and Blodgett
lwc	- liquid water content
mvd	- median volume diameter droplet
R	- Macklin correlation parameter for rotating cylinder ice density
R'	- revised Macklin parameter for correlation of ρ_0
R_c	- circular cylinder diameter
Re	- droplet Reynolds number based on the free-stream velocity
Re_d	- droplet Reynolds number based on the relative velocity
r_d	- droplet radius
T	- temperature

- T_h - thickness of ice layer
 T_l - tail length, added to α_{max}
 T_s - mean surface temperature of ice layer
 $T_{s,0}$ - surface temperature of ice at the stagnation line
 Δt - integration time step for droplet trajectories
 U - free-stream air speed
 u_x, u_y - air speed coordinates
 V - relative speed of droplet with respect to the air
 V_r - impact speed of droplet in the direction normal to the cylinder surface
 v_0 - droplet impact speed at the stagnation line
 v - absolute velocity of droplet
 v_x, v_y - droplet speed coordinates
 x_0, y_0 - initial droplet coordinates
 Δy - initial separation of trajectory pair
 Δl - final separation in arc length of the trajectory pair
 α - angle between surface normal and the free-stream
 α' - scaled surface angle for Equation V.7
 α_0 - angular position of maximum β
 α_{max} - angular position of accretion limit
 α_m - accretion limit plus tail length, T_l

- β - local collision efficiency
- β_0 - local collision efficiency at the stagnation line
- ξ - Stallabrass correlation parameter
- θ - position angle on circular cylinder
- μ - dynamic viscosity of air
- ρ - local ice density
- ρ_a - density of air
- ρ_d - density of the water droplet
- ρ_0 - local ice density at the stagnation line
- τ - ice layer time step
- Φ - angle of attack of the free-stream
- ϕ - non-dimensional Langmuir flow parameter, or Stokes number
- ψ - potential flow streamfunction

I. Introduction

'Icing' presents a problem occasionally to pastry cooks, sometimes to hockey players, and always to those concerned with the natural phenomenon of ice accretion.

In cold climates, ice accretion may result from atmospheric cloud droplets, rain, snow, or sea spray. It may cause serious hazards for aircraft, power lines and transmission towers, ships, and off-shore oil rigs. All of these represent human enterprises that involve many lives and dollars, which may be jeopardized during icing events. So, the primary aim in studying icing is the prediction of its occurrence, whether of a particular event or of the probability of extreme events, and ultimately the prevention of costly and often disastrous accidents.

The icing phenomenon may appear straightforward at first glance: water is collected on a cold surface and freezes there. However, a deeper look reveals many layers of complexity in the physical processes involved, and serious practical difficulties in the observational, experimental, and theoretical aspects of the problem. The development of a predictive model is therefore not an easy task, but it is nonetheless one of some importance.

As with other physical problems, there are two approaches that may be taken in model building. The first is a statistical approach, in which a very large number of events (predictands) are observed, as well as their antecedent or concurrent conditions (predictors). A

statistical analysis will then look for correlations between the predictors and predictands. Considerable computational effort may be required to establish a 'best guess' for the most significant predictors, and for the form of the predictive relation.

The reliability of the outcome is highly dependent on the number and quality of the observations. The advantage of this method is that a predictive relation may be derived and applied in the absence of any further understanding of the physical processes involved, which may be complex. But if the observations are adequate, and a good correlation can be found, it is the quickest way of achieving practical forecasting results.

However, the predictive skill of this method is limited by the strength of the discovered correlation, and its applicability is limited to the range of conditions defined by the original observations. For icing studies, this of course includes the geographical range, since the character of icing problems has a large regional variability.

The other approach to modelling is the physical one. This usually means a mathematical model, solved numerically using a digital computer, in which an attempt is made to simulate the intermediate steps, and to understand the causal relationships between the input conditions and the output predictions. Producing such a model does take considerably more time and effort than producing a statistical correlation, and the requirements for the

observational data are just as stringent. Furthermore, no mathematical model can perfectly reproduce a given physical process or situation - there must always be simplifying assumptions.

But the knowledge gained from a physical model is less restricted in its application, within those assumptions, than is any purely statistical relationship, and it can provide a useful testing ground for theory. Even the simplest physical model might at least suggest what the most effective predictors will be for a statistical study; thus if it is found that liquid water content and cloud droplet size are of prime importance in determining model ice accretion rates, then collectors of field data should take note, even if these things are very difficult to observe.

A. The Icing Problem

A model of the complete ice accretion process involves the solution of a series of problems. First, an approximation to the airflow around the accreting object must be found. If potential flow is assumed, and there is no analytical solution (as there is for circular cylinders or Joukowski airfoils) then the partial differential equation for the velocity potential must be solved numerically, as in Hess and Smith (1967), or Kennedy and Marsden (1976), for example.

Once it is possible to calculate the air velocity at any point, the trajectories of water droplets carried by the

4

airstream toward the object may be determined. Again, simplifying assumptions are applied to the droplet's equation of motion in order to reduce the computational time needed to integrate it numerically.

An ensemble of droplet trajectories is calculated, and their points of impact on the accretion surface are determined. This information is necessary to derive the impingement characteristics of the accretion shape. These are: the distribution of the local collision efficiency, the overall collision efficiency, the maximum impingement angle, and impact speed of the droplets. The collection efficiency is the product of the collision efficiency and the sticking efficiency. Since the latter is unknown, but usually assumed to be unity, only the collision efficiency is dealt with. These quantities and their symbols are defined for a circular cylinder in Figure II.1.

Langmuir and Blodgett (1946) authored the classical solution to this problem, for collision efficiencies of cylinders, spheres, and ribbons in a potential flow field. More recent, but less extensive calculations have been made by McComber and Touzot (1981), and by Egelhofer, et al. (1984). The experimental work of Ranz and Wong (1952) qualitatively validates the theory of Langmuir and Blodgett, if not their numerical calculations.

The impingement characteristics depend on the cylinder size, droplet size, the free-stream air speed, and the air temperature and pressure. If more than one droplet size is

present, the impingement characteristics of each size, or size interval, must be determined. A common simplification to this requirement for droplet spectra is made through the substitution of the impingement characteristics of a single droplet size, that of the median volume droplet of the size spectrum. The usefulness of this simplification is examined in Appendix VI, although it is used throughout the thesis.

Only when all of these calculations are completed can ice begin to accrete in the model. For obvious reasons then, most modelers have turned to standard accretion shapes for which these calculations are simpler, for which much data already exist, and for ease of comparison between models. Thus we have the ubiquitous horizontal circular cylinder in a uniform cross-flow, which appears in the models of Macklin and Payne (1967), McComber and Touzot (1981), Lozowski, Stallabrass and Hearty (1983), Horjen (1983), Egelhofer, et al. (1984) and Makkonen (1984). The more difficult problem of accretion on airfoils has been treated by Oleskiw (1982), Gent and Cansdale (1985), and MacArthur, et al. (1982).

The cloud water is usually assumed to be at the temperature of the air stream, and to arrive at the accreting surface in a uniform flux determined by the liquid water content, or lwc, (defined as the mass of water contained in a unit volume of air), the air speed and the object's collision efficiency. The density of the accreted ice also determines the thickness and shape of the deposit.

On rotating cylinders, accreted rime ice densities have been examined by Macklin (1962), and by Makkonen and Stallabrass (1985). On non-rotating objects, the shape of the deposit is also partly dependent on the variation of the local ice density along its surface. Bain and Gayet (1982) have suggested one form for this variation.

If the flux of super-cooled water is large enough so that the latent heat of freezing cannot be radiated, conducted or convected away from the surface fast enough, then the surface temperature may rise to the melting point. When this happens the ice may become 'wet', rather than 'dry', meaning that all of the impinging water is no longer able to freeze on impact. Now the problem becomes even more complex since a detailed heat balance must be calculated for the accretion surface, in order to determine how much of the impinging water is able to freeze, and how much is shed, or remains in the accretion as liquid water. Calculation of the heat balance is made especially difficult since the heat transfer properties of the ice surfaces and even of rough circular cylinders are very poorly known (Makkonen, 1985).

Models in which a computation of the heat balance on cylinders is attempted using empirical heat transfer data include those of Lozowski, Stallabrass and Hearty (1984), Macklin and Payne (1967), Egelhofer, et al. (1984), and Makkonen (1984). However, such data are scarce, especially for non-cylindrical shapes, and for rough surfaces. Some modelers have thus used numerically calculated heat transfer

for cylinders (Makkonen, 1985) or for airfoils (Cansdale and McNaughton, 1977, Cansdale and Gent 1983).

Models developed specifically for marine applications must contend with the further complications of salinity, droplet distributions and liquid water contents that vary with height, and intermittent sprays. Models including these effects are currently under development by various researchers.

The models developed for this thesis are intended as 'operational' icing models, which would be efficient and inexpensive enough to be used regularly in the laboratory for predictive purposes, or for numerical experiments into specific aspects of icing. Previous models have often been such too costly to be used in such a way. To reduce computational time several 'shortcuts', or parameterizations, have been introduced which help to simplify some of the calculations needed in this problem. Specifically, the local collision efficiency and local ice density are approximated by analytical functions of the surface slope. Such an approach naturally involves some loss of accuracy, but this loss must be balanced against unavoidable uncertainties in the input data and the required precision of output predictions.

Two models are described, for circular cylinders in Chapter III, and in Chapter V for airfoils, that could also be applied to other arbitrary shapes. Both models are limited to rime ice accretion, i.e. there is no heat balance

8

calculation, and a uniform air speed and flux of pure water droplets are assumed. This is so that the performance of the parameterizations can be easily compared with real ice accretions whose shape and mass are not dependent on the poorly known heat transfer distribution.

In the course of model development, significant improvements were made in two specific aspects, the theoretical calculation of collision efficiencies on smooth circular cylinders, (Chapter II) and the distribution of local density in non-rotating circular cylinder rime accretions (Chapter IV).

Experiments for model verification were carried out in the University of Alberta's original icing wind-tunnel, known as the Facility for Research On Solidification and Thawing, or FROST tunnel. A full description of the facility may be found in Gates (1981), or Lozowski and Gates (1984). All wind-tunnel experiments were performed under the direction of Professor Gates.

References

- Bain, M. and Gayet, J-F. 1982: Contribution to the Modelling of the Ice Accretion Process: Ice Density Variation with the Impacted Surface Angle. Proceedings, First International Workshop on Atmospheric Icing of Structures, Hanover, 13-20.
- Cansdale, J.T. and Gent, R.W. 1983: Ice Accretion on Aerofoils in Two-Dimensional Compressible Flow - A Theoretical Model. British Royal Aircraft Establishment Technical Report 82128, 31 pp. + 31 fig.s.
- Cansdale, J.T. and McNaughtan, I.I. 1977: Calculation of Surface Temperature and Ice Accretion Rate in a Mixed Water Droplet / Ice Crystal Cloud. British Royal Aircraft Establishment, Technical Report 77090, 24 pp. + 6 fig.s.
- Egelhofer, K.Z., Ackley, S.F. and Lynch, D.R. 1984: Computer Modelling of Atmospheric Ice Accretion and Aerodynamic Ice Loading of Transmission Lines. Proceedings, Second International Workshop on Atmospheric Icing of Structures, Trondheim, (in press).
- Gates, E.M. 1981: FROST Tunnel. Departmental Report No. 26, Department of Mechanical Engineering, The University of

Alberta. 10 pp.

Gent, R.W. and Cansdale, J.T. 1985: The Development of Mathematical Modelling Techniques for Helicopter Rotor Icing. AIAA Publication 85-0336, 10 pp.

Hess, J.L. and Smith, A.M.O. 1967: Calculation of Potential Flow About Arbitrary Bodies, *Progress in Aeronautical Sciences, Vol. 8*, Pergamon Press, 1-138.

Horjen, I. 1983: Icing on Offshore Structures Atmospheric Icing. *Norwegian Maritime Research*, II, No. 3, 9-21.

Kennedy, J.L. and Marsden D.J. 1976: Potential Flow Velocity Distributions on Multi-Component Airfoil Sections. *Can. Aero. and Space Jour.*, 22, 243-256.

Langmuir, I. and Blodgett, K. 1946: A Mathematical Investigation of Water Droplet Trajectories. *Collected Works of Irving Langmuir, Vol. 10*, Pergamon Press, 348-393.

Lozowski, E.P. and Gates, E.M. 1984: Ice Accretion in a Marine Environment. *Proceedings, 3rd International Symposium on Offshore Mechanics and Arctic Engineering*, New Orleans, 8 pp.

Lozowski, E.P., Stallabrass, J.R. and Hearty, P.F. 1983: The Icing of an Unheated, Non-rotating Cylinder Part I: A Simulation Model. *J. Climate and App. Meteor.*, 22, 2053-2074.

MacArthur, C.D. Keller, J.L. and Luers, J.K. 1982: Mathematical Modelling of Ice Accretion on Airfoils. AIAA Publication No. 82-0284.

McComber, P. and Touzot, G. 1981: Calculation of the Impingement of Cloud Droplets in a Cylinder by the Finite Element Method. *J. Atmos. Sci.*, 38, 1027-1036.

Macklin, W.C. 1962: The Density and Structure of Ice Formed by Accretion. *Quart. Jour. Roy. Meteor. Soc.* 88, 30-50.

Macklin, W.C. and Payne, G.S. 1967: A Theoretical Study of the Ice Accretion Process. *Quart. Jour. Roy. Meteor. Soc.*, 93, 195-213.

Makkonen, L. 1984: Modelling of Ice Accretion on Wires. *Jour. Climate and App. Meteor.*, 23, 929-939.

Makkonen, L. 1985: Heat Transfer and Icing of a Rough Cylinder. *Cold Regions Science and Technology*, 10, 105-116.

Makkonen, L. and Stallabrass, J.R. 1984: Ice Accretion on
Cylinders and Wires. National Research Council,
Mechanical Engineering Division, Technical Report
TR-LT-005, 50 pp.

Poots, G. 1984: Theoretical Solutions of Ice Accretion on
Cables. Proceedings, Second International Workshop on
Atmospheric Icing of Structures, (in press).

Ranz, W.E. and Wong, J.B. 1952: Impaction of Dust and Smoke
Particles. *Industrial Engineering Chemistry*, 44,
1371-1381.

II. Cloud Droplet Trajectories Updated

A. Introduction

For many years the standard reference work for cloud droplet trajectories in an airstream flowing around an obstacle has been Langmuir and Blodgett (1946), hereafter LB. This was one of the first published treatments of the problem which used an analog computer to integrate the equations of motion for water droplets in a steady potential flow about an infinitely long circular cylinder.

These calculations are of interest in studies of atmospheric and marine ice accretion, in which the characteristics of droplet impingement on cylinders and other objects are important factors in modelling the icing process. However, since the calculations were done so long ago, on what would now be considered a primitive machine, and because the original reference can be difficult to obtain, a need was perceived to recalculate the droplet trajectories and to publish the results in the open literature. The effect of replacing the drag coefficient formulation used by LB with a more recent one, that of Beard and Pruppacher (1969), has also been investigated.

Functional fits have been devised by several authors to the original tabulated data of LB. A number of these are compared to show the need for improving and standardizing them. Toward this end, a non-linear regression fit to the new data has been found for the range of conditions

pertaining to airborne, land structure and marine icing.

B. Impingement Parameters and Droplet Trajectories

From trajectory calculations may be derived the overall collision efficiency, E , the local collision efficiency at a point on the surface represented by its local surface slope, $\beta(\alpha)$, the local collision efficiency at the stagnation line, β_0 , the maximum impingement angle on the cylinder surface, α_{\max} , and the non-dimensional impact velocity at the stagnation line, V_0 . V_0 is normalized by the free stream speed, U . The local surface angle, α , is defined as the angle between the local surface normal and the free stream direction. The other quantities are defined in Figure II.1.

Values of E , β_0 , α_{\max} and V_0 are given by LB for a large number of cases which vary in droplet size, cylinder size, and air speed. These results are tabulated in terms of the non-dimensional parameters, K :

$$K = (\rho_d D_d^2 U) / (9 \mu D_c), \quad \text{II.1}$$

and ϕ :

$$\phi = Re^2 / K, \quad \text{II.2}$$

with the droplet Reynolds number based on the free-stream velocity, Re , given by:

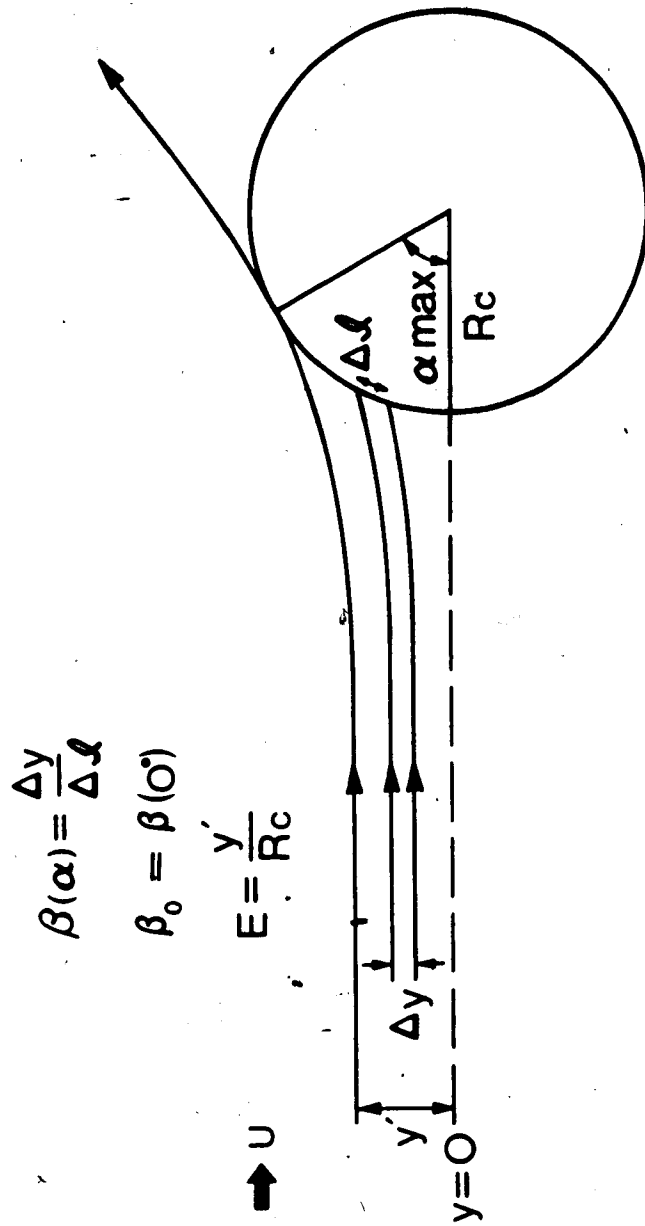


Figure II.1 - Droplet trajectories impinging on a circular cylinder, giving the definitions of $\beta(\alpha)$, β_0 , E and α . On the accretion surface α is the angle between the local surface normal and the free stream direction.

$$Re = U D_d \rho_a / \mu. \quad \text{II.3}$$

Here ρ_d is the density of water, ρ_a the density of air, μ the dynamic viscosity of air, D_d the droplet diameter, D_c the cylinder diameter, and U the free stream air speed.

The K parameter measures the inertia of the droplet, and is also known as the Stokes number. To aid in solving problems in which the droplet size is the unknown quantity, LB presented their data in terms of a second non-dimensional parameter, ϕ , that is independent of D_d .

The case $\phi = 0$ corresponds to Stokes, or creeping flow:

$$C_d Re_d / 24 = 1, \quad \text{II.4}$$

where C_d is the droplet drag coefficient, and Re_d is the droplet Reynolds number based on the relative velocity with respect to the air, V , so that:

$$Re_d = |V| Re / U. \quad \text{II.5}$$

In component form, the droplet equations of motion

$$dv_x / dt = -(v_x - u_x) (U C_d Re_d) / (12 D_c K)$$

$$dv_y / dt = -(v_y - u_y) (U C_d Re_d) / (12 D_c K),$$

where t is time, v_x , v_y and u_x , u_y are the droplet and air

speed components, respectively. This set of equations is in dimensional form, with the origin at the cylinder axis and U in the positive x direction. Gravity and the effects of droplet acceleration on the drag have been neglected, as in the original theory of LB.

The air speed components for potential flow around a cylinder (Green, 1937) are:

$$u_x(x,y) = U \left(1 + (R_c^2 (y^2 - x^2) / (x^2 + y^2)^2) \right)$$

II.7

$$u_y(x,y) = -(2 U R_c^2) (x y) / (x^2 + y^2)^2.$$

In order to permit a direct comparison with the original solutions by LB some trajectories have been integrated using their empirical formulation for the steady-state drag coefficient:

$$C_d Re_d / 24 = 1 + 0.197 Re_d^{0.63} + 2.6 \cdot 10^{-4} Re_d^{1.38} \quad \text{II.8}$$

More recent studies have improved the accuracy of C_d approximations at low Reynolds numbers, however, so in further calculations over the complete range of conditions the formulation of Beard and Pruppacher (1969) has been substituted when Re_d is less than 200. This formulation is:

$$C_d Re_d/24 = 1 + 0.102 Re_d^{0.955}, \text{ for } 0.2 \leq Re_d \leq 2.0$$

$$C_d Re_d/24 = 1 + 0.115 Re_d^{0.802}, \text{ for } 2.0 \leq Re_d \leq 21.0 \quad 11.9$$

$$C_d Re_d/24 = 1 + 0.189 Re_d^{0.632}, \text{ for } 21.0 \leq Re_d \leq 200.0$$

A comparison of a variety of theoretical and experimental results for the drag coefficients of spheres is given by Beard (1976), in which the above formulation is shown to be an accurate analytical approximation.

The integration is carried out by the Heun method as described in Mesinger and Arakawa (1976). The droplet trajectories are begun at ten cylinder radii upstream of the origin with speeds at the initial position (x_0, y_0) assumed to be:

$$v_x(x_0, y_0) = u_x(x_0, y_0) \quad 11.10$$

$$v_y(x_0, y_0) = 0.5 u_y(x_0, y_0)$$

At this initial upstream distance, the final results are not greatly influenced by the choice of initial droplet speed as long as it lies in between the local air speed and the undisturbed upstream air speed. Tests indicate differences in collision efficiency of less than 0.5 percent, when the initial droplet speeds are varied within this range.

Other factors which influence the accuracy of the integration are the time step, Δt , and the initial upstream distance, x_0 . A value of $x_0 = 10$ cylinder radii has been chosen, which, when compared to the results with $x_0 = 20$ cylinder radii, agrees to within 0.7 percent. At this initial distance, the size of the time step made less than a 0.5 percent difference in the results, as long as $\Delta t < 0.0033 (D_c/U)$. The value used is $0.0025 (D_c/U)$. Double precision is used throughout the program.

Values of the air viscosity and air density used are based on an assumed air temperature of -10°C . Within the temperature range of interest for most dry icing, i.e. -20 to 0°C , the collision efficiencies vary by a maximum of ± 1 percent.

An air pressure of 100 kPa was assumed. The calculations of LB were carried out for an atmospheric pressure of 78.5 kPa, for application to Mt. Washington, or to airborne icing in general. At this pressure value, the present results differed from the 100 kPa results by less than 0.5 percent. The new results should therefore be applicable to both ground-level and airborne icing.

Two complete trajectories must be integrated in order to calculate one value of the local collision efficiency $\beta(\alpha)$, where α is the mean angle of the two impact points. As illustrated in Figure II.1, $\beta(\alpha)$ is defined as the ratio of the initial vertical separation of the two trajectories, to the final separation in arc length of the two impact

points. In the present model, the initial y separation of the two trajectories is always 10^{-8} metres, an arbitrarily small distance for use in the finite difference approximation to dy/dt , the definition of local collision efficiency. The stagnation line value, β_0 , is calculated from the case where the first trajectory's initial position $y_0 = 0$.

The maximum impingement angle, α_{\max} , is found from the droplet trajectory which is tangent to the cylinder surface at its point of impact. This 'grazing' trajectory is found by increasing the initial position y_0 by successively smaller amounts until the tangent trajectory is reached.

The total collision efficiency E may then be calculated from the ratio of the initial vertical distance y_0 (graze) to the cylinder radius.

The Fortran77 code written for these calculations is included in Appendix I.

C. Results

In Figure II.2 three curves of β_0 vs. K are shown for the value $\phi = 10^3$, to illustrate the differences between LB's original calculations, the re-calculation of their results, and the re-calculation using Beard and Pruppacher's formulation for drag coefficient. The data for this Figure are listed in Table II.1.

A comparison between the first two curves shows that the LB results are too large for small K ($K \leq 0.4$), by up to

K	β_0 (LB), old C_d	β_0 (new), old C_d	β_0 (new), new C_d
.144	0.048	0.007	0.011
.196	0.095	0.058	0.073
.256	0.146	0.116	0.137
.4	0.233	0.224	0.247
.625	0.323	0.335	0.359
.9	0.398	0.425	0.447
1.6	0.513	0.558	0.575
3.6	0.680	0.714	0.724
6.4	0.778	0.798	0.806
10.	0.837	0.848	0.854
19.6	0.901	0.902	0.906
32.4	0.932	0.929	0.932
62.5	0.959	0.953	0.955
90.	0.969	0.962	0.963
160.	0.980	0.972	0.973
360.	0.989	0.981	0.981
640.	0.993	0.984	0.984
1000.	0.995	0.986	0.986

Table II.1 - $\beta_0(K)$ for $\phi = 10^3$. A comparison between Langmuir and Blodgett's results and the new results.

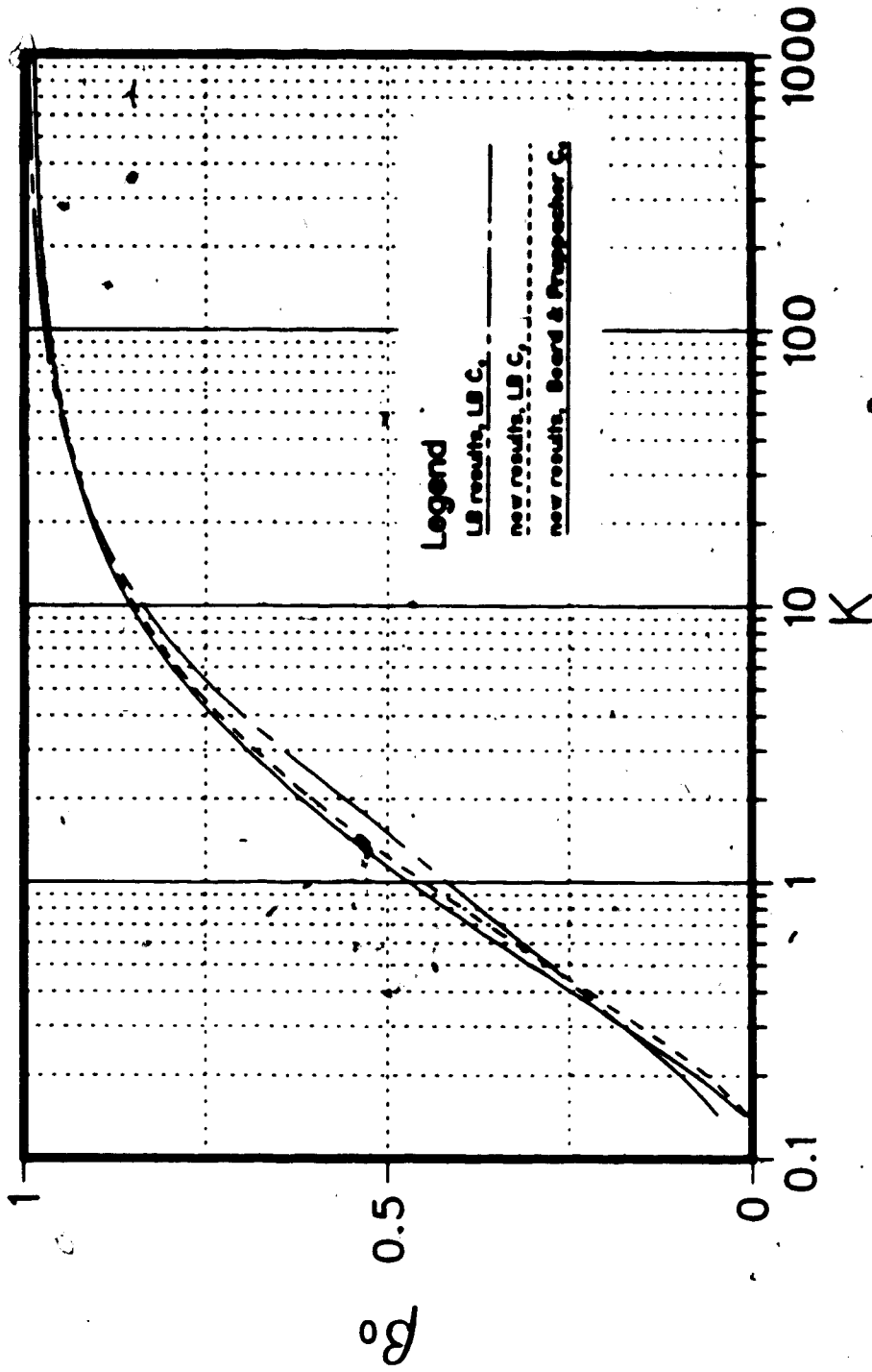


Figure II.2 - Comparison of β_0 vs. K for one value of $\phi = 10^3$.

several hundred percent. In the range $0.4 < K < 20.0$ their results are too small, by amounts near 10 percent in the middle of the range. For larger K , their values are again larger than the new results, but only by a few percent. The use of the revised drag coefficients (dotted curve, Figure II.2) gives another small increase over the LB results for all $K < 200.0$. A noticeable difference is that the new results for β_0 reach an effective value of zero for $K = 0.14$, rather than at LB's theoretical value of 0.125. This difference is as yet unexplained. Results for other ϕ values, and for α_{\max} , E and V_0 are quantitatively similar in differences between the old and new results.

It is concluded from the comparisons in Figure II.2 and Table II.1, that the original LB calculations are accurate only for very large K , but that when K is less than about 200 they may be significantly in error. The new results are suggested for future use. These are shown for β_0 , α_{\max} , E and V_0 for a complete range of ϕ and K in Tables II.2 to II.3, and in Figures II.3 through II.6, where the tabulated data have been fit by spline curves.

D. Curve Fitting

LB also drew smooth curves through their data, and derived analytical expressions in K and ϕ to fit them. Subsequently other authors have made attempts to improve on or to simplify these relations, and have then applied them

K	$\varphi = 10^2$			$\varphi = 10^4$			$\varphi = 10^6$		
	β_0	α_{max}	E	β_0	α_{max}	E	β_0	α_{max}	E
.16	0.034	0.054	0.001	0.021	0.035	0.0006	0.005	0.011	0.00004
.25	0.153	0.282	0.032	0.094	0.168	0.012	0.026	0.051	0.001
.36	0.257	0.466	0.088	0.164	0.287	0.034	0.050	0.089	0.003
.64	0.415	0.720	0.212	0.281	0.468	0.095	0.103	0.176	0.013
1.	0.528	0.889	0.325	0.374	0.609	0.163	0.157	0.260	0.029
1.96	0.676	0.997	0.500	0.518	0.817	0.296	0.251	0.380	0.067
3.24	0.763	1.219	0.617	0.617	0.958	0.406	0.319	0.488	0.112
6.25	0.848	1.336	0.743	0.726	1.115	0.547	0.424	0.633	0.191
9.	0.882	1.387	0.797	0.777	1.187	0.618	0.482	0.712	0.243
16.	0.921	1.446	0.863	0.838	1.278	0.711	0.570	0.832	0.333
36.	0.955	1.501	0.922	0.899	1.379	0.812	0.680	0.982	0.463
64.	0.968	1.523	0.946	0.927	1.434	0.864	0.745	1.080	0.550
100.	0.975	1.536	0.959	0.944	1.465	0.894	0.787	1.143	0.612
196.	0.982	1.548	0.972	0.960	1.497	0.927	0.839	1.227	0.693
324.	0.985	1.554	0.978	0.969	1.517	0.944	0.869	1.282	0.744
625.	0.987	1.558	0.983	0.977	1.533	0.959	0.900	1.337	0.799
900.	0.988	1.559	0.985	0.980	1.538	0.966	0.913	1.366	0.824

Table II.2 - continued.

K	V ₀					K	V ₀				
	$\psi = 0$	$\psi = 10$	$\psi = 10^3$	$\psi = 10^5$	$\psi = 10^2$		$\psi = 10^4$	$\psi = 10^6$			
.144	0.0002	0.0002	0.0002	0.0001	.16	0.002	0.0009	0.0001			
.196	0.018	0.017	0.012	0.003	.25	0.051	0.021	0.003			
.256	0.065	0.061	0.041	0.010	.36	0.133	0.059	0.010			
.4	0.195	0.183	0.122	0.033	.64	0.297	0.144	0.029			
.625	0.348	0.327	0.227	0.068	1.	0.428	0.228	0.055			
.9	0.471	0.443	0.317	0.111	1.96	0.604	0.379	0.116			
1.6	0.638	0.604	0.459	0.200	3.24	0.708	0.491	0.162			
3.6	0.804	0.772	0.640	0.346	6.25	0.810	0.625	0.251			
6.4	0.879	0.852	0.742	0.447	9.	0.853	0.690	0.306			
10.	0.918	0.896	0.806	0.528	16.	0.904	0.768	0.396			
19.6	0.956	0.940	0.876	0.642	36.	0.948	0.854	0.520			
32.4	0.973	0.960	0.913	0.715	64.	0.967	0.897	0.603			
62.5	0.986	0.977	0.945	0.793	100.	0.977	0.922	0.659			
90.	0.990	0.983	0.957	0.828	196.	0.986	0.948	0.732			
160.	0.994	0.989	0.971	0.872	324.	0.990	0.962	0.777			
360.	0.997	0.995	0.983	0.910	625.	0.994	0.975	0.826			
640.	0.999	0.997	0.989	0.936	900.	0.996	0.980	0.849			
1000.	0.999	0.998	0.992	0.950							

Table II.3 - Numerically calculated values of V₀ as a function of K and ψ .

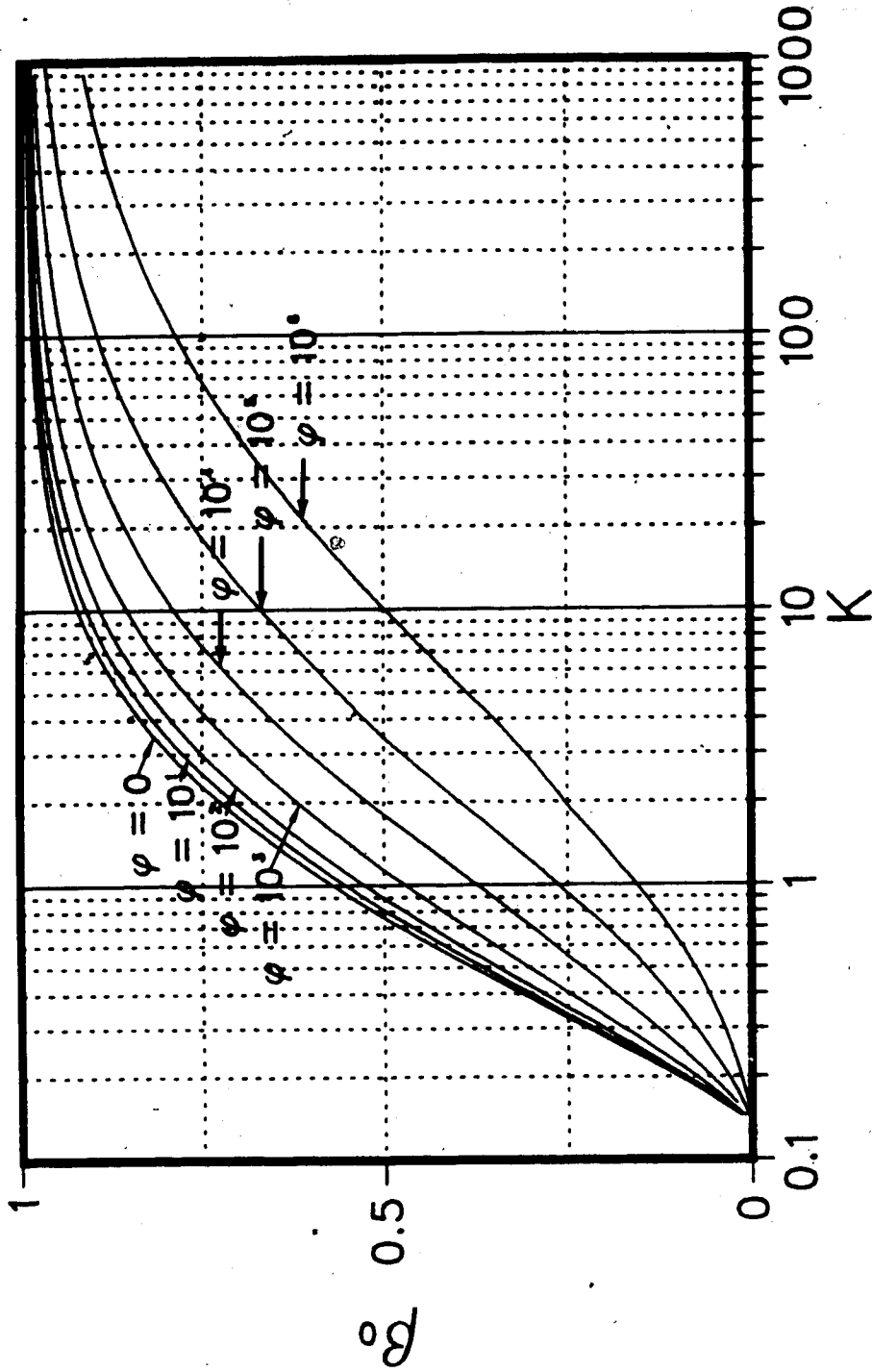


Figure II.3 - Smooth curves drawn for the numerical data of β_0 vs. K and ϕ .

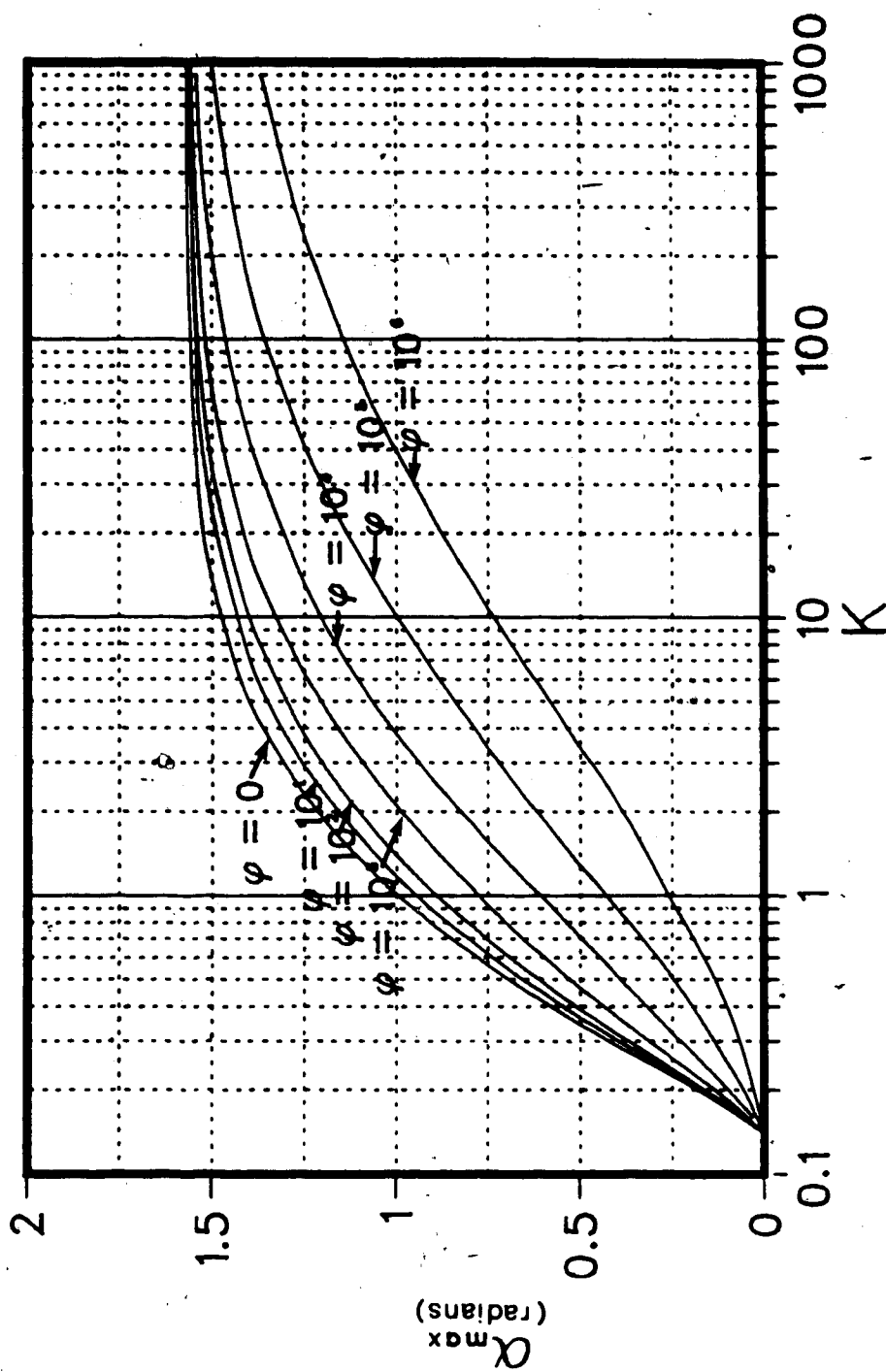


Figure II.4 - Smooth curves drawn for the numerical data of α_{\max} vs. K and ϕ .

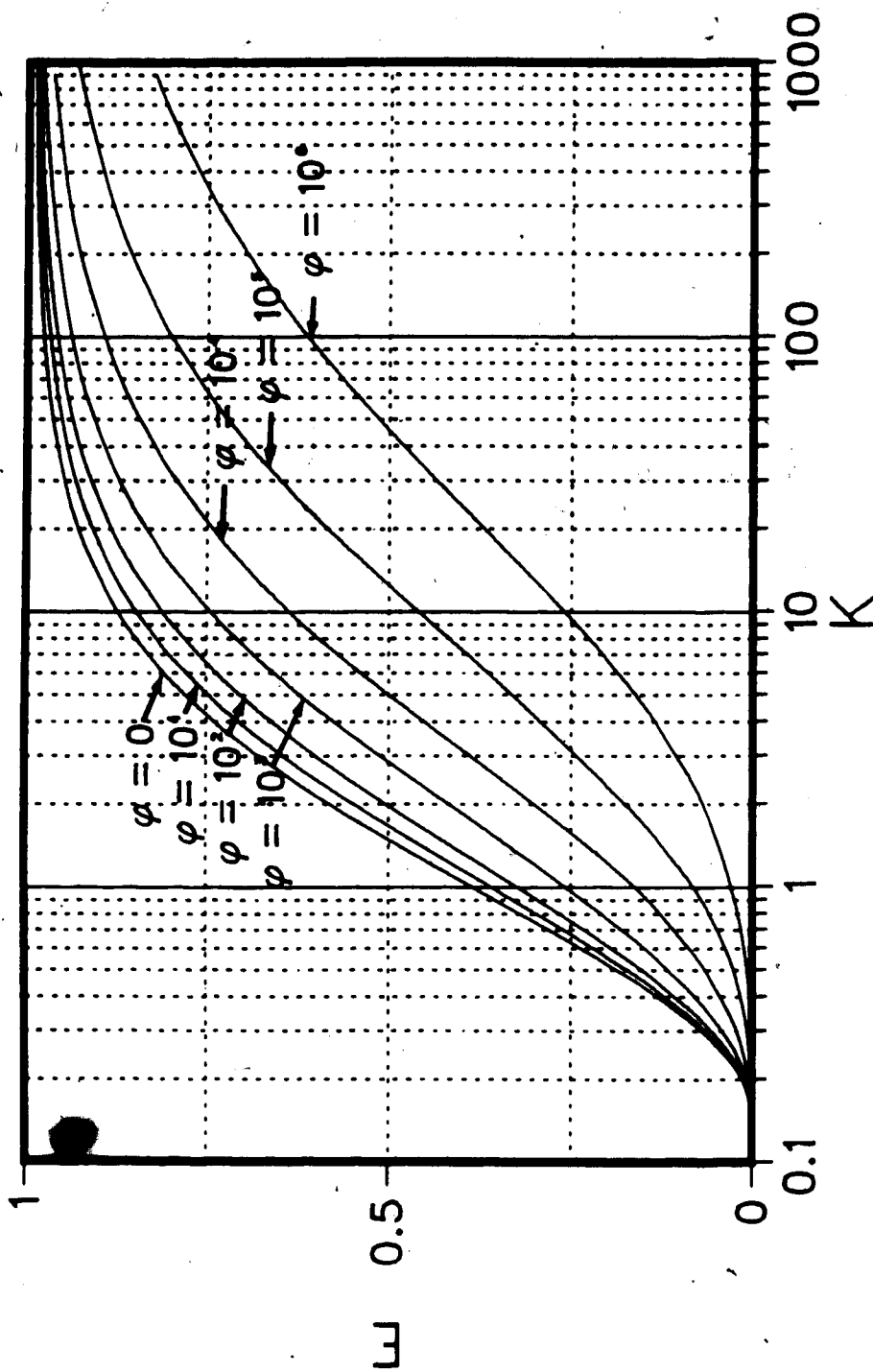


Figure II.5 - Smooth curves drawn for the numerical data of E vs. K and ϕ .

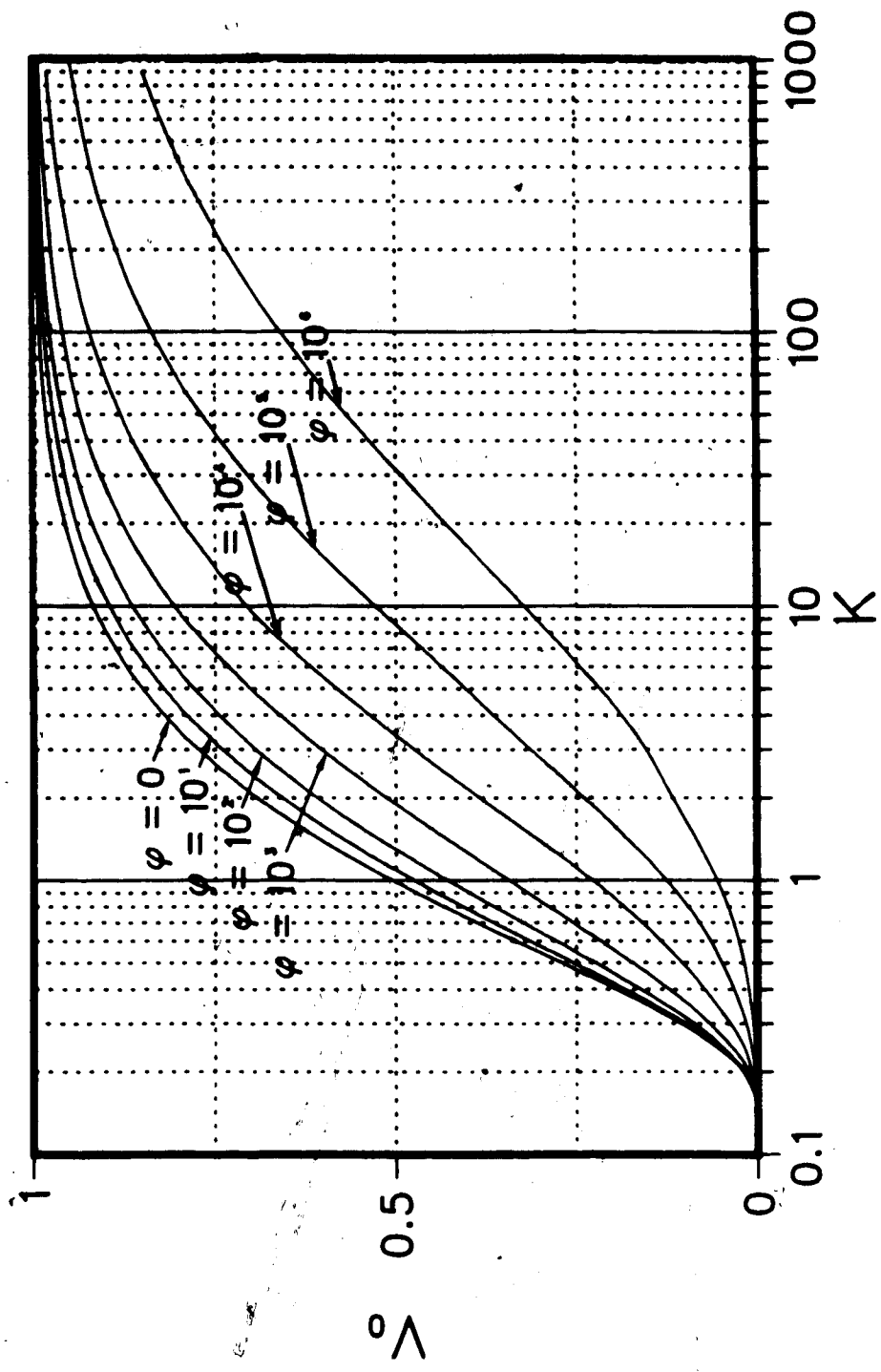


Figure II.6 - Smooth curves drawn for the numerical data of V_0 vs. K and ϕ .

Author(s)	$K_o(K, Re), \zeta(U, D_d, D_c)$	$E(K_o), E(K, Re), E(\delta)$	Range
Langmuir and Blodgett	$K_o = .125 + \frac{(K - .125)}{1 + .0967 Re^{.6367}}$	$E = .466 (\log_{10} (8K_o))^2$ $E = \frac{K_o}{K_o + 2}$ $E = \frac{K}{K + \frac{\pi}{2} \cdot .112 Re^{.63} + .75 \cdot 10^{-4} Re^{1.38}}$	$.125 < K_o < 1.1$ $K_o > 1.1$ $E > 0.5$
Lozowski, Stallabrass and Hearty	$K_o = .125 + \frac{(K - .125)}{1 + .0967 Re^{.6367}}$	$E = .489 (\log_{10} (8K_o))^{1.978}$ $E = \frac{K_o}{K_o + 2}$	$.125 < K_o < 0.9$ $K_o > 0.9$
Cansdale and McHaughton	$K_o = \frac{K}{1 + .087 Re^{(.76 Re^{-.027})}}$	$E = .53 (\log_{10} (8K_o))^{1.8}$ $E = \frac{K_o^{1.1}}{K_o^{1.1} + 1.223}$	$.125 < K_o < 1.1$ $K_o > 1.1$
Makkonen	$K_o = \frac{K}{1 + .087 Re^{(.76 Re^{-.027})}}$	$E = .5 (\log_{10} (8K_o))^{1.6}$ $E = \frac{K_o^{1.1}}{K_o^{1.1} + 1.426}$	$.125 < K_o < 0.8$ $K_o > 0.8$
Stallabrass	$\zeta = \frac{U^{.6} D_d^{1.6}}{D_c}$	$E = \frac{\zeta - 3200}{\zeta + 27000}$ $E = 0.1$	$\zeta > 3200$ $\zeta \leq 3200$

Table II.4 - Approximations to the numerical data of Langmuir and Blodgett derived by various authors.

to various numerical icing models (Cansdale and McNaughtan, 1977, Stallabrass, 1980, Lozowski; Stallabrass and Hearty, 1983, Makkonen, 1984). A number of these fitted relations for $E(K, \phi)$ are listed in Table II.4.

In order to compare these relations, values computed from each are listed with a selection of the original data in Table II.5. The data all fall within a range of ϕ between 10^2 and 10^4 , since some of the fitting functions were specifically designed for similar ranges, and because this range should apply to most physical applications, corresponding to $10 \leq D_d \leq 4000$ microns, $0.01 \leq D_c \leq 1.0$ metre, $5 \leq U \leq 200$ metres per second and $-20^\circ\text{C} \leq T \leq 0^\circ\text{C}$. It is worth noting that the natural range is actually narrower than this, since the largest drops do not occur together with the highest wind speeds (e.g. marine icing), nor do the smallest droplets occur at the lowest speeds (e.g. aircraft icing).

Langmuir and Blodgett's own fit is the most accurate, since it includes a correction table for $E < 0.5$, and for larger values of K , (giving E values > 0.5), they give theoretically derived functions for β_0 , α_{\max} , and E , which assume essentially straight-line trajectories. For this more elaborate scheme, the standard error (computed with respect to the numerical data) is generally an order of magnitude smaller than it is for the other fitting schemes. Even more important, however, is the fact that the variation among the values calculated by the various empirical

formulae for a given case can exceed 10 percent. These discrepancies will add to the difficulty of making comparisons among the icing predictions made by the various models which use these relations.

To reduce any further confusion, the new data have been fitted with approximating functions of improved form and greater accuracy. These functions are described below.

The approach taken by other authors to derive the formulae of Table II.4 has been to collapse a family of curves, such as that in Figure II.3, into a single curve via the ratio K_0/K , calculated as a function of Re , or in the case of Stallabrass (1980), via the parameter ξ , a function of D_d , U , and D_c (see Table II.4). K_0 is the K value read from the $\phi = 0$ curve which yields the same value of β_0 , α_{max} , E or V_0 as do the original K and ϕ . Extensive manipulation of the new data has revealed major problems with this approach. Specifically, the three families of curves for β , α_{max} and E are not collapsible by the same ratio K_0/K , but require three different ratios. Only LB take this into account for small values of E , by using their correction table, and theoretical approximations for larger E . Furthermore, the K_0/K 's are *not* single-valued functions of Re (see Figure II.7), as has usually been assumed.

In the Stallabrass (1980) method, although ξ is used instead of K and ϕ , a similar problem arises for his curves, since they collapse to a single curve only for very large values of ξ .

	K	LB (numerical)	LB (approx.)	Lozowski, et al.	Canadale	Makkonen	Stallabrass
10 ²	.16	0.004	0.004	0.004	0.002	0.005	0.056
	.64	0.181	0.183	0.181	0.191	0.202	0.284
	3.24	0.591	0.588	0.568	0.630	0.594	0.634
	16.	0.855	0.854	0.836	0.884	0.867	0.867
	100.	0.966	0.965	0.958	0.975	0.972	0.966
10 ³	625.	0.992	0.992	0.989	0.995	0.994	0.992
	.196	0.009	0.009	0.010	0.0	0.0	0.017
	.625	0.127	0.129	0.132	0.120	0.134	0.170
	3.6	0.542	0.540	0.509	0.560	0.522	0.536
	19.6	0.830	0.825	0.796	0.852	0.831	0.827
10 ⁴	90.	0.942	0.939	0.925	0.956	0.949	0.943
	640.	0.986	0.985	0.942	0.992	0.990	0.988
	.25	0.012	0.013	0.014	0.0	0.0	0.0
	1.	0.148	0.142	0.146	0.120	0.134	0.152
	6.25	0.546	0.539	0.499	0.557	0.518	0.531
	36.	0.820	0.811	0.778	0.850	0.829	0.831
	196.	0.937	0.934	0.921	0.960	0.954	0.951
	900.	0.974	0.974	0.972	0.988	0.987	0.985
standard error:			0.003	0.018	0.017	0.010	0.019

Table II.5 - Comparison of some original E values calculated numerically by Langmuir and Blodgett, and those derived from the approximations of Table II.4.

For these reasons, an accurate fit to the entire range of data given is difficult to find and awkward to use. Consequently, an approximating function is given here only for ϕ between 10^2 and 10^4 , which is the range applicable to most atmospheric, land-based and marine icing problems.

A non-linear regression analysis on this range gives the following result for $0.17 \leq K \leq 10^3$:

$$X(K, \phi) = (C_{X,1} K^{C_{X,2}} \exp(C_{X,3} K^{C_{X,4}} + C_{X,5}) - (C_{X,6} (\phi - 100)^{C_{X,7}})) \quad \text{II.11}$$

$$(C_{X,8} K^{C_{X,9}} \exp(C_{X,10} K^{C_{X,11}}) + C_{X,12}),$$

where X is either β_0 , α_{\max} , E or V_0 , and the constants $C_{X,n}$ are as listed in Table II.6. The basic form of this function is a standard fitting function supplied by the BMDP non-linear regression package (Dixon, et al., 1981).

Values for $K < 0.17$ and $K > 10^3$ may be read from the curves or roughly approximated as follows:

$$\beta_0 = \alpha_{\max} = E = V_0 = 0.97, \text{ for } K < 0.17, \quad \text{II.12}$$

and

$$\beta_0 = E = V_0 = 0.99, \text{ for } K > 10^3, \quad \text{II.13}$$

$$\alpha_{\max} = 1.56, \text{ for } K > 10^3.$$

$K_{0,\beta}/K$ vs. Re

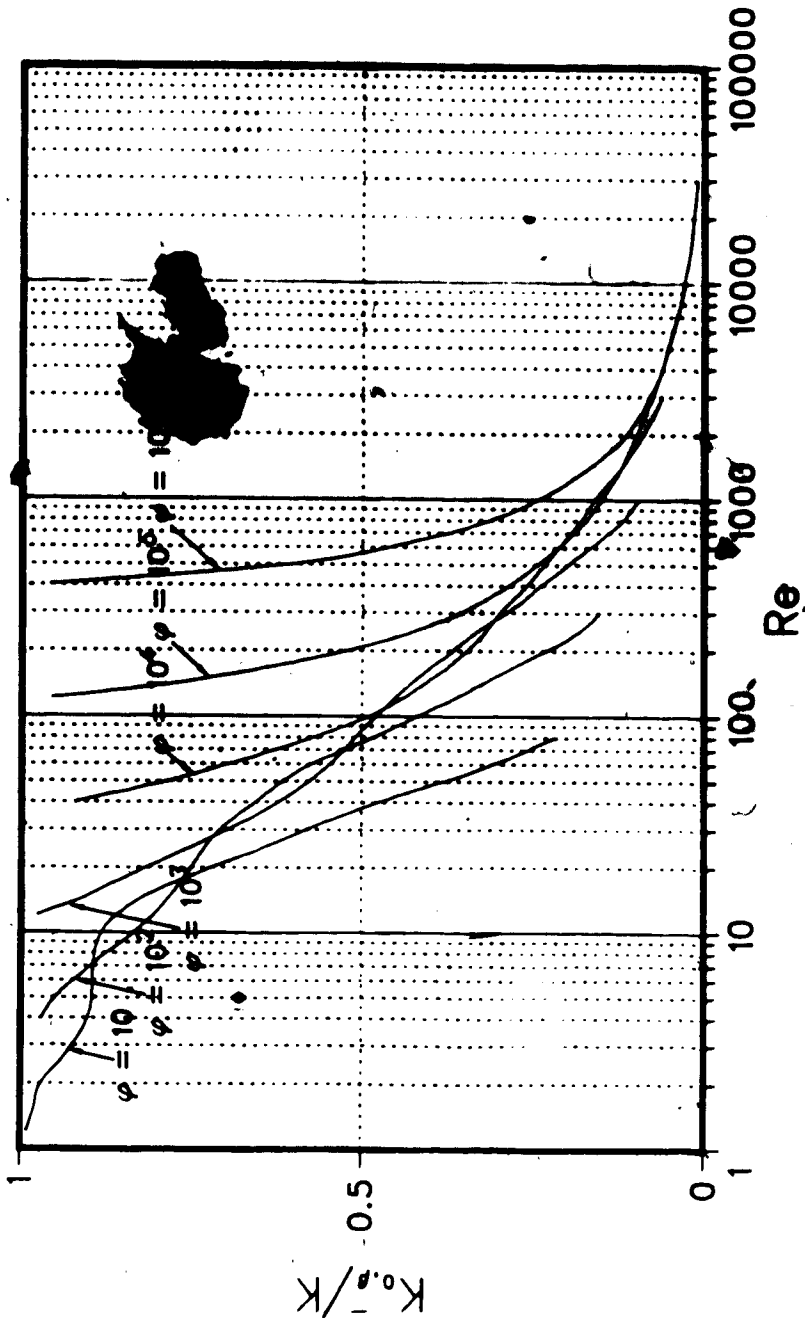


Figure 14.7 The dependence of $\frac{K_{0,\beta}}{K}$ on Reynolds Number Re . $K_{0,\beta}$ is defined by: $\beta_0(K,\varphi) = \beta_0(K_{0,\beta},0)$

	$X = \beta_0$	$X = \alpha_{max}$	$X = E$	$X = V_0$
$C_{X,1}$	1.218	2.433	1.066	1.030
$C_{X,2}$	$-6.70 \cdot 10^{-3}$	$-4.70 \cdot 10^{-3}$	$-6.16 \cdot 10^{-3}$	$1.68 \cdot 10^{-3}$
$C_{X,3}$	-0.551	-0.375	-1.103	-0.796
$C_{X,4}$	-0.643	-0.576	-0.688	-0.780
$C_{X,5}$	-0.170	-0.781	-0.028	-0.040
$C_{X,6}$	$3.05 \cdot 10^{-3}$	$8.50 \cdot 10^{-3}$	$6.37 \cdot 10^{-3}$	$9.44 \cdot 10^{-3}$
$C_{X,7}$	0.430	0.383	0.381	0.344
$C_{X,8}$	2.220	1.757	3.641	2.657
$C_{X,9}$	-0.450	-0.298	-0.498	-0.519
$C_{X,10}$	-0.767	-0.420	-1.497	-1.060
$C_{X,11}$	-0.806	-0.960	-0.694	-0.842
$C_{X,12}$	-0.068	-0.179	-0.045	-0.029

Table 11.6 Coefficients for approximating impingement parameters by the expression:

$$X(K, \varphi) = (C_{X,1} K^{C_{X,2}} \exp(C_{X,3} K^{C_{X,4}}) + C_{X,5}) \cdot (C_{X,6} (\varphi - 100)^{C_{X,7}}) (C_{X,8} K^{C_{X,9}} \exp(C_{X,10} K^{C_{X,11}}) + C_{X,12})$$

Within the range of $0.17 < K < 10^3$ the standard error of the fit with respect to the numerical data is given in Table II.7. It compares very favorably to the errors given in Table II.5 for the fitting schemes previously discussed.

E. Limitations of LB Theory

The collision efficiency theory of Langmuir and Blodgett assumes that the air is in potential flow about the collecting cylinder, that only steady-state drag forces are exerted on the water droplets by the flow, and that the flow itself remains unaffected by the presence of the droplets.

The potential flow field about an infinitely long, circular cylinder is as described by Equations II.7^a, and illustrated in Figure II.8(a). Figure II.8(b) illustrates the analogous situation for viscous flow at a cylinder Reynolds number of $\approx 10^4$, corresponding to $D_c = 0.0254$ m, $U = 10$ m/sec, and $T = -10^\circ$ C. The upstream flow in Figure II.8(b), which determines the accretion, deviates slightly from the potential flow case due to the presence of a sizable wake on the downstream side. The cylinder plus wake will be felt by the flow further upstream, decreasing the streamline curvature, and thus increasing the collision efficiency. In most situations, however, the effect will be small.

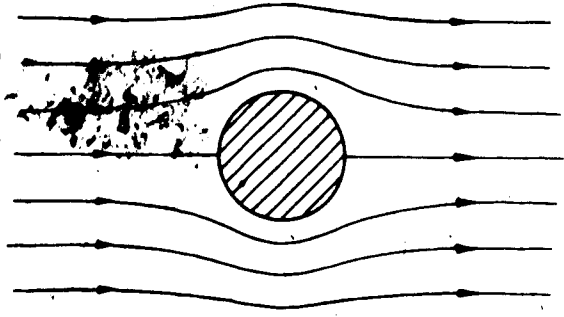
The potential flow assumption also ignores the cylinder boundary layer, which will be of negligible depth for a

numerical approximated

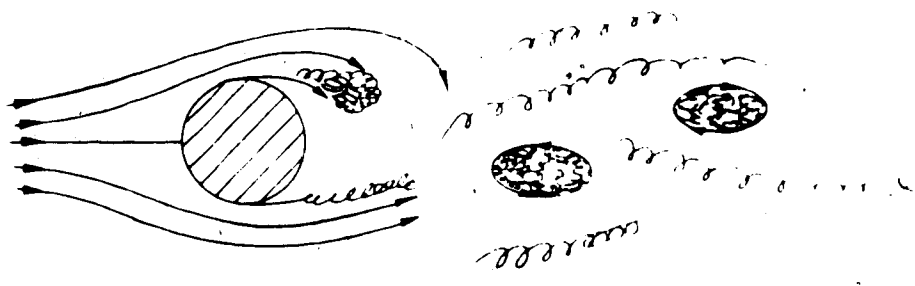
φ	numerical				approximated			
	β_0	α_{max}	E	V_0	β_0	α_{max}	E	V_0
10^2	.16	0.034	0.001	0.002	0.036	0.054	0.0	0.0
	.64	0.415	0.212	0.297	0.416	0.720	0.210	0.293
	3.24	0.763	0.617	0.708	0.763	1.219	0.619	0.710
	16.	0.921	0.863	0.904	0.920	1.445	0.861	0.904
10^3	100.	0.975	0.959	0.977	0.978	1.538	0.961	0.975
	625.	0.987	0.983	0.994	0.986	1.558	0.983	0.995
	.196	0.073	0.007	0.012	0.075	0.135	0.005	0.013
	.625	0.359	0.157	0.227	0.363	0.611	0.159	0.220
10^4	3.6	0.725	0.553	0.640	0.728	1.139	0.557	0.639
	19.6	0.906	0.832	0.876	0.904	1.401	0.825	0.869
	90.	0.963	0.935	0.957	0.964	1.503	0.931	0.951
	640.	0.984	0.976	0.989	0.983	1.549	0.974	0.989
	.25	0.094	0.012	0.015	0.098	0.179	0.012	0.024
	.1	0.374	0.163	0.228	0.379	0.610	0.162	0.225
	6.25	0.726	0.547	0.625	0.726	1.115	0.548	0.637
	36.	0.899	0.812	0.854	0.899	1.380	0.816	0.865
	196.	0.960	0.927	0.948	0.962	1.497	0.930	0.954
	900.	0.980	0.966	0.980	0.980	1.543	0.967	0.986

standard error: 0.002 0.005 0.003 0.006

Table II.7 - Comparisons between a selection of numerically calculated values, and approximated values calculated according to Table II.6.



(a)



(b)

Figure II.8 - (a):Potential flow streamlines about a cylinder in cross-section. (b):Viscous flow streamlines about a cylinder at a Reynolds number of 10,000.

smooth cylinder, but may become significant for rough surfaces. The effect, if any, of a deep, possibly turbulent boundary layer on the collision efficiency is unknown. In particular, the onset of accretion may be affected if the roughness elements are large enough to act as individual collectors.

The assumption of the airflow being undisturbed by the droplets carried in it, is a reasonable one given typical cloud liquid water contents.

In determining the deceleration of the drop by the flow, LB's steady-state viscous drag coefficient ignores buoyancy and gravitational forces, the influence of vorticity diffusion from the accelerating droplet surface, and the induced mass increase of the drop as a result of accelerating the air immediately surrounding it.

A 20 micron droplet falls in air with a terminal speed of 0.012 m/sec (Mason, 1971). Thus the vertical deviation of such a droplet approaching a 0.0254 m diameter cylinder from five diameters upstream, at a free-stream speed of 10 m/sec, is about 0.15 mm. This is only about one percent of the maximum vertical deviation due to the flow, under those conditions. At some point on the cylinder surface, the deviation due to the flow will be comparable to the gravitational drift, but since the relative difference in two adjacent trajectories will be much smaller, the collision efficiencies should not be affected.

Much larger drops, such as occur in sea spray icing, will have a correspondingly larger gravitational drift. Preliminary numerical calculations by Szilder (personal communication, 1986) indicate that there is still a very small effect on the collision efficiency, but this is a question which should be investigated further.

The other two effects on the drag are incorporated into the 'history' term, which, expressed as an acceleration, is:

$$-\frac{18\rho_a}{(2\rho_d + \rho_a) D_d} \sqrt{\frac{\mu}{\pi\rho_a}} \int_{-\infty}^t \frac{d\vec{v}}{dr} \frac{dr}{\sqrt{t-\tau}} \quad \text{II.14}$$

The relative importance of the history term is often measured by the acceleration modulus (Norment, 1980):

$$N_A = D_d \left| \frac{dv}{dt} \right| / v^2, \quad \text{II.15}$$

where v is the droplet's absolute velocity. If this quantity is < 0.01 , the history term may be safely omitted from the droplet's equation of motion.

Numerical results from the trajectory integration model presented above show that N_A is well within this limit under most conditions of accretion on cylinders. However, for $K \leq 0.5$, N_A may reach values ≥ 0.01 just before impact, and for $K \leq 0.20$, the limit is exceeded as much as a few millimetres in front of the cylinder surface.

For these small K values then, the effect of the history term is to decrease the droplet's deceleration and

increase both its total velocity near the surface, and the resulting collision efficiency. Numerical integrations by Oleskiw (1982) for $K = 0.196$, $\phi = 1000$ show an increase in E of 350%, and in β_0 of 167% when the history term is included.

Thus the 'cut-off' K value, for zero collision efficiency, which arises from LB theory, is not valid for real flow. In light of these results, it may be advisable to consider Equations II.11, II.12, and II.13 as valid only for $K > 0.25$. Below this limit, the trajectories should be recalculated using the complete drag terms in the droplet equation of motion.

The last assumption listed, that of an airflow undisturbed by the presence of water droplets, is probably a reasonable one for the small liquid water contents typical of clouds, $< 5 \text{ g/m}^3$. The case for heavy spray icing may, however, be very different, and this is another question which warrants further study.

F. Summary

Earlier results for water droplet trajectories at freezing temperatures have been re-examined and improved upon. The new results differ from LB by as much as 10 percent. Tabulated data are provided to replace those of Langmuir and Blodgett for the collisional parameters of water droplets on cylinders, and a good approximating function to the data has been found which will be of use to

modellers. These results should only be applied, however, to real situations when $K > 0.25$, below which the non-steady-state drag terms have a significant effect on collision efficiencies.

References

- Beard, K.V. 1976: Terminal Velocity and Shape of Cloud and Precipitation Drops Aloft. *J. Atmos. Sci.* , 33, 851-864. *J. Atmos. Sci.*, 33, 851-864.
- Beard, K.V. and Pruppacher, H.R. 1969: A Determination of the Terminal Velocity and Drag of Small Water Droplets by Means of a Wind Tunnel. *J. Atmos. Sci.*, 26, 1066-1072.
- Cansdale, J.T. and McNaughton, I.I. 1977: Calculation of Surface Temperature and Ice Accretion Rate in a Mixed Water Droplet / Ice Crystal Cloud. Royal Aircraft Establishment Technical Report 77090, 29 pp.
- Dixon, W.J., Chief Editor, et. al. 1980: Chapter 14 - Nonlinear Regression. In: BMDP Statistical Software. University of California Press, 289-309.
- Green, S. L. 1937: Hydro-and-Aero-Dynamics. Pitman and Sons, p. 26.
- Langmuir, I. and Blodgett, K. 1946: A Mathematical Investigation of Water Droplet Trajectories.

Collected Works of Irving Langmuir Vol. 10,
Pergamon Press, 348-393.

Lozowski, E.P., Stallabrass, J.R. and Hearty, P.F. 1983: The
Icing of an Unheated, Non-Rotating Cylinder Part
I: A Simulation Model. *J. Climate and App.
Meteor.*, 22, 2053-2074.

Mesinger, F. and Arakawa, A. 1976: Numerical Methods used in
Atmospheric Models, Vol. 1. W.M.O. GARP
Publications Series No. 17, 64 pp.

Mason, B.J. 1971: The Physics of Clouds, 2nd Edition.
Clarendon Press, p. 594.

Makkonen, L. 1984: Modelling of Ice Accretion on Wires. *J.
Climate and App. Meteor.*, 23, 929-939.

Norment, H.G. 1980: Calculation of Water Drop Trajectories
to and About Three-Dimensional Bodies in Potential
Airflow. NASA Contractor Report 3291, 82 pp.

Oleskiw, M.M. 1982: A Computer Simulation of Time-Dependent
Rime Icing on Airfoils. Ph.D. thesis, The
University of Alberta, 302 pp.

Stallabrass, J.R. 1980: Trawler Icing: A Compilation of Work

Done at NRC. NRC Report MD-56, NRC No. 19372, 103

1 pp.

III. An Operational Model for Rime Ice Accretion

A. Introduction

Modelling of the many physical processes involved in ice accretion can be a complex and time-consuming exercise. The cost of running such models tends to limit their use as investigative tools, or for predictive purposes of an operational character. In an attempt to alleviate part of this problem, simple parameterization methods have been developed which make possible a more practical, inexpensive and realistic model. In this chapter these methods, and their application in a computer simulation of rime icing on circular cylinders will be described.

The computer model was developed with several specific purposes in mind. The first was to reduce the computational time necessary, in particular, for the calculation of impingement parameters. The quantities E , β_0 and α_{max} for circular cylinders are available from the tabulated data and analytical fitting functions of Chapter II. Values of local collision efficiency between the stagnation line and maximum impingement angle usually have to be determined from a series of droplet trajectory pairs. Oleskiw (1982) has calculated the distributions of local collision efficiency

' It has been suggested (McComber and Touzot, 1981) that the variation of the local radial velocity of impact be used as an approximation to the local collision efficiency. It has been previously shown (Lozowski, Finstad and Gates, 1985) that for realistic cases this can be a poor approximation at the stagnation line (compare Figures II.3 and II.6), and that the relative error increases dramatically with distance toward the accretion limit.

for several cases, from numerically integrated trajectories. From these, it was possible to derive a parameterized general form of the $\beta(\alpha)$ curve which depends only on the parameters β_0 and α_{max} .

Use of this parameterization is the major time-saving device in the model. Several other options are provided for simulating the effect on the $\beta(\alpha)$ distribution of a droplet size spectrum which cannot be adequately modelled by the median volume size. This effect is principally in the extension of the maximum accretion angle.

A second major purpose in developing this model was to incorporate the local ice density variations into the shape of the rime ice accretions. An empirical, parameterized function is used to describe this variation, and it is shown to be reasonably successful in reproducing observed accretion shapes on non-rotating cylinders, under a variety of conditions.

A third purpose was to attempt to simulate a slow rotation of the collecting cylinder about its long axis. This is meant to imitate the effects of a gravitational torque on an ice-loaded cable. Although this capability has now been built into the model, it has not yet been possible to test it against laboratory or field data.

In order to effectively examine the validity of these methods, only dry, rime ice accretions are considered. This is so that any comparisons with experimental results are not dependent on poorly known quantities, such as heat transfer,

which affect wet, icing processes.

In the experimental accretion experiments used to aid in model development and verification, a crucial measurement is the droplet size spectrum, and its median volume diameter. All droplet spectra were measured by the oil slide method, an outline of which is given in Mason (1971). However, the mvd's derived from such measurements have been found to show a systematic error by Makkonen and Stallabrass (1984). We therefore apply their empirical correction formula to our data in all but a few cases, which fall outside the range of validity for the correction. The procedure followed in these cases is described in Appendix III.

To ensure rime icing under the conditions typical of the wind-tunnel experiments, in which collectors with diameters of 2 to 5 cm were exposed to typical atmospheric liquid water contents and wind speeds, the air temperature in the model is assumed to be always at or below -10° C. For application to general conditions, the model should include a calculation of the critical liquid water content, or 'Ludlam limit', (Ludlam, 1951) in order to determine whether the ice will be wet or dry.

B. Parameterization for Local Collision Efficiency

For the idealized situation of straight-line droplet trajectories the local collision efficiency is given simply by $\cos \alpha$, where α is the angle of the local surface normal

with respect to the free stream direction. The collision efficiency has a maximum value of unity at the stagnation line, and a minimum of zero at $\alpha = \pi/2$.

In a more realistic situation, the trajectories curve away from the free stream direction as they approach the cylinder. The stagnation line collision efficiency is reduced from 1, and the local value reaches zero for some $\alpha = \alpha_{\max} < \pi/2$. This situation can be well approximated (especially for large droplets whose trajectory curvature is small) by directly scaling the $\cos \alpha$ distribution to these two extreme values, as follows:

$$\beta(\alpha) = \beta_0 \cos \left(\left(\frac{\alpha}{\alpha_{\max}} \right) \left(\frac{\pi}{2} \right) \right), \quad \text{III.1}$$

where the two parameters β_0 and α_{\max} are determined from tabulated values or approximating functions given in Chapter II.

A form of time dependence is built into this method since the collision efficiency at a point depends on its local surface angle, which changes with time as the ice layers are accreted on top of one another. The parameters β_0 and α_{\max} do not change with time, an approximation which becomes worse as the accretion shape grows, and departs from a circular cross-section.

For smaller droplets the simple approximation of Equation III.1 fails, since the trajectories are curved by much larger amounts. It has been found that, for a $\beta_0 <$

0.65, the $\beta(\alpha)$ curve is more closely approximated by:

$$\beta(\alpha) = \beta_0 - (\beta_0 (1 - \cos^{0.5} \alpha) \cos^{0.5} \alpha_{\max})). \quad \text{III.2}$$

For a 0.0254 m diameter cylinder at typical ground level wind speeds of a few tens of metres per second, this corresponds to water droplets of less than 20 microns diameter.

Figure III.1 illustrates the goodness of fit of these functions against local collision efficiency curves calculated numerically by Oleskiw (1982), and approximated by Lozowski, Stallabrass and Hearty (1983).

In both Equations III.1 and III.2, a monodisperse droplet size population has been assumed, or at least a distribution for which the collision efficiency may be reasonably approximated by the collision efficiency of the median volume droplet, or mvd. The results of Appendix VI suggest that, for typical ground-level wind speeds, the single droplet size approximation holds well for $\beta_0 \geq 0.5$.

Otherwise, the effect of the size spectrum, and particularly its larger drops, should be accounted for. Droplet size distributions for icing purposes are commonly described by volume percentages in several size bins of finite width (see, for example, Figure III.2). Applying either Equation III.1 or III.2 to the median volume droplet of each size bin, a volume-weighted average distribution may be calculated. Such a weighted curve then illustrates the

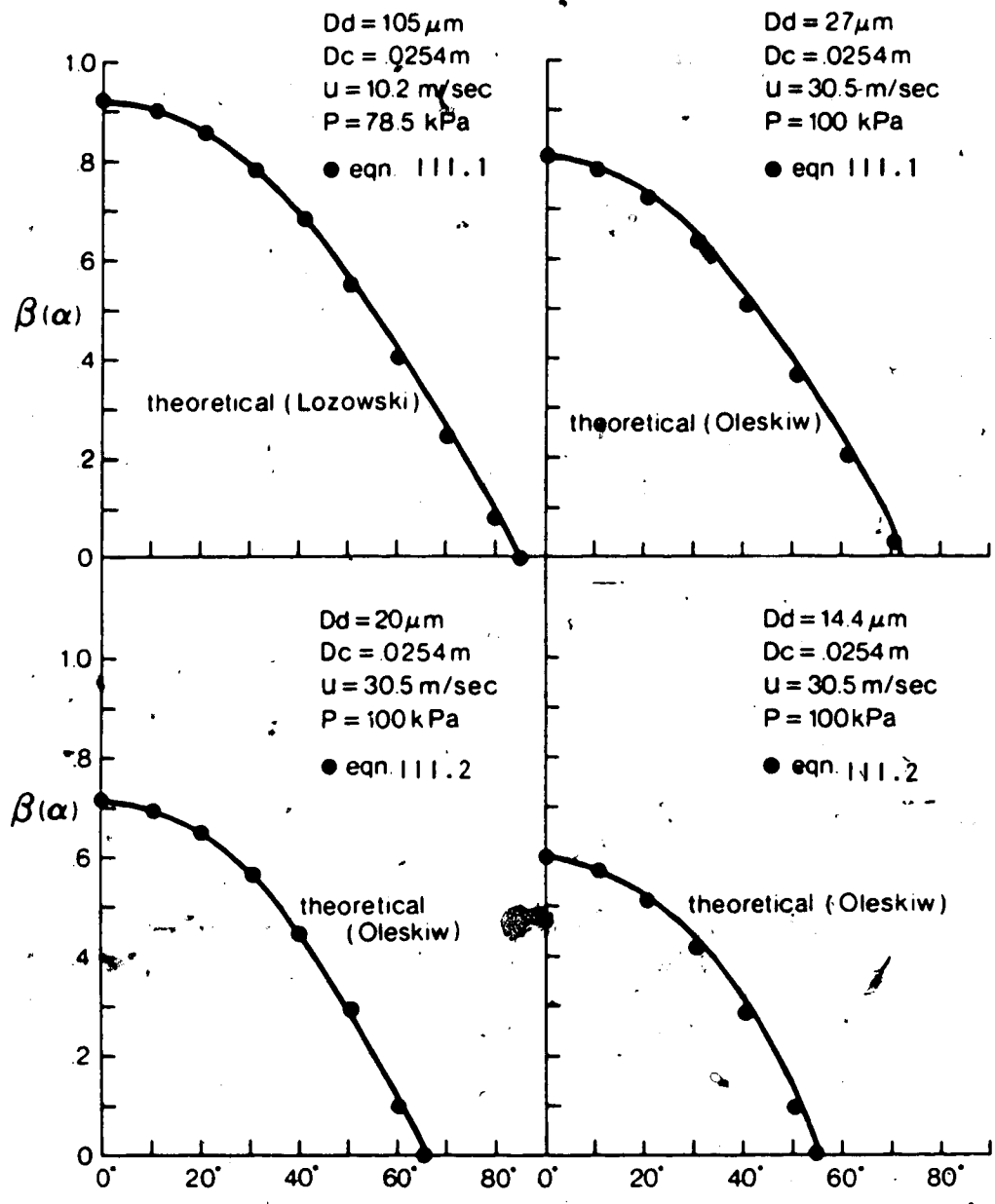


Figure III.1 - Parameterized $\beta(\alpha)$ values from Equations III.1 and III.2, compared to numerically calculated curves of Oleskiw (1982), and parameterized curve after Lozowski, Stallabrass, and Hearty (1983).

effect of the smaller droplets in extending the maximum accretion limit.

This weighting procedure, for a given input size spectrum, may be carried out within the model. This is the "weighted spectrum" option. However, the nature of the averaging procedure eventually gives rise to first-order discontinuities in the $\beta(\alpha)$ curve, and thus on the accretion surface. For this reason, the weighted spectrum option is not recommended when more than three ice layers are accreted, no matter how thin these layers are.

An alternative option is included to avoid this problem, which has been called the "simulated spectrum" option. It is another form of the $\beta(\alpha)$ curve, this time based on weighted average curves (from laboratory measured spectra) which have been scaled and fitted with polynomial functions.

for $\beta_0 < 0.65$:

$$\beta(\alpha/\alpha_m) = \beta_0 (1 + 0.22(\alpha/\alpha_m) - 3.08(\alpha/\alpha_m)^2 + 1.86(\alpha/\alpha_m)^3),$$

III.3

and for $\beta_0 > 0.65$:

$$\beta(\alpha/\alpha_m) = \beta_0 (1 + 0.029(\alpha/\alpha_m) - 1.94(\alpha/\alpha_m)^2 + 2.48(\alpha/\alpha_m)^3 - 4.11(\alpha/\alpha_m)^4 + 2.54(\alpha/\alpha_m)^5),$$

III.4

where $\alpha_m = \alpha_{\max} + T_1$, and T_1 is the "tail length", an extension to α_{\max} , derived from numerical results and correlated to the mvd. For $\beta_0 < 0.65$:

$$T_1 = 0.52 \exp(-mvd / 70) \quad \text{III.5}$$

and for $\beta_0 > 0.65$:

$$T_1 = 0.37 \exp(-mvd / 70). \quad \text{III.6}$$

Here mvd is in μm and T_1 is in radians. Equations III.3 and III.4 are compared in Figure III.2 with two weighted average curves for the cloud droplet spectra shown.

Although these methods may seem to have become very superficial, they do retain the desired economy of computation with an acceptably small loss of accuracy.

C. Variation of Local Density

A study of the local density variations in circular cylinder rime accretions will be discussed in some detail in Chapter IV. Here the result is presented briefly; an empirical curve describing local density as a function of surface slope.

Based on cross-sectional thickness measurements of several shallow rime layers grown in the laboratory under known conditions, the following function was derived for $\alpha/\alpha_m < 1$:

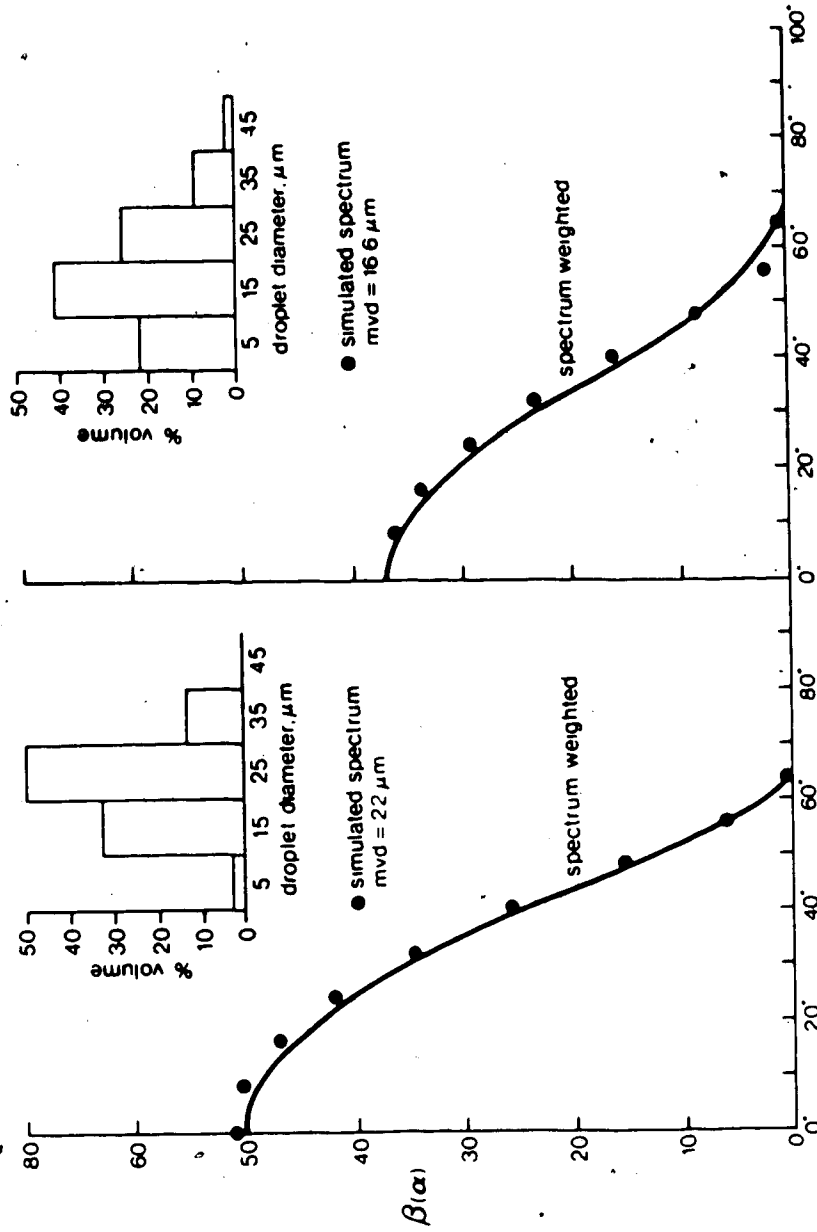


Figure III.10 - Parameterized $\beta(\alpha)$ values from Equations III.3 and III.4, compared to weighted average curves for the cloud droplet spectra shown. These spectra are derived from the distribution of Best (1951).

$$\rho/\rho_0 = (1 - 0.143(\alpha/\alpha_m) - 0.246(\alpha/\alpha_m)^2$$

$$- 0.309(\alpha/\alpha_m)^3).$$

III.7

Here α_m is defined as for Equations III.3 and III.4, and in this version of the model, $\rho_0 = 890 \text{ kg / m}^3$. This assumption is made for simplicity; in reality the rime densities may be much lower, and this will affect the accretion thickness and overall shape. Chapter IV will discuss methods for estimating more realistic values of ρ_0 .

The remainder of this section will examine the predictive success of the model under a variety of input conditions. Figure III.3 compares accretion profiles and masses from the model against ice accretions grown in wind tunnel experiments carried out in the University of Alberta's FROST tunnel (this facility and our experimental methods are described in Gates, 1981 and Lozowski and Gates, 1984). For the ranges shown of mvd , liquid water content and free-stream speed the modelled mass is always within 10% of the observed mass, and the major features of the experimental shapes are reproduced in the profiles.

However, it is not expected that the model will reproduce such features as ridges or troughs near the stagnation line. These are most likely due to changes in the flow pattern as the accretion grows, and the resulting

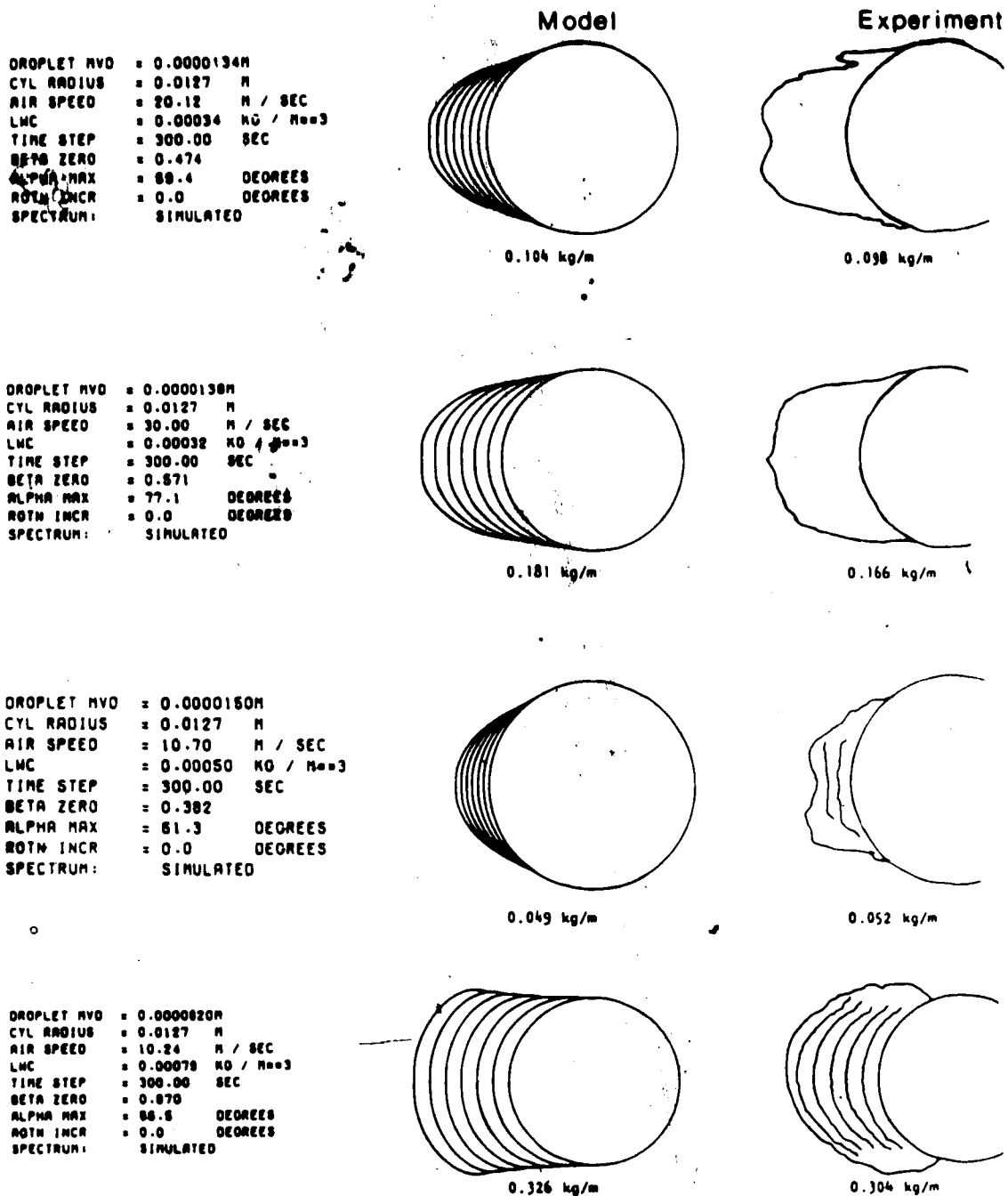


Figure III.3 - Comparisons between modelled and experimental profiles and masses per unit length for the conditions listed at left. The lower two experimental profiles have layer-outlines which were marked by spray paint.

changes in the impingement characteristics.

In particular, the value of β_0 will change with time, while the model assumes a constant value. Even with this assumption, however, it is able to distinguish between widening and narrowing profiles for small differences in growth conditions, and can produce the flat front surface which often precedes the formation of ridges and troughs in the experiments.

D. Rotation

An option has been included in the model which will allow the cylinder plus accretion to be rotated with respect to the free stream by a small amount after each layer is accreted. No attempt is made to calculate the correct rotation rate due to the gravitational and aerodynamic torque; the rotation speed in degrees per layer must be specified as one of the input parameters.

In order to achieve this effect within the model algorithm, the local collision efficiency and local density must be calculated as functions of the position angle rather than the surface angle on the current surface. (The position angle at a surface point is the angle between a line joining the point to the centre of the cylinder, and the free-stream direction.) This somewhat less accurate method was adopted in order to avoid problems when accreting over top of the previous layers' accretion limit.

There are presently no laboratory or field data available with which to test this part of the model. It is presented here only as an option for future study. An example of a rotating case is shown in Figure III.4.

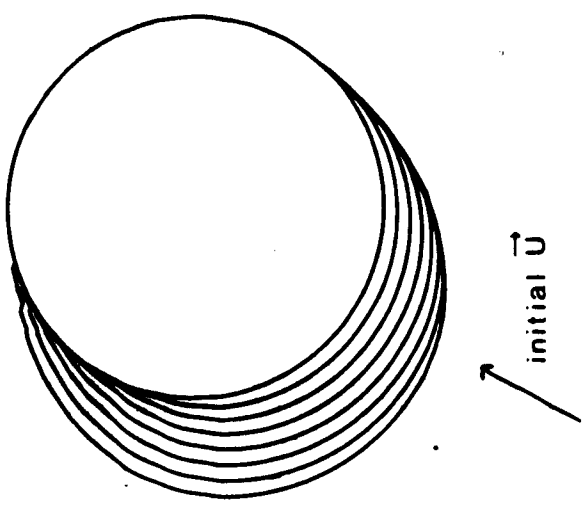
The Fortran77 code written for the model is included in Appendix II. The code will also run on an IBM or compatible personal computer fitted with a math co-processor and graphics capability; a six layer rotated accretion takes about 90 seconds to compute on a regular PC.

E. Model Applications

This model is intended for use in the laboratory, in conjunction with wind-tunnel experiments. There the required input data are readily available, as accurately as present equipment and methods can determine them.

However, if this model or some future version of it were to be applied in the field, the situation becomes very different. Good estimates of the input data (duration, wind speed, liquid water content, droplet mvd and type of spectrum) must somehow be obtained. In addition, a field version should be able to predict at least the transition to wet icing, and so the air temperature will also be required as input.

These data are rarely available for a remote site. Local meteorological services may provide estimates or forecasts for duration, wind speed, air temperature, and precipitation, but usually not liquid water content or



DROPLET MVD = 0.0000200M
CYL RADIUS = 0.0080 M
AIR SPEED = 12.00 M / SEC
LWC = 0.00050 KG / M³
TIME STEP = 150.00 SEC
BETA ZERO = 0.652
ALPHA MAX = 82.2 DEGREES
ROTN INCR = 10.0 DEGREES
SPECTRUM: SIMULATED

final U

Figure III.4 - An example of the model output for a rotating cylinder.

cloud droplet size.

Clearly, real-time icing forecasting with such a model is a long way off. However, the model could conceivably be used to determine icing climatologies for different regions where adequate meteorological data have been obtained. This would mean sufficiently long-term observations of liquid water contents and droplet sizes (i.e. cloud type) to give an idea of the typical values of these quantities under the typical meteorological situations which lead to icing events in a given region.

However, given the current state of knowledge of field conditions, the best application for this model remains in furthering the understanding of what is happening under controlled rime icing conditions in the laboratory, which it is capable of doing much more efficiently and cheaply than previous models.

References

- Gates, E.M. 1981: FROST Tunnel. Departmental Report No. 26, Department of Mechanical Engineering, The University of Alberta. 10 pp.
- Langmuir, I. and Blodgett, K. 1946: A Mathematical Investigation of Water Droplet Trajectories. In: Collected Works of Irving Langmuir, Vol. 10. Pergamon Press, 348-393.
- Lozowski, E.P., Finstad, K.J. and Gates, E.M. 1985: Comments on "Calculation of the Impingement of Cloud Droplets by the Finite-Element Method". *J. Atmos. Sci.*, 42, 306-307.
- Lozowski, E.P. and Gates, E.M. 1984: Ice Accretion on Structures in a Marine Environment. Proceedings, Third International Symposium on Offshore Mechanics and Arctic Engineering, New Orleans, 8 pp.
- Lozowski, E.P., Stallabrass, J.R. and Hearty, P.F. 1983: The Icing of an Unheated, Non-Rotating Cylinder Part I: A Simulation Model. *J. Climate and App. Meteor.*, 22, 2053-2074.

Ludlam, F.H. 1951: The Heat Economy of a Rimed Cylinder.
Quart. Jour. Roy. Met. Soc., 77, 663-667.

Mason, B.J. 1971: *The Physics of Clouds*, 2nd Edition,
Clarendon Press, p. 93.

McComber, P. and Touzot, G. 1981: Calculation of the
Impingement of Cloud Droplets in a Cylinder by the
Finite Element Method. *J. Atmos. Sci.*, 38,
1027-1036.

Oleskiw, M. 1982: A Computer Simulation of Icing on
Airfoils. Ph.D. Thesis, The University of
Alberta, 302 pp.

IV. Local Densities of Circular Cylinder Rime Accretions

A. Introduction

A situation very commonly described for the study of rime ice accretion is that of a non-rotating, circular cylinder, enveloped in a steady cross-flow of cold, cloudy air. Rime ice is formed when all of the impinging cloud droplets are able to freeze completely at the point of impact, and before the arrival of another droplet. Rime ice is always 'dry', which means there is no liquid water on the surface or trapped within the ice. The conditions necessary for dry ice to form are described by the so-called "Ludlam limit" (Ludlam, 1951), a maximum value of cloud liquid water content computed as a function of air temperature, cylinder size and air speed. Above this limiting value, the accretion will be 'wet', or glaze ice, where the droplets may run along the surface before freezing, or are incorporated into pockets of liquid water within the ice. This results in a much higher and more uniform density of ice. This study deals only with rime ice.

Examination of a rime accretion in cross-section (Figure IV.1) reveals details of the internal structure which govern the local density. Air bubbles and channels are apparent, usually increasing in number and size toward the lateral edges, away from the stagnation line. At the extreme edges of the accretion are often found the individual elongated or fan-shaped structures known as



Figure IV.1 - A 1.5 cm thick cross-section of a circular cylinder rime accretion, viewed in transmitted light. The accretion conditions are those of Sample 1 in Table IV.1.

'rime feathers', which seem to merge into the accretion from the sides. These are seen more easily in a lateral view (Figure IV.2).

It is apparent even from such a cursory examination that there should be a trend in the local ice density, decreasing from the stagnation line out toward the edges. When averaged over intervals larger than the typical air channel size, a smooth distribution should emerge. The actual shape of this distribution and how it arises are of interest to modellers of the icing process.

Numerical models have been devised which predict the results of accretion experiments performed in wind tunnels under controlled conditions, e.g. Oleskiw (1982), Lozowski, Stallabrass and Hearty (1983), McComber and Touzot (1981). The parameters which determine the rate of ice growth in such models are the accretion object's size, the air temperature and pressure, air speed, liquid water content and the sizes and relative number distribution of the water droplets in the air stream. These quantities are needed to calculate the local and overall collision efficiencies on the collecting object, which together with the local ice density determines the mass and the shape of the modelled ice deposit.

Although collision efficiency and its local distribution have been well studied, at least for circular cylinders (see for example, Oleskiw, 1982, McComber and Touzot, 1981, Langmuir and Blodgett, 1946), the density of

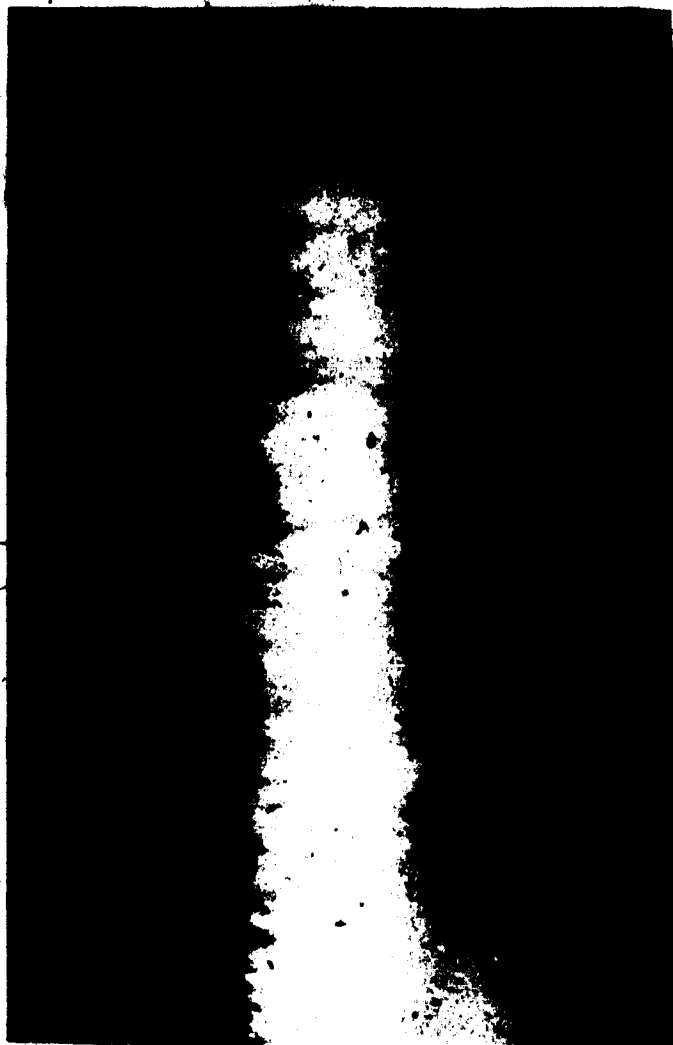


Figure IV.2 - A typical circular cylinder accretion showing rime feathers.

rime has not received as much attention. Some studies have dealt with the densities of ice accretions on rotating cylinders or hailstones (e.g. Macklin, 1962, List, Cantin and Ferland, 1970, Makkonen and Stallabrass, 1984).

Bain and Gayet (1983) have attempted to adapt these results to the fixed cylinder case; their method will be covered in the next section. Problems with this method, very similar to those outlined by Rasmussen and Heymsfield (1985) are also discussed, and a new density distribution is derived directly from experimental accretion shapes. Both distributions are tested in the model, and also against direct laboratory measurements of local density.

B. Rotating Cylinder Densities Applied to the Non-rotating Case

Macklin (1962) made extensive measurements of the bulk densities of rotating cylinder ice deposits. The results were found to correlate best with the parameter, called R, given by:

$$R = r_d^3 V_0 / T_s \quad \text{IV.1}$$

where r_d is the radius of the median volume droplet, V_0 is the impact speed of that droplet at the stagnation line, and T_s is the mean surface temperature of the accretion. Similar correlations were found for the experimental results of Bain and Gayet (1983) and Makkonen and Stallabrass (1984)

on rotating cylinders, although the latter found significantly larger densities in the lower range of R .

Makkonen and Stallabrass attribute this difference to their method of measuring droplet sizes with optical probes. Macklin's droplets were measured using the oil slide method, which according to Makkonen and Stallabrass, has underestimated sizes, in comparison with the optical probe method. Makkonen and Stallabrass' correlation for the range $0.2 < R < 100$ is:

$$\rho(R) = 0.378 + 0.42 \log_{10}(R) - 0.0823(\log_{10}(R))^2 \quad \text{IV.2}$$

Bain and Gayet (1983) made an attempt to apply the earlier correlation of Macklin to densities on a fixed cylinder accretion, by introducing local variations into the R parameter as follows:

$$R(\theta) = r V_r(\theta) / T_s(\theta), \quad \text{IV.3}$$

where now $V_r(\theta)$ is the radial component of droplet impact velocity as a function of the radius angle θ (measured with respect to the stagnation line). Bain and Gayet derive the total droplet speed at impact from an assumed cosine distribution of speed with cylinder radius angle, scaled to the stagnation line value as calculated by Langmuir and Blodgett. $T_s(\theta)$ is the variation of local surface temperature calculated from the model of Lozowski,

4.71

Stallabrass and Harty (1983).

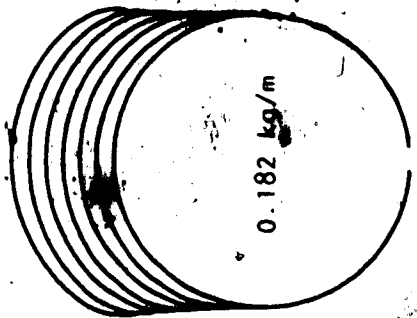
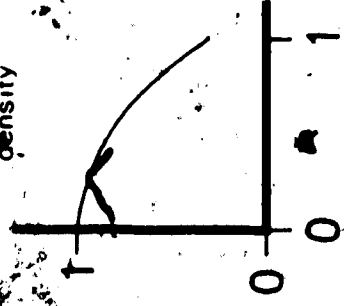
An initial objection to this approach is philosophical. Macklin's correlation is a purely empirical one; it is not a physical model and therefore should not be extended to a physical situation so different from that which provided the original data.

On the fixed cylinder, $V_r(\theta)$ is not even analogous to V_0 on the rotating cylinder, which is the maximum impact speed felt at any one point during one rotation. Furthermore, on the rotating cylinder, the droplets arrive at a given point from a large range of angles, which should perhaps result in closer packing of the droplets and a higher density. More importantly, the shadowing effects of feather structures and the formation of air channels between them is not accounted for.

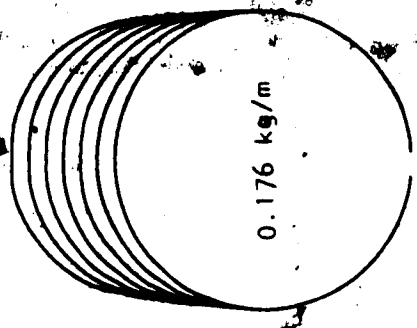
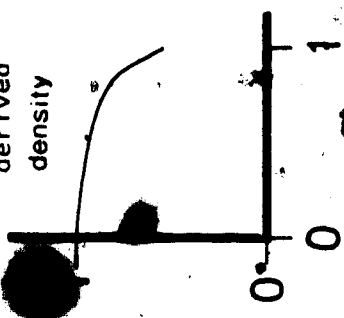
However, a more concrete objection is found by comparing this type of distribution to that found by direct measurement of the density, and by comparing the model accretion shapes and masses it produces to experimental profiles. The first comparison will be discussed in Section D of this Chapter. For the model comparison the simple rime accretion model described in Chapter III is used.

The experimental accretion profile shown on the left in Figure IV.3 was grown, under the conditions listed, in the University of Alberta FROST tunnel. Also shown are model profiles produced by three different distributions of local

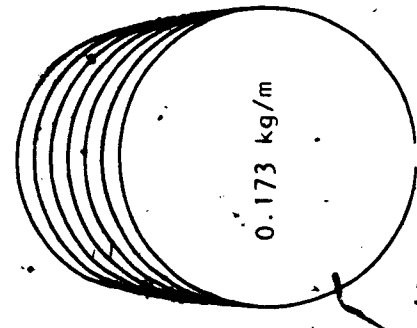
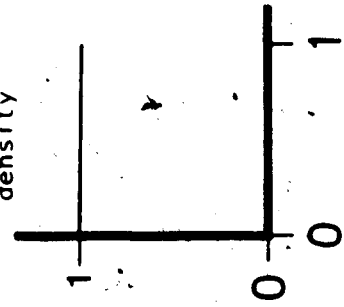
profile-derived density



rotating-cylinder derived density



constant density



experimental profile

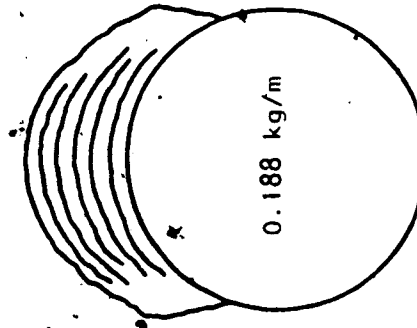


Figure IV.3 - Experimental and three model accretions showing the effects of three different density distributions (plotted above as ρ/ρ_0 vs. a/α_{max}). Conditions are: $D_p = 51 \mu m$, $D_c = 0.0254 m$, $U = 10.7 m/sec$, $lvc = 0.49 g/m^3$, $\tau = 390 sec$

density. The profile at centre left results from a constant density, that at centre right from a distribution that is derived following Bain and Gayet. The profile at the far right uses a third distribution which is described below.

The three density distributions are illustrated above their respective profiles. For easy comparison, each is plotted as ρ/ρ_0 vs. x/a_m , where ρ_0 is the local density at the stagnation line, α is the local angle of the surface normal with respect to the free stream direction, and a_m is defined in Chapter III. On the bare cylinder, α is identical with θ , but not for subsequent ice layers. The angle α is used rather than θ , so that the density distribution will be time-dependent, changing as the ice shape changes.

The middle distribution is derived from Equation IV.1, using $V_r(\alpha)$ as calculated by Bain and Gayet, and $T_s(\alpha)$ calculated by the model of Lozowski, Stallabrass and Hearty. The resulting curve is fitted with a third-order polynomial:

$$\rho(\alpha/a_m) / \rho_0 = (1 - 0.303 (\alpha/a_m) + 0.936 (\alpha/a_m)^2 - 1.074 (\alpha/a_m)^3).$$

IV.4

The second modelled profile is very similar to the first, constant density profile, which was too narrow in comparison with the experimental shape. Both of the modelled masses are less than the observed mass, by 8 and 6

percent, respectively. The result using the third distribution shown is in better agreement with the experimental shape, by having a widening profile, and a mass within 3 percent of observation. This distribution and its derivation are described next.

C. Profile-Derived Density Distribution

The thickness (Th) of ice deposited in time τ at a given point on the bare cylinder surface, which we describe by its surface angle α , is

$$Th(\alpha) = \beta(\alpha) U l_{wc} \tau / \rho(\alpha), \quad IV.5$$

where U is the free-stream speed, and l_{wc} is the liquid water content. This version of the dry-growth equation ignores curvature effects, e.g. as described by Lozowski, Stallabrass and Hearty (1983). This is a reasonable simplification given the very small spacing of the points which define the icing surface in the model.

Given IV.5 then, if both the local thickness and the local collision efficiency $\beta(\alpha)$ are known, and if the interval τ is assumed to be small enough that $\beta(\alpha)$ and the density $\rho(\alpha)$ remain essentially constant, IV.5 may be solved for $\rho(\alpha)$.

Figure IV.4 shows another experimental accretion grown in the FROST tunnel, and its growth conditions. The total accretion time was 30 minutes. Every five minutes, a layer



Figure IV.4 - A circular cylinder rime deposit in profile, with paint layers marking the surface at five minute intervals. Conditions are those of Case B in Table III.1.

of paint was sprayed onto the surface, allowing changes in the shape of the ice surface to be followed with time. It also allowed local thickness measurements of thin layers to be obtained, which are unaffected by the melting or sublimation losses that must occur on the top surface, between the time of the end of the test and photography of the profile.

The distribution of local collision efficiency was calculated from the median volume diameter, and an assumed droplet size distribution, scaled to the mvd, based on measurements taken in the same wind tunnel. The mvd was originally measured by the oil slide method, which is known from the work of Makkonen and Stallabrass (1984) to be an overestimate; but for Case B of Table IV.1 the oil slide estimate falls outside of the size range for which Makkonen and Stallabrass' empirical correction formula is valid. Therefore, an mvd has been adopted which was derived from the stagnation line thickness measurement, the liquid water content measurement, and an assumed local density for the stagnation line of 890 kg / m^3 (a reasonable density in this case based on visual inspection of the accretion). The method used to derive this estimate of the mvd is described in Appendix III.

For Case A of the same table it was possible to make use of the correction formula mentioned above to correct the oil slide measured mvd.

In this way the distribution $\rho(\alpha)$ has been found for several layers of two different accretions. The data are listed in Table IV.1 and plotted in Figure IV.5. A cubic polynomial fit (solid curve, Figure IV.5) gives:

$$\rho(\alpha/\alpha_m) / \rho_0 = (1 - 0.143 (\alpha/\alpha_m) - 0.246 (\alpha/\alpha_m)^2 - 0.309 (\alpha/\alpha_m)^3)$$

IV.6

The relative distribution is thus assumed independent of v_w and air temperature; this assumption implies that these factors only come into the determination of the scaling parameter ρ_0 . Normalization of the distribution by the two parameters ρ_0 and α_m makes the expression above easy to use in an icing model, assuming that it is generally applicable to a range of accretion conditions. Evidence for this was presented in Figure III.3 of the last Chapter, where the model results are compared to several independent wind tunnel experiments.

B. Laboratory Measurements of Local Density

For further evidence to support our proposed distribution of local density, a series of direct measurements were made from wind-tunnel accretions.

Following the techniques described by List, Cantin and Ferland (1970), local densities were measured by drilling small holes (2.5 - 3.0mm diameter, less than 1 cm depth) in

	(degrees)	Th (mm)	β (a)	ρ (kg/m ³)
Case A	0	3.34	0.407	767
	10	3.12	0.393	792
	20	3.25	0.334	646
	30	2.9	0.249	540
	40	1.7	0.155	574
	50	0.9	0.069	482
	Case B	0	1.48	0.842
10		1.48	0.825	871
20		1.48	0.776	820
30		1.40	0.699	780
40		1.33	0.592	696
50		1.03	0.458	695
60		0.81	0.302	583

Table IV.1 - Local densities as a function of surface slope derived from thickness measurements of shallow ice layers accreted at -10°C under the following conditions:

	D_d (μ m)	D_c (m)	l_{wc} (g/m ³)	U (m/sec)	τ (sec)
Case A	15.5	0.0254	0.98	10.7	600
Case B	51.0	0.0254	0.49	10.7	300

β (a) is calculated from Equations II.11, III.3 and III.4.

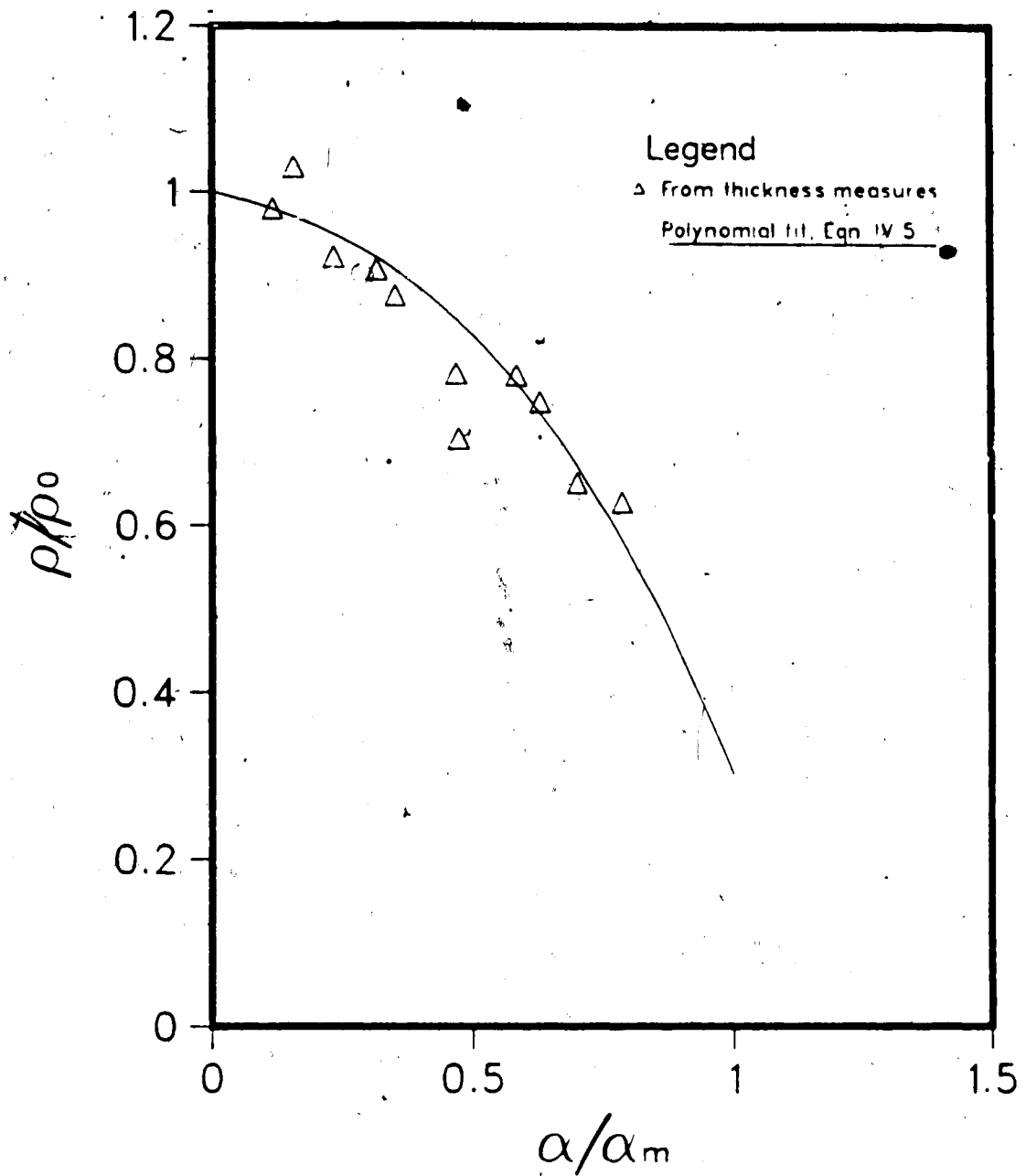


Figure IV.5 - Local densities derived from thickness measurements of shallow ice layers from Table IV.1. The solid curve is a polynomial fit to the data (Equation IV.3).

cross sectional cuts from two different rime accretions (see Figure IV.6). The location, volume and mass loss were recorded for each hole. The mass was measured to within 0.00005 g with a Mettler model H20 balance. For the data of Sample 1, Table IV.2, the hole depths and diameters from three sections of a single accretion were measured to within .05 mm with a Vernier caliper. For Sample 2 of Table IV.2, holes from two sections of accretions grown under nearly identical conditions were measured to 0.01mm in depth and 0.001mm in diameter, with the same bore and depth gauges used by List et al. (1970) to determine local densities in hailstones. The surface angles were approximated by the more easily measured radius angles, since paint layers to define the intermediate surfaces would have altered the densities. This is a good assumption for shallow layers, at any rate, and measurements have been used only from the layer immediately above the cylinder surface. The error in using the radius angle approximation is estimated to be \pm five degrees.

Another source of error is mass loss from the entire sample through sublimation and handling during the hole drilling procedure. Several experimental estimates were made of the size of this error, and the average (0.001 g) was subtracted from the measured mass losses from the holes.

The resulting density measurements are shown in Table IV.2 and in Figures IV.7 and IV.8. The solid and dashed curves shown in each of these figures are from Equations



Figure IV.6 - An accretion section of about 1.5 cm.

thickness, showing the holes drilled for the local density measurements. The condition are those of Sample 1 in Table IV.2

Sample 1		Sample 2	
α ($\pm 5^\circ$)	ρ ($\pm 60 \text{ kg/m}^3$)	α ($\pm 5^\circ$)	ρ ($\pm 30 \text{ kg/m}^3$)
2	786	2	907
2	667	3	902
2	660	4	723
6	719	6	747
8	620	7	770
8	792	8	909
10	714	13	788
12	645	15	815
12	688	17	766
12	685	19	724
15	629	23	823
18	519	24	683
20	715		
21	630		
27	675		
28	427		
30	681		
30	733		
30	701		
35	539		
38	580		
42	749		
50	504		

Table IV.2 - Experimentally measured local densities as a function of surface slope taken from accretions grown under the following conditions:

D_d (m)	D_c (m)	lwc (g/m^3)	U (m/sec)	T ($^\circ\text{C}$)
16.4	0.046	0.53	14.9	-14
14.0	0.0254	0.36	30.0	-10

IV.2 and IV.4, respectively, where the choice of ρ_0 has been based on the density measurements, and α_{\max} is calculated from the median volume diameter droplet, following the methods of Chapters II and III.

The scatter of points in both figures is considerable, and is much larger than the measurement errors represented by the error bars will allow. The most likely cause of the large scatter is in the nature of the rime itself. The internal air channels are scattered at random, and since they are often of the same size as the holes, this will introduce a natural scatter. Also, in the very fragile rime, the drilling process may cause walls between adjacent air channels to collapse, resulting in additional mass loss. This problem is especially bothersome near the edges of the accretion, where the density is lowest. Here, walls between the holes themselves will sometimes collapse, making it very difficult to obtain density values at large surface angles. Part of the problem might be alleviated by using accretions samples grown on a larger diameter cylinder, so that the holes do not have to be drilled so close together to get the same interval of surface angle. Unfortunately, the only accretions available were grown on cylinders of one and two inches in diameter.

For whatever reason, the results are too scattered to allow a clear choice between one parameterized distribution and the other. This is due, in part, to the lack of data at

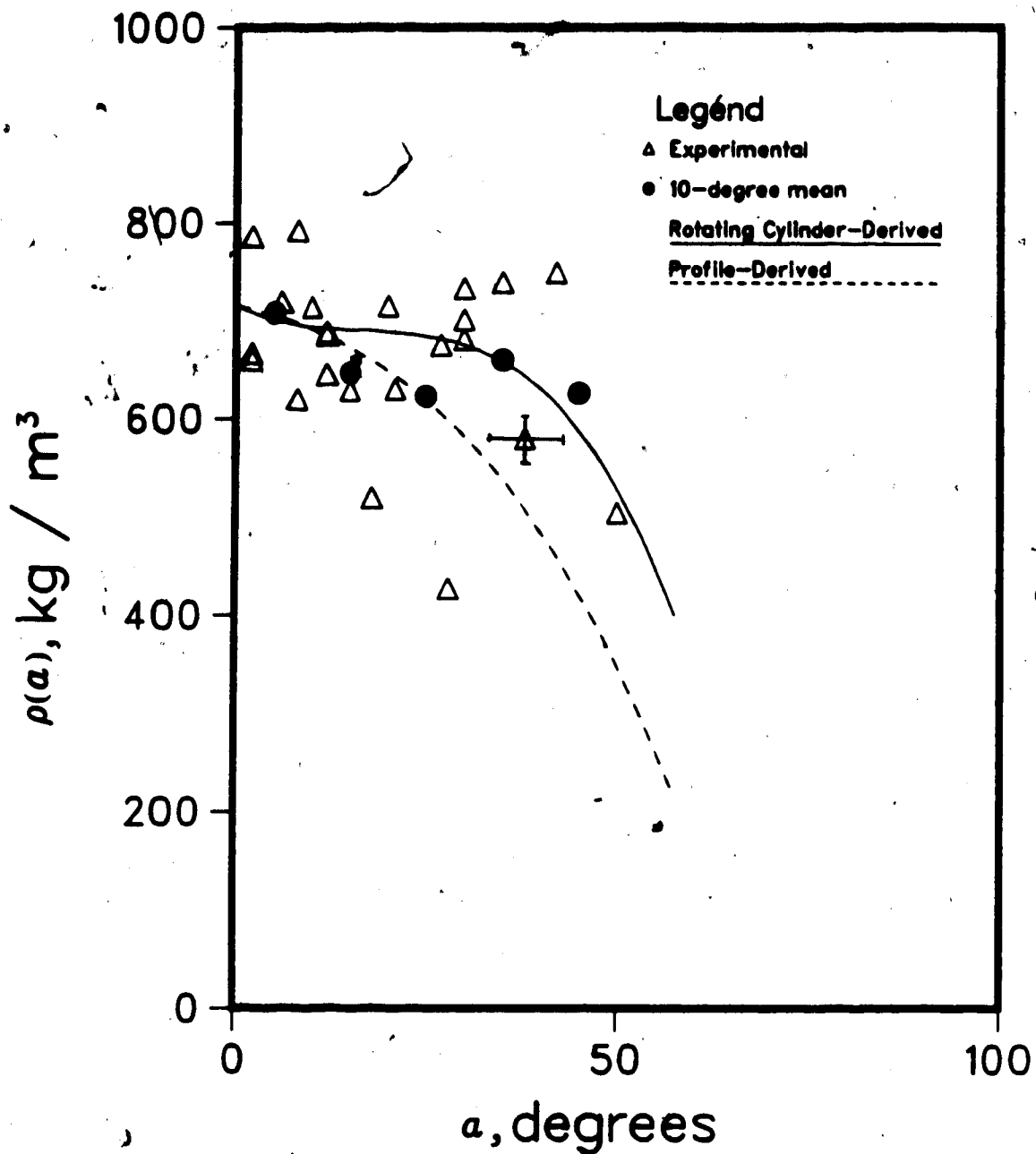


Figure IV.7 - Local density vs. surface angle; experimental measures and parameterized curves for the conditions of Sample 1 in Table IV.2. The filled symbols represent mean values for 10° intervals in surface slope.

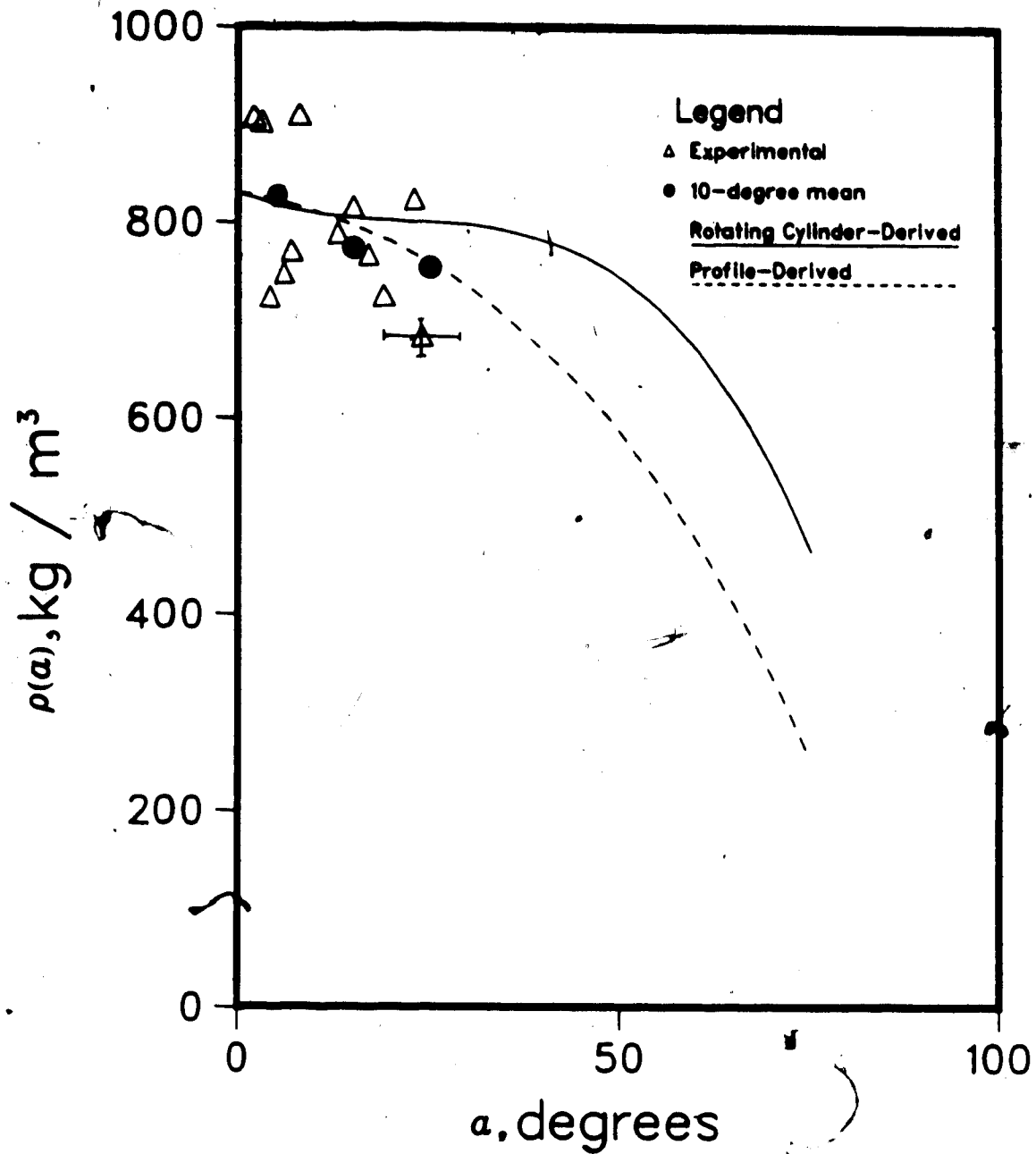


Figure IV.8 - Local density vs. surface angle; experimental measures and parameterized curves for the conditions of Sample 2 in Table IV.2. The filled symbols represent mean values for 10° intervals in surface angle.

large surface angles. When averaged over 10 degree intervals (filled symbols) the experimental data in both figures favour the profile-derived curve up to a surface angle of 30° , but for larger angles in Figure IV.7 they lie closer to the rotating cylinder-derived curve. However, there are far fewer points defining the averages for the larger angles, and none at all for Figure IV.8.

Although these direct density measurements have not been conclusive, the model results and the practical advantages of the profile-derived distribution justify its adoption over the other. The application of this method is efficient and inexpensive, assuming that the scaling parameters may be easily determined. One of these parameters, the maximum accretion angle, α_{\max} , may be quickly approximated according to the analytical function given in Chapter II, but ρ_0 remains to be determined.

E. Local Density at the Stagnation Line

Qualitative observations of many rime accretions show that the stagnation line density also varies with the environmental conditions. Since there are, at present, insufficient quantitative data on this variation, the correlation for rotating cylinder densities, Equation IV.1, may perhaps be applied. The justification for doing so here, but not for the entire density distribution, is that there is no shadowing at the stagnation line, and the conditions are more nearly analogous to the rotating

cylinder case.

However, some important differences must be noted between the two situations. In the rotating cylinder correlation, the parameter V_0 is the impact speed of the median volume droplet at the stagnation line only. Over the remainder of the accretion surface, droplets impact at speeds ranging between zero and V_0 , so the average impact speed, at least for cases with large α_{\max} , is roughly one half V_0 , and perhaps somewhat less if α_{\max} is small. Thus, V_0 for the rotating cylinder is \leq twice the average speed of impact. On the stagnation line of the non-rotating cylinder, the impact speed is constant and equal to V_0 , so in order to substitute into the R parameter the correct analogy for twice the average speed, we use twice V_0 . V_0 is estimated from Equation II.11.

The R parameter is further altered by substituting for the mean surface temperature, the value at the stagnation line ($T_{s,0}$) which is determined using the model of Lozowski, Stallabrass and Hearty (1983). The new correlation parameter is then:

$$R' = 2 r_d V_0 / T_{s,0} \quad \text{IV.7}$$

The results are shown in Figure IV.9, for five accretions for which ρ_0 has been experimentally measured by the methods described in the last section. The fit to Equation IV.1 is quite good, considering the size of the

measurement errors in ρ_0 (i.e., the same size as for Figure IV.8). Until more experimental data are available, this is an acceptable method for estimating ρ_0 .

F. Summary

Previous methods for estimating the local variation of rime ice density are examined, and found to be inadequate. A new method is derived empirically, and tested in model accretions, and against direct laboratory measurements of local density. The laboratory measured distribution is inconclusive, but model results show the new method to be more successful than the old for predicting the shapes and masses of circular cylinder rime ice accretions.

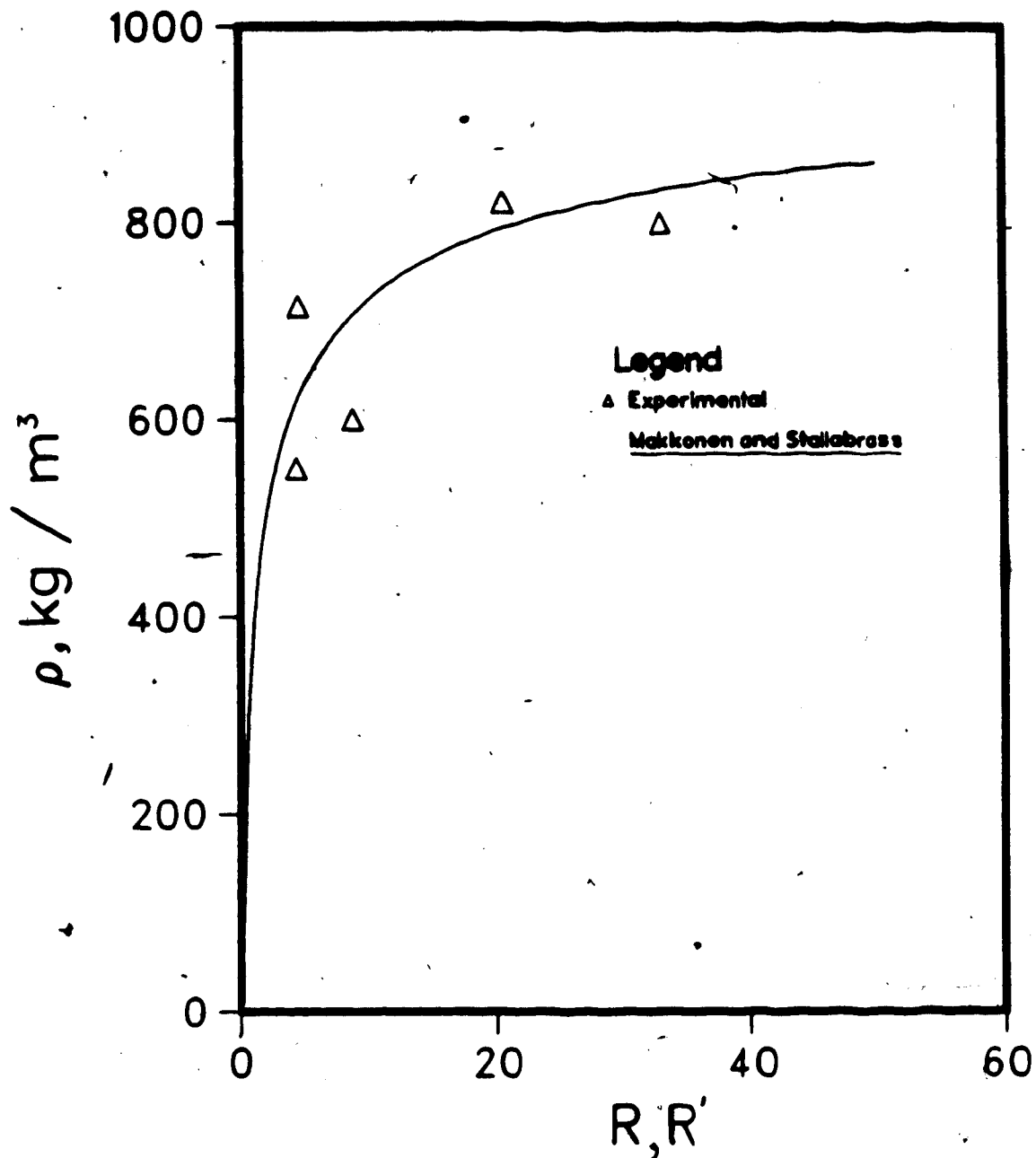


Figure IV.9 - Stagnation line density measurements vs. R' (symbols), and the rotating cylinder density correlation of Makkonen and Stallabross, Equation IV.2, vs. R (solid line). R and R' are defined in Equations IV.1 and IV.7, respectively.

References

- Bain, W. and Gayet, J.P. 1983: Etude de L'accretion de la Glace Atmospherique II. Modelisation Numerique avec Parametrisation de la Variation de la Mass Specificque du Givre en Fonction de la Position Angulaire sur un Cylindre. *J. Rech. Atmos.*, 17, 299-311.
- Langmuir, I. and Blodgett, K. 1946: A Mathematical Investigation of Water Droplet Trajectories. Collected Works of Irving Langmuir, Vol 10. Pergamon Press, 348-393.
- List, R. Cantin, J.-G. and Ferland, M. 1970: Structural Properties of Two Hailstone Samples. *J. Atmos. Sci.*, 27, 1080-1090.
- Lozowski, E.P., Stallabrass, J.R. and Hearty, P.F. 1983: The Icing of an Unheated, Rotating Cylinder Part I: A Simulation Mod Model. *J. Climate and App. Meteor.*, 22, 2053-2074.
- Ludlam, F. H. 1951: The Heat Economy of a Rimed Cylinder. *Quart. J. Roy. Meteor. Soc.*, 77, 663-666.
- Macklin, W.C. 1962: The Density and Structure of Ice Formed

by Accretion. *Quart. J. Roy. Meteor. Soc.*, 11,
30-50.

→ Makkonen, L. and Stallebrass, J. 1984: Ice Accretion on
Cylinders and Wires. National Research Council
Technical Report TR-LT-005, NRC No. 23649, 43 pp.

McComber, P. and Toussot, G. 1981: Calculation of the
Impingement of Cloud Droplets in a Cylinder by the
Finite Element Method. *J. Atmos. Sci.* 38,
1027-1036.

Rasmussen, R.M. and Heymsfield, A.J. 1985: A Generalized
Form for Impact Velocities Used to Determine
Graupel Accretional Densities. *J. Atmos. Sci.* 42,
2275-2279.

V. Rime Icing on Airfoils

A. Introduction

A numerical simulation of ice accretion on an arbitrary airfoil section involves greater computational difficulty than does the corresponding problem of icing on circular cylinders. The major reason is the requirement for numerical integration of the impinging droplet trajectories in order to determine collision efficiencies. Unlike the cylinder case, there is (except for the Joukowski airfoil) no analytical solution of the potential flow to simplify the task, nor are there convenient tables of previously calculated collision efficiencies as functions of the flow and inertia parameters.

This requirement adds considerably to the model's consumption of computing time and resources. Previous airfoil accretion models (e.g. Oleskiw, 1982, MacArthur et al., 1982, Cansdale and Gent, 1983) have thus tended to be expensive to run, and may be prone to numerical instabilities.

However, from the results of one such model (Oleskiw 1982), simple parameterizations have been derived for the local collision efficiency distribution with surface slope on NACA 0015 and 0012 airfoils. Three separate analytical functions approximate this distribution for monodisperse or average droplet spectra, or for any spectrum when the angle of attack is non-zero. Use of these functions requires the

determination of only one value of local collision efficiency, that at the stagnation line; thus considerably reducing the computation time. This single value may then be re-determined at intervals during the accretion to give the model a true time-dependence.

These parameterizations have been incorporated into a new, more efficient numerical icing model. Other computational simplifications include the representation of the airfoil and ice surfaces by straight line segments rather than by a spline curve, and a straightforward algebraic method to determine the droplet's point of collision with the surface. An approximate distribution function for the local density has also been introduced. Again, rime icing only is considered, i.e. the air temperature is assumed to be below -10° C, and the impinging water is assumed to freeze immediately and completely. Most of the parameterizations and simplifications could also be used in a model for wet accretion.

The model results are presented in comparison with those of Oleskiw (1982) and with real accretions grown in wind tunnel experiments.

B. Model Outline

A brief outline of the model algorithm is as follows:

Step 1. Specify the x, y coordinates of the original airfoil surface. The coordinates are dimensional,

with the origin at the nose of the airfoil.

- Step 2.** Find the local collision efficiency at the stagnation line, β_0 , by the following procedure:
1. Solve for the potential flow field about the airfoil or accretion shape by the method of Kennedy and Marsden (1976).
 2. Integrate two droplet trajectories near the stagnation line and find their collision points.
 3. Calculate β_0 from $\Delta y / \Delta l$, the ratio of initial separation normal to the free-stream of the trajectories to their final separation in arc length on the surface.
- Step 3.** For each surface point, calculate the thickness accreted perpendicular to the surface during one layer time step τ . The local collision efficiency at each point is approximated from one of three parameterized functions of β_0 and the local surface slope, α , depending on the type of droplet size spectrum and the angle of attack, ϕ (defined as the angle between the free-stream direction and the airfoil chord). The local density distribution is also approximated from a parameterized function of surface slope, α .

Step 4. Calculate the mass and mean density of the accreted ice layer.

Step 5. Repeat Steps 3 and 4 for the number of layers requested. Repeat Step 2 only for every fifth layer. The layer time step, τ , should be chosen so that the combined stagnation line thickness of five layers is not more than 1/10 of the original chord length.

Step 7. Plot the original airfoil and all accreted layers.

The sections below will discuss each of Steps 1 through 4 in detail.

C. Specifying the Airfoil Shape

This version of the model employs the standard airfoil section known as the NACA (United States National Advisory Committee on Aeronautics) four-digit wing section, for which Abbott and von Doenhoff (1959) give the thickness distribution in non-dimensional x, y -coordinates normalized to the chord length, as:

$$y = 0.05 h_0 (0.2969 x^{0.5} - 0.126 x - 0.3516 x^2 + 0.2843 x^3 - 0.1015 x^4)$$

V.1

The number h_0 gives the maximum airfoil thickness as a

percentage of the chord length, as shown in Figure V.1, and also makes up the last two digits of the "four-digit" designation. The first two digits represent c_m , the maximum camber as a percentage of the chord, and c_p , the abscissa of the camber ordinate in tenths of the chord. All of the parameterizations used in the model are derived assuming that both c_m and c_p are zero. The maximum thickness h_0 is entered as model input, but expressed as a fraction of the chord, rather than a percentage.

Although defined above for non-dimensional coordinates, the model carries the airfoil and accretion profiles in dimensional coordinates throughout most of the calculations, because the chord length (initial chord plus accumulated ice thickness) is changing with every layer step. Where a non-dimensional profile is required for the potential flow calculation, the coordinates are normalized using the current chord length.

Since the profile is always represented by a vector of coordinate points, the points must be of sufficiently high density to ensure that the curved surfaces are well approximated by straight line segments joining them. This avoids the expensive computational process of fitting a few surface points with a spline curve, which may be prone to instabilities. It also simplifies the determination of trajectory impact points, but it does require more data storage. However, even this can be minimized by using a point distribution scheme which concentrates points in the

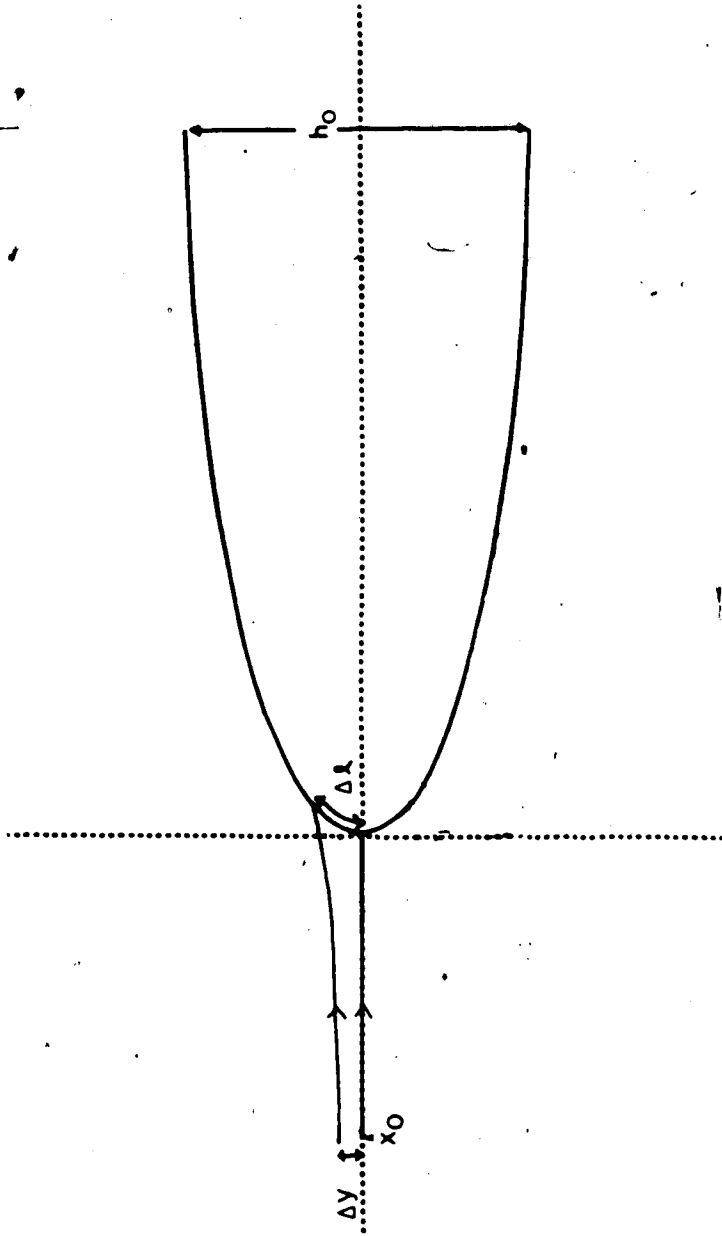


Figure V.1 - Determination of collision efficiency on an airfoil. $\beta = \frac{dy}{d\ell} = \frac{\Delta y}{\Delta \ell}$. Also illustrated is the definition of ϕ , the angle of attack.

regions of strong curvature at the nose and tail.

One such scheme is that suggested by Kennedy and Marsden (1976), in which the distribution of non-dimensional x-coordinates is given by:

$$x_i = 0.5 (1 - \cos(2\pi i / N)) \quad V.2$$

where i lies between 1 and N , an even integer. This scheme was found to give good results with $N = 600$ to specify the complete airfoil section for plotting purposes, although only half this number of points, defining the front portion of the airfoil, is allowed to accrete ice.

In the potential flow solution, a profile consisting of a much smaller number of points is desired to reduce the computational requirements; Kennedy and Marsden suggest that 40 points is an optimum number. This can be simply constructed from either the original airfoil profile, or from subsequent accretion shapes by taking every 15th point of the denser profile. The new sparse profile will also retain the desired distribution pattern of points.

Accretion thicknesses are calculated for each surface point in the direction perpendicular to the local surface slope. This causes the point separation to increase near the nose with each succeeding layer. After several layers, the separation may have become too large for a reasonable representation of the surface by straight line segments, and has destroyed the original point distribution.

A way to remedy the situation is to shift each coordinate point, after each layer is accreted, closer to the nose along the straight line segment joining it and its nearest neighbour (whose position has already been shifted). The amount of the shift must be carefully chosen to preserve the desired distribution of points, and an accurate profile. Because the original distribution concentrated points near the nose, and because points near the nose diverge faster than elsewhere, those points must be shifted by larger amounts (relative to the segment length) than points further away.

A shift of half the segment length at the nose, decreasing linearly to one eighth at about half the chord length gives the desired results. To test that profiles produced by this scheme are accurate, model profiles were also made with four times the optimum point density. There was no noticeable difference in the resulting plotted profiles.

D. Local Collision Efficiency

Parameterization schemes were derived in Chapter III for local collision efficiency β on circular cylinders as a scaled cosine function of local surface slope α . If the numerical results of Oleskiw (1982) for local collision efficiency on a NACA airfoil at 0° angle of attack are plotted against surface slope, they also closely follow a cosine curve, but one which is displaced negatively along

the abscissa. The form holds for several cases computed by Oleskiw, as seen in Figures V.2, V.3 and V.4, and is described by:

$$\beta(\alpha) = \cos(\alpha) - (1 - \beta_0), \quad \text{V.3}$$

where β_0 is the value of β at the stagnation line. This is the only parameter required to approximate the entire distribution, since the maximum accretion angle α_{\max} , in radians, follows from:

$$\alpha_{\max} = \arccos(1 - \beta_0). \quad \text{V.4}$$

Appendix IV gives a geometrical derivation of Equation V.3.

So far, a monodisperse droplet population has been assumed. In practice, of course, a spectrum of droplet sizes is present. Often the collision efficiency of the entire population is modelled by a single droplet size at the median volume diameter of the spectrum. This is generally a good approximation to the weighted average $\beta(\alpha)$ distribution calculated according to the relative volumes of the droplet sizes in the spectrum, as discussed in Appendix VI.

In real populations, when relatively large numbers of very small droplets are present in the population, they can change the shape of the β distribution, as well as force the mvd-based maximum accretion limit to a smaller value.

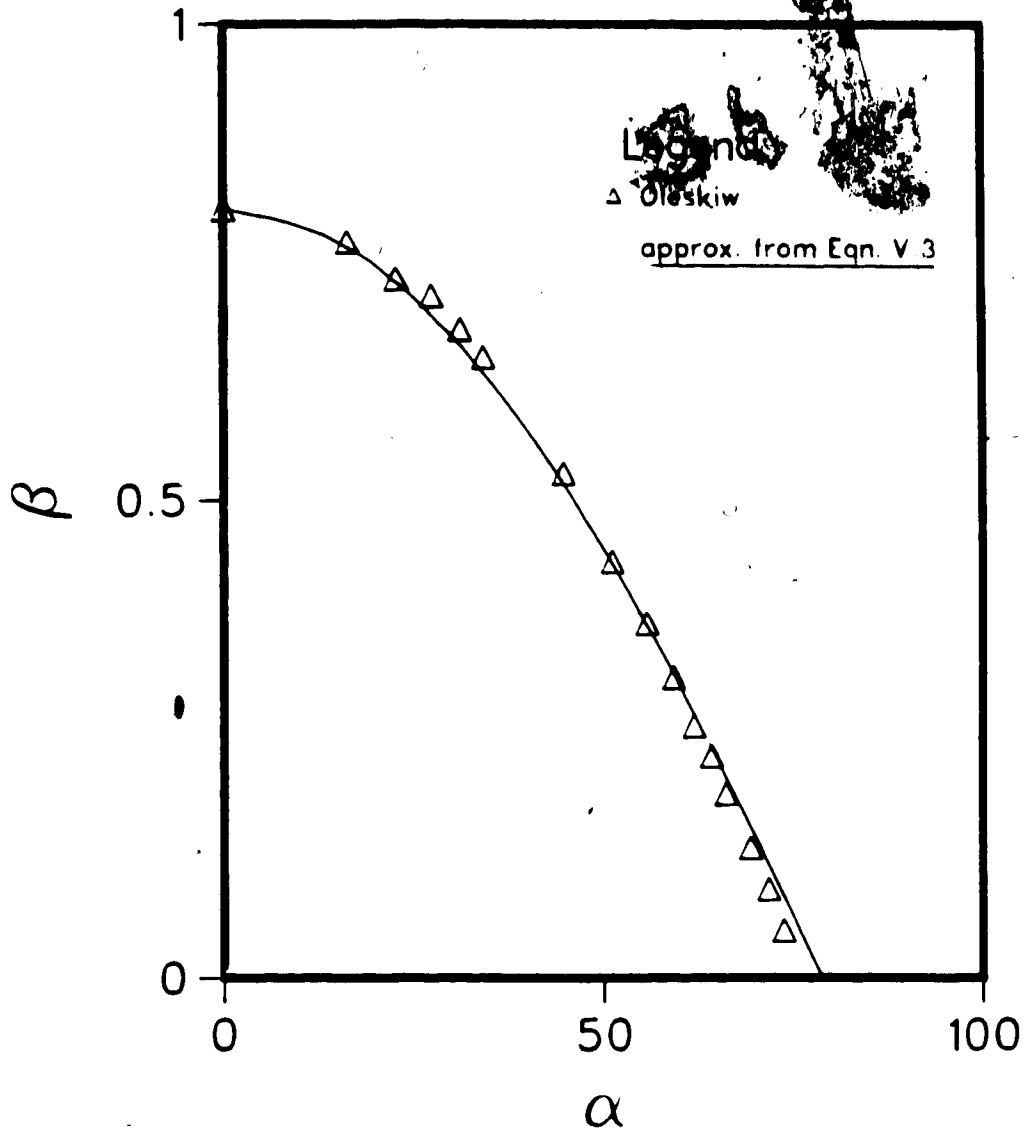


Figure V.2 - Comparison of Oleskiw's numerical results and Equation V.3, for collision efficiency of a single drop size. Airfoil is a NACA 0015, $U = 61$ m/sec, Chord = 0.213 m, $D_d = 20$ μ m.

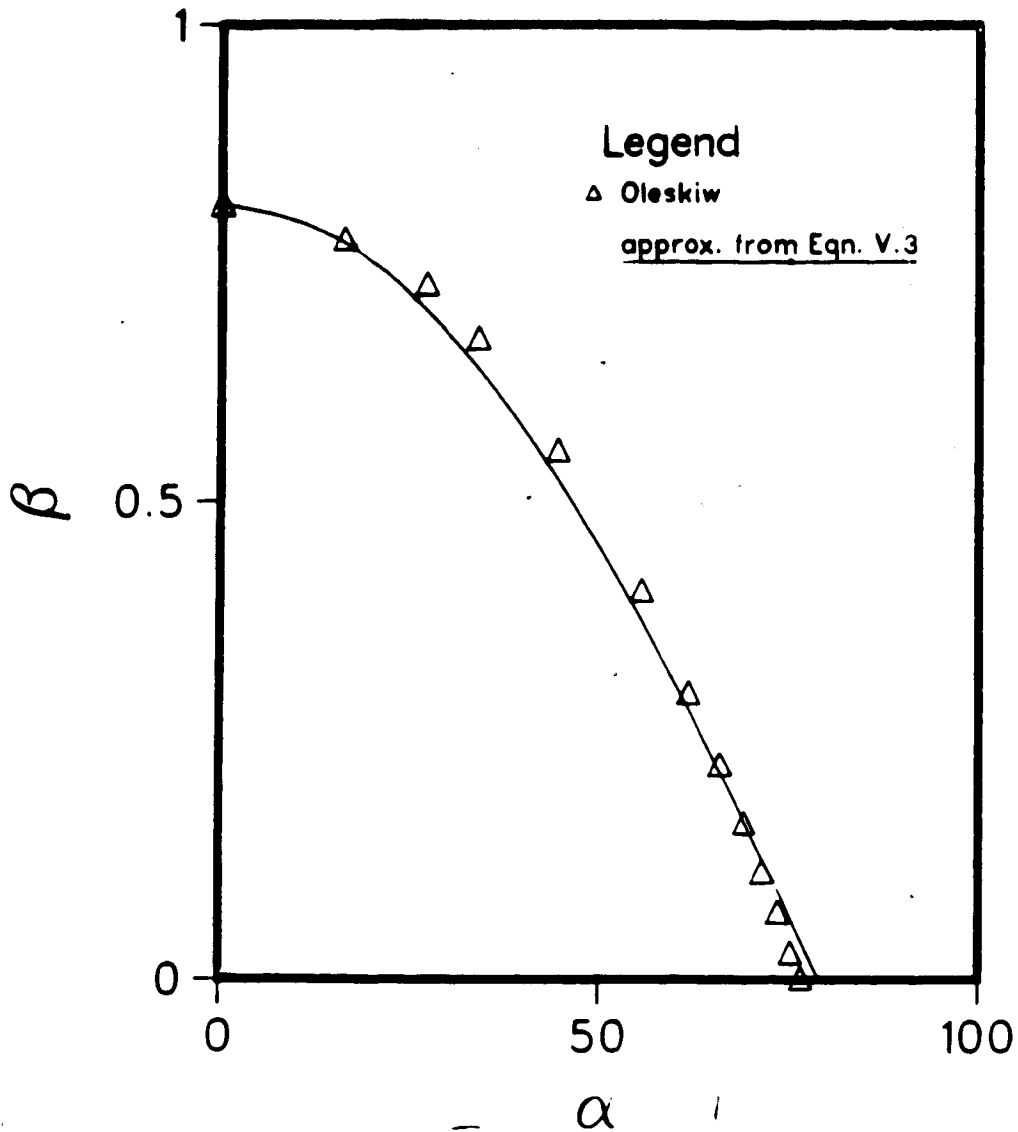


Figure V.3 - Comparison of Oleskiw's numerical results and Equation V.3, for collision efficiency of a single drop size. Airfoil is a Joukowski 15%, $U = 78.2$ m/sec, Chord = 0.33 m, $D_d = 25.5 \mu\text{m}$.

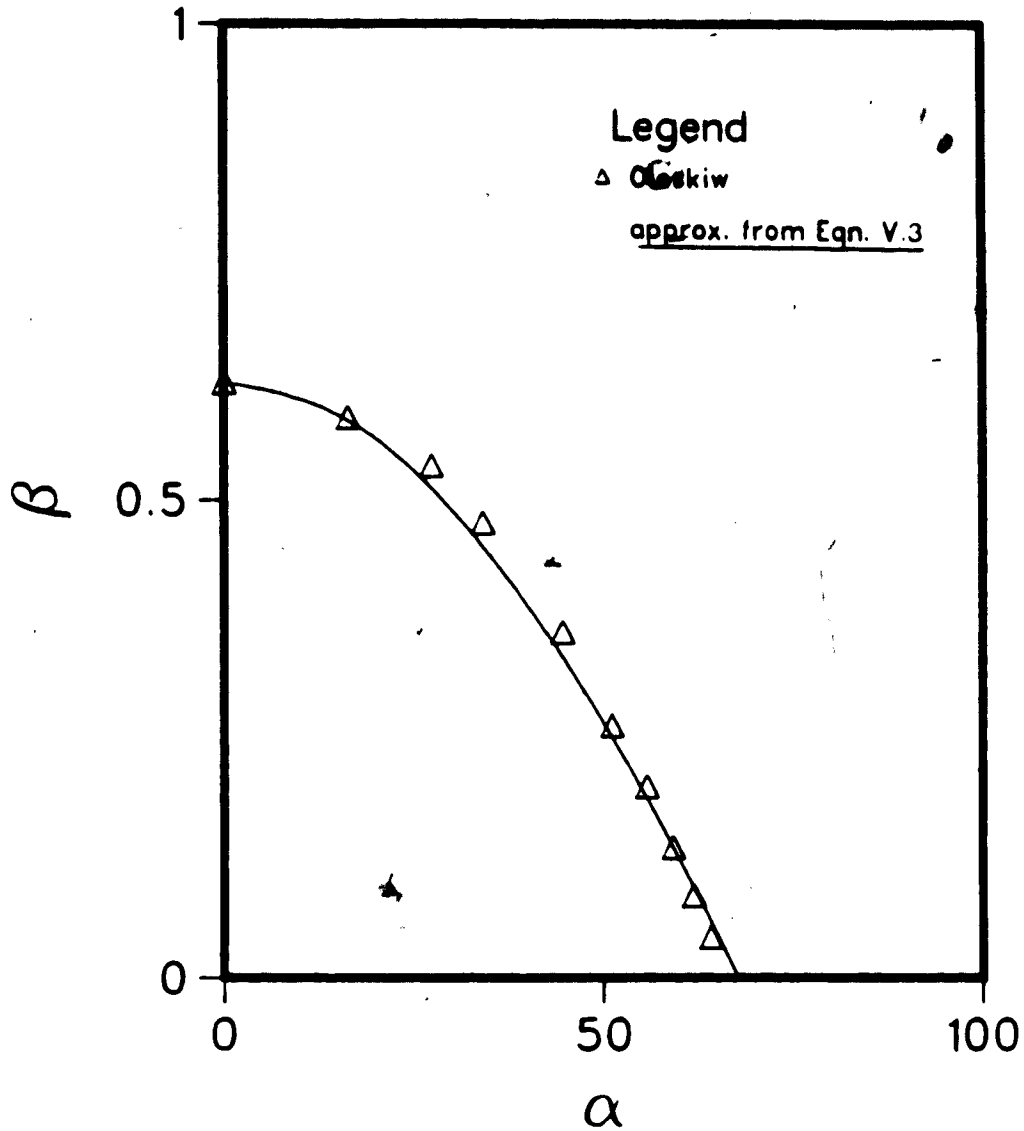


Figure V.4 - Comparison of Oleskiw's numerical results and Equation V.3, for collision efficiency of a single drop size. Airfoil is a Joukowski 15%, $U = 78.2$ m/sec, Chord = 0.33 m, $D_d = 13.2 \mu\text{m}$.

than actually occurs. For airfoils, the effect becomes important for β_0 less than about 0.8. For these cases, an alternative parameterization is proposed. It is derived from a polynomial fit to an average of several spectrum-weighted $\beta(\alpha)$ curves calculated by the author for droplet spectra observed in the FROST tunnel at the University of Alberta. The form of the parameterization is:

$$\begin{aligned} \beta(\alpha/\alpha_m) = & \beta_0 (1 + 0.039(\alpha/\alpha_m) - 1.842(\alpha/\alpha_m)^2 \\ & - 0.543(\alpha/\alpha_m)^3 + 1.792(\alpha/\alpha_m)^4 \\ & - 0.444(\alpha/\alpha_m)^5, \end{aligned} \quad \text{V.5}$$

where $\beta_0 = \beta_{0,mvd}$, and

$$\alpha_m = \alpha_{max,mvd} + 0.13 \exp(-mvd / 70). \quad \text{V.6}$$

Here α_m is again in radians, and mvd is in μm . In Figures V.5 and V.6, the approximation of Equation V.5 is compared with spectrum-weighted distributions for two other observed droplet spectra, which appear in Table A.1 as "Battan and Reitan stratus" (Battan and Reitan, 1957), and "FROST 3", a spectrum measured in the FROST tunnel. These figures also show the difference in β_0 between the spectrum-weighted value and that derived from the mvd for these cases.

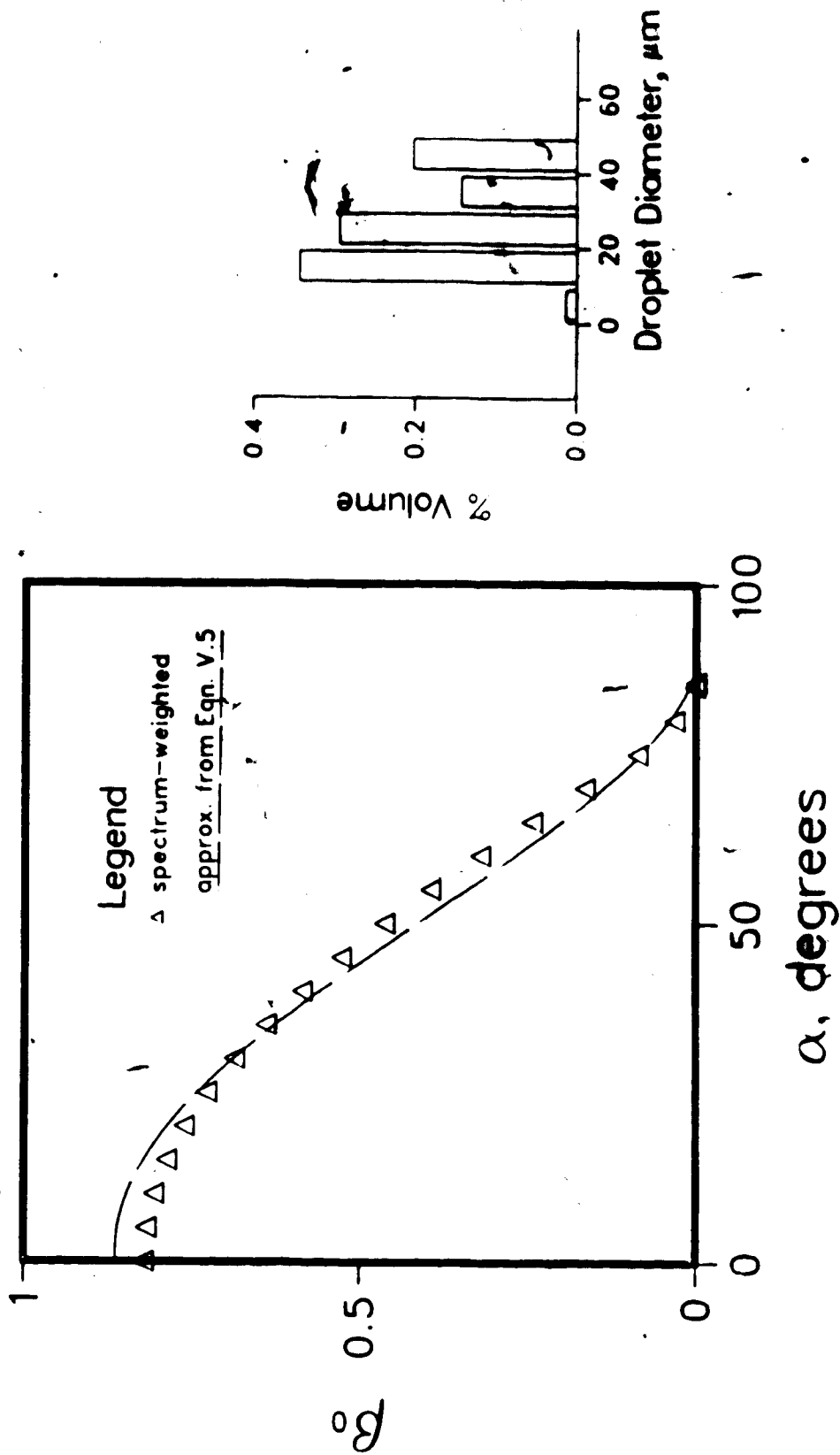


Figure V.5 - Comparison of spectrum-weighted collision efficiencies and Equation V.5 for the spectrum shown (mvd = 26.2 μm) on a NACA 0015, U = 50 m/sec, chord = 0.2 m.

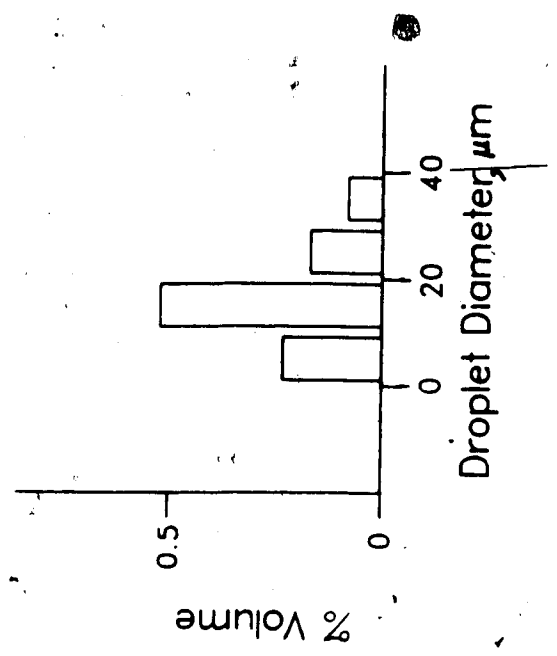
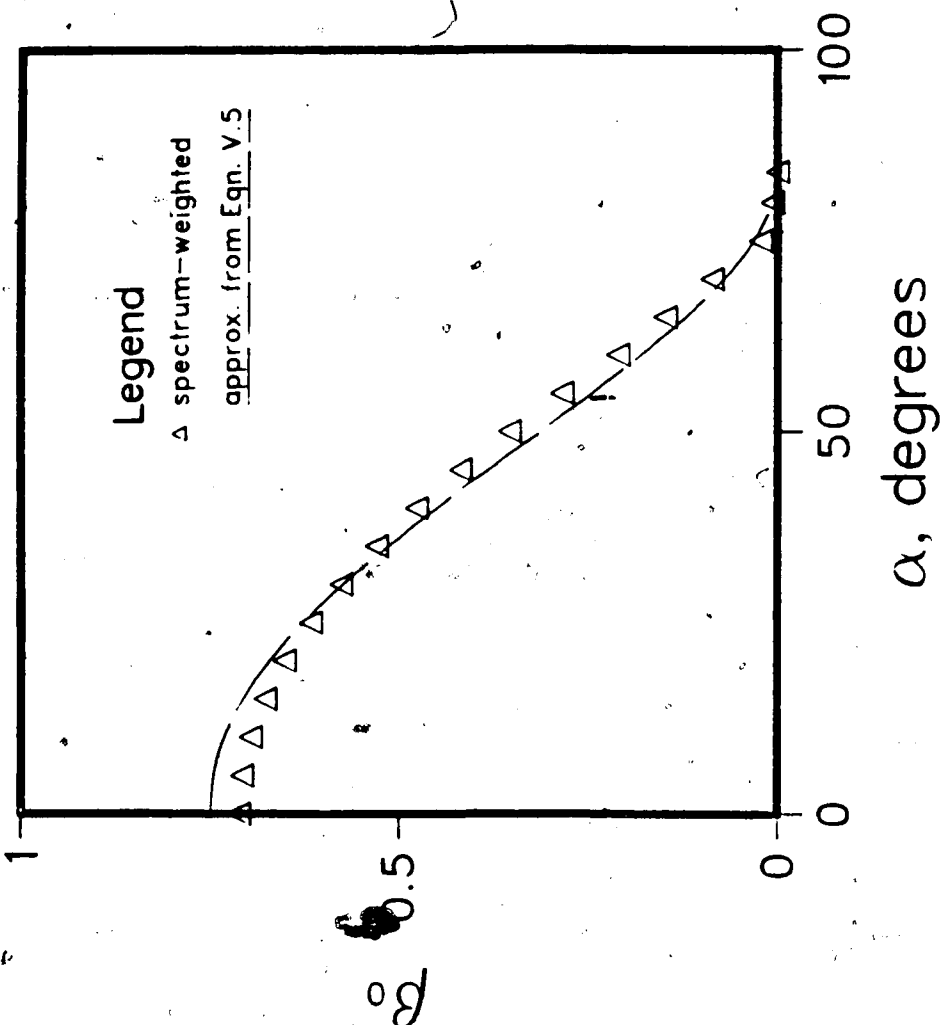


Figure V.6 - Comparison of spectrum-weighted collision efficiencies and Equation V.5 for the spectrum shown (mvd = 17.2 μm) on a NACA 0015, $U = 50 \text{ m/sec}$, chord = 0.2 m.

When the angle of attack (Φ) is non-zero, Oleskiw's numerical results have been fitted with the following function:

$$\beta(\alpha') = 0.95 \beta_0 \cos(\alpha'), \quad \text{V.7}$$

where β_0 is calculated as for the $\Phi = 0$ case, and

$$\alpha' = ((\pi/2) (\alpha_0 - \alpha) / (\pi/2 - \alpha)). \quad \text{V.8}$$

The position of maximum collision efficiency has been designated by α_0 , and may be approximated by:

$$\alpha_0 = \pi \log_{10} ((180 \Phi/\pi) + 1) / (0.180 \exp(30.5 h_0)), \quad \text{V.9}$$

where α_0 and Φ are in radians.

Unfortunately, there are only two numerical cases currently available (from Oleskiw, 1982) to test this fit, as illustrated in Figures V.7 and V.8. Further calculations at some time in the future may help to refine the approximation. In the meantime, it does give a rough estimate for the $\beta(\alpha)$ distribution when Φ is non-zero, which is otherwise very costly to compute.

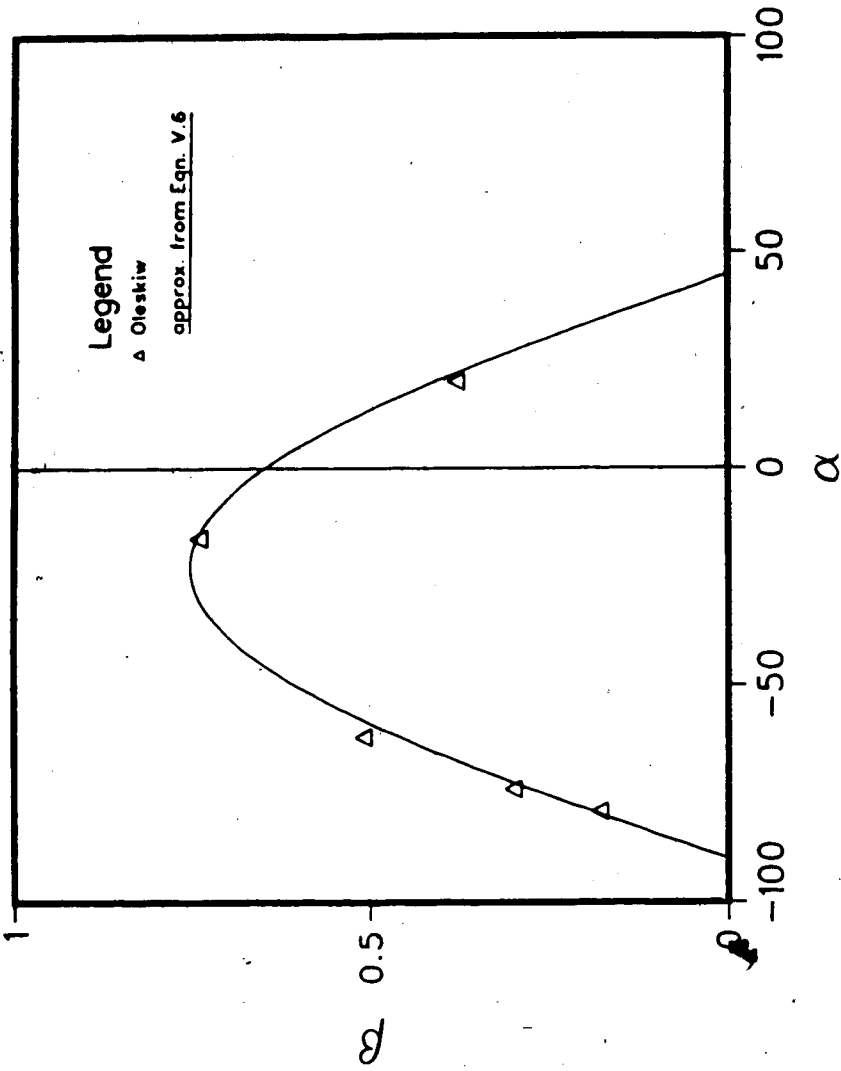


Figure V.7 - Comparison of Oleskiw's numerical results and Equation V.7, for collision efficiency on a NACA 0015 at an angle of attack = 8°, U = 30.5 m/sec, Chord = 0.169 m, $D_d = 20 \mu\text{m}$.

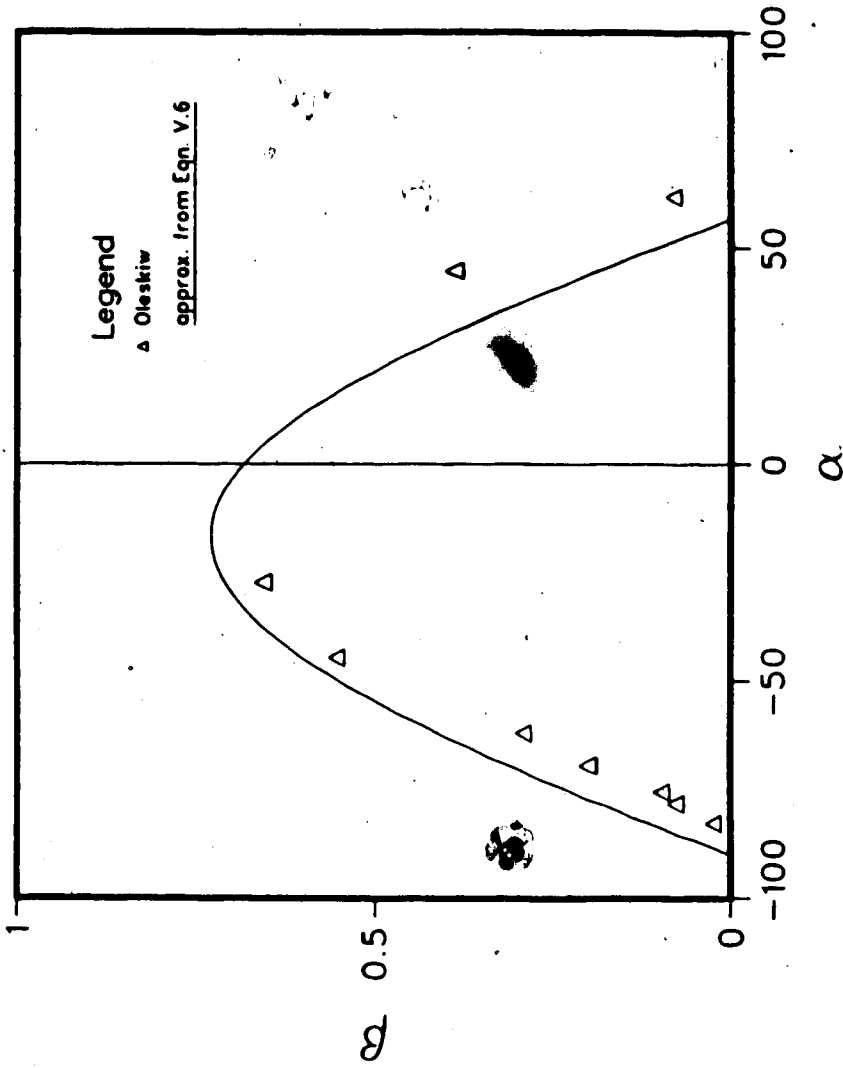


Figure V.8 - Comparison of Oleskiw's numerical results and Equation V.7, for collision efficiency on a Joukowski 15% at an angle of attack = 4° , $U = 78.2$ m/sec, Chord = 0.33 m, $D_d = 18.6$ μ m.

E. Integration of Droplet Trajectories

The equations of motion of a cloud droplet carried by the air stream, in a more general form than for the cylinder problem (Equation II.6), are:

$$dv_x/dt = -3/4 (\rho_a / \rho_d) (C_d/D_d) v (v_x - u_x)$$

V.10

$$dv_y/dt = -3/4 (\rho_a / \rho_d) (C_d/D_d) v (v_y - u_y)$$

In this steady-state formulation the additional term due to gravity has been neglected, as has the "history" term, arising from the droplet's acceleration with respect to the flow. Neglect of these terms is justified by the results of Oleskiw (1982), and also by examination of the "acceleration modulus", (Norment, 1980):

$$N_A = D_d \left| \frac{dv}{dt} \right| / v^2$$

V.11

If this quantity is less than about 0.01, the history term may be safely neglected. The results of Oleskiw and of Norment showed that this limit is not exceeded in most aeronautical modelling situations.

The drag coefficient is again estimated from the the expressions of Beard and Pruppacher (1969), Equation II.9. The droplet trajectories are integrated by the Heun method (Mesinger and Arakawa, 1976), similar to the calculations in

Chapter II, except for the determination of the air speeds u_x and u_y .

The streamfunction ψ of the potential flow field about the current accretion shape is numerically calculated following the method of Kennedy and Marsden (1976). This is a version of the surface singularity method originated by Hess and Smith (1967), in which the airfoil surface is represented by a set of point vortices. Kennedy and Marsden have slightly altered, at the trailing edge, the usual boundary condition of a constant streamfunction along the airfoil surface. They claim this gives a very accurate result with a minimum of computing time. Full details are available in their paper. The air speeds may then be approximated from a finite-difference calculation of the streamfunction derivatives, with the spatial differences equal to the droplet diameter.

The droplet's initial x-coordinate is five chord lengths upstream of the nose, and the initial separation of the two trajectories, Δy , is 10^{-8} metres. An optimum time step was found to be $\Delta t = 0.0025 (U/\text{chord})$. The justification for these choices is given by Table V.1, which examines the sensitivity of the model results to changes in these parameters.

As the droplet approaches the airfoil, the model begins testing for its position with respect to the current accretion surface. At each time step Δt , the array of accreting surface points is searched for the pair of

Δt (chord/U)	β_0 ($x_0 = 10 \cdot \text{chord}$)	β_0 ($x_0 = 5 \cdot \text{chord}$)
0.005	0.787	0.812
0.0033	0.794	0.804
0.0025	0.796	0.801
0.002	0.798	0.799

Table V.1 - Sensitivity of the integration results to the time step size Δt , and the initial x-position x_0 . Trajectory is for a 20 micron drop impinging on a NACA 0015 airfoil of 0.213 m chord, in a 61 m/sec airstream.

adjacent points which bracket the current y-coordinate of the droplet. The droplet's x-coordinate is then compared to the x-coordinates of these two points. If either or both of them are greater than the droplet's x-coordinate, the current droplet position lies inside the accretion surface.

The collision point is then estimated by solving for the intersection of the straight line segments, one joining the two bracketing surface points, and one joining the current and immediately previous droplet positions (see Figure V.9). The arc length Δl separating the two collision points on the surface is also approximated as a straight line. β_0 is then just $\Delta y / \Delta l$.

All of these straight line approximations, and the simple integration method, are sufficiently accurate because of the very small distances between surface points near the nose, the small Δt and initial Δy of the trajectories.

A comparison of the integration results with those of Oleskiw for his Case 55 shows very good agreement. Oleskiw calculates $\beta_0 = 0.805$ for a 20 μm drop impinging on a 10 mm chord NACA 0015, at 0° angle of attack and 61 m/s. The present model result is 0.801 for the same initial conditions. The small difference is easily accounted for by the use of a slightly different formulation for drag coefficient and by Oleskiw's method of approximating β_0 . This is from a spline fit to several $\beta(\alpha)$ points that are distributed along the surface, away from the stagnation line.

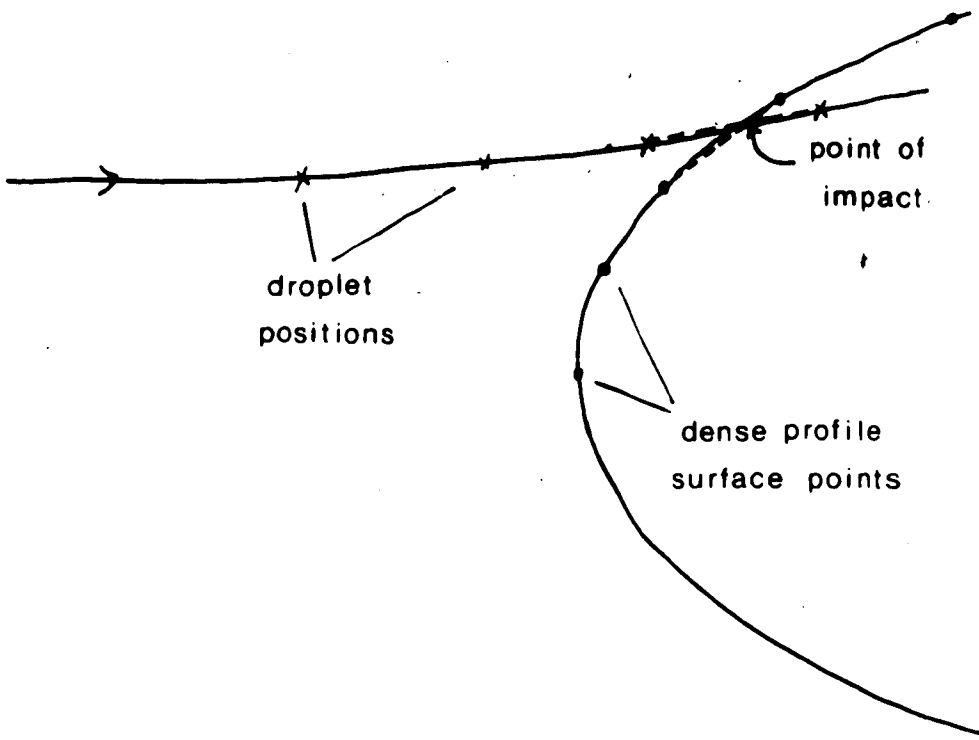


Figure V.9 - Determination of droplet impact point on the surface.

F. Local Density Variations

Once β_0 has been determined, α_{\max} and the distribution of local collision efficiency may be approximated from Equations V.3, V.5 or V.7. The local ice thickness (Th) accreted over a layer time step τ at each surface point is then given by the dry growth equation:

$$Th = \beta(\alpha) U lwc \tau / \rho(\alpha), \quad V.12$$

where now a suitable distribution for $\rho(\alpha)$ must be found.

This would ideally be done using the same techniques that were used in Chapter IV, to investigate circular cylinder accretion densities by direct measurement of local densities and of layer thicknesses. However, the wind tunnel experiments on airfoils which were performed in the FROST tunnel for this study, were grown on airfoils with thicknesses less than one inch. This is too small to allow effective measurements by the hole drilling technique, and the layers outlined by paint spray for some of the experiments were too thick to allow good results using the layer method.

Therefore, an approximate distribution was derived by plugging the above-mentioned circular cylinder curve into the model, and adjusting it until it could produce reasonable profiles. The result works best when used with the 'simulated spectrum' parameterization for local

collision efficiency. We emphasize that this distribution is not yet supported by any empirical evidence, and that it should be adjusted further when such evidence is available. For the present however, a good estimate for the density distribution is:

$$\rho(\alpha/\alpha_m) = \rho_0 (1 - 0.163 (\alpha/\alpha_m) + 0.235(\alpha/\alpha_m)^2 - 2.357(\alpha/\alpha_m)^3 + 1.374(\alpha/\alpha_m)^4 + 0.019(\alpha/\alpha_m)^5),$$

V.13

where ρ_0 is assumed, for simplicity, to be always 890 kg/m^3 . In certain conditions, the maximum density may be less than this value, but the model has no capability to determine this, at present.

The mass and mean density of each layer are calculated in the same way as for the circular cylinder described in Chapter III.

G. Model Results

Available data for model validation include the numerical results of Oleskiw, and a number of wind tunnel experiments carried out in the University of Alberta FROST tunnel, at NASA/Lewis and described in Olsekiw (1982b), at the National Aeronautical Establishment by Stallabrass (1958), and at the National Research Council Low Temperature Laboratory by Lozowski and Stallabrass (1978). In all of the experimental cases, the droplet sizes were determined by the

oil slide method, and have been corrected by us according to the calibration of Makkonen and Stallabrass (1984) discussed in Appendix III. An exception is the case taken from Stallabrass (1958), for which the liquid water content given by Stallabrass was derived from the observed ice thickness and the oil slide measurement of mvd. Stallabrass' numbers have thus been retained for both the droplet size and lwc. In all other cases, however, the accretion conditions were measured independently of the resulting thicknesses.

Figure V.10 illustrates the modelled profiles of Oleskiw and of the present model for identical accretion conditions. Since a constant local density was used, the agreement in shape of the layers between the two models reflects the accuracy of the parameterized collision efficiency distribution, for this case Equation V.3. The present model also lacks the surface instabilities which are already appearing in the Oleskiw model profile, arising from the spline curve approximation to the layer surface. Most importantly, the bottom profile of Figure V.10 represents a reduction in computational costs of a factor of ten over the Oleskiw model.

The conditions of Figure V.10 were chosen to agree with those of an experimental case grown in the NASA/Lewis tunnel. This experimental profile appears in Figure V.11, together with a corresponding model simulation using a constant local density, and one using the 'simulated spectrum' version of the local collision efficiency

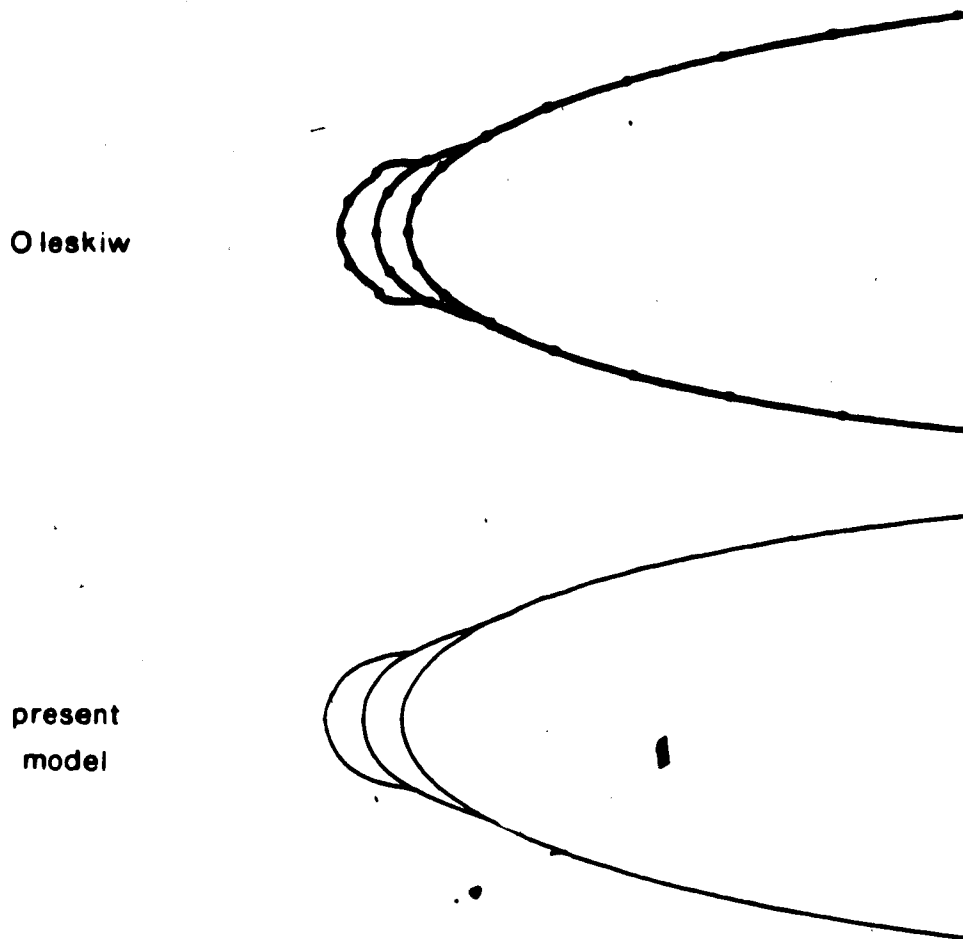


Figure V.10 - Comparison of present model results with those of Oleskiw (1982b) for a constant density accretion on a NACA 0015 at $\Phi = 0^\circ$, $U = 58$ m/sec, $lwc = 1.02$ g/m³, chord = 0.533 m, $t = 5$ min. A monodisperse droplet population at 12 μ m diameter is assumed, and an air temperature of -15° C.

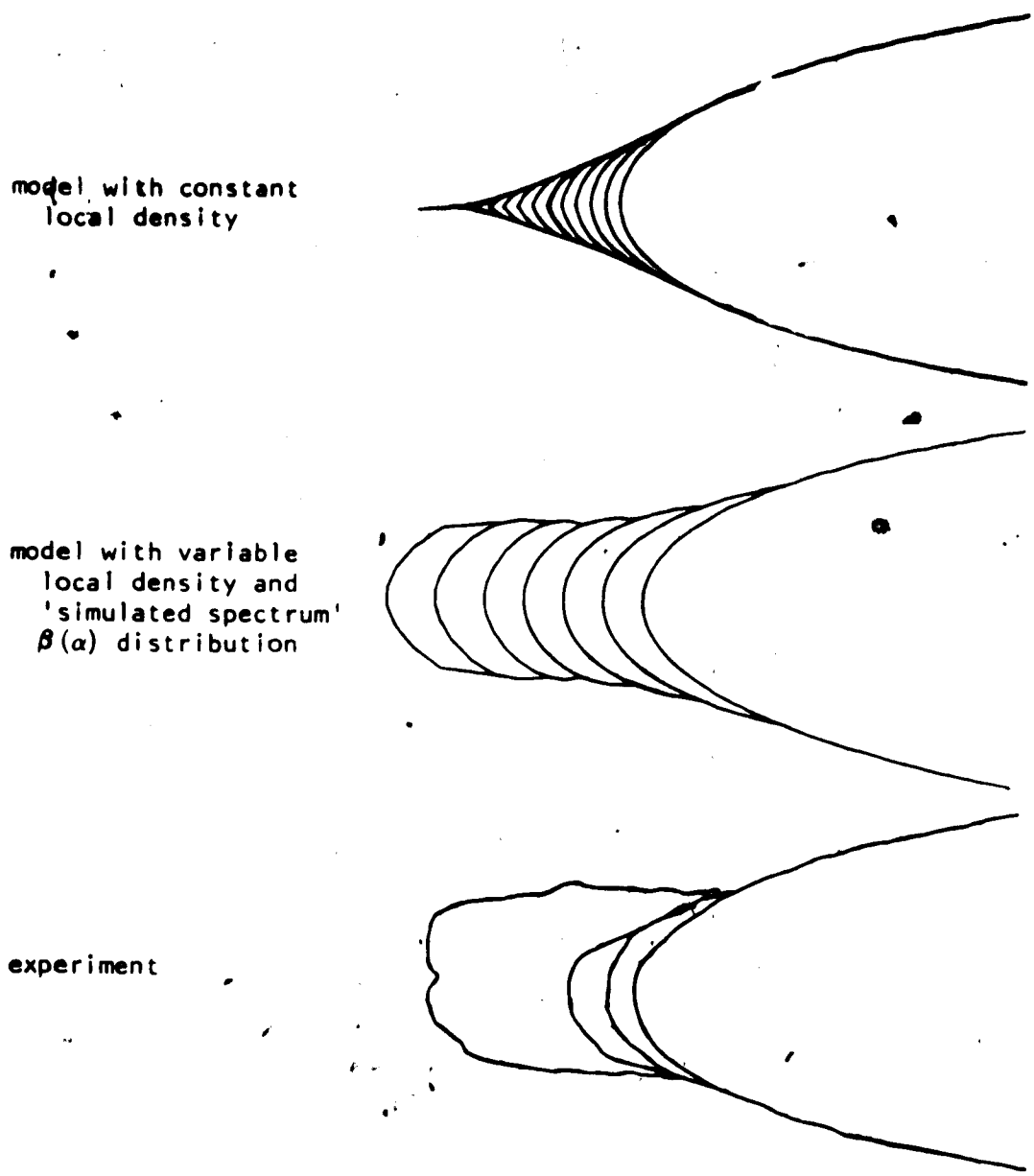


Figure V.11 - Comparison of present model results with an experimental accretion grown in the NASA/Lewis tunnel and described in Oleskiw (1982b), for the same conditions as in Figure V.10, but for a NACA 0012 airfoil, $t = 15$ min. Intermediate profiles at $t = 2$ and 5 minutes are also marked.

distribution, Equation V.5, together with the local density distribution of Equation V.12.

The two modelled profiles demonstrate a great improvement, in terms of a realistic accretion shape, in using the new local density and 'simulated spectrum' distributions over the old constant density and monodisperse spectrum versions. The model profiles are also seen to be free of surface instabilities and thus capable of accreting many more layers than the Oleskiw model.

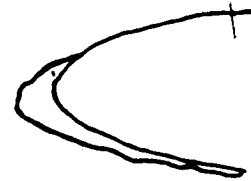
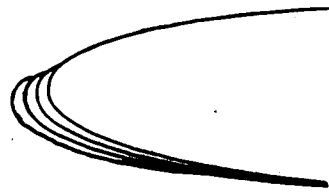
Except for the forward surface of the experimental accretion, which seems to contain a small central trough, the agreement in shape is very good. Central troughs and ridges are features which are often seen to form on wind-tunnel accretions. They most probably arise from disturbances in the laminar flow pattern near the nose, as the ice layer alters its shape. The simple, potential flow model does not include such effects, and such features are not expected to show up in these simulations.

The experimental results of Lozowski and Stallabrass (1978) and of Stallabrass (1958) allow a test of Equation V.7, for local collision efficiency at non-zero angles of attack. Figure V.12 shows four experimental accretions and the corresponding model profiles, all including density variation and local collision efficiencies estimated for the $\phi \neq 0$ case from Equation V.7. Since the method of approximating accretion limits for $\phi \neq 0$ is somewhat crude,

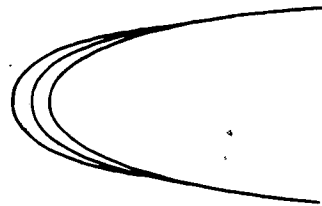
chord = 0.417 m
 $\Phi = 5.7^\circ$
 $D_d = 30 \mu\text{m}$
 $l_{wc} = 0.22 \text{ g/m}^3$
 $U = 60 \text{ m/sec}$
 $t = 14.3 \text{ min}$

model

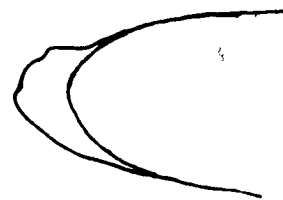
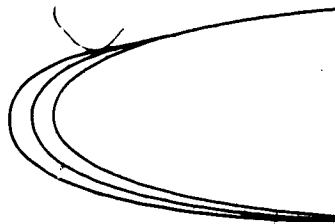
experiment



chord = 0.213 m
 $\Phi = 0^\circ$
 $D_d = 14.2 \mu\text{m}$
 $l_{wc} = 0.40 \text{ g/m}^3$
 $U = 61 \text{ m/sec}$
 $t = 5 \text{ min}$



chord = 0.213 m
 $\Phi = 4^\circ$
 $D_d = 14.2 \mu\text{m}$
 $l_{wc} = 0.36 \text{ g/m}^3$
 $U = 91.5 \text{ m/sec}$
 $t = 4 \text{ min}$



chord = 0.213 m
 $\Phi = 8^\circ$
 $D_d = 14.2 \mu\text{m}$
 $l_{wc} = 0.41 \text{ g/m}^3$
 $U = 61 \text{ m/sec}, t = 5 \text{ min}$

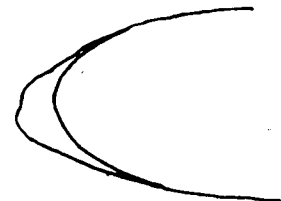
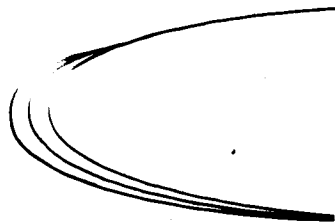


Figure V.12 - Comparison of present model results with experimental profiles from Stallabrass (1958, top profile, NACA 0012) and Stallabrass and Lozowski (1978, lower three profiles, Air temperature is -15° C).

comparison in this region shows only rough agreement. However, the general agreement in shape and stagnation line thicknesses is encouraging. These cases at least illustrate that the approach taken in Equation-V.9, to approximate the position of maximum collision efficiency α_0 , is worth pursuing and refining, especially given the large computational costs of determining this position from a series of droplet trajectory integrations.

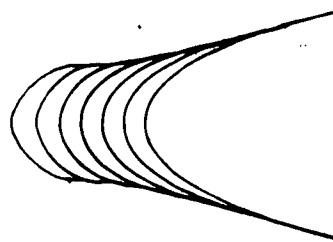
For all of the cases mentioned so far, accretion masses have not been available. However, a series of wind-tunnel experiments were carried out in the University of Alberta FROST tunnel, for which was measured the mass of ice accreted on a 15 cm length of a NACA 0012 airfoil under various conditions. These results, with intermediate layers as marked by paint spray, are shown in Figure V.13 together with the modelled masses and profiles.

The differences between the model masses and the experimental masses for the two cases are 11 and 16 percent. This is of the same order as typical measurement errors for input parameters such as droplet size and liquid water content.

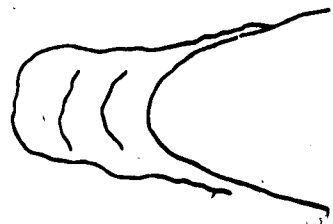
These examples have shown the usefulness of a simple approach toward numerical methods for ice accretion modelling. The present results are comparable to and much less costly than those of the Oleskiw model, and are of

$D_d = 15.9 \mu\text{m}$
 $lwc = 0.6 \text{ g/m}^3$
 $U = 11.0 \text{ m/sec}$
 $t = 30 \text{ min}$

model mass = 6.7 g

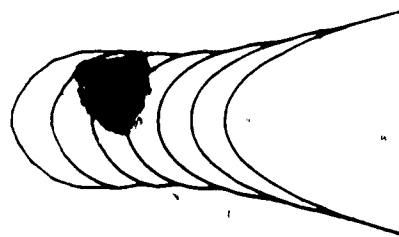


expt. mass = 8.0 g



$D_d = 15.9 \mu\text{m}$
 $lwc = 0.91 \text{ g/m}^3$
 $U = 11.2 \text{ m/sec}$
 $t = 30 \text{ min}$

model mass = 12 g



expt. mass = 13.4 g

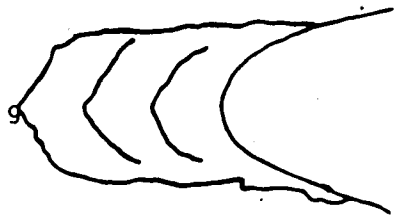


Figure V.13 - Comparison of present model results with experimental profiles and masses of accretions grown in The University of Alberta FROST tunnel on a NACA 0012 at $\phi = 0^\circ$, chord = 0.176 m, air temperature = -10° C .

sufficient accuracy to allow practical and realistic comparisons with rime experiments. Such methods will also help to make the modelling problem for wet icing more tractable.

References

- Abbott, I.H. and von Doenhoff, A.E. 1959: Theory of Wing Sections Including a Summary of Airfoil Data. Dover, 693 pp.
- Beard, K.V. and Pruppach, H.R. 1969: A Determination of the Terminal Velocity and Drag of Small Water Drops by Means of a Wind Tunnel. *J. Atmos. Sci.*, 26, 1066-1072.
- Cansdale, J.T. and Gent, R.W. 1983: Ice Accretion on Airfoils in Two-Dimensional Compressible Flow - A Theoretical Model. British Royal Aircraft Establishment Technical Report No. 82128, 31 pp. plus 33 fig.s.
- Hess, J.L. and Smith, A.M.O. 1967: Calculation of Potential Flow about Arbitrary Bodies. *Progress In Aeronautical Sciences*, Vol. 8. Pergamon Press, 1-138.
- Kennedy, J.L. and Marsden, D.J. 1976: Potential Flow Velocity Distributions on Multi-Component Airfoil Sections. *Can. Aero. and Space Jour.*, 22, 243-256.

- MacArthur, C.D., Keller, J.L. and Luers, J.K. 1982:
Mathematical Modelling of Ice Accretion on
Airfoils. AIAA Publication No. 82-0284.
- Makkonen, L. and Stallabrass, J.R. 1984: Ice Accretion on
Cylinders and Wires. National Research Council,
Division of Mechanical Engineering, Technical
Report TR-LT-005, 50 pp.
- Mesinger, F. and Arakawa, A. 1976: Numerical Methods used in
Atmospheric Models, Vol. 1. W.M.O.GARP
Publications Series No. 17, 64 pp.
- Norment, H.G. 1980: Calculation of Water Drop Trajectories
to and About Arbitrary Three-Dimensional Bodies in
Potential Airflow. NASA Contractor Report 3291,
82 pp.
- Oleskiw, M.M. 1982: Numerical Simulation of Icing on
Airfoils. Ph.D. Thesis, The University of
Alberta, 302 pp.
- Oleskiw, M.M. 1982b: Contribution to NASA/Lewis Icing
Workshop, unpublished.
- Stallabrass, J.R. 1958: Icing Flight Trials of a Sikorsky
HO4S-2 Helicopter. National Aeronautical

Establishment, Laboratory Report LR-219, 25 pp.

Stallabrass, J.R. and Lozowski, E.P. 1978: Ice Shapes on
Cylinders and Rotor Blades. Presented to NATO
Panel X Symposium on Helicopter Icing, London.

VI. Concluding Remarks

In the four separate, but interrelated studies of this thesis several improvements have been put forward for physical models of ice accretion. Since conclusions were given within each chapter, these remarks will summarise the results, and give suggestions for future research.

Chapter II presented a re-calculation of the long-established work of Langmuir and Blodgett on collision efficiencies and other impingement parameters of circular cylinders. High-speed digital computer results for droplet trajectory integrations have provided a small improvement over the old analog computer results, but a larger improvement has been made in the application of a non-linear regression fit to the tabulated numerical values of collision efficiency, impact speed and accretion limit. This new analytical approximation could be very useful to modellers, who presently use a variety of functions to approximate the same thing, none of which is as accurate as the new expression.

These results are equally applicable to all types of icing, wet or dry, from transmission lines to marine structures, as long as it occurs on circular cylinders. A possibility for future work here is to extend the re-calculations to the spheres and flat ribbons also considered by Langmuir and Blodgett.

The circular cylinder rime model of Chapter III makes use of these new collision efficiencies, as well as of new

parameterizations for the distribution of local collision efficiency under various conditions. The efficiency and accuracy of these methods was well demonstrated in that chapter, by model results which reproduced realistic profiles, and accreted masses to within 10 percent of observation. The speed of the model; a few seconds on the University of Alberta Amdahl 580, and about 90 seconds on an IBM PC; make it highly practical.

The cylinder model also represents an improvement on older models in its version of local ice density distribution, derived in Chapter IV. Based on empirical data, this distribution is more realistic than previous versions, based on rotating cylinder correlations, have been. Since an attempt to validate the density distribution by direct measurement was inconclusive, further work, perhaps using different measurement techniques, would be valuable.

A logical extensions to the circular cylinder model would be the addition of gravitational and aerodynamic torque calculations in order to determine the correct rate of rotation. Another would be the determination of stagnation line density, following the method described in Chapter IV. The stagnation line density is required as a scaling parameter of the empirical density distribution. This would require a simple heat balance calculation at the stagnation line in order to determine the surface temperature there.

The airfoil model of Chapter V shows that parameterization methods similar to those of Chapter III may also be found for more difficult shapes, where the potential saving in computational costs is much larger. Here the parameterization for $\rho(\alpha)$ is in particular need of empirical validation, and the collision efficiency approximations would benefit from further verification and refinement using numerical results for a wider range of conditions.

The airfoil model has the capability to update the potential flow approximation, from which the β_0 parameter is derived, at intervals throughout the accretion period. Although a suggestion was made for the length of this interval, it was only an estimate. More numerical experiments should be carried out to discover the optimum interval, since this procedure is an expensive one.

Both models fail in the prediction of the troughs and ridges which sometimes form along the stagnation line of experimental accretions, often after the formation of a flat forward surface. An interesting exercise would be to investigate the flow patterns and droplet trajectories about these flat surfaces, in an attempt to understand how such features are formed. Experimental data should be gathered on the conditions under which troughs and ridges form, since they are not always present. Such studies may discover ways to model their formation.

Appendix I

Program Listing: GRAZE

- o' -
)


OPTIONS IN EFFECT: NOLIST NOMAP NOXREF NOGOSTMT NOCHECK SOURCE /TERM OBJECT FIXED SEQ
 OPTIMIZE(O) LANGVL(77) NOFIPS FLAG(I) NAME(MAIN) LINECOUNT(60) MDTST

```

1 C ..... 1 2 3 4 5 6 7 8 9
2 C ..... GRAZE .....
3 C
4 C Karen J. Finstad June, 1986
5 C
6 C This program calculates trajectory pairs for water
7 C droplets in an air flow field around a circular cylinder,
8 C and determines the stagnation line collision efficiency,
9 C maximum accretion angle and overall collision efficiency.
10 C The air is assumed to be at a temperature of -10 degrees
11 C C, and a pressure of 100 kPa.
12 C
13 C The equation of motion of the droplet is integrated
14 C using the Heun scheme (Mesinger, F. and Arakawa, A. 1976
15 C Numerical Methods Used in Atmospheric Models, Vol. 1
16 C W.M.O. GARP Publications Series No. 17, 64pp.) The time
17 C step is set to 1/400 of the time to travel one cylinder
18 C radius at the free stream speed. A maximum of 7000 steps
19 C are allowed, by which time the droplet is assumed to have
20 C collided with the cylinder or to have passed it.
21 C
22 C Note that the droplet's initial x-coordinate is set
23 C to be 10 cylinder radii upstream of the cylinder axis.
24 C The initial x-component speed is set equal to the air's
25 C x-component, and the y-component is set to half the
26 C air's y-component.
27 C
28 C A first trajectory is integrated beginning at the
29 C input initial x-coordinate, which is then incremented
30 C by a very small amount (DELTA) for the second trajectory.
31 C If both trajectories intercept the cylinder, the normal
32 C impact velocity, impact angle, impact position, and local
33 C collision efficiency are calculated.
34 C
35 C The grazing trajectory is determined by successively halving
36 C the distance between a pair of initial y-coordinates which
37 C bracket the initial y-coordinate of the grazing trajectory.
38 C The initial values of y-min and y-max are input by the user;
39 C a judicious choice will decrease the number of trajectories
40 C needed to determine the grazing one.
41 C If a Stokes flow calculation is requested (i.e. Langmuir phi
42 C parameter = 0), the drag coefficient is set to 24 / Reynolds
43 C number. Otherwise, the formulation of Beard and Pruppacher is
44 C used for the drag coefficient.
45 C
46 C All operations are carried out in double precision.
47 C Output is written to EMSOURCE.
48 C
49 C To compile on a PC enter:
50 C $RUN *FORTRANVS SCARDS-GRAZE SPUNCH-GRAZERUN
51 C
52 C To run, enter $RUN GRAZERUN. You will be prompted for
53 C the following input parameters:

```

1 2 3 4 5 6 7 8 9

```

52 C Droplet DIAMETER in microns
53 C
54 C Cylinder RADIUS in metres
55 C
56 C Free stream air speed in metres per second
57 C
58 C Initial droplet y position in metres
59 C
60 C Initial value for y-min
61 C
62 C Initial value for y-max
63 C
64 C Y(es) or n(o) for Stokes flow option
65 C
66 C ..... Subprograms .....
67 C
68 C
69 C SUBROUTINE TRAJEC - calculates droplet trajectories
70 C by integrating the droplet equations of motion by
71 C the trapezoid rule with one iteration step.
72 C
73 C SUBROUTINE ITERAT - calculates the air speeds (from
74 C the analytical flow solution) and droplet
75 C accelerations (from the equations of motion) for
76 C the current iteration and time step.
77 C
78 C SUBROUTINE COLLID -calculates final impact position
79 C if the droplet collides with the surface.
80 C
81 C ..... Variable Dictionary .....
82 C
83 C
84 C ARC1 - arc lengths along cylinder surface
85 C ARC2 - from stagnation line to the impact points
86 C of the two trajectories
87 C
88 C BETA - local collision efficiency
89 C
90 C CYLRAD - cylinder radius in metres (INPUT)
91 C
92 C DELTAT - time step in seconds
93 C
94 C DELTAY - difference in initial y coordinate of
95 C the two trajectories, in metres
96 C DROPLD - droplet diameter (input in microns, but
97 C converted to metres (INPUT))
98 C
99 C FINVX, - average values of the final velocities
100 C FINVY
101 C
102 C FINVX1, - x-components of droplet velocity at
103 C FINVX2 - impact
104 C
105 C FINVY1, - as above, for y-components
106 C FINVY2

```


1 2 3 4 5 6 7 8 9

```

107 C HALFPI - pi / 2 (FORTRAN77 constant parameter)
108 C
109 C HIT1, - logical flags for each trajectory
110 C HIT2 - which indicate whether a collision
111 C with the cylinder has occurred
112 C
113 C NOTRAJ - no. of trajectories used to find grazing traj
114 C
115 C NSTEPS - maximum number of time steps to be
116 C integrated
117 C
118 C PHI - angle of trajectory to the surface
119 C normal at impact
120 C
121 C STK - input character variable to set Stokes
122 C flow flag
123 C
124 C STOKES - logical flag for Stokes flow option
125 C
126 C THETA - average of THETA1 and THETA2
127 C
128 C THETA1, - position angles of the impact points
129 C THETA2 - of the two trajectories
130 C
131 C VEL - free stream air speed in metres/sec (INPUT)
132 C
133 C VNORM - droplet velocity normal to the cylinder
134 C surface at impact
135 C
136 C XINIT - initial droplet x-coordinate in metres
137 C
138 C YINIT - initial droplet y-coordinate in metres (INPUT)
139 C
140 C YMIN, - minimum and maximum initial y-coordinates
141 C YMAX - which bracket the graze coordinate
142 C
143 C .....
144 C DOUBLE PRECISION DROPI,VEL,CYLRAD,XINIT,YINIT,FINVX,
145 C + FINVY,VNORM,PHI,THETA,THETA1,THETA2,
146 C + BETA,FINVX1,FINVX2,FINVY1,FINVY2,
147 C + ARC1,ARC2,DELTAT,DELTAY,YMIN,YMAX
148 C
149 C INTEGER NSTEPS,NOTRAJ
150 C
151 C LOGICAL HIT1,HIT2,STOKES
152 C
153 C CHARACTER*1 RESPNS,STK
154 C
155 C PARAMETER (HALFPI = 3.1415926535897932/2.0)
156 C
157 C Prompt user for input parameters
158 C
159 C WRITE (6,10)
160 C FORMAT (///, '***** Droplet Trajectories about a',
161 C
162 C
163 C
164 C
165 C

```

```

ISN 1
ISN 2
ISN 3
ISN 4
ISN 5
ISN 6
ISN 7

```


1.....2.....3.....4.....5.....6.....7.....8.....9.....

```

222. C
223. C Integrate first trajectory
224. C
225. C CALL TRAJEC (XINIT,YINIT,DROPI,VEL,CYLRAD,DELTAT,NSTEPS,
226. C STOKES,THETA1,ARC1,HIT1,FINVX1,FINVY1)
227. C
228. C Correct initial y position and integrate second trajectory
229. C
230. C YINIT = YINIT + DELTAY
231. C CALL TRAJEC (XINIT,YINIT,DROPI,VEL,CYLRAD,DELTAT,NSTEPS,
232. C STOKES,THETA2,ARC2,HIT2,FINVX2,FINVY2)
233. C
234. C Test for result of trajectory (miss, graze or collision)
235. C
236. C IF (.NOT.(HIT1) .AND. (HIT2)) THEN
237. C
238. C Calculate impact parameters and local collision efficiency
239. C
240. C IF (YINIT-DELTAY .NE. 0.0) YMIN = YINIT - DELTAY
241. C BETA = DELTAY / (ARC2 - ARC1)
242. C THETA = (THETA1 + THETA2) / 2.0
243. C FINVX = (FINVX1 + FINVX2) / 2.0
244. C FINVY = (FINVY1 + FINVY2) / 2.0
245. C PHI = HALFPI - DATAN(FINVX/FINVY) + THETA
246. C VNORM = DSORT((FINVX * FINVX) + (FINVY * FINVY))
247. C
248. C
249. C Write results to screen
250. C
251. C WRITE (6,20)THETA,VNORM,PHI,BETA
252. C FORMAT (//,' Both trajectories collided with cylinder',
253. C //,' Position angle at impact point: ',F7.3
254. C //,' Velocity normal to surface at impact: ',F7.3,
255. C //,' Angle of trajectory to surface normal: ',F7.3
256. C //,' Local collision efficiency: ',F5.3,/)
257. C
258. C ELSE IF (HIT1) THEN
259. C WRITE (6,30) THETA1
260. C FORMAT (//,' First trajectory grazed cylinder',
261. C //,' Surface angle of max accretion point: ',F7.3,/)
262. C
263. C WRITE (6,*) ' overall coll. eff.: ', (YINIT - DELTAY)/CYLRAD
264. C WRITE (6,*) ' no of trajectories: ', NOTRAU
265. C GO TO 200
266. C ELSE
267. C YMAX = YINIT - DELTAY
268. C WRITE (6,40)
269. C FORMAT (//,' Both trajectories missed the cylinder',)
270. C
271. C Determine new initial position and start next trajectory pair
272. C
273. C YINIT = (YMAX + YMIN) / 2.0
274. C GO TO 100
275. C
276. C 200 STOP
277. C END

```

LEVEL 1.1.1 (DEC 81) VS FORTRAN DATE: JUL 24, 1986 13:13:40 NAME: MAIN PAGE: 6

STATISTICS SOURCE STATEMENTS = 69, PROGRAM SIZE = 2732 BYTES, PROGRAM NAME = MAIN PAGE: 1.

STATISTICS NO DIAGNOSTICS GENERATED.

***** END OF COMPILATION 1 *****

OPTIONS IN EFFECT: NOLIST NOMAP NOXREF NOGOSTMT NODECK SOURCE TERM OBJECT FIXED
 OPTIMIZE(O) LANGLVL(77) NOFIPS FLAG(1) NAME(MAIN) LINECOUNT(60) NOTEST SEO

1.....2.....3.....4.....5.....6.....7.....8.....9.....

```

277. C .....
278. C .....
279. C .....
280. C .....
281. C .....
282. C .....
283. C .....
284. C .....
285. C .....
286. C .....
287. C .....
288. C .....
289. C .....
290. C .....
291. C .....
292. C .....
293. C .....
294. C .....
295. C .....
296. C .....
297. C .....
298. C .....
299. C .....
300. C .....
301. C .....
302. C .....
303. C .....
304. C .....
305. C .....
306. C .....
307. C .....
308. C .....
309. C .....
310. C .....
311. C .....
312. C .....
313. C .....
314. C .....
315. C .....
316. C .....
317. C .....
318. C .....
319. C .....
320. C .....
321. C .....
322. C .....
323. C .....
324. C .....
325. C .....
326. C .....
327. C .....
328. C .....
329. C .....

SUBROUTINE TRAJEC
.....
Integrates trajectory of droplet whose initial
position is specified in the parameter list. Calls
ITERAT for iterative calculations, and COLLID to
determine impact parameters for colliding trajectories.

INPUT VARIABLES:
XINIT - initial x position
YINIT - initial y position
DROPLD - droplet diameter
CYLRAD - cylinder radius
VEL - free stream velocity
DELTAT - time step
NSTEPS - maximum number of time steps
STOKES - logical flag for Stokes flow

OUTPUT VARIABLES:
THETA - surface angle of impact
ARC - arc length along cylinder surface
from stagnation line to impact
point
HIT - logical flag set to .TRUE. if
a collision occurs
FINVX - droplet x velocity on impact
FINVY - droplet y velocity on impact

OTHER VARIABLES:
X,Y - arrays containing x,y positions
for each time step
VX,VY - arrays containing x,y components
of droplet speed for each step
DVX, - arrays containing x,y components
DVY - of droplet accelerations

SUBROUTINE TRAJEC(XINIT,YINIT,DROPLD,VEL,CYLRAD,DELTAT,
+ NSTEPS,STOKES,THETA,ARC,HIT,FINVX,FINVY)
C
DOUBLE PRECISION X(7000),Y(7000),
+ VX(7000),VY(7000),DVX(7000),DVY(7000)
C
DOUBLE PRECISION XINIT,YINIT,DROPLD,CYLRAD,VEL,DELTAT,
+ THETA,ARC,FINVX,FINVY
C
INTEGER NSTEPS
C
LOGICAL HIT,STOKES
C
C Initialize values for integration
    
```

```

330.
331.
332.
333.
334.
335.
336.
337.
338.
339.
340.
341.
342.
343.
344.
345.
346.
347.
348.
349.
350.
351.
352.
353.
354.
355.
356.
357.
358.
359.
360.
361.
362.
363.
364.
365.
366.
367.
368.
369.
370.
371.
372.
373.
374.
375.
376.
377.
378.
379.
380.
381.
382.
383.
384.
385.
386.
387.
388.
389.
390.
391.
392.
393.
394.
395.
396.
397.
398.
399.
400.
401.
402.
403.
404.
405.
406.
407.
408.
409.
410.
411.
412.
413.
414.
415.
416.
417.
418.
419.
420.
421.
422.
423.
424.
425.
426.
427.
428.
429.
430.
431.
432.
433.
434.
435.
436.
437.
438.
439.
440.
441.
442.
443.
444.
445.
446.
447.
448.
449.
450.
451.
452.
453.
454.
455.
456.
457.
458.
459.
460.
461.
462.
463.
464.
465.
466.
467.
468.
469.
470.
471.
472.
473.
474.
475.
476.
477.
478.
479.
480.
481.
482.
483.
484.
485.
486.
487.
488.
489.
490.
491.
492.
493.
494.
495.
496.
497.
498.
499.
500.
501.
502.
503.
504.
505.
506.
507.
508.
509.
510.
511.
512.
513.
514.
515.
516.
517.
518.
519.
520.
521.
522.
523.
524.
525.
526.
527.
528.
529.
530.
531.
532.
533.
534.
535.
536.
537.
538.
539.
540.
541.
542.
543.
544.
545.
546.
547.
548.
549.
550.
551.
552.
553.
554.
555.
556.
557.
558.
559.
560.
561.
562.
563.
564.
565.
566.
567.
568.
569.
570.
571.
572.
573.
574.
575.
576.
577.
578.
579.
580.
581.
582.
583.
584.
585.
586.
587.
588.
589.
590.
591.
592.
593.
594.
595.
596.
597.
598.
599.
600.
601.
602.
603.
604.
605.
606.
607.
608.
609.
610.
611.
612.
613.
614.
615.
616.
617.
618.
619.
620.
621.
622.
623.
624.
625.
626.
627.
628.
629.
630.
631.
632.
633.
634.
635.
636.
637.
638.
639.
640.
641.
642.
643.
644.
645.
646.
647.
648.
649.
650.
651.
652.
653.
654.
655.
656.
657.
658.
659.
660.
661.
662.
663.
664.
665.
666.
667.
668.
669.
670.
671.
672.
673.
674.
675.
676.
677.
678.
679.
680.
681.
682.
683.
684.
685.
686.
687.
688.
689.
690.
691.
692.
693.
694.
695.
696.
697.
698.
699.
700.
701.
702.
703.
704.
705.
706.
707.
708.
709.
710.
711.
712.
713.
714.
715.
716.
717.
718.
719.
720.
721.
722.
723.
724.
725.
726.
727.
728.
729.
730.
731.
732.
733.
734.
735.
736.
737.
738.
739.
740.
741.
742.
743.
744.
745.
746.
747.
748.
749.
750.
751.
752.
753.
754.
755.
756.
757.
758.
759.
760.
761.
762.
763.
764.
765.
766.
767.
768.
769.
770.
771.
772.
773.
774.
775.
776.
777.
778.
779.
780.
781.
782.
783.
784.
785.
786.
787.
788.
789.
790.
791.
792.
793.
794.
795.
796.
797.
798.
799.
800.
801.
802.
803.
804.
805.
806.
807.
808.
809.
810.
811.
812.
813.
814.
815.
816.
817.
818.
819.
820.
821.
822.
823.
824.
825.
826.
827.
828.
829.
830.
831.
832.
833.
834.
835.
836.
837.
838.
839.
840.
841.
842.
843.
844.
845.
846.
847.
848.
849.
850.
851.
852.
853.
854.
855.
856.
857.
858.
859.
860.
861.
862.
863.
864.
865.
866.
867.
868.
869.
870.
871.
872.
873.
874.
875.
876.
877.
878.
879.
880.
881.
882.
883.
884.
885.
886.
887.
888.
889.
890.
891.
892.
893.
894.
895.
896.
897.
898.
899.
900.
901.
902.
903.
904.
905.
906.
907.
908.
909.
910.
911.
912.
913.
914.
915.
916.
917.
918.
919.
920.
921.
922.
923.
924.
925.
926.
927.
928.
929.
930.
931.
932.
933.
934.
935.
936.
937.
938.
939.
940.
941.
942.
943.
944.
945.
946.
947.
948.
949.
950.
951.
952.
953.
954.
955.
956.
957.
958.
959.
960.
961.
962.
963.
964.
965.
966.
967.
968.
969.
970.
971.
972.
973.
974.
975.
976.
977.
978.
979.
980.
981.
982.
983.
984.
985.
986.
987.
988.
989.
990.
991.
992.
993.
994.
995.
996.
997.
998.
999.
1000.

```

1 2 3 4 5 6 7 8 9

386 C
387 RETURN
388 END

STATISTICS SOURCE STATEMENTS = 33, PROGRAM SIZE = 338354 BYTES, PROGRAM NAME = TRAJEC PAGE: 7.
STATISTICS NO DIAGNOSTICS GENERATED.
***** END OF COMPILATION 2 *****

OPTIONS IN EFFECT: NOLIST NOMAP NOXREF NOGOSTMT NODECK SOURCE TERM OBJECT FIXED
 OPTIMIZE(O) LANGLVL(77) NOFIPS FLAG(I) NAME(MAIN) LINECOUNT(60)

1 2 3 4 5 6 7 8 9

```

389. C *****
390. C
391. C * SUBROUTINE ITERAT - calculates for the current step:
392. C * air speed components from analytical solution to
393. C * flow around a cylinder, the droplet Reynolds
394. C * number, drag coefficient according to the formula-
395. C * tion of Beard and Pruppacher, and the droplet
396. C * acceleration components from the equations of motion.
397. C *
398. C * INPUT VARIABLES :
399. C * X,Y - current droplet positions
400. C * VX,VY, - current droplet speeds
401. C * VEL - free stream air speed
402. C * CYLRAD - cylinder radius
403. C * DROPDI - droplet diameter
404. C * STOKES - logical flag for Stokes flow
405. C *
406. C * OUTPUT VARIABLES :
407. C * DVX,DVY - current droplet accelerations
408. C *
409. C * OTHER VARIABLES :
410. C * UX,UY - current air speed components
411. C * DROPRE - droplet Reynolds number
412. C * DRAGCO - drag coefficient
413. C * COEFF - combined coefficients of the
414. C * equations of motion
415. C * DENOM - denominator of air speed
416. C * equations
417. C *
418. C *
419. C
420. C
421. C
422. C SUBROUTINE ITERAT(X,Y,VX,VY,VEL,CYLRAD,DROPDI,STOKES,DVX,DVY)
423. C DOUBLE PRECISION X,Y,VX,VY,DVX,DVY,VEL,CYLRAD,DROPDI,
424. C DROPRE,DRAGCO,COEFF,UX,UY,DENOM
425. C LOGICAL STOKES
426. C
427. C Calculate air speeds
428. C
429. C DENOM = ((X * X) + (Y * Y)) ** 2
430. C UX = VEL * (1 + ((CYLRAD**2) * ((Y * Y) - (X * X))/(DENOM)))
431. C UY = DABS(2 * VEL * (CYLRAD**2) * ((X * Y) / DENOM))
432. C
433. C Calculate Reynolds number and drag coefficient
434. C
435. C DROPRE = DROPDI * DSORT(((VX - UX) ** 2) + ((VY - UY)
436. C * ** 2)) / 1.262E-5
437. C IF (STOKES) THEN
438. C DRAGCO = 24.0 / DROPRE
439. C ELSE IF (DROPRE .LT. 2.0) THEN
440. C DRAGCO = (24.0 / DROPRE) + (2.45 / (DROPRE ** 0.045))
441. C ELSE IF (DROPRE .LT. 21.0) THEN

```


1
2
3
4
5
6
7
8
9

```

442. DRAGCO = (24.0 / DROPRE) + (2.76 / (DROPRE ** 0.198))
443. ELSE IF (DROPRE .GT. 200.0) THEN
444. DRAGCO = (24.0 / DROPRE) + (4.73 / (DROPRE ** 0.37))
445. + (6.24E-3 * (DROPRE ** 0.38))
446. ELSE
447. DRAGCO = (24.0 / DROPRE) + (4.536 / (DROPRE ** 0.368))
448. ENDIF
449.
450. C Calculate accelerations
451. C
452. C
453. C
454. COEFF = 9.92E-4 * (DRAGCO / DROPRE)
455. DVX = COEFF * DSORT(((VX - UX) ** 2) + ((VY - UY) ** 2))
456. + (VX - UX)
457. DVY = -COEFF * DSORT(((VX - UX) ** 2) + ((VY - UY) ** 2))
458. + (VY - UY)
459. C
460. RETURN
461. END

```

STATISTICS SOURCE STATEMENTS = 23. PROGRAM SIZE = 1380 BYTES. PROGRAM NAME = ITERAT PAGE: 10.

STATISTICS NO DIAGNOSTICS GENERATED.

***** END OF COMPILATION 3 *****

OPTIONS IN EFFECT: NOLIST NOMAP NOXREF NOGOSTMT NODCK SOURCE TERM OBJECT FIXED OPTIMIZE(O) L ANGLVL(77) NOFIPS FLAG(I) NAME(MAIN) LINECOUNT(60)

1 2 3 4 5 6 7 8 9

```

462. C .....
463. C .....
464. C * SUBROUTINE COLLID - Calculates the x,y position
465. C of impact on the cylinder surface, position angle
466. C of the impact point, and arc length measured from
467. C the stagnation line.
468. C .....
469. C * INPUT VARIABLES:
470. C XOUT, - last droplet position outside
471. C YOUT the cylinder
472. C XIN, - first droplet position inside
473. C YIN the cylinder
474. C CYLRAD - cylinder radius
475. C .....
476. C * OUTPUT VARIABLES:
477. C THETA - position angle of impact point
478. C on the cylinder measured from
479. C the stagnation line
480. C ARC - arc length from stagnation line
481. C to the impact point
482. C .....
483. C * OTHER VARIABLES:
484. C SLOPE - slope of the trajectory segment
485. C which crosses the cylinder surface
486. C i.e., between XOUT,YOUT and
487. C XIN,YIN
488. C A,B,C - coefficients of the quadratic
489. C equation to solve for the intercept
490. C of the trajectory and cylinder
491. C surface
492. C IMPX, - impact position on the surface
493. C IMPY
494. C .....
495. C .....
496. C .....
497. C SUBROUTINE COLLID (XOUT,XIN,YOUT,YIN,CYLRAD,THETA,ARC)
498. C .....
499. C DOUBLE PRECISION XOUT,XIN,YOUT,YIN,CYLRAD,THETA,ARC,
500. C SLOPE,A,B,C,IMPX,IMPY
501. C .....
502. C Calculate slope of trajectory at impact point
503. C
504. C SLOPE = (YIN - YOUT) / (XIN - XOUT)
505. C XOUT = XOUT / CYLRAD
506. C XIN = XIN / CYLRAD
507. C YOUT = YOUT / CYLRAD
508. C YIN = YIN / CYLRAD
509. C .....
510. C Find impact point by solving quadratic equation with
511. C coefficients as follows
512. C
513. C A = (SLOPE * SLOPE) + 1.0
514. C B = (2.0 * SLOPE * YOUT) - (2.0 * (SLOPE * SLOPE) * XOUT)

```

```

10 ISN 10 C = -(2.0 * SLOPE * XOUT * YOUT) + ((SLOPE * SLOPE) *
11 ISN 11 (XOUT * XOUT)) + (YOUT * YOUT) - 1.0
12 ISN 12 IMPX = (-B - DSORT((B * B) - (4 * A * C))) / (2 * A)
13 ISN 13 IMPY = (SLOPE * (IMPX - XOUT)) + YOUT
14 ISN 14 C Calculate impact point angle and arc length
15 ISN 15 THETA = DATAN (IMPY / DABS(IMPX))
16 ISN 16 ARC = CYLRAD * THETA
17 ISN 17 RETURN
18 ISN 18 END

```

STATISTICS SOURCE STATEMENTS = 16, PROGRAM SIZE = 840 BYTES, PROGRAM NAME = COLLID PAGE: 12

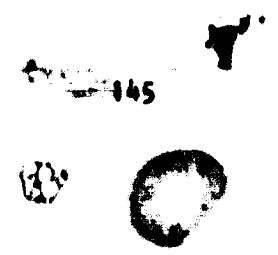
STATISTICS NO DIAGNOSTICS GENERATED.

***** END OF COMPILATION 4 *****

SUMMARY OF MESSAGES AND STATISTICS FOR ALL COMPILATIONS

STATISTICS SOURCE STATEMENTS = 69, PROGRAM SIZE = 2732 BYTES, PROGRAM NAME = MAIN PAGE: 1
STATISTICS NO DIAGNOSTICS GENERATED.
***** END OF COMPILATION 1 *****
STATISTICS SOURCE STATEMENTS = 33, PROGRAM SIZE = 338354 BYTES, PROGRAM NAME = TRAJEC PAGE: 7
STATISTICS NO DIAGNOSTICS GENERATED.
***** END OF COMPILATION 2 *****
STATISTICS SOURCE STATEMENTS = 23, PROGRAM SIZE = 1380 BYTES, PROGRAM NAME = ITERAT PAGE: 10
STATISTICS NO DIAGNOSTICS GENERATED.
***** END OF COMPILATION 3 *****
STATISTICS SOURCE STATEMENTS = 16, PROGRAM SIZE = 840 BYTES, PROGRAM NAME = COLLID PAGE: 12
STATISTICS NO DIAGNOSTICS GENERATED.
***** END OF COMPILATION 4 *****

***** SUMMARY STATISTICS ***** 0 DIAGNOSTICS GENERATED. HIGHEST SEVERITY CODE IS 0.



Appendix II

Program Listing: OMNICYL

CTIONS IN EFFECT: NOLIST NOMAP NOXREF NOGOSTMT NODACK SOURCE TERM OBJECT FILMED NOTEST SEQ
 OPTIMIZE(O) LANGVL(77) NOFIPS FLAG(I) NAME(MAIN) LINECOUNT(60)

1 2 3 4 5 6 7 8 9

C Cylinder Rime Icing Model

C Karen J. Finstad June, 1986

C This program will calculate and plot rime ice accretion
 C layers on a cylinder, as well as calculate the mass and
 C mean density of each layer. Local collision efficiencies
 C for each point on the surface are calculated as a cosine
 C function of the current local surface angle
 C and scaled to the value of stagnation line collision
 C efficiency (Beta zero), and maximum accretion angle
 C (Alpha max).

C Two forms of this function are used for droplet diameters
 C above and below 20 microns. Beta zero and Alpha max are
 C estimated from a non-linear regression fit to data computed
 C by droplet trajectory program GRAZE.

C Two optional procedures are available for treating
 C the effects of droplet size spectra, when the assumption
 C of a monodisperse population at the median-volume
 C diameter (mvd) becomes inaccurate (roughly, when the
 C mvd is less than 50 micron, for ground level wind speeds):
 C 1. The user may enter weighting factors for each
 C of 16 size bins of width 10 microns, or
 C 2. use a "simulated spectrum" curve for the local
 C collision efficiency (l.c.e.), which differs principally
 C from the cosine approximation by the addition of a "tail"
 C onto the maximum accretion limit. The length of this
 C tail is a function of the mvd. Again, there is a
 C slightly different form of the curve for mvd above and
 C below 20 microns.

C The first of these options is recommended only when
 C three or less layers are to be accreted, since the weighted
 C averaging procedure eventually produces first-order
 C discontinuities in the l.c.e. curve, and thus on the
 C modelled ice surface.

C Local density is calculated from an empirically-
 C derived function of local surface slope

C The cylinder may be rotated, clockwise, after each
 C layer is accreted. The rotation increment is included
 C in the input parameter list. When this option is
 C chosen, (i.e., if the input rotation increment is greater
 C than zero), the l.c.e. and local density are calculated
 C as a function of position angle, instead of surface angle
 C This somewhat less accurate method is necessary to avoid
 C problems when accreting over top of the previous layers.
 C accretion limit

C Also please note that rotation of more than 90 degrees
 C in total is not possible in this version.

17
 18
 19
 20
 21
 22
 23
 24
 25
 26
 27
 28
 29
 30
 31
 32
 33
 34
 35
 36
 37
 38
 39
 40
 41
 42
 43
 44
 45
 46
 47
 48
 49
 50
 51

1.....2.....3.....4.....5.....6.....7.....8.....9.....

The output consists of a plot description file written into -pdf attached to unit 8, and a mass and density table written into -mass attached to unit 9. (These are temporary files.)

The plot description file is produced using the system subroutine library *PLOTLIB. All of the plotting is done in a single program subroutine, so that other available plotting routines may be substituted if desired. Please note: in order to run *PLOTLIB subroutines (or any subroutines which have not been compiled in Fortran77 and which contain character strings or variables in their argument list), in conjunction with this program. (or any Fortran77 program) the command ePROCESS(list of subroutines) MUST appear in ROW 1, COLUMN 1 if the subroutines are called directly from MAIN. If they are called from another subroutine, the ePROCESS command must be placed in COLUMN 1 OF THE LINE IMMEDIATELY FOLLOWING THE END STATEMENT OF THE PREVIOUS ROUTINE.

This code will also run on the IBM Professional Fortran compiler for PC's and PC compatibles. A math co-processor and graphics capability is required. (Graphics routines must be supplied. A 6-layer accretion with rotation takes about 90 seconds on a standard PC. Storage needed is about 370,000 bytes.

To compile (on MTS), first empty -mass and -pdf. Then \$RUN *FORTRANVS SCARDS=OMNIC SPUNCH=CYLRUN.

To run, enter \$RUN CYLJUN*PLOTLIB. You will be prompted for the following input parameters:

- median volume droplet DIAMETER in microns
- y or n to enter full spectrum, followed by weights, entered individually
- y or n to simulated spectrum option
- cylinder RADIUS in metres
- free stream air speed in metres per second
- liquid water content in kg per cubic metre
- time step per layer in seconds
- total number of layers
- rotation increment in degrees

..... Subprograms

INTERNAL:

52. C
53. C
54. C
55. C
56. C
57. C
58. C
59. C
60. C
61. C
62. C
63. C
64. C
65. C
66. C
67. C
68. C
69. C
70. C
71. C
72. C
73. C
74. C
75. C
76. C
77. C
78. C
79. C
80. C
81. C
82. C
83. C
84. C
85. C
86. C
87. C
88. C
89. C
90. C
91. C
92. C
93. C
94. C
95. C
96. C
97. C
98. C
99. C
100. C
101. C
102. C
103. C
104. C
105. C
106. C
107. C

1 2 3 4 5 6 7 8 9

108. C SUBROUTINE DRAW - Plots cylinder profile and all
109. C accreted ice layers with appropriate legend.
110. C
111. C
112. C DOUBLE PRECISION FUNCTION MONBET - Estimates local
113. C collision efficiency as a function of surface slope for
114. C a monodisperse droplet population at the mvd. The
115. C function has two forms for use with mvd smaller or
116. C larger than 20 microns.
117. C
118. C SUBROUTINE PARAM - Estimates the stagnation line
119. C collision efficiency and maximum accretion angle
120. C for bare cylinders at atmospheric pressure of 100 kPa
121. C from a non-linear regression fit to data derived from
122. C droplet trajectory calculations.
123. C
124. C SUBROUTINE ROTAT1 - When the rotation increment
125. C is non-zero, this subroutine calculates the array
126. C of position angles for the current surface, to replace
127. C surface angles in the array ALPHA.
128. C
129. C SUBROUTINE ROTAT2 - shifts the array indices of
130. C the current LAYRX and LAYRY arrays to face the new
131. C free stream direction, which has been rotated
132. C according to the rotation increment.
133. C
134. C DOUBLE PRECISION FUNCTION SPCBET - Estimates local
135. C collision efficiency as a function of surface slope
136. C which simulates the effect of a typical droplet size
137. C spectrum centred on the mvd. The function has two forms
138. C for use with mvd smaller or larger than 20 microns.
139. C
140. C SUBROUTINE WT BET - Calculates weighted average of
141. C local collision efficiency estimates from FUNCTION
142. C MONBET, for droplet spectrum weights in 18 10-micron
143. C size bins.
144. C
145. C
146. C
147. C
148. C
149. C
150. C
151. C
152. C
153. C
154. C
155. C
156. C
157. C
158. C
159. C
160. C
161. C
162. C
163. C

EXTERNAL:

*PLOTLIB - The subroutines PLOTS, METRIC, PLOT, AXIS2,
LINE, SYMBOL and NUMBER (called from SUBROUTINE DRAW) are
found in the public system subroutine library *PLOTLIB.
(See note above regarding external subroutines in Fortran77).
..... Variable Dictionary

ALPHA - array of angles between surface normal
and the free stream direction

ALPHAM - Alpha max, the maximum impingement angle

AM - array of maximum impingement angles for
each size category of the droplet size
spectrum

1
2
3
4
5
6
7
8
9

164. C AREA - cross sectional area between
165. C adjacent points in the current layer
166. C (dimensioned in metres)
167. C
168. C BETA - local collision efficiency
169. C
170. C BZERO - stagnation line value of the local collision
171. C efficiency
172. C
173. C BZ - array of Bzero values for each size
174. C category of the droplet size spectrum
175. C
176. C CYLRAD - radius of cylinder in metres (INPUT)
177. C
178. C CYLX,CYLY - arrays containing non - dimensional x and
179. C y coordinates of the cylinder surface
180. C
181. C DI - array of 18,10-micron wide droplet
182. C diameter size bins
183. C
184. C DIAG - cross diagonal of the quadrilateral
185. C area used in mass calculations
186. C
187. C DROPLDI - droplet diameter in microns (INPUT)
188. C
189. C HALFPI - pi/2 (Fortran77 constant PARAMETER)
190. C
191. C LAREA - cross sectional area of the current layer
192. C in sq. metres
193. C
194. C LAYERS - integer number of layers
195. C
196. C LAYRX,LAYRY - array containing non - dimensional x and y
197. C coordinates of the accretion surfaces for
198. C up to 30 accretion layers
199. C
200. C LDENS - mean density of the current layer in kg/cubic m
201. C
202. C LMASS - mass of the current layer in kg per unit length
203. C
204. C LWC - liquid water content in kg per cubic metre
205. C (INPUT)
206. C
207. C L1,L2,L3 - dimensioned sides of the quadrilateral area
208. C defined by two adjacent points on the
209. C current surface and two on the surface below
210. C
211. C MASS - array of masses per unit length for areas
212. C defined by adjacent points, in kg
213. C
214. C PI - pi (Fortran77 constant PARAMETER)
215. C
216. C R - temporary variable for storing real result
217. C during conversion of the rotation increment
218. C an integer number of surface points
219. C

1 2 3 4 5 6 7 8 9

220. C RHO - array of local densities in kg/cubic metre
 221. C ROTN - no. of surface points in a rotation increment
 222. C RSPEED - rotation increment per layer in radians (INPUT)
 223. C SIMSPC - logical variable, true if simulated spectrum option is chosen
 224. C SIMOPT - character variable for reading in response to simulated spectrum option query (INPUT)
 225. C SLOPE - array of local surface slopes calculated at each surface point
 226. C SMOROP - logical flag for droplet size, which determines function used to calculate local c.e.
 227. C SPCOPT - character variable for reading in response to spectrum weighting option query (INPUT)
 228. C SPEC - logical variable, true if spectrum weighting option is chosen
 229. C S1,S2 - quantities used to determine the quadrilaterals for the layer area calculation
 230. C TAILEN - filter length for optional smoothing filter applied to c. e. curve
 231. C TAU - accretion time step in seconds (INPUT)
 232. C THICK - array of ice thicknesses normal to surface (non - dimensional)
 233. C TMASS - total mass of the accretion
 234. C VEL - free stream air speed in m per sec (INPUT)
 235. C WGT - array of droplet spectrum volume percentages for each size bin (INPUT)

.....

DOUBLE PRECISION ALPHA(600), CYLX(1202), CYLY(1202),
 LAYRX(30,600), LAYRY(30,600),
 RHO(600), SLOPE(600), THICK(600),
 DI(18), WGT(18), BZ(18), AM(18)

DOUBLE PRECISION ALPHA, AREA, BETA, BZERO, CYLRAD, DIAG,
 DROPTI, LAREA, LDENS, LMASS, LWC, L1, L2,
 L3, L4, MASS, RSPEED, S1, S2, TAILEN, TAU,
 TMASS, VEL

REAL R

ISN 1

ISN 2

ISN 3

1 2 3 4 5 6 7 8 9

```

276. C
277. C
278. C
279. C
280. C
281. C
282. C
283. C
284. C
285. C
286. C
287. C
288. C
289. C
290. C
291. C
292. C
293. C
294. C
295. C
296. C
297. C
298. C
299. C
300. C
301. C
302. C
303. C
304. C
305. C
306. C
307. C
308. C
309. C
310. C
311. C
312. C
313. C
314. C
315. C
316. C
317. C
318. C
319. C
320. C
321. C
322. C
323. C
324. C
325. C
326. C
327. C
328. C
329. C
330. C
331. C

ISN 4
ISN 5
ISN 6
ISN 7
ISN 8

ISN 9

ISN 10
ISN 11

ISN 12
ISN 13

ISN 14
ISN 15

ISN 16
ISN 17

ISN 18
ISN 19
ISN 21

ISN 22

      INTEGER          LAYERS,ROTN
      CHARACTER*1     SIMOPT,SPCOPT
      LOGICAL         SIMSPC,SMDROP,SPEC
      PARAMETER (PI = 3.1415926535897932,HALFPI = PI/2)
      COMMON CYLX,CYLY,LAYRX,LAYRY
      C Fill array of droplet diameter bins
      DATA (DI(I),I=1,18)/5.E-6,15.E-6,25.E-6,35.E-6,45.E-6,
      + 55.E-6,65.E-6,75.E-6,85.E-6,95.E-6,105.E-6,
      + 115.E-6,125.E-6,135.E-6,145.E-6,155.E-6,
      + 165.E-6,175.E-6/
      C Prepare mass table and plot description files.
      OPEN (UNIT = 8, FILE = '-MASS', STATUS = 'OLD')
      OPEN (UNIT = 9, FILE = '-PDF', STATUS = 'OLD')
      C Set up headings for mass and density table in -MASS.
      WRITE (8,110)
      110 FORMAT (///,15X,' Mass of Ice Accreted',//,5X,' Layer no.',
      + 7X,' Mass',7X,' Mean Density',///,
      + 20X,' (kg/m)',9X,' (kg/cu.m)',///,
      + '.....')
      C Write program title and intro to screen.
      WRITE (6,120)
      120 FORMAT (////, '..... CYLINDER RIME ICING MODEL .....',
      + '.....',//,20X,' Version Feb. 17, 1986',///,
      + 22X,' K. J. Finstad',//,19X,
      + ' Meteorology Division',//,15X,' The University of Alberta',
      + '///', ' Please enter parameters to begin accretion: ',///)
      C Prompt user for input parameters.
      WRITE (6,*) 'Median Volume Droplet DIAMETER in microns?'
      READ (5,*) DROPLDI
      C Set droplet size flag
      SMDROP = .FALSE.
      IF (DROPLDI.LT. 20) SMDROP = .TRUE.
      DROPLDI = DROPLDI*1.OE-6
      C Set flags for requested treatment of droplet spectrum.
      C If full spectrum weighting is requested, input volume
      C weights for each size bin.
      WRITE (6,*)
    
```

1.....2.....3.....4.....5.....6.....7.....8.....9.....

```

332. WRITE (6,*) 'Do you wish to enter full droplet spectrum?'
333. READ (5,9) SPCOPT
334. FORMAT (1A1)
335. SPEC = .FALSE.
336. IF ((SPCOPT.EQ. 'Y') OR. (SPCOPT.EQ. 'Y')) THEN
337. SPEC = .TRUE.
338. WRITE (6,*)
339. WRITE (6,*) 'Enter weight for the following size ranges:'
340. DO 13 I=1,18
341. WRITE (6,*)
342. WRITE (6,*) DI(I)/1.0E-6, 'microns'
343. READ (5,*) WGT(I)
344. CONTINUE
345. ELSE
346. WRITE (6,*)
347. WRITE (6,*) 'Do you wish simulated spectrum weighting?'
348. READ (5,8) SIMOPT
349. FORMAT (1A1)
350. ENDIF
351.
352. C For simulated spectrum, calculate 'tail' length from
353. C median volume diameter.
354. C
355. IF ((SIMOPT.EQ. 'Y') OR. (SIMOPT.EQ. 'Y')) THEN
356. SIMSPC = .TRUE.
357. IF (SIMDROPT) THEN
358. TAILLEN = 0.52 * DDEXP(-DROPTI / 7.0E-5)
359. ELSE
360. TAILLEN = 0.37 * DDEXP(-DROPTI / 7.0E-5)
361. ENDIF
362. ELSE
363. SIMSPC = .FALSE.
364. TAILLEN = 0.0
365. ENDIF
366.
367. WRITE (6,*)
368. WRITE (6,*) 'Cylinder RADIUS in metres?'
369. READ (5,*) CYLRAD
370.
371. WRITE (6,*)
372. WRITE (6,*) 'Free stream speed in m / sec?'
373. READ (5,*) VEL
374.
375. WRITE (6,*)
376. WRITE (6,*) 'Liquid water content in kg / cubic metre?'
377. READ (5,*) LWC
378.
379. WRITE (6,*)
380. WRITE (6,*) 'Time step per layer in seconds?'
381. READ (5,*) TAU
382.
383. WRITE (6,*)
384. WRITE (6,*) 'Total number of layers?'
385. READ (5,*) LAYERS
386.
387. C Bare cylinder will be layer 1, so add 1 to LAYERS

```

```

388. C
389. C
390. C
391. C
392. C
393. C
394. C
395. C
396. C
397. C
398. C
399. C
400. C
401. C
402. C
403. C
404. C
405. C
406. C
407. C
408. C
409. C
410. C
411. C
412. C
413. C
414. C
415. C
416. C
417. C
418. C
419. C
420. C
421. C
422. C
423. C
424. C
425. C
426. C
427. C
428. C
429. C
430. C
431. C
432. C
433. C
434. C
435. C
436. C
437. C
438. C
439. C
440. C
441. C
442. C
443. C
444. C
445. C
446. C
447. C
448. C
449. C
450. C
451. C
452. C
453. C
454. C
455. C
456. C
457. C
458. C
459. C
460. C
461. C
462. C
463. C
464. C
465. C
466. C
467. C
468. C
469. C
470. C
471. C
472. C
473. C
474. C
475. C
476. C
477. C
478. C
479. C
480. C
481. C
482. C
483. C
484. C
485. C
486. C
487. C
488. C
489. C
490. C
491. C
492. C
493. C
494. C
495. C
496. C
497. C
498. C
499. C
500. C
501. C
502. C
503. C
504. C
505. C
506. C
507. C
508. C
509. C
510. C
511. C
512. C
513. C
514. C
515. C
516. C
517. C
518. C
519. C
520. C
521. C
522. C
523. C
524. C
525. C
526. C
527. C
528. C
529. C
530. C
531. C
532. C
533. C
534. C
535. C
536. C
537. C
538. C
539. C
540. C
541. C
542. C
543. C
544. C
545. C
546. C
547. C
548. C
549. C
550. C
551. C
552. C
553. C
554. C
555. C
556. C
557. C
558. C
559. C
560. C
561. C
562. C
563. C
564. C
565. C
566. C
567. C
568. C
569. C
570. C
571. C
572. C
573. C
574. C
575. C
576. C
577. C
578. C
579. C
580. C
581. C
582. C
583. C
584. C
585. C
586. C
587. C
588. C
589. C
590. C
591. C
592. C
593. C
594. C
595. C
596. C
597. C
598. C
599. C
600. C
601. C
602. C
603. C
604. C
605. C
606. C
607. C
608. C
609. C
610. C
611. C
612. C
613. C
614. C
615. C
616. C
617. C
618. C
619. C
620. C
621. C
622. C
623. C
624. C
625. C
626. C
627. C
628. C
629. C
630. C
631. C
632. C
633. C
634. C
635. C
636. C
637. C
638. C
639. C
640. C
641. C
642. C
643. C
644. C
645. C
646. C
647. C
648. C
649. C
650. C
651. C
652. C
653. C
654. C
655. C
656. C
657. C
658. C
659. C
660. C
661. C
662. C
663. C
664. C
665. C
666. C
667. C
668. C
669. C
670. C
671. C
672. C
673. C
674. C
675. C
676. C
677. C
678. C
679. C
680. C
681. C
682. C
683. C
684. C
685. C
686. C
687. C
688. C
689. C
690. C
691. C
692. C
693. C
694. C
695. C
696. C
697. C
698. C
699. C
700. C
701. C
702. C
703. C
704. C
705. C
706. C
707. C
708. C
709. C
710. C
711. C
712. C
713. C
714. C
715. C
716. C
717. C
718. C
719. C
720. C
721. C
722. C
723. C
724. C
725. C
726. C
727. C
728. C
729. C
730. C
731. C
732. C
733. C
734. C
735. C
736. C
737. C
738. C
739. C
740. C
741. C
742. C
743. C
744. C
745. C
746. C
747. C
748. C
749. C
750. C
751. C
752. C
753. C
754. C
755. C
756. C
757. C
758. C
759. C
760. C
761. C
762. C
763. C
764. C
765. C
766. C
767. C
768. C
769. C
770. C
771. C
772. C
773. C
774. C
775. C
776. C
777. C
778. C
779. C
780. C
781. C
782. C
783. C
784. C
785. C
786. C
787. C
788. C
789. C
790. C
791. C
792. C
793. C
794. C
795. C
796. C
797. C
798. C
799. C
800. C
801. C
802. C
803. C
804. C
805. C
806. C
807. C
808. C
809. C
810. C
811. C
812. C
813. C
814. C
815. C
816. C
817. C
818. C
819. C
820. C
821. C
822. C
823. C
824. C
825. C
826. C
827. C
828. C
829. C
830. C
831. C
832. C
833. C
834. C
835. C
836. C
837. C
838. C
839. C
840. C
841. C
842. C
843. C
844. C
845. C
846. C
847. C
848. C
849. C
850. C
851. C
852. C
853. C
854. C
855. C
856. C
857. C
858. C
859. C
860. C
861. C
862. C
863. C
864. C
865. C
866. C
867. C
868. C
869. C
870. C
871. C
872. C
873. C
874. C
875. C
876. C
877. C
878. C
879. C
880. C
881. C
882. C
883. C
884. C
885. C
886. C
887. C
888. C
889. C
890. C
891. C
892. C
893. C
894. C
895. C
896. C
897. C
898. C
899. C
900. C
901. C
902. C
903. C
904. C
905. C
906. C
907. C
908. C
909. C
910. C
911. C
912. C
913. C
914. C
915. C
916. C
917. C
918. C
919. C
920. C
921. C
922. C
923. C
924. C
925. C
926. C
927. C
928. C
929. C
930. C
931. C
932. C
933. C
934. C
935. C
936. C
937. C
938. C
939. C
940. C
941. C
942. C
943. C
944. C
945. C
946. C
947. C
948. C
949. C
950. C
951. C
952. C
953. C
954. C
955. C
956. C
957. C
958. C
959. C
960. C
961. C
962. C
963. C
964. C
965. C
966. C
967. C
968. C
969. C
970. C
971. C
972. C
973. C
974. C
975. C
976. C
977. C
978. C
979. C
980. C
981. C
982. C
983. C
984. C
985. C
986. C
987. C
988. C
989. C
990. C
991. C
992. C
993. C
994. C
995. C
996. C
997. C
998. C
999. C
1000. C

```

```

LEVEL 1.1.1 (DEC 81)
VS FORTRAN DATE: JUL 24, 1986 TIME: 13:15:27 NAME: MAIN PAGE: 9
1.....1.....2.....3.....4.....5.....6.....7.....8.....9.....
444. 99 200 CONTINUE
445. C
446. C Initialize total mass and begin loop to accrete ice layers.
447. C
448. TMASS = 0.0
449. DO 300 J = 2,LAYERS
450. C
451. C Calculate slope and surface angle from finite differences for
452. C each point on current surface. If rotation increment is
453. C non-zero, call subroutine to calculate slopes and
454. C position angles instead.
455. C
456. IF (ROTN .GT. 0) THEN
457.   CALL ROTAT1(J,RSPEED,SLOPE,ALPHA)
458. ELSE
459.   DO 400 I = 2,599
460.     SLOPE(I) = (LAYRX(J-1,I+1) - LAYRX(J-1,I-1)) /
461.     + DABS(LAYRY(J-1,I+1) - LAYRY(J-1,I-1))
462.     IF (LAYRY(J-1,I+1) .LT. LAYRY(J-1,I-1)) THEN
463.       ALPHA(I) = DABS(PI - DATAN(SLOPE(I)))
464.     ELSE
465.       ALPHA(I) = DABS(DATAN(SLOPE(I)))
466.     ENDIF
467.   ENDIF
468. ENDIF
469. C
470. C Calculate for each point local density, collision efficiency and
471. C ice thickness. The method of calculation for Beta depends on
472. C the values of SMDROP, SPEC and SIMSPC.
473. C
474. DO 500 I = 2,599
475.   RHO(I) = 890.
476.   + (1.0 - .143 * (ALPHA(I))/(ALPHM+TAILEN)) -
477.   + .246 * ((ALPHA(I))/(ALPHM+TAILEN)) ** 2) -
478.   + .309 * ((ALPHA(I))/(ALPHM+TAILEN)) ** 3)
479. C
480. C Make sure density does not become too small
481. C
482. IF (RHO(I) .LT. 175.) RHO(I) = 175.
483. C
484. C Calculate local collision efficiency
485. C
486. IF (SPEC) THEN
487.   CALL WTBTET(ALPHA(I),SMDROP,BZ,AM,WGHT,BETA)
488. ELSE IF (SIMSPC) THEN
489.   BETA = SPCBET(ALPHA(I),SMDROP,BZERO,ALPHM,TAILEN)
490. ELSE
491.   BETA = MONBET(ALPHA(I),SMDROP,BZERO,ALPHM)
492. ENDIF
493. C
494. C Calculate local ice thickness perpendicular to surface
495. C (in non-dimensional units)
496. C
497. THICK(I) = BETA * VEL * TAU * LWC / (RHO(I) * CYLRAD)
498. C
499. C Define new layer surface coordinates.

```

```

500. C
501. IF (LAVRY(J-1,I) .LT. LAVRY(J-1,I-1)) THEN
502.   LAVRX(J,I) = LAVRX(J-1,I) + (THICK(I) *
503.     DCOS(DATAN(SLOPE(I))))
504. ELSE
505.   LAVRX(J,I) = LAVRX(J-1,I) - (THICK(I) *
506.     DCOS(DATAN(SLOPE(I))))
507. ENDIF
508. LAVRY(J,I) = LAVRY(J,I) + (THICK(I) *
509.   DSIN(DATAN(SLOPE(I))))
510. CONTINUE
511. LAVRX(J,1) = LAVRX(J-1,1)
512. LAVRX(J,600) = LAVRX(J-1,600)
513. LAVRY(J,1) = LAVRY(J-1,1)
514. LAVRY(J,600) = LAVRY(J-1,600)
515.
516. C Calculate mass and mean density of the layer from
517. C the sum of areas between surface points on successive
518. C layers. First, initialize layer mass and area.
519. C
520. LMASS = 0.0
521. LAREA = 0.0
522. DO 560 I = 2,598
523.   IF ((THICK(I) .GT. 0.0) .AND. (THICK(I+1) .GT. 0.0)) THEN
524.     L4 = THICK(I) * CYLRAD
525.     L1 = DSORT((LAVRX(J-1,I+1) - LAVRX(J-1,I))**2 + (LAVRY
526.       (J-1,I+1) - LAVRY(J-1,I))**2) * CYLRAD
527.     L3 = DSORT((LAVRX(J,I+1) - LAVRX(J,I))**2 + (LAVRY
528.       (J,I+1) - LAVRY(J,I))**2) * CYLRAD
529.     DIAG = DSORT((LAVRX(J,I+1)-LAVRX(J-1,I))**2 + (LAVRY
530.       (J,I+1) - LAVRY(J-1,I))**2) * CYLRAD
531.     S1 = 0.5 * (DIAG+L1+L2)
532.     S2 = 0.5 * (DIAG+L3+L4)
533.     AREA = DSORT(S1 * (S1-DIAG) + (S1-L1) * (S1-L2)) +
534.       DSORT(S2 * (S2-DIAG) + (S2-L3) * (S2-L4))
535.     MASS = ((RHO(I) + RHO(I+1)) / 2.0) * AREA
536.     LMASS = LMASS + MASS
537.     LAREA = LAREA + AREA
538.   ENDIF
539. CONTINUE
540.
541. C Calculate mean density.
542.
543. C
544. LDENS = LMASS/LAREA
545.
546. C Write results to mass table.
547. C
548. WRITE (8,570) J-1,LMASS,LDENS
549. FORMAT (//.8X,12.7X,19.5,7X,F9.5)
550.
551. C Add mass of current layer to total mass.
552. C
553. TMASS = TMASS + LMASS
554. C
555. C Call subroutine to rotate array indices if required.

```

1 2 3 4 5 6 7 8 9

```

556. C
557. C
558. C
559. C
560. C
561. C
562. C
563. C
564. C
565. C
566. C
567. C
568. C
569. C
570. C
571. C

```

```

      IF (ROTN .GT. 0) CALL ROTAT2(J,ROTN)
      300 CONTINUE
      Write total mass accreted to table
      WRITE (8,590) TMASS
      590 FORMAT ('X:/// Total mass accreted per metre: ',F9.5)
      Call subroutine to plot cylinder and accreted layers
      CALL DRAW(ALPHM,BZERO,CYLRAD,DROFDI,LAYERS,LWC,RSPEED,
      + SIMSPC,SPEC,TAILEN,TAU,VEL)
      999 STOP
      END

```

```

*STATISTICS* SOURCE STATEMENTS = 161, PROGRAM SIZE = 27174 BYTES, PROGRAM NAME = MAIN PAGE: 1
*STATISTICS* NO DIAGNOSTICS GENERATED.
***** END OF COMPILATION 1 *****

```


REQUESTED OPTIONS (PROCESS): SC(AXIS2,SYMBOL)

OPTIONS IN EFFECT: NOLIST NOMAP NOXREF NOGOSTMT NODACK SOURCE TERM OBJECT FIXED NOTEST / SEQ
 OPTIMIZE(O) LANGVL(77) NOFIPS FLAG(I) NAME(MAIN) LINECOUNT(60)

1 2 3 4 5 6 7 8 9

```

573 C
574 C
575 C SUBROUTINE DRAW - to plot cylinder and all accretion
576 C layers, with appropriate information
577 C in the legend. This subroutine uses
578 C the plotting library *PLOTLIB
579 C
580 C Input Variables : as defined for Main program :
581 C ALPHM,BZERO,CYLRAD,DROPDI,LAYERS,LWC,
582 C RSPEED,SIMSPC,SPEC,TAILEN,TAU,VEL
583 C
584 C Common Variables : CYLX,CVLY,LAYRX,LAYRY
585 C
586 C Other Variables : PLOTX,PLOTY - arrays containing x,y
587 C plotting data and scaling information
588 C for accretion layer currently being
589 C plotted
590 C
591 C
592 C
593 C SUBROUTINE DRAW(ALPHM,BZERO,CYLRAD,DROPDI,LAYERS,
594 C LWC,RSPEED,SIMSPC,SPEC,TAILEN,TAU,VEL)
595 C
596 C
597 C
598 C
599 C
600 C
601 C
602 C
603 C
604 C
605 C
606 C
607 C
608 C
609 C
610 C
611 C
612 C
613 C
614 C
615 C
616 C
617 C
618 C
619 C
620 C
621 C
622 C
623 C
624 C
625 C
626 C
627 C
628 C
629 C
630 C
631 C
632 C
633 C
634 C
635 C
636 C
637 C
638 C
639 C
640 C
641 C
642 C
643 C
644 C
645 C
646 C
647 C
648 C
649 C
650 C
651 C
652 C
653 C
654 C
655 C
656 C
657 C
658 C
659 C
660 C
661 C
662 C
663 C
664 C
665 C
666 C
667 C
668 C
669 C
670 C
671 C
672 C
673 C
674 C
675 C
676 C
677 C
678 C
679 C
680 C
681 C
682 C
683 C
684 C
685 C
686 C
687 C
688 C
689 C
690 C
691 C
692 C
693 C
694 C
695 C
696 C
697 C
698 C
699 C
700 C
701 C
702 C
703 C
704 C
705 C
706 C
707 C
708 C
709 C
710 C
711 C
712 C
713 C
714 C
715 C
716 C
717 C
718 C
719 C
720 C
721 C
722 C
723 C
724 C
725 C
726 C
727 C
728 C
729 C
730 C
731 C
732 C
733 C
734 C
735 C
736 C
737 C
738 C
739 C
740 C
741 C
742 C
743 C
744 C
745 C
746 C
747 C
748 C
749 C
750 C
751 C
752 C
753 C
754 C
755 C
756 C
757 C
758 C
759 C
760 C
761 C
762 C
763 C
764 C
765 C
766 C
767 C
768 C
769 C
770 C
771 C
772 C
773 C
774 C
775 C
776 C
777 C
778 C
779 C
780 C
781 C
782 C
783 C
784 C
785 C
786 C
787 C
788 C
789 C
790 C
791 C
792 C
793 C
794 C
795 C
796 C
797 C
798 C
799 C
800 C
801 C
802 C
803 C
804 C
805 C
806 C
807 C
808 C
809 C
810 C
811 C
812 C
813 C
814 C
815 C
816 C
817 C
818 C
819 C
820 C
821 C
822 C
823 C
824 C
825 C
826 C
827 C
828 C
829 C
830 C
831 C
832 C
833 C
834 C
835 C
836 C
837 C
838 C
839 C
840 C
841 C
842 C
843 C
844 C
845 C
846 C
847 C
848 C
849 C
850 C
851 C
852 C
853 C
854 C
855 C
856 C
857 C
858 C
859 C
860 C
861 C
862 C
863 C
864 C
865 C
866 C
867 C
868 C
869 C
870 C
871 C
872 C
873 C
874 C
875 C
876 C
877 C
878 C
879 C
880 C
881 C
882 C
883 C
884 C
885 C
886 C
887 C
888 C
889 C
890 C
891 C
892 C
893 C
894 C
895 C
896 C
897 C
898 C
899 C
900 C
901 C
902 C
903 C
904 C
905 C
906 C
907 C
908 C
909 C
910 C
911 C
912 C
913 C
914 C
915 C
916 C
917 C
918 C
919 C
920 C
921 C
922 C
923 C
924 C
925 C
926 C
927 C
928 C
929 C
930 C
931 C
932 C
933 C
934 C
935 C
936 C
937 C
938 C
939 C
940 C
941 C
942 C
943 C
944 C
945 C
946 C
947 C
948 C
949 C
950 C
951 C
952 C
953 C
954 C
955 C
956 C
957 C
958 C
959 C
960 C
961 C
962 C
963 C
964 C
965 C
966 C
967 C
968 C
969 C
970 C
971 C
972 C
973 C
974 C
975 C
976 C
977 C
978 C
979 C
980 C
981 C
982 C
983 C
984 C
985 C
986 C
987 C
988 C
989 C
990 C
991 C
992 C
993 C
994 C
995 C
996 C
997 C
998 C
999 C
1000 C
    
```

```

624. C
625. C Draw 6 by 9 inch box
626. C
627. CALL PLOT(2.0,2.0,-3)
628. CALL PLOT(0.0,6.0,3)
629. CALL PLOT(8.0,6.0,2)
630. CALL PLOT(9.0,0.0,2)
631. C
632. C Label axes and draw tics
633. C
634. CALL AXIS2(0.0,0.0,'X/CYL RAD',-8.9,0.0,0.0,-6.0,1.0,1.0)
635. CALL AXIS2(0.0,0.0,'Y/CYL RAD',8.6,0.90,0.0,-3.0,1.0,0.5)
636. C
637. C Write legends to top left corner
638. C
639. CALL SYMBOL(1.5,4.0,10,'DROPLET MVD' = ,0.0,15)
640. CALL NUMBER(2.6,5.4,0.10,DROPLD,0.0,07)
641. CALL SYMBOL(3.5,4.0,10,'M' ,0.0,01)
642. CALL SYMBOL(1.5,2.0,10,'CYL RADIUS' = ,0.0,15)
643. CALL NUMBER(2.6,5.2,0.10,CYL RAD,0.0,04)
644. CALL SYMBOL(3.5,5.2,0.10,'M' ,0.0,01)
645. CALL SYMBOL(1.5,0.0,10,'AIR SPEED' = ,0.0,15)
646. CALL NUMBER(2.6,5.0,0.10,VEL,0.0,02)
647. CALL SYMBOL(3.5,5.0,0.10,'M / SEC' ,0.0,07)
648. CALL SYMBOL(1.4,8.0,10,'LWC' = ,0.0,15)
649. CALL NUMBER(2.6,4.8,0.10,LWC,0.0,05)
650. CALL SYMBOL(3.5,4.8,0.10,'KG / M**3' ,0.0,09)
651. CALL SYMBOL(1.4,6.0,10,'TIME STEP' = ,0.0,15)
652. CALL NUMBER(2.6,4.6,0.10,TAU,0.0,02)
653. CALL SYMBOL(3.5,4.6,0.10,'SEC' ,0.0,03)
654. CALL SYMBOL(1.4,4.0,10,'BETA ZERO' = ,0.0,15)
655. CALL NUMBER(2.6,4.4,0.10,BZERO,0.0,03)
656. CALL SYMBOL(1.4,2.0,10,'ALPHA MAX' = ,0.0,15)
657. CALL NUMBER(2.6,4.2,0.10,(ALPH+TAILEN)*360/6.283,0.0,01)
658. CALL SYMBOL(3.5,4.2,0.10,'DEGREES' ,0.0,07)
659. CALL SYMBOL(1.4,0.0,10,'ROIN IMCR' = ,0.0,15)
660. CALL NUMBER(2.6,4.0,0.10,RSPEED*360/6.283,0.0,01)
661. CALL SYMBOL(3.5,4.0,0.10,'DEGREES' ,0.0,07)
662. CALL SYMBOL(1.3,8.0,10,'SPECTRUM' ,0.0,09)
663. IF (SPEC) THEN
664. CALL SYMBOL(2.6,3.8,0.10,'YES' ,0.0,03)
665. ELSE IF (SIMSPC) THEN
666. CALL SYMBOL(2.6,3.8,0.10,'SIMULATED' ,0.0,09)
667. ELSE
668. CALL SYMBOL(2.6,3.8,0.10,'NO' ,0.0,02)
669. ENDIF
670. C
671. C Draw initial cylinder surface
672. C
673. CALL LINE(CYLX,CYLY,4200,2.0)
674. C
675. C Transfer each layer in turn to the array holding
676. C the scaling parameters
677. C
678. DO 610 J = 2,LAYERS
679. DO 700 L = 1,600
    
```

1 2 3 4 5 6 7 8 9

```

ISN 57 PLOTX(L) = LAYRX(J,L)
ISN 58 PLOTY(L) = LAYRY(J,L)
ISN 59 CONTINUE
700 CONTINUE
C
C Draw accretion layer
683 C
684 C
685 C
686 C CALL LINE(PLOTX,PLOTY,600,2,0)
ISN 60 610 CONTINUE
ISN 61 C Close plotting library
C
C CALL PLOT(1.0,1.0,999)
ISN 62 RETURN
ISN 63 END
ISN 64

```

STATISTICS SOURCE STATEMENTS = 64, PROGRAM SIZE = 12132 BYTES, PROGRAM NAME = DRAW PAGE: 12.

STATISTICS NO DIAGNOSTICS GENERATED.

***** OF COMPILATION 2 *****

OPTIONS IN EFFECT: NOLIST NOMAP NOXREF NOGOSTMT NOCHECK SOURCE TERM OBJECT FIXED OPTIMIZE(Q) LANGVL(77) NOFIPS FLAG(I) NAME(MAIN) LIMECOUNT(60)

1 2 3 4 5 6 7 8

```

694 C .....
695 C .....
696 C .....
697 C .....
698 C .....
699 C .....
700 C .....
701 C .....
702 C .....
703 C .....
704 C .....
705 C .....
706 C .....
707 C .....
708 C .....
709 C .....
710 C .....
711 C .....
712 C .....
713 C .....
714 C .....
715 C .....
716 C .....
717 C .....
718 C .....
719 C .....
720 C .....
721 C .....
722 C .....
723 C .....

```

FUNCTION MONBET - Calculates local τ_e

estimate for monodisperse droplet populations at and either above or below 20 microns using a cosine curve scaled to the stagnation line c_s and the maximum accretion angle

Input Variables: as defined for main program: ALPHA, BZERO, ALPHA, SMDROP

DOUBLE PRECISION FUNCTION MONBET(ALPHA, SMDROP, BZERO, ALPHA)

DOUBLE PRECISION BZERO, ALPHA, ALPHA

LOGICAL SMDROP

PARAMETER (HALFPI = 3.1415926535897932/2.)

IF (ALPHA .GE. ALPHA) THEN
MONBET = 0.0

ELSE IF (SMDROP) THEN
MONBET = BZERO * (BZERO * (DSORT(DCOS(ALPHA)) - 1.0)) /
(1.0 - DSORT(DCOS(ALPHA)))

ELSE
MONBET = BZERO * (DCOS((ALPHA/ALPHA) * HALFPI))

ENDIF
RETURN
END

ISN 1 2 3 4 5 6 7 8 9 10 11 12 13

STATISTICS SOURCE STATEMENTS = 13, PROGRAM SIZE = 586 BYTES, PROGRAM NAME = MONBET PAGE: 15

STATISTICS NO DIAGNOSTICS GENERATED

***** END OF COMPILATION 3 *****

OPTIONS IN EFFECT: NOLIST NOMAP NOXREF NOGOSTMT NODDECK SOURCE TERM OBJECT FIXED
OPTIMIZE(O) LANGVL(77) NDFIPS FLAG(I) NAME(MAIN) LINECOUNT(60)

1 2 3 4 5 6 7 8 9

```

724 C .....
725 C .....
726 C * Subroutine PARAM - Estimates Beta zero and alpha max
727 C * from the input parameters according to
728 C * an empirical fit to droplet trajectories
729 C * calculated with program DROPSION.
730 C .....
731 C * Input variables : as defined for Main program:
732 C * CYLRAD, DROPDI, VEL
733 C .....
734 C * Output variables : as defined for Main program:
735 C * ALPHM, BZERO
736 C .....
737 C * Other variables :
738 C * RE - free stream Reynolds number
739 C * K - Langmuir inertia parameter
740 C * PHI - Langmuir parameter
741 C * TERM1, - terms used in the fitting function
742 C * TERM2,
743 C * TERM3
744 C * A(2,12) - array containing constants for
745 C * the fitting functions
746 C .....
747 C .....
748 C .....
749 C .....
750 C .....
751 C .....
752 C .....
753 C .....
754 C .....
755 C .....
756 C .....
757 C .....
758 C .....
759 C .....
760 C .....
761 C .....
762 C .....
763 C .....
764 C .....
765 C .....
766 C .....
767 C .....
768 C .....
769 C .....
770 C .....
771 C .....
772 C .....
773 C .....
774 C .....
775 C .....
776 C .....

```

```

SUBROUTINE PARAM (DROPDI,VEL,CYLRAD,BZERO,ALPHM)
DOUBLE PRECISION ALPHM,BZERO,CYLRAD, DROPDI,K,
PHI,RE,TERM1,TERM2,TERM3,VEL
DOUBLE PRECISION A(2,12)
DATA (A(1,I), I=1,12)/1.215,-7.42D-3,-0.561,-0.644,-0.164,
3.05D-3,0.43D,2.22,-0.45,-0.767,-0.806,-0.068,
DATA (A(2,I), I=1,12)/2.327,-4.09D-3,-0.388,-0.593,-0.689,
8.5D-3,0.383,1.757,-0.298,-0.42,-0.96,-0.179/

```

```

C Calculate free stream Reynolds number, phi and K assuming
C water density is 1000, air density 1.323 and air
C viscosity 1.669 in MKS units. These correspond to
C an air temperature of -10 C and pressure 100 kPa.
RE = DROPDI * VEL / 1.262E-5
K = (VEL * DROPDI * DROPDI** 3.329E6) / CYLRAD
PHI = (RE * RE) / K

```

```

C Calculate Beta zero and alpha max
DO 10 I = 1,2
TERM1 = (A(I,7) * (K ** A(I,2))) * DEXP(A(I,3) * K ** A(I,4)))
+ A(I,5)
TERM2 = A(I,6) * (PHI ** A(I,7))

```

```

1 ..... 1 ..... 2 ..... 3 ..... 4 ..... 5 ..... 6 ..... 7 ..... 8 ..... 9 .....
12 777. TERM3 = (A(I,8) * (K ** A(I,9))) * DEXP(A(I,10) * K ** A(I,11))
13 778. + A(I,12)
14 779. IF (I .EQ. 1) THEN
15 780. BZERO = TERM1 - (TERM2 * TERM3)
16 781. ELSE
17 782. ALPHM = TERM1 - (TERM2 * TERM3)
18 783. ENDIF
19 784. 10 CONTINUE
20 785. C
21 786. C Check for extreme values of K
22 787. C
23 788. IF (K .LT. 0.17) THEN
24 789. ALPHM = 0.0
25 790. BZERO = 0.0
26 791. ELSE IF (K .GT. 1000.) THEN
27 792. ALPHM = 1.56
28 793. BZERO = 0.99
29 794. ENDDIF
30 795. RETURN
31 796. END

```

STATISTICS SOURCE STATEMENTS = 27, PROGRAM SIZE = 1362 BYTES, PROGRAM NAME = PARAM PAGE: 16.

STATISTICS NO DIAGNOSTICS GENERATED.

***** END OF COMPILATION 4 *****


```

1 .....2 .....3 .....4 .....5 .....6 .....7 .....8 .....9
ISN 17      ENDIF
ISN 18      ENDIF
      C Calculate position angles.
853.      C
854.      IF (LAYRX(J-1,I) .EQ. 1.0) THEN
855.          ALPHA(I) = DABS(HALFPI - ((J-2) * RSPEED))
856.      ELSE IF (LAYRX(J-1,I) .GT. 1.0) THEN
857.          ALPHA(I) = HALFPI - ((J-2)*RSPEED) +
858.              DATAN((LAYRX(J-1,I) - 1.) / LAYRY(J-1,I))
859.      ELSE
860.          IF (DABS(LAYRY(J-1,I)) .LT. 1.00-10) LAYRY(J-1,I) = 0.0
861.          IF (DABS(LAYRX(J-1,I)) .LT. 1.00-10) LAYRX(J-1,I) = 0.0
862.          ALPHA(I) = DABS(DATAN(LAYRY(J-1,I) /
863.              (1.0 - LAYRX(J-1,I))) - ((J-2)*RSPEED))
864.
865.      ENDIF
866.      590 CONTINUE
867.      C
868.      RETURN
869.      END

```

STATISTICS SOURCE STATEMENTS = 29, PROGRAM SIZE = 1998 BYTES, PROGRAM NAME = ROTAT1 PAGE: 18.

STATISTICS NO DIAGNOSTICS GENERATED.

*..... END OF COMPILATION 5

OPTIONS IN EFFECT: NOLIST NOMAP NOXREF NOGOSTMT NODECK SOURCE TERM ORANGE FIXED OPTIMIZE(O) LANGVL(77) NOFIPS FLAG(F) NAME(MAIN) INECOUNT(60) NOTEST SEO

1 2 3 4 5 6 7 8 9

```

914 C .....
915 C .....
916 C * Function SPCBET - Estimates Beta(alpha) for a
917 C * simulated droplet size distribution. for an
918 C * mvd either smaller or larger than 20 microns.
919 C * The polynomial function is scaled to (alpha
920 C * max + tail length), where the tail length
921 C * is a function of the mvd.
922 C .....
923 C * Input Variables : as defined for Main program:
924 C * ALPHA,ALPHM,BZERO,SMDROP,TAILEN
925 C .....
926 C * Other Variables : X - scaled angle = Alpha /
927 C * (Alpha + Tailen)
928 C .....
929 C .....
930 C .....
931 C .....
932 C .....
933 C .....
934 C * DOUBLE PRECISION.FUNCTION SPCBET(ALPHA,SMDROP,BZERO,
935 C * ALPHM,TAILEN)
936 C .....
937 C .....
938 C .....
939 C .....
940 C .....
941 C .....
942 C .....
943 C .....
944 C .....
945 C .....
946 C .....
947 C .....
948 C .....
949 C .....
950 C .....
951 C .....
952 C .....
953 C .....
954 C .....
955 C .....
956 C .....
957 C .....
958 C .....
959 C .....
960 C .....
961 C .....
962 C .....
963 C .....
964 C .....
965 C .....
966 C .....
967 C .....
968 C .....
969 C .....
970 C .....
971 C .....
972 C .....
973 C .....
974 C .....
975 C .....
976 C .....
977 C .....
978 C .....
979 C .....
980 C .....
981 C .....
982 C .....
983 C .....
984 C .....
985 C .....
986 C .....
987 C .....
988 C .....
989 C .....
990 C .....
991 C .....
992 C .....
993 C .....
994 C .....
995 C .....
996 C .....
997 C .....
998 C .....
999 C .....

```

STATISTICS SOURCE STATEMENTS = 16, PROGRAM SIZE = 708 BYTES, PROGRAM NAME = SPCBET PAGE: 21
STATISTICS NO DIAGNOSTICS GENERATED.
***** END OF COMPILATION 7 *****

OPTIONS IN EFFECT: NOLIST,NOMAP,NOMSET,NODGSTMT,NODECK,SOURCE,TERM,OBJECT,FIXED,OPTIMIZE(O),LANGVL(77),NOFIPS,FLAG(I),NAME(MAIN),LINECOUNT(60),NOTEST,SEO

1 2 3 4 5 6 7 8 9

```

954. C .....
955. C .....
956. C SUBROUTINE WTBTET - Calculates the average local .....
957. C collision efficiency according to .....
958. C the input volume weighted droplet .....
959. C size spectrum. ....
960. C .....
961. C Input Variables : as defined for Main program. ....
962. C ALPHA,AM,BZ,SMDROP,WGHT .....
963. C .....
964. C Output Variables : as defined for Main program: .....
965. C BETA .....
966. C .....
967. C .....
968. C .....

```

969. C SUBROUTINE WTBTET(ALPHA,SMDROP,BZ,AM,WGHT,BETA)

970. C DOUBLE PRECISION AM(18),BZ(18),WGHT(18)

971. C DOUBLE PRECISION ALPHA,BETA

972. C LOGICAL SMDROP.

973. C BETA = 0.0

974. C DO 22 L=1,18

975. C IF (WGHT(L) .NE. 0.0) THEN

976. C BETA = BETA + WGHT(L) * MONSET(

977. C ALPHA(I),BZ(L),AM(L),SMDROP)

978. C ENDIF

979. C 22 CONTINUE

980. C RETURN

981. C END

982. C

983. C

984. C

985. C

986. C

987. C

988. C

989. C

990. C

991. C

992. C

STATISTICS SOURCE STATEMENTS = 12, PROGRAM SIZE = 654 BYTES, PROGRAM NAME = WTBTET PAGE: 22

STATISTICS NO DIAGNOSTICS GENERATED.

***** END OF COMPILATION 8 *****

SUMMARY OF MESSAGES AND STATISTICS FOR ALL COMPILATIONS

STATISTICS SOURCE STATEMENTS = 161, PROGRAM SIZE = 27174 BYTES, PROGRAM NAME = MAIN PAGE: 1
STATISTICS NO DIAGNOSTICS GENERATED. 4
***** END OF COMPILATION 1 *****
STATISTICS SOURCE STATEMENTS = 64, PROGRAM SIZE = 12132 BYTES, PROGRAM NAME = DRAW PAGE: 12
STATISTICS NO DIAGNOSTICS GENERATED.
***** END OF COMPILATION 2 *****
STATISTICS SOURCE STATEMENTS = 13, PROGRAM SIZE = 586 BYTES, PROGRAM NAME = MONBET PAGE: 15
STATISTICS NO DIAGNOSTICS GENERATED.
***** END OF COMPILATION 3 *****
STATISTICS SOURCE STATEMENTS = 27, PROGRAM SIZE = 1362 BYTES, PROGRAM NAME = PARAM PAGE: 16
STATISTICS NO DIAGNOSTICS GENERATED.
***** END OF COMPILATION 4 *****
STATISTICS SOURCE STATEMENTS = 29, PROGRAM SIZE = 1998 BYTES, PROGRAM NAME = ROTAT1 PAGE: 18
STATISTICS NO DIAGNOSTICS GENERATED.
***** END OF COMPILATION 5 *****
STATISTICS SOURCE STATEMENTS = 16, PROGRAM SIZE = 780 BYTES, PROGRAM NAME = ROTAT2 PAGE: 20
STATISTICS NO DIAGNOSTICS GENERATED.
***** END OF COMPILATION 6 *****
STATISTICS SOURCE STATEMENTS = 16, PROGRAM SIZE = 708 BYTES, PROGRAM NAME = SPCBET PAGE: 21
STATISTICS NO DIAGNOSTICS GENERATED.
***** END OF COMPILATION 7 *****
STATISTICS SOURCE STATEMENTS = 12, PROGRAM SIZE = 654 BYTES, PROGRAM NAME = WT BET PAGE: 22
STATISTICS NO DIAGNOSTICS GENERATED.
***** END OF COMPILATION 8 *****
***** SUMMARY STATISTICS ***** 0 DIAGNOSTICS GENERATED HIGHEST SEVERITY CODE IS 0

Appendix III

Approximation of the mvd from Stagnation Line Thickness

The measurement of water droplet sizes and size distributions is one of the major experimental problems in icing studies. The very common measurement technique, known as the oil slide method, has been shown by Makkonen and Stallabrass (1984) to overestimate the median volume diameters of observed droplet spectra in comparison to measurements made with an optical sizing probe, the Forward Scattering Spectrometer Probe, or FSSP, manufactured by Particle Measuring Systems and described by Knollenberg (1981). Makkonen and Stallabrass provide an empirical correction formula for oil slide measured mvds in the range 10 to 40 μm , as follows:

$$\text{mvd}_{\text{FSSP}} = 8.8 + 0.27 \text{ mvd}_{\text{oil slide}} \quad \text{A.1}$$

All of the wind tunnel experiments performed in the FROST tunnel and described in this thesis have had droplet size distributions determined by the oil slide method. The mvds derived from this data appear to be too large, not only in light of Makkonen and Stallabrass' results, but also because the theoretical collection efficiencies calculated

for these mvd's imply a minimum stagnation line thickness much larger than that observed.

In order to supply the most accurate input data possible to the model, these oil slide measurement should be corrected. However, some of the circular cylinder cases lie outside of the range given for Equation A.1. For these cases an approximate mvd has been derived from the observed stagnation line thicknesses of accreted ice, using the method outlined below, similar to the rotating cylinder methods which have been used for the same purpose.

For cases which lie inside the range of validity, these approximate mvd's agree well (within about 10 per cent) with the results of Equation A.1. The correlation of Makkonen and Stallabrass has therefore been used for all cases within the appropriate range.

Outside of that range, however, it is important to remember that the approximation given here is derived independently of the actual size spectrum, and represents a droplet size corresponding to the average value of β_0 for the time period of the accretion layer. It has been used here only because of the absence of a reliable calibration for oil slide measurements of droplets larger than 40 μm .

The method is as follows:

1. The stagnation line thickness (T_h) of the chosen layer is measured from a photograph of the accretion in cross-section.
2. A first estimate of β_0 is calculated from applying

the dry growth equation to the stagnation line:

$$\beta_0 = (\rho_0 Th) / (U lwc \tau) \quad A.2$$

A best estimate of ρ_0 may be made as in Chapter IV. For lwc , the first guess is made using the oil slide mvd , and the measured rate of mass collected on a small rotating cylinder, and calculated by the algorithm given by Stallabrass (1978)

3. Calculate the Stokes parameter

$$\phi = 9 \rho_a^2 D_c U / (\mu \rho_d) \quad A.3$$

then read from Figure II.3, a value of K corresponding to ϕ and β_0 .

4. Derive a new value of mvd from the definition of K :

$$K = (\rho_d / 18 \mu) (mvd^2 U / D_c) \quad A.4$$

5. Recalculate lwc using the new mvd .
6. Recalculate β_0 from new lwc . Repeat steps 2 through 6 until the values of β_0 , mvd and lwc appear to have converged.

For the examples given below, the rotating cylinder diameter was 2.46 mm.

Example 1:

oil slide mvd = 24.2 μm

Th = 1.49 mm

U = 10.7 m/sec

τ = 600 sec

ρ_0 = 750 kg/m^3

rotating cylinder mass = 0.029 g/min

revised mvd = 13.8 μm

mvd from Equation A.1 = 15.3 μm

Example 2:

oil slide mvd = 136 μm

Th = 13.5 mm

U = 10.24 m/sec

τ = 1800 sec

ρ_0 = 890 kg/m^3

rotating cylinder mass = 0.122 g/min

revised mvd = 62 μm

References

Knollenberg, R.G. 1981: Techniques for Probing Cloud Microstructure. Clouds, Their Formation, Optical Properties, and Effects, ed.s P.V. Hobbs and A. Deepak. Academic Press, 15-92.

Makkonen, L. and Stallabrass, J.R. 1984: Ice Accretion on Cylinders and Wires. National Research Council, Division of Mechanical Engineering, Technical Report TR-LT-005, 50 pp.

Stallabrass, J.R. 1978: National Research Council, Division of Mechanical Engineering, Technical Report TR-LT-92, 26 pp., 7 fig.s, + 2 App.s.

Appendix IV

A Geometrical Derivation of Equation V.3

Figure A.1 illustrates two droplet trajectories impinging on an airfoil, at zero angle of attack. If the initial separation of the trajectories is Δy , then the distance separating them (in the direction normal to the lower trajectory) will have increased at the point of impact to, say, $(\Delta y + a)$. Referring to Figure A.1, if the angle γ is the departure from horizontal of the tangent to the upper trajectory at the point X, it follows that for small Δl :

$$\cos(\alpha + \gamma) = (\Delta y + a) / \Delta l = \beta + (a / \Delta l), \quad \text{A.5}$$

using the definition of β given in Chapter II.

For airfoils, γ is always $\ll \alpha$, so:

$$\cos(\alpha + \gamma) = \cos \alpha \quad \text{A.6}$$

Now if it is assumed that $(a / \Delta l)$ is approximately a constant, and applying the boundary condition at $\alpha = 0$; this gives:

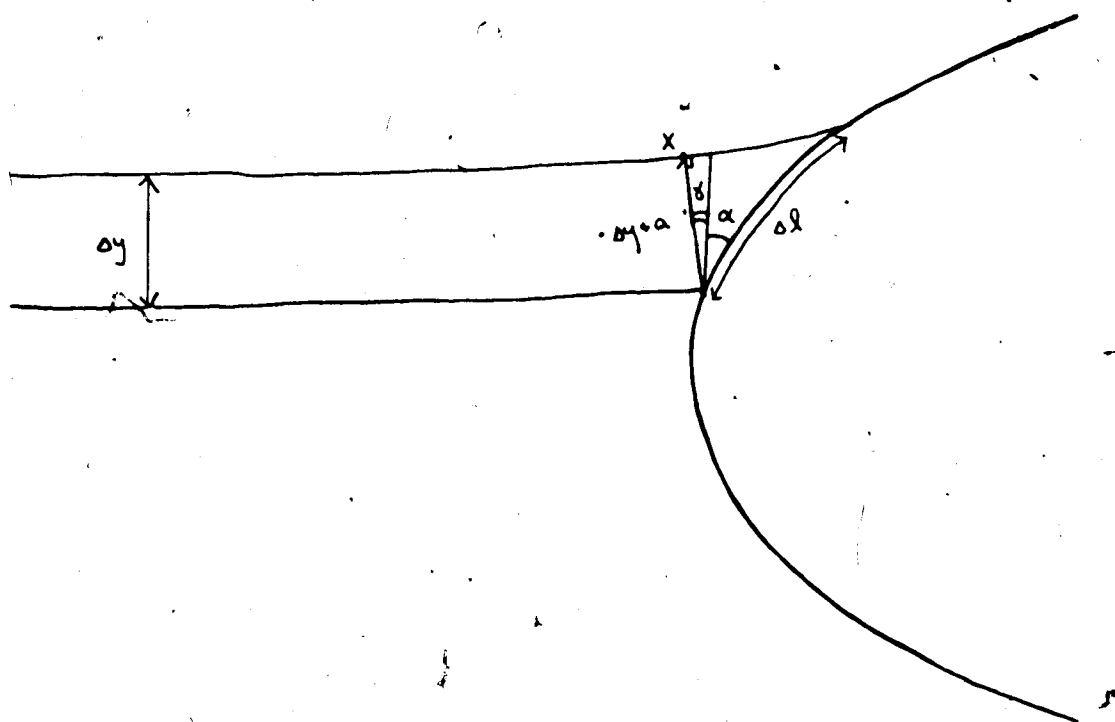


Figure A.1 - Droplet trajectories impinging on an airfoil.

$$\beta = \cos \alpha - (1 - \beta_0),$$

A.7

which is Equation V.3. The above approximation should then hold when the impinging trajectories have small curvature.

Appendix V

Program Listing: OMNIFOIL

NOTEST SEQ

OPTIONS IN EFFECT: NOLIST NOMAP NOXREF NOGDSTMT NMODECK SOURCE TERM OBJECT FIXED
OPTIMIZE(O) LANGLVL(77) NOFIPS FLAG(I) NAME(MAIN) LINECOUNT(6Q)

1. 2. 3. 4. 5. 6. 7. 8. 9.

***** Airfoil Rime Icing Model *****

Karen J. Finstad June, 1986

This program will calculate and plot rime ice accretion layers on an airfoil, as well as calculate the mass and mean density of each layer. Local collision efficiencies for each point on the surface are calculated as a cosine function of the current local surface angle and scaled to the value of stagnation line collision efficiency (Beta zero), which is determined from droplet trajectory calculations.

Beta zero is updated on every fourth layer to account for the changing flow around the accretion. Layer time steps should be chosen so that Beta zero is updated at reasonable intervals, say after a maximum thickness of no more than 1/10 of the chord length has been accreted.

The maximum accretion angle, alpha max, is determined from Beta zero.

When the angle of attack is zero, a "skewed spectrum" version of local collision efficiency distribution may be used to approximate the effects of droplet size spectra with median volume diameters less than about 20 microns. Larger drops are well represented by the monodisperse version of collision efficiency parameterisation at the mvd.

For other angles of attack, an approximate "skewed" distribution is used, which should apply to all droplet sizes.

Local density is approximated by a polynomial function of the local surface slope.

The output consists of a plot description file written into -pdf attached to unit 8, and a mass and density table written into -mass attached to unit 9. (A negative sign identifies temporary files on MTS.)

The plot description file is produced using the system subroutine library *PLOTLIB. All of the plotting is done in a single program subroutine, so that other available plotting routines may be substituted if desired.

An additional external subroutine, from the *IMSLDPLIB library, is used in the solution of the potential flow. Other matrix inversion routines may be substituted.

Please note: in order to run *PLOTLIB subroutines (or any subroutines which have not been compiled in Fortran77 and which contain character strings or variables in their

1. C
2. C
2.2 C
2.4 C
3. C
4. C
5. C
6. C
7. C
8. C
9. C
10. C
11. C
12. C
13. C
14. C
15. C
16. C
17. C
18. C
19. C
20. C
21. C
22. C
23. C
24. C
25. C
26. C
27. C
28. C
29. C
30. C
31. C
32. C
33. C
34. C
35. C
36. C
37. C
38. C
39. C
40. C
41. C
42. C
43. C
44. C
45. C
46. C
47. C
48. C
49. C
50. C
51. C

1 2 3 4 5 6 7 8 9

argument list), in conjunction with this program, or any
 Fortran77 program) the command ePROCESS(list of subroutines)
 MUST appear in ROW 1, COLUMN 1 if the subroutines are
 called directly from MN. If they are called from
 another subroutine, the ePROCESS command must be placed
 in COLUMN 1 OF THE LINE IMMEDIATELY FOLLOWING THE END
 STATEMENT OF THE PREVIOUS ROUTINE.

To compile (on MTS), first empty -mass and -pdf. Then
 \$RUN *FORTRANVS SCARDS=OMNIFOIL SPUNCH=FOILRUN

To run, enter \$RUN FOILRUN+*IMSLDPLIB+*PLOTLIB.
 You will be prompted for the following input parameters:

median volume droplet DIAMETER in microns.

y or n to simulated spectrum option

airfoil chord length in metres

NACA airfoil height as fraction of chord

free stream air speed in metres per second

liquid water content in kg per cubic metre

time step per layer in seconds

total number of layers

angle of attack of the free stream in degrees

OR, input data may be entered in a file. You must
 then specify "5 = filename" in the \$RUN command.

..... Subprograms

INTERNAL:

SUBROUTINE DRAW - Plots airfoil profile and all
 accreted ice layers with appropriate legend.

SUBROUTINE DROPS - Integrates droplet trajectories
 and calculates stagnation line collision efficiency.
 Subroutines called only from within DROPS (COLLID,
 FLOWXY, KCALC, POFLO, TRAJEC) are described in the program
 summary to DROPS.

DOUBLE PRECISION FUNCTION ONEBET - Estimates local
 collision efficiency as a function of surface slope for
 a monodisperse droplet population at the end.

DOUBLE PRECISION FUNCTION PHIBET - calculates local
 collision efficiency as a function of slope w.r.t to
 free stream direction, and distance from the maximum

52. C
 53. C
 54. C
 55. C
 56. C
 57. C
 58. C
 59. C
 60. C
 61. C
 62. C
 63. C
 64. C
 65. C
 66. C
 67. C
 68. C
 69. C
 70. C
 71. C
 72. C
 73. C
 74. C
 75. C
 76. C
 77. C
 78. C
 79. C
 80. C
 81. C
 82. C
 83. C
 84. C
 85. C
 86. C
 87. C
 88. C
 89. C
 90. C
 91. C
 92. C
 93. C
 94. C
 95. C
 96. C
 97. C
 98. C
 99. C
 100. C
 101. C
 102. C
 103. C
 104. C
 105. C
 106. C
 107. C

1.....2.....3.....4.....5.....6.....7.....8.....9.....

108 local value of collision efficiency (set to 0.95 times
 109 the value for zero angle of attack). The location of
 110 the maximum is estimated from a correlation derived
 111 from previous numerical results
 112
 113
 114
 115
 116
 117
 118
 119
 120
 121
 122
 123
 124
 125
 126
 127
 128
 129
 130
 131
 132
 133
 134
 135
 136
 137
 138
 139
 140
 141
 142
 143
 144
 145
 146
 147
 148
 149
 150
 151
 152
 153
 154
 155
 156
 157
 158
 159
 160
 161
 162
 163

DOUBLE PRECISION FUNCTION SPBET - Estimates local
 collision efficiency as a function of surface slope
 for an average distribution shape of droplet sizes,
 scaled to the mvd. The function assumes that small
 droplets dominate in the spectrum, with mvd less than
 about .20 microns.

EXTERNAL:

*IMSLDPLIB - The subroutine LEQ1IF is used to solve
 the matrix of potential vorticities for the potential
 flow calculation in subroutine DROPS.
 *PLOTLIB - The subroutines PLOTS, METRIC, PLOT, AXIS2,
 LINE, SYMBOL and NUMBER (called from SUBROUTINE DRAW) are
 found in the public system subroutine library *PLOTLIB.
 (See note above regarding external subroutines in Fortran77).

***** Variable Dictionary *****

- ALPHA - array of angles between surface normal
and the free stream direction
- ALPHM - Alpha max, the maximum impingement surface
angle
- APHI - parameter for determining the distribution
of collision efficiency and of density
about the position of maximum c.e. when
phi is non-zero.
- AREA - cross sectional area between
adjacent points in the current layer
(dimensioned in metres)
- AZERO - the surface angle of maximum collision
efficiency when phi is non-zero.
determined from an approximating
expression.
- BETA - local collision efficiency.
- BZERO - stagnation line value of the local collision
efficiency
- CHORD - length of airfoil chord plus accreted ice
- CHORD1 - length of bare airfoil chord in metres

1 2 3 4 5 6 7 8 9

- 164. C (INPUT)
- 165. C
- 166. C - cross diagonal of the quadrilateral of AREA
- 167. C
- 168. C - droplet diameter in microns (INPUT)
- 169. C
- 170. C - airfoil thickness as a fraction of the chord length (INPUT)
- 171. C
- 172. C
- 173. C
- 174. C - pi/2 (Fortran77 constant PARAMETER)
- 175. C
- 176. C - cross sectional area of the current layer in sq. metres
- 177. C
- 178. C
- 179. C - integer number of layers
- 180. C
- 181. C - array containing non - dimensional x and y coordinates of the accretion surfaces for up to 30 accretion layers
- 182. C
- 183. C
- 184. C
- 185. C - mean density of the current layer in kg/cubic m
- 186. C
- 187. C - mass of the current layer in kg per unit length
- 188. C
- 189. C - liquid water content in kg per cubic metre (INPUT)
- 190. C
- 191. C
- 192. C - dimensional sides of the quadrilateral area defined by two adjacent points on the current surface and two on the surface below
- 193. C
- 194. C
- 195. C
- 196. C - array of masses per unit length for areas defined by adjacent points, in kg
- 197. C
- 198. C
- 199. C - number of points defining the initial airfoil surface (note not the same as for potential flow calculation)
- 200. C
- 201. C
- 202. C
- 203. C - arrays of non-dimensional x,y points of the front of the initial surface, for plotting
- 204. C
- 205. C
- 206. C
- 207. C - angle of attack of the free stream (INPUT)
- 208. C
- 209. C - pi (Fortran77 constant PARAMETER)
- 210. C
- 211. C
- 212. C
- 213. C - array of local densities in kg/cubic metre
- 214. C
- 215. C - logical variable, true if simulated spectrum option is chosen
- 216. C
- 217. C - character variable for reading in response to simulated spectrum option query (INPUT)
- 218. C
- 219. C

1 2 3 4 5 6 7 8 9

```

220. C
221. C
222. C
223. C
224. C
225. C
226. C
227. C
228. C
229. C
230. C
231. C
232. C
233. C
234. C
235. C
236. C
237. C
238. C
239. C
240. C
241. C
242. C
243. C
244. C
245. C
246. C
247. C
248. C
249. C
250. C
251. C
252. C
253. C
254. C
255. C
256. C
257. C
258. C
259. C
260. C
261. C
262. C
263. C
264. C
265. C
266. C
267. C
268. C
269. C
270. C
271. C
272. C
273. C
274. C
275. C

SLOPE - array of local surface slopes calculated
        at each surface point

S1,S2 - quantities used to determine the quadrilaterals
        for the layer area calculation

TAILEN - filter length for optional smoothing filter
        applied to C. e. curve

TAU - accretion time step in seconds (INPUT)

TH - accumulated stagnation line thickness

THICK - array of ice thicknesses normal to surface

TMASS - total mass of the accretion

VEL - free stream air speed in m per sec (INPUT)

XFOIL, - arrays containing dimensional x and
YFOIL, y coordinates of the airfoil surface

.....

DOUBLE PRECISION ALPHA(600), GAMMA(41), LAYRX(20,300),
+ LAYRY(20,300), PFOILX(302), PFOILY(302),
+ RHO(300), SLOPE(300), THICK(300),
+ XFOIL(600), YFOIL(600)

DOUBLE PRECISION AZERO, ALPHA, APhi, AREA, BETA, BZERO,
+ CHORD, CHORD1, DIAG, DROPOI, H, LAREA, LDENS,
+ LMASS, LWC, L1, L2, L3, L4, MASS, PHI, S1,
+ S2, TAILLEN, TAU, TH, TMASS, VEL

INTEGER LAYERS, NPOINT

CHARACTER*1 SIMOPT

LOGICAL SIMSPC

PARAMETER (PI = 3.1415926535897932, HALFPI = PI/2)

COMMON /MN/XFOIL, YFOIL, GAMMA/DR/LAYRX, LAYRY, PFOILX, PFOILY

Prepare mass table and plot description files.

OPEN (UNIT = 8, FILE = '-MASS', STATUS = 'UNKNOWN')
OPEN (UNIT = 9, FILE = '-PDF', STATUS = 'UNKNOWN')

Set up headings for mass and density table in -MASS.

WRITE (8,110)
110 FORMAT (///,15X, 'Mass of Ice Accreted',///,5X, 'Layer no.',
+ 7X, 'Mass', 7X, 'Mean Density',///,
+ 20X, '(kg/m)', 9X, '(kg/cu.m)',///)

```

```

1 ..... 2 ..... 3 ..... 4 ..... 5 ..... 6 ..... 7 ..... 8 ..... 9 .....
+ .....
C Write program title and intro to screen.
C
C
C WRITE (6,120)
C FORMAT (////, 'AIRFOIL RIME ICING MODEL', //, 'Version Mar. 12, 1986', //,
C '20X, K. J. Finstad', //, '17X, Meteorology Division', //, '12X, The University of Alberta',
C '///, Please enter parameters to begin accretion', //)
C
C Prompt user for input parameters.
C
C WRITE (6,*) 'Median Volume Droplet DIAMETER in microns?'
C READ (5,*) DRODPI
C
C Convert to metres
C
C DRODPI = DRODPI*1.0E-6
C
C Set flags for requested treatment of droplet spectrum.
C
C WRITE (6,*)
C WRITE (6,*) 'Do you wish simulated spectrum weighting?'
C READ (5,8) SIMOPT
C FORMAT ('AT')
C
C For simulated spectrum calculate 'tail' length from
C median volume diameter
C
C IF ((SIMOPT.EQ.'Y') .OR. (SIMOPT.EQ.'y')) THEN
C SIMSPC = TRUE
C TAILLEN = 0.13 * DEXP(-DRODPI / 7.0E-5)
C ELSE
C SIMSPC = FALSE
C TAILLEN = 0.0
C ENDIF
C
C WRITE (6,*)
C WRITE (6,*) 'Airfoil chord length in metres?'
C READ (5,*) CHORD1
C
C Set current chord length equal to bare airfoil
C
C CHORD = CHORD1
C
C WRITE (6,*)
C WRITE (6,*) 'Airfoil height as fraction of chord?'
C READ (5,*) H
C
C WRITE (6,*)
C WRITE (6,*) 'Free stream speed in m / sec?'
C READ (5,*) VEL
C
C WRITE (6,*)
C WRITE (6,*) 'Liquid water content in kg / cubic metre?'
C

```

```

332. 40 ISN READ (5.0) LWC
333.
334. 41 ISN WRITE (6.0)
335. 42 ISN WRITE (6.0) 'Time step per layer in seconds?'
336. 43 ISN READ (5.0) TAU
337.
338. 44 ISN WRITE (6.0)
339. 45 ISN WRITE (6.0) 'Total number of layers?'
340. 46 ISN READ (5.0) LAYERS
341.
342. C Bare surface will be layer 1., so add 1 to LAYERS
343. C
344. C LAYERS = LAYERS + 1
345. C
346. 48 ISN WRITE (6.0)
347. 49 ISN WRITE (6.0) 'Angle of attack in degrees?'
348. 50 ISN READ (5.0) PHI
349.
350. C Convert angle of attack to radians, and calculate
351. C surface angle of the max collision efficiency point
352. C for non-zero attack angles (AZERO).
353. C
354. 51 ISN AZERO = DLOG10(PHI + 1) / (0.001 * DEXP(30.5 * H))
355. 52 ISN PHI = (PHI * 2.0 * PI) / 360.0
356. 53 ISN AZERO = (AZERO * 2.0 * PI) / 360.0
357.
358. C Fill array of points defining the initial surface of the
359. C airfoil in dimensional coordinates. The complete
360. C surface contains NPOINT points.
361. C
362. 54 ISN NPOINT = 600
363. C
364. 55 ISN DO 100 I = 1, NPOINT
365. 56 ISN XFOIL(I) = 0.5 * (1.0 - DCOS(2.0 * PI * DBLE(I-1)) /
366. DBLE(NPOINT))
367. 57 ISN YFOIL(I) = 5.0 * H * (0.2969 * DSORT(XFOIL(I))
368. + 0.126 * XFOIL(I) - 0.3516 * XFOIL(I) ** 2
369. + 0.2843 * XFOIL(I) ** 3
370. + 0.1015 * XFOIL(I) ** 4) * CHORD
371. 58 ISN IF (I GT 301) YFOIL(I) = -YFOIL(I)
372. 60 ISN XFOIL(I) = XFOIL(I) * CHORD
373. 61 ISN YFOIL(I) = YFOIL(I) * CHORD
374.
375. C 100 CONTINUE
376. C
377. C Fill arrays of non-dimensional coordinates for later plotting.
378. C
379. 62 ISN DO 101 I = 1, 150
380. 63 ISN PFOILX(150+I) = XFOIL(I) / CHORD
381. 64 ISN PFOILY(150+I) = YFOIL(I) / CHORD
382. 65 ISN PFOILX(I) = XFOIL(450+I) / CHORD
383. 66 ISN PFOILY(I) = YFOIL(450+I) / CHORD
384. 67 ISN
385. C 101 CONTINUE
386. C
387. C Copy front part of surface to array, which will contain
388. C all of the layers.
389. C
390. 68 ISN DO 200 I = 1, NPOINT / 4

```

1 2 3 4 5 6 7 8 9

```

388 LAYRX(1,1) = XFOIL((3 * NPOINT / 4) + 1)
389 LAYRY(1,1) = YFOIL((3 * NPOINT / 4) + 1)
390 CONTINUE
391 DO 210 I = (NPOINT / 4) + 1, NPOINT / 2
392 LAYRX(1,1) = XFOIL(I - (NPOINT / 4))
393 LAYRY(1,1) = YFOIL(I - (NPOINT / 4))
394 CONTINUE
395
396 C Call Subroutine DROPS to calculate Beta zero. Alpha max is
397 C then determined from Beta zero.
398
399 CALL DROPS(DROPS, VEL, CHORD, NPOINT, BZERO)
400 ALPHA = DACOS(1.0 - BZERO)
401
402 C Initialize total mass and begin loop to accrete ice layers.
403
404 TMASS = 0.0
405 DO 300 J = 2, LAYERS
406
407 C Check for recalculation of BZERO every fifth layer
408
409 IF ((J.EQ. 6) .OR. (J.EQ. 11) .OR. (J.EQ. 16)) THEN
410
411 C Copy new shape to arrays for potential flow calculation in DROPS
412
413 DO 220 I=1,NPOINT / 4
414 XFOIL(I + (3*NPOINT/4)) = LAYRX(J-1,1)
415 YFOIL(I + (3*NPOINT/4)) = LAYRY(J-1,1)
416 CONTINUE
417 DO 230 I = (NPOINT / 4) + 1, NPOINT / 2
418 XFOIL(I - NPOINT / 4) = LAYRX(J-1,1)
419 YFOIL(I - NPOINT / 4) = LAYRY(J-1,1)
420 CONTINUE
421
422 C Update length of airfoil chord plus accreted ice
423
424 CHORD = .CHORD + (((J-2) * BZERO * VEL * LWC * TAU) / 890.0)
425
426 C Update BZERO, and ALPHA if necessary
427
428 CALL DROPS(DROPS, VEL, CHORD, NPOINT, BZERO)
429 IF (DACOS(1.0 - BZERO) LT ALPHA) ALPHA =
430 + DACOS(1.0 - BZERO)
431 ENDIF
432
433 C Calculate slope and surface angle from finite differences for
434 C each point on current surface
435
436 DO 400 I = 2, 299
437 SLOPE(I) = (LAYRX(J-1, I+1) - LAYRX(J-1, I-1)) /
438 + DABS(LAYRY(J-1, I+1) - LAYRY(J-1, I-1))
439
440 IF (LAYRY(J-1, I+1) EQ. LAYRY(J-1, I-1))
441 SLOPE(I) = 1.0E10
442 IF (LAYRY(J-1, I+1) LT. LAYRY(J-1, I-1)) THEN
443 ALPHA(I) = PI - DATAN(SLOPE(I))

```

1 2 3 4 5 6 7 8

```

444 ISN 100      ELSE
445 ISN 101      ALPHA(I) = DATAN(SLOPE(I))
446 ISN 102      ENDIF
447 ISN 103      400 CONTINUE
448
449 C
450 C Calculate for each point local density, collision efficiency and
451 C ice thickness. The method of calculation for Beta and rho
452 C depends on the values of SIMSPC and PHI
453 C
454 DO 500 I = 2,288
455   IF (PHI.EQ.0.0) THEN
456     RHO(I) = 880.0
457     * (1.0 - 0.163 * DABS(ALPHA(I))/(ALPHA+TAILEN)) *
458     * 0.235 * (DABS(ALPHA(I))/(ALPHA+TAILEN)) ** 2) -
459     * 2.357 * (DABS(ALPHA(I))/(ALPHA+TAILEN)) ** 3) +
460     * 1.374 * (DABS(ALPHA(I))/(ALPHA+TAILEN)) ** 4) +
461     * 0.0188 * (DABS(ALPHA(I))/(ALPHA+TAILEN)) ** 5))
462   ELSE
463     APHI = ((-ALPHA(I) - AZERO) / (HALFPI - AZERO)
464             * HALFPI)
465     RHO(I) = 880.0 *
466     * (1.0 - (0.163 * DABS(APHI/HALFPI)) *
467     * (0.235 * DABS(APHI/HALFPI) ** 2) -
468     * (2.357 * DABS(APHI/HALFPI) ** 3) +
469     * (1.374 * DABS(APHI/HALFPI) ** 4) +
470     * (0.0188 * DABS(APHI/HALFPI) ** 5))
471   ENDIF
472 IF (ALPHA(I) .GT. HALFPI) RHO(I) = 170.
473
474 C
475 C Make sure density does not become too small
476 IF (RHO(I) .LT. 170.) RHO(I) = 170.
477
478 C
479 C Calculate local collision efficiency
480 IF (PHI .NE. 0.0) THEN
481   BETA = 0.95 * SPCBET(APHI,BZERO,HALFPI,0.0)
482 ELSE IF (SIMSPC) THEN
483   BETA = SPCBET(ALPHA(I),BZERO,ALPHA,TAILEN)
484 ELSE
485   BETA = ONEBET(ALPHA(I),BZERO,ALPHA)
486 ENDIF
487
488 C
489 C Calculate local ice thickness perpendicular to surface
490 THICK(I) = BETA * VEL * TAU * LWC / RHO(I)
491
492 C
493 C Define new layer surface coordinates.
494 LAYRX(J,I) = LAYRX(J-1,I) - (THICK(I) *
495   * DCOS(DATAN(SLOPE(I))))
496 LAYRY(J,I) = LAYRY(J-1,I) + (THICK(I) *
497   * DSIN(DATAN(SLOPE(I))))
498
499 500 CONTINUE
500 LAYRX(J,1) = LAYRX(J-1,1)
500 LAYRY(J,300) = LAYRY(J-1,300)

```

1 2 3 4 5 6 7 8 9 10

```

500 LAYR(J,1) = LAYR(J-1,1)
501 LAYR(J,300) = LAYR(J-1,300)
502
503 C Calculate mass and mean density of the layer from
504 C the sum of areas between surface points on successive
505 C layers. First, initialize layer mass and area
506
507 LMASS = 0.0
508 LAREA = 0.0
509 DO 560 I = 2,298
510 IF ((THICK(I) .GT. 0.0) .AND. (THICK(I+1) .GT. 0.0)) THEN
511 L4 = THICK(I)
512 L2 = THICK(I+1)
513 L1 = DSORT((LAYRX(J-1,I+1) - LAYRX(J-1,I))**2 + (LAYR
514 (J-1,I+1) - LAYR(J-1,I))**2)
515 L3 = DSORT((LAYRX(J,I+1) - LAYRX(J,I))**2 + (LAYR
516 (J,I+1) - LAYR(J,I))**2)
517 DIAG = DSORT((LAYRX(J,I+1)-LAYRX(J-1,I))**2 + (LAYR
518 (J,I+1) - LAYR(J-1,I))**2)
519 S1 = 0.5 * (DIAG+L1+L2)
520 S2 = 0.5 * (DIAG+L3+L4)
521 AREA = DSORT(S1 * (S1-DIAG) + (S1-L1) * (S1-L2)) +
522 DSORT(S2 * (S2-DIAG) + (S2-L3) * (S2-L4))
523 MASS = ((RND(I) + RND(I+1)) / 2.0) * AREA
524 LMASS = LMASS + MASS
525 LAREA = LAREA + AREA
526
527 ENDIF
528 CONTINUE
529
530 C Calculate mean density
531
532 LDEMS = LMASS/LAREA
533
534 C Write results to mass table
535
536 WRITE (8,570) J-1,LMASS,LDEMS
537 FORMAT (//,BX,12,7X,F9.5,7X,F9.5)
538
539 C Add mass of current layer to total mass
540
541 TMASS = TMASS + LMASS
542
543 C Shift surface points closer to nose by a decreasing
544 C interval between points
545
546 IF ((J .GT. 2) .AND. (PHI EQ. 0.0)) THEN
547 DO 580 I=1,149
548 IF (THICK(I+1-I) .GT. 0.0) THEN
549 LAYRX(J,I+1-I) = LAYRX(J,I+1-I) -
550 ((0.4 * (20./DBLE(I+19))) *
551 DABS(LAYRX(J,I+1-I) - LAYR(J,I+1-I)) +
552 LAYR(J,I+1-I) - LAYR(J,I+1-I)) *
553 ((0.4 * (20./DBLE(I+19))) *
554 DABS(LAYR(J,I+1-I) - LAYR(J,I+1-I)) +
555 LAYR(J,I+1-I) - LAYR(J,I+1-I))
556 ENDIF
557 IF (THICK(L+151) .GT. 0.0) THEN

```

1 2 3 4 5 6 7 8 9

```

556. LAYRX(J,I+151) = LAYRX(J,I+151) -
557. ((0.4 * (20./DBLE(I+19)))) *
558. DABS(LAYRX(J,I+150)-LAYRX(J,I+151)))
ISN 157 LAYRY(J,I+151) = LAYRY(J,I+151) -
559. ((0.4 * (20./DBLE(I+19)))) *
560. DABS(LAYRY(J,I+150)-LAYRY(J,I+151)))
ISN 158 ENDIF
ISN 159 580 CONTINUE
ISN 160 ENDIF
ISN 161 900 CONTINUE
566. C
567. C Write total mass accreted to table
568. C
569. C
570. WRITE (8,590) TMASS
ISN 162 590 FORMAT (8X,/, ' Total mass accreted per metre: ',F9.5)
ISN 163
572. C Call subroutine to plot airfoil and accreted layers
573. C
574. C CALL DRAW(ALPHM,BZERO,CHORD1,DROPI,LAYERS,LWC,PHI,
575. SIMSPC,TAILEN,TAU,VEL)
ISN 164
576. C
577. C
ISN 165 999 STOP
ISN 166 END

```

STATISTICS SOURCE STATEMENTS = 162, PROGRAM SIZE = 21362 BYTES, PROGRAM NAME = MAIN PAGE: 1

STATISTICS NO DIAGNOSTICS GENERATED.

***** END OF COMPILATION 1 *****

REQUESTED OPTIONS (PROCESS): SC(AXIS2.SYMBOL)

OPTIONS IN EFFECT: NOLIST NOMAP NOXREF NOGOSTMT NODECK SOURCE TERM OBJECT FIXED
 OPTIMIZE(O) LANGVL(77) NOFIPS FLAG(I) NAME(MAIN) LINECOUNT(60)

*.....1.....2.....3.....4.....5.....6.....7.....8.....9.....

```

581. C
582. * SUBROUTINE DRAW - to plot airfoil and all accretion
583. * layers, with appropriate information
584. * in the legend. This subroutine uses
585. * the plotting library *PLOTLIB
586. *
587. *
588. * Input Variables : as defined for Main program :
589. * ALPHM,BZERO,CHORD1,DROPTD,LAYERS,LWC,
590. * PHI,SIMSPC,TAILEN,TAU,VEL
591. *
592. * Common Variables :LAYRX,LAYRY,PFOILX,PFOILY
593. *
594. * Other Variables : PLOTX,PLOTY - arrays containing x,y
595. * plotting data and scaling information
596. * for accretion layer currently being
597. * plotted
598. *
599. *
600. C
601. + SUBROUTINE DRAW(ALPHM,BZERO,CHORD1,DROPTD,LAYERS,
602. * LWC,PHI,SIMSPC,TAILEN,TAU,VEL)
603. C
604. + DOUBLE PRECISION PFOILX(302),PFOILY(302),LAYRX(20,300),
605. * LAYRY(20,300),PLOTX(302),PLOTY(302)
606. C
607. + DOUBLE PRECISION ALPHM,BZERO,CHORD,DROPTD,LWC,PHI,
608. * TAILEN,TAU,VEL
609. C
610. C INTEGER LAYERS
611. C LOGICAL SIMSPC
612. C COMMON /DR/LAYRX,LAYRY,PFOILX,PFOILY
613. C
614. C To plot airfoil surface.
615. C place scaling data at the end of coordinate arrays.
616. C
617. C PFOILX(301) = -0.4
618. C PFOILX(302) = 0.1
619. C PFOILY(301) = -0.25
620. C PFOILY(302) = 0.1
621. C PLOTX(301) = -0.4
622. C PLOTX(302) = 0.1
623. C PLOTY(301) = -0.25
624. C PLOTY(302) = 0.1
625. C
626. C
627. C
628. C Open plotting library
629. C
630. C CALL PLOTS
631. C CALL METRIC(O)
    
```

1 2 3 4 5 6 7 8 9

```

632 C
633 C Draw 4 by 6 inch box
634 C
635 CALL PLOT(2.0,2.0,-3)
636 CALL PLOT(0.0,6.0,3)
637 CALL PLOT(9.0,6.0,2)
638 CALL PLOT(9.0,0.0,2)
639 C
640 C Label axes and draw tics
641 C
642 CALL AXIS2(0.0,0.0,'X/CHORD',-7.9,0.0,0.0,-0.4,0.1,1.0)
643 CALL AXIS2(0.0,0.0,'Y/CHORD',7.6,0.90,0.0,-0.25,0.1,0.5)
644 C
645 C Write legends to top left corner
646 C
647 CALL SYMBOL(1.1,5.4,0.10,'DROPLET MVD' = '.0.0.15)
648 CALL NUMBER(2.6,5.4,0.10,DROPLDI,0.0,0.07)
649 CALL SYMBOL(3.5,5.4,0.10,'M' ,0.0,0.1)
650 CALL SYMBOL(1.1,5.2,0.10,'CHORD' = '.0.0.15)
651 CALL NUMBER(2.6,5.2,0.10,CHORD1,0.0,0.04)
652 CALL SYMBOL(3.5,5.2,0.10,'M' ,0.0,0.1)
653 CALL SYMBOL(1.1,5.0,0.10,'AIR SPEED' = '.0.0.15)
654 CALL NUMBER(2.6,5.0,0.10,VEL,0.0,0.02)
655 CALL SYMBOL(3.5,5.0,0.10,'M / SEC',0.0,0.07)
656 CALL SYMBOL(1.1,4.8,0.10,'LWC' = '.0.0.15)
657 CALL NUMBER(2.6,4.8,0.10,LWC,0.0,0.05)
658 CALL SYMBOL(3.5,4.8,0.10,'KG / M**3',0.0,0.09)
659 CALL SYMBOL(1.1,4.6,0.10,'TIME STEP' = '.0.0.15)
660 CALL NUMBER(2.6,4.6,0.10,TAU,0.0,0.02)
661 CALL SYMBOL(3.5,4.6,0.10,'SEC',0.0,0.03)
662 CALL SYMBOL(1.1,4.4,0.10,'BETA ZERO' = '.0.0.15)
663 CALL NUMBER(2.6,4.4,0.10,BZERO,0.0,0.03)
664 CALL SYMBOL(1.1,4.2,0.10,'ALPHA MAX' = '.0.0.15)
665 CALL NUMBER(2.6,4.2,0.10,(ALPHM+TAILEN)*360./6.283,0.0,0.1)
666 CALL SYMBOL(3.5,4.2,0.10,'DEGREES',0.0,0.07)
667 CALL SYMBOL(1.1,4.0,0.10,'ATTACK ANGLE' = '.0.0.15)
668 CALL NUMBER(2.6,4.0,0.10,PHI*360./6.283,0.0,0.07)
669 CALL SYMBOL(3.5,4.0,0.10,'DEGREES',0.0,0.07)
670 CALL SYMBOL(1.1,3.8,0.10,'SPECTRUM',0.0,0.09)
671 IF ((SYMSPC).OR.(PHI.NE.0.0)) THEN
672 CALL SYMBOL(2.6,3.8,0.10,'SIMULATED',0.0,0.09)
673 ELSE
674 CALL SYMBOL(2.6,3.8,0.10,'NO',0.0,0.02)
675 ENDIF
676 C
677 C Draw initial airfoil surface
678 C
679 CALL LINE(PFOILX,PFOILY,300,2.0)
680 C
681 C Transfer each layer in turn to the array holding
682 C the scaling parameters
683 C
684 DO 610 J = 2,LAYERS
685 DO 700 L = 1,300
686 PLOTX(L) = LAYRX(J,L) / CHORD1
687 PLOTY(L) = LAYRY(J,L) / CHORD1
688 C
689 C
690 C
691 C
692 C
693 C
694 C
695 C
696 C
697 C
698 C
699 C
700 C
701 C
702 C
703 C
704 C
705 C
706 C
707 C
708 C
709 C
710 C
711 C
712 C
713 C
714 C
715 C
716 C
717 C
718 C
719 C
720 C
721 C
722 C
723 C
724 C
725 C
726 C
727 C
728 C
729 C
730 C
731 C
732 C
733 C
734 C
735 C
736 C
737 C
738 C
739 C
740 C
741 C
742 C
743 C
744 C
745 C
746 C
747 C
748 C
749 C
750 C
751 C
752 C
753 C
754 C
755 C
756 C
757 C
758 C
759 C
760 C
761 C
762 C
763 C
764 C
765 C
766 C
767 C
768 C
769 C
770 C
771 C
772 C
773 C
774 C
775 C
776 C
777 C
778 C
779 C
780 C
781 C
782 C
783 C
784 C
785 C
786 C
787 C
788 C
789 C
790 C
791 C
792 C
793 C
794 C
795 C
796 C
797 C
798 C
799 C
800 C
801 C
802 C
803 C
804 C
805 C
806 C
807 C
808 C
809 C
810 C
811 C
812 C
813 C
814 C
815 C
816 C
817 C
818 C
819 C
820 C
821 C
822 C
823 C
824 C
825 C
826 C
827 C
828 C
829 C
830 C
831 C
832 C
833 C
834 C
835 C
836 C
837 C
838 C
839 C
840 C
841 C
842 C
843 C
844 C
845 C
846 C
847 C
848 C
849 C
850 C
851 C
852 C
853 C
854 C
855 C
856 C
857 C
858 C
859 C
860 C
861 C
862 C
863 C
864 C
865 C
866 C
867 C
868 C
869 C
870 C
871 C
872 C
873 C
874 C
875 C
876 C
877 C
878 C
879 C
880 C
881 C
882 C
883 C
884 C
885 C
886 C
887 C
888 C
889 C
890 C
891 C
892 C
893 C
894 C
895 C
896 C
897 C
898 C
899 C
900 C
901 C
902 C
903 C
904 C
905 C
906 C
907 C
908 C
909 C
910 C
911 C
912 C
913 C
914 C
915 C
916 C
917 C
918 C
919 C
920 C
921 C
922 C
923 C
924 C
925 C
926 C
927 C
928 C
929 C
930 C
931 C
932 C
933 C
934 C
935 C
936 C
937 C
938 C
939 C
940 C
941 C
942 C
943 C
944 C
945 C
946 C
947 C
948 C
949 C
950 C
951 C
952 C
953 C
954 C
955 C
956 C
957 C
958 C
959 C
960 C
961 C
962 C
963 C
964 C
965 C
966 C
967 C
968 C
969 C
970 C
971 C
972 C
973 C
974 C
975 C
976 C
977 C
978 C
979 C
980 C
981 C
982 C
983 C
984 C
985 C
986 C
987 C
988 C
989 C
990 C
991 C
992 C
993 C
994 C
995 C
996 C
997 C
998 C
999 C
1000 C

```


OPTIONS IN EFFECT: NOLIST NOMAP NOXREF NOGOSTMT NODECK SOURCE TERM OBJECT FIXED
 OPTIMIZE(O) LANGLVL(77) NOFIPS FLAG(1) NAME(MAIN) LINECOUNT(60)

1.....2.....3.....4.....5.....6.....7.....8.....9.....

```

700 C .....
701 C * FUNCTION ONEBET - Calculates local collision efficiency*
702 C * estimate for a monodisperse droplet populations *
703 C *
704 C *
705 C * Input Variables : as defined for main program:
706 C * ALPHM,BZERO,ALPHA,SMDROP
707 C *
708 C *
709 C DOUBLE PRECISION FUNCTION ONEBET(ALPHA,BZERO,ALPHM)
710 C
711 C DOUBLE PRECISION BZERO,ALPHM,ALPHA
712 C
713 C
714 C
715 C IF (DABS(ALPHA) .GE. ALPHM) THEN
716 C ONEBET = 0.0
717 C ELSE
718 C ONEBET = DCOS(ALPHA) - (1.0 - BZERO)
719 C ENDIF
720 C RETURN
721 C END
    
```

STATISTICS SOURCE STATEMENTS = 9, PROGRAM SIZE = 870 BYTES, PROGRAM NAME = ONEBET PAGE: 15

STATISTICS NO DIAGNOSTICS GENERATED.

***** END OF COMPILATION 3 *****

OPTIONS IN EFFECT: NOLIST NOMAP NOXREF NOGOSTMT MODECK SOURCE TERM OBJECT FIXED
 OPTIMIZE(O) LANGVL(77) NOFIPS FLAG(1) NAME(MAIN) LINECOUNT(60)

.....1.....2.....3.....4.....5.....6.....7.....8.....9.....

```

722. C .....
723. C .....
724. C * Function SPCBET - Calculates the local c.e. for a
725. C * simulated droplet size distribution
726. C * scaled to the median volume droplet,
727. C * and to (alpha max + tail). The tail
728. C * length was determined in the main program.
729. C .....
730. C * Input Variables : as defined for Main program:
731. C * ALPHA,ALPHA,BZERO,SMDROP,TAILEN
732. C .....
733. C * Other Variables : X - scaled angle = Alpha /
734. C * (Alpha + Tailen)
735. C .....
736. C .....
737. C .....
738. C .....
739. C .....
740. C .....
741. C .....
742. C .....
743. C .....
744. C .....
745. C .....
746. C .....
747. C .....
748. C .....
749. C .....
750. C .....
751. C .....
752. C .....
753. C .....
754. C .....
755. C .....

DOUBLE PRECISION FUNCTION SPCBET(ALPHA,BZERO,
ALPHA,TAILEN)
+
DOUBLE PRECISION ALPHA,ALPHA,BZERO,TAILEN,X
C
ALPHA = DABS(ALPHA)
IF (ALPHA .GE. (ALPHA+TAILEN)) THEN
ELSE
X = ALPHA / (ALPHA+TAILEN)
SPCBET = BZERO * (1.000 + 0.039 * X - 1.842 *
(X ** 2) - 0.543 * (X ** 3)
+ 1.792 * (X ** 4) - 0.444 * (X ** 5))
IF (SPCBET .LT. 0.0) SPCBET = 0.0
IF (SPCBET .GT. BZERO) SPCBET = BZERO
ENDIF
RETURN
END

```

STATISTICS SOURCE STATEMENTS = 13, PROGRAM SIZE = 608 BYTES, PROGRAM NAME = SPCBET PAGE: 16

STATISTICS NO DIAGNOSTICS GENERATED.

***** END OF COMPILATION 4 *****

OPTIONS IN EFFECT: NOLIST NOMAP NOXREF NOGOSTMT NODACK SOURCE TERM OBJECT FIXED NOTEST SEQ
 OPTIMIZE(O) LANGVL(77) NOFIPS FLAG(I) - NAME(MAIN) LINECOUNT(60)

.....1.....2.....3.....4.....5.....6.....7.....8.....9.....

```

756. C .....
757. C .....
758. C SUBROUTINE DROPS .....
759. C .....
760. C This routine calculates a trajectory pair for water
761. C droplets in a potential flow field around a NACA airfoil or
762. C similar accretion shape. The stagnation line collision
763. C efficiency is then determined.
764. C
765. C The equation of motion of the droplet is integrated
766. C by the Heun method (Mesinger and Arakawa, 1976; Numerical
767. C Methods used in Atmospheric Models, Volume I, W.M.O. GARP
768. C Publications Series No. 17). The time step is set to
769. C 1/400 of the time to travel one chord length at the free
770. C stream speed. A maximum of 3000 steps are allowed,
771. C by which time the droplet is assumed to have collided
772. C with the airfoil or to have passed it.
773. C
774. C The droplet's initial x-coordinate is set to an
775. C upstream distance of 5.0 chord lengths. At this
776. C distance the x-speed is assumed to be equal to the air
777. C speed in the x-direction, and the droplet y-speed is
778. C set to zero.
779. C
780. C A first trajectory is integrated beginning at y = zero,
781. C which is then incremented by a small amount (DELTAY)
782. C for the second trajectory. If both trajectories
783. C intercept the airfoil, the local collision efficiency, and
784. C the angle between the local surface normal and free stream
785. C direction are calculated.
786. C
787. C The formulation of Beard and Pruppacher (J.A.S., Vol. 26,
788. C p. 1066, 1969) is used for the drag coefficient. Potential
789. C flow calculations are made according to the method of Kennedy
790. C and Marsden (Can. Aero. and Space J., Vol. 22, p. 243,
791. C 1976).
792. C
793. C The external subprogram is required, from the IMSL library;
794. C the subroutine LEQTF, to solve a system of equations
795. C in the potential flow calculation.
796. C
797. C The following internal subprograms are called from DROPS:
798. C ..... Subprograms .....
799. C .....
800. C
801. C SUBROUTINE COLLID - calculates final impact position,
802. C if the droplet collides with the surface.
803. C
804. C SUBROUTINE FLOWXY - calculates the air speeds at a
805. C given x,y location using the results of POFLO,
806. C and droplet accelerations (from the equations of
807. C motion) for the current iteration and time step.
808. C

```

```

1. .... 2. .... 3. .... 4. .... 5. .... 6. .... 7. .... 8. .... 9. ....
C SUBROUTINE KCALC - calculates the matrix elements
C K used in POFLO and FLOWXY.
C
C SUBROUTINE POFLO - calculates the potential vorticities
C at the surface of the airfoil according to the
C method of Kennedy and Marsden.
C
C SUBROUTINE TRAJEC - calculates droplet trajectories
C by integrating the droplet equations of motion by
C the trapezoid rule with one iteration step.
C
Input Variables:
C
CHORD - airfoil chord length in metres
C
DROPLDI - droplet diameter in microns
C
NPOINT - number of points in the complete airfoil
C surface (must be divisible by 15)
C
VEL - free stream air speed in metres per second
C
Output Variables:
C
BZERO - stagnation line collision efficiency
C
Common Variables: (with Main)
C
GAMMA - vector of potential vorticities for
C potential flow calculation
C
XFOIL - vectors containing points which define
C the complete dimensioned airfoil surface.
C
Other Variables:
C
ALPHA - angle between the local surface normal
C and the free stream direction at
C the impact point
C
ARC - arc length along the airfoil surface
C between the impact points of the two
C trajectories (estimated by a straight
C line segment)
C
DELTAT - time step in seconds
C
DELTAY - difference in initial y position of
C the two trajectories
C
FINX1 - x-positions of the droplets at impact
C FINX2 - for each trajectory
C
FINY1 - y-positions of the droplets at impact
C FINY2 - for each trajectory
C
809.
810.
811.
812.
813.
814.
815.
816.
817.
818.
819.
820.
821.
822.
823.
824.
825.
826.
827.
828.
829.
830.
831.
832.
833.
834.
835.
836.
837.
838.
839.
840.
841.
842.
843.
844.
845.
846.
847.
848.
849.
850.
851.
852.
853.
854.
855.
856.
857.
858.
859.
860.
861.
862.
863.
864.

```

1.....2.....3.....4.....5.....6.....7.....8.....9.....

```

C 865. HALFPI - pi / 2 (FORTRAN77 constant parameter)
C 866.
C 867.
C 868. HIT1, - logical flags for each trajectory
C 869. HIT2 - which indicate whether a collision
C 870. with the airfoil has occurred
C 871.
C 872. NSTEPS - maximum number of time steps to be
C 873. integrated
C 874.
C 875. PI - pi (FORTRAN77 constant parameter)
C 876.
C 877. SLOPE1, - slopes of the airfoil or accretion
C 878. SLOPE2 - surface at the impact points
C 879.
C 880. XINIT, - initial droplet x,y position in metres
C 881. YINIT
C 882.
C 883.
C 884.
C 885.
C 886. SUBROUTINE DROPS(DROPOI,VEL,CHORD,NPOINT,BZERO)
C 887.
C 888. DOUBLE PRECISION XFOIL(600),YFOIL(600),GAMMA(41)
C 889.
C 890. DOUBLE PRECISION ARC,BZERO,CHORD,DELTA,DELTA1,DELTA2,
C 891. DROPOI,FINX1,FINX2,FINY1,FINY2,
C 892. SLOPE1,SLOPE2,VEL,XINIT,YINIT
C 893.
C 894. INTEGER NSTEPS,NPOINT
C 895.
C 896. LOGICAL HIT1,HIT2
C 897.
C 898. PARAMETER (PI = 3.1415926535897932,HALFPI = PI / 2.0)
C 899.
C 900. COMMON /MN/ XFOIL,YFOIL,GAMMA
C 901.
C 902.
C 903. Set maximum number of time steps, initial x-coordinate, and
C 904. the difference in initial y-coordinates
C 905.
C 906. NSTEPS = 3000
C 907. DELTA = 1.0E-8
C 908. XINIT = 5.0 * CHORD
C 909. YINIT = 0.0
C 910.
C 911. Calculate time step
C 912.
C 913. DELTA = CHORD / (VEL * 400)
C 914.
C 915. Calculate potential vorticity matrix for air speed calculations
C 916.
C 917. CALL POFLO(NPOINT,CHORD)
C 918.
C 919. Integrate first trajectory
C 920.

```


1 2 3 4 5 6 7 8 9

```

921. 14 CALL TRAJEC (XINIT,YINIT,DRODDI,VEL,CHORD,DELTAI,NSTEPS,
922.      + NPOINT,HIT1,FINX1,FINY1,SLOPE1)
923.
924. C Correct initial y position and integrate second trajectory
925. C
926.      YINIT = YINIT + DELTAY
927.      CALL TRAJEC (XINIT,YINIT,DRODDI,VEL,CHORD,DELTAI,NSTEPS,
928.      + NPOINT,HIT2,FINX2,FINY2,SLOPE2)
929.
930. C Test for result of trajectory (miss, graze or collision)
931. C
932.      IF ((HIT1) .AND. (HIT2)) THEN
933.
934. C Calculate impact parameters and local collision efficiency
935. C
936.      ARC = DSORT(((FINX2 - FINX1)**2) + ((FINY1 - FINY2)
937.      + **2))
938.      BZERO = DELTAY / ARC
939.
940. C If droplet didn't hit the foil, write message to screen
941. C
942.      ELSE IF ((.NOT. HIT1) .OR. (.NOT. HIT2)) THEN
943.      WRITE (6,40)
944.      FORMAT (//,'Droplet did not reach the airfoil.')
945.      ENDIF
946. C
947.      RETURN
948.      END

```

•STATISTICS* SOURCE STATEMENTS = 25, PROGRAM SIZE = 926 BYTES, PROGRAM NAME = DROPS PAGE 17
•STATISTICS* NO DIAGNOSTICS GENERATED
***** END OF COMPILATION 5 *****

OPTIONS IN EFFECT: NOLIST NOMAP NOXREF NOGOSTMT NODDECK SOURCE TERM OBJECT FIXED
 OPTIMIZE(O) L ANGLVL(77) NOFIPS FLAG(I) NAME(MAIN) LINECOUNT(GO) NOTEST SEO

1.....2.....3.....4.....5.....6.....7.....8.....9.....

```

949. C .....
950. C .....
951. C .....
952. C .....
953. C .....
954. C .....
955. C .....
956. C .....
957. C .....
958. C .....
959. C .....
960. C .....
961. C .....
962. C .....
963. C .....
964. C .....
965. C .....
966. C .....
967. C .....
968. C .....
969. C .....
970. C .....
971. C .....
972. C .....
973. C .....
974. C .....
975. C .....
976. C .....
977. C .....
978. C .....
979. C .....
980. C .....
981. C .....
982. C .....
983. C .....
984. C .....
985. C .....
986. C .....
987. C .....
988. C .....
989. C .....
990. C .....
991. C .....
992. C .....
993. C .....
994. C .....
995. C .....
996. C .....
997. C .....
998. C .....
999. C .....
1000. C .....
1001. C .....

SUBROUTINE TRAJEC
.....
Integrates trajectory of droplet whose initial
position is specified in the parameter list. Calls
POFLO to set up matrix for potential flow calculations.
FLOWXY for iterative calculations of air speed and
droplet acceleration, and COLLID to determine
impact points.

INPUT VARIABLES:
CHORD - airfoil chord length
DELTA - time step
DROPLD - droplet diameter
NPOINT - number of surface points
NSTEPS - maximum number of time steps
VEL - free stream air speed
XINIT - initial x position
YINIT - initial y position

OUTPUT VARIABLES:
FINALX - droplet x velocity on impact
FINALY - droplet y velocity on impact
HIT - logical flag set to .TRUE. if
a collision occurs
SLOPE - slope of the surface at impact

COMMON VARIABLES:
CO - vector of cosines of angles of the
control elements
DELTA - vector of half-lengths of the
control elements
GAMMA - output array of POFLO, passed to
FLOWXY
SI - vector of sines of angles of the
control elements
XCON, - x,y coordinates of the control
YCON points
XFOIL, - vectors of initial surface
YFOIL coordinates

OTHER VARIABLES:
DVX, - arrays containing x,y components
DVY of droplet accelerations
L - counter for searching surface array.
LIMIT - initial value of counter L
VX,VY - arrays containing x,y components
of droplet speed for each step
X,Y - arrays containing x,y positions
for each time step
    
```

```

1002. C
1003. C
1004. C
1005. C
1006. C
1007. C
1008. C
1009. C
1010. C
1011. C
1012. C
1013. C
1014. C
1015. C
1016. C
1017. C
1018. C
1019. C
1020. C
1021. C
1022. C
1023. C
1024. C
1025. C
1026. C
1027. C
1028. C
1029. C
1030. C
1031. C
1032. C
1033. C
1034. C
1035. C
1036. C
1037. C
1038. C
1039. C
1040. C
1041. C
1042. C
1043. C
1044. C
1045. C
1046. C
1047. C
1048. C
1049. C
1050. C
1051. C
1052. C
1053. C
1054. C
1055. C
1056. C
1057. C

1 ISN SUBROUTINE TRAJEC(XINIT,YINIT,DROPOI,VEL,CHORD,DELTAT,
+ NSTEPS,NPOINT,HIT,FINALX,FINALY,SLOPE)
C
2 ISN DOUBLE PRECISION X(2500),Y(2500),GAMMA(41),XFOIL(600),
+ YFOIL(600),VX(2500),VY(2500),DVX(2500),
+ DVY(2500),DELTA(40),CO(40),SI(40),
+ XCON(41),YCON(41)
C
3 ISN DOUBLE PRECISION XINIT,YINIT,DROPOI,CHORD,VEL,DELTAT,
+ FINALX,FINALY,SLOPE
C
4 ISN INTEGER NSTEPS,NPOINT,LIMIT
C
5 ISN LOGICAL HIT
C
6 ISN COMMON /MN/ XFOIL,YFOIL,GAMMA/DRP/DELTA,CO,SI,XCON,YCON
C
7 ISN C Initialize values for integration
8 ISN X(1) = XINIT
9 ISN Y(1) = YINIT
10 ISN VX(1) = 0.0
11 ISN VY(1) = 0.0
12 ISN I = 0
13 ISN HIT = .FALSE.
14 ISN C Begin integration
15 ISN 100 I = I+1
16 ISN IF (I .GE. NSTEPS) GOTO 250
17 ISN C Calculate current step air speeds and accelerations
18 ISN CALL FLOWXY(X(I),Y(I),VX(I),VY(I),VEL,CHORD,DROPOI,
+ NPOINT,DVX(I),DVY(I))
19 ISN C Calculate next step droplet speeds and positions
20 ISN VX(I+1) = VX(I) - (DELTAT * DVX(I))
21 ISN VY(I+1) = VY(I) + (DELTAT * DVY(I))
22 ISN X(I+1) = X(I) + (VX(I) * DELTAT) - (0.5 * DVX(I)
+ (DELTAT * DELTAT))
23 ISN Y(I+1) = Y(I) + (VY(I) * DELTAT) + (0.5 * DVY(I)
+ (DELTAT * DELTAT))
24 ISN C Calculate next step air speeds and accelerations
25 ISN CALL FLOWXY(X(I+1),Y(I+1),VX(I+1),VY(I+1),VEL,
+ CHORD,DROPOI,NPOINT,DVX(I+1),DVY(I+1))
26 ISN C Iterate calculations of next step droplet speed and
27 ISN position using averaged values of accelerations
28 ISN VX(I+1) = VX(I) + ((DELTAT / 2.0) * (DVX(I) +

```

1 2 3 4 5 6 7 8 9

```

1058      DVX(I+1) = DVX(I+1)
1059      VY(I+1) = VY(I) + ((DELTA / 2.0) * (DVY(I) +
1060      DVY(I+1)))
1061      X(I+1) = X(I) + (VX(I) * DELTA) - (0.25 *
1062      (DVX(I) + DVX(I+1)) * (DELTA * DELTA))
1063      Y(I+1) = Y(I) + (VY(I) * DELTA) + (0.25 *
1064      (DVY(I) + DVY(I+1)) * (DELTA * DELTA))
1065
1066      C If trajectory has reached the nose
1067      C test whether trajectory has intercepted the airfoil surface
1068      C
1069      C Set LIMIT to begin search on upper or lower surface
1070      C if the droplet has reached to within one current chord
1071      C length of the nose
1072      C
1073      LIMIT = 0
1074      L = LIMIT
1075      L = L + 1
1076      IF (L .GE. (LIMIT + 125)) GOTO 100
1077
1078      C Search for adjacent pair of points which bracket the
1079      C y-coordinate of current trajectory position (if pair
1080      C cannot be found, continue with next integration step)
1081      C
1082      IF ((YFOIL(L+1) .GT. Y(I+1)) .AND. (YFOIL(L) .LT.
1083      Y(I+1))) THEN
1084
1085      C Check if current position has passed the airfoil surface
1086      C between the two points
1087      C
1088      IF ((XFOIL(L+1) .LT. X(I+1)) .OR. (XFOIL(L) .LT.
1089      X(I+1))) THEN
1090      HIT = .TRUE.
1091
1092      C Determine the impact point on the surface, and local
1093      C surface slope at that point, then exit from subroutine
1094      C
1095      CALL COLLID(X(I),X(I+1),Y(I),Y(I+1),XFOIL(L),
1096      YFOIL(L),XFOIL(L+1),YFOIL(L+1),
1097      FINALX,FINALY)
1098      SLOPE = (YFOIL(L+1) - YFOIL(L)) / (XFOIL(L+1) -
1099      XFOIL(L))
1100      GOTO 250
1101      ELSE
1102
1103      C If not inside surface, continue integration
1104      C
1105      GOTO 100
1106      ENDIF
1107      ELSE
1108
1109      C Else continue search for bracketing pair
1110      C
1111      GOTO 200
1112      ENDIF
1113
1114
1115
1116
1117
1118
1119
1120
1121
1122
1123
1124
1125
1126
1127
1128
1129
1130
1131
1132
1133
1134
1135
1136
1137
1138
1139
1140
1141
1142
1143
1144
1145
1146
1147
1148
1149
1150
1151
1152
1153
1154
1155
1156
1157
1158
1159
1160
1161
1162
1163
1164
1165
1166
1167
1168
1169
1170
1171
1172
1173
1174
1175
1176
1177
1178
1179
1180
1181
1182
1183
1184
1185
1186
1187
1188
1189
1190
1191
1192
1193
1194
1195
1196
1197
1198
1199
1200
1201
1202
1203
1204
1205
1206
1207
1208
1209
1210
1211
1212
1213
1214
1215
1216
1217
1218
1219
1220
1221
1222
1223
1224
1225
1226
1227
1228
1229
1230
1231
1232
1233
1234
1235
1236
1237
1238
1239
1240
1241
1242
1243
1244
1245
1246
1247
1248
1249
1250
1251
1252
1253
1254
1255
1256
1257
1258
1259
1260
1261
1262
1263
1264
1265
1266
1267
1268
1269
1270
1271
1272
1273
1274
1275
1276
1277
1278
1279
1280
1281
1282
1283
1284
1285
1286
1287
1288
1289
1290
1291
1292
1293
1294
1295
1296
1297
1298
1299
1300
1301
1302
1303
1304
1305
1306
1307
1308
1309
1310
1311
1312
1313
1314
1315
1316
1317
1318
1319
1320
1321
1322
1323
1324
1325
1326
1327
1328
1329
1330
1331
1332
1333
1334
1335
1336
1337
1338
1339
1340
1341
1342
1343
1344
1345
1346
1347
1348
1349
1350
1351
1352
1353
1354
1355
1356
1357
1358
1359
1360
1361
1362
1363
1364
1365
1366
1367
1368
1369
1370
1371
1372
1373
1374
1375
1376
1377
1378
1379
1380
1381
1382
1383
1384
1385
1386
1387
1388
1389
1390
1391
1392
1393
1394
1395
1396
1397
1398
1399
1400
1401
1402
1403
1404
1405
1406
1407
1408
1409
1410
1411
1412
1413
1414
1415
1416
1417
1418
1419
1420
1421
1422
1423
1424
1425
1426
1427
1428
1429
1430
1431
1432
1433
1434
1435
1436
1437
1438
1439
1440
1441
1442
1443
1444
1445
1446
1447
1448
1449
1450
1451
1452
1453
1454
1455
1456
1457
1458
1459
1460
1461
1462
1463
1464
1465
1466
1467
1468
1469
1470
1471
1472
1473
1474
1475
1476
1477
1478
1479
1480
1481
1482
1483
1484
1485
1486
1487
1488
1489
1490
1491
1492
1493
1494
1495
1496
1497
1498
1499
1500
1501
1502
1503
1504
1505
1506
1507
1508
1509
1510
1511
1512
1513
1514
1515
1516
1517
1518
1519
1520
1521
1522
1523
1524
1525
1526
1527
1528
1529
1530
1531
1532
1533
1534
1535
1536
1537
1538
1539
1540
1541
1542
1543
1544
1545
1546
1547
1548
1549
1550
1551
1552
1553
1554
1555
1556
1557
1558
1559
1560
1561
1562
1563
1564
1565
1566
1567
1568
1569
1570
1571
1572
1573
1574
1575
1576
1577
1578
1579
1580
1581
1582
1583
1584
1585
1586
1587
1588
1589
1590
1591
1592
1593
1594
1595
1596
1597
1598
1599
1600
1601
1602
1603
1604
1605
1606
1607
1608
1609
1610
1611
1612
1613
1614
1615
1616
1617
1618
1619
1620
1621
1622
1623
1624
1625
1626
1627
1628
1629
1630
1631
1632
1633
1634
1635
1636
1637
1638
1639
1640
1641
1642
1643
1644
1645
1646
1647
1648
1649
1650
1651
1652
1653
1654
1655
1656
1657
1658
1659
1660
1661
1662
1663
1664
1665
1666
1667
1668
1669
1670
1671
1672
1673
1674
1675
1676
1677
1678
1679
1680
1681
1682
1683
1684
1685
1686
1687
1688
1689
1690
1691
1692
1693
1694
1695
1696
1697
1698
1699
1700
1701
1702
1703
1704
1705
1706
1707
1708
1709
1710
1711
1712
1713
1714
1715
1716
1717
1718
1719
1720
1721
1722
1723
1724
1725
1726
1727
1728
1729
1730
1731
1732
1733
1734
1735
1736
1737
1738
1739
1740
1741
1742
1743
1744
1745
1746
1747
1748
1749
1750
1751
1752
1753
1754
1755
1756
1757
1758
1759
1760
1761
1762
1763
1764
1765
1766
1767
1768
1769
1770
1771
1772
1773
1774
1775
1776
1777
1778
1779
1780
1781
1782
1783
1784
1785
1786
1787
1788
1789
1790
1791
1792
1793
1794
1795
1796
1797
1798
1799
1800
1801
1802
1803
1804
1805
1806
1807
1808
1809
1810
1811
1812
1813
1814
1815
1816
1817
1818
1819
1820
1821
1822
1823
1824
1825
1826
1827
1828
1829
1830
1831
1832
1833
1834
1835
1836
1837
1838
1839
1840
1841
1842
1843
1844
1845
1846
1847
1848
1849
1850
1851
1852
1853
1854
1855
1856
1857
1858
1859
1860
1861
1862
1863
1864
1865
1866
1867
1868
1869
1870
1871
1872
1873
1874
1875
1876
1877
1878
1879
1880
1881
1882
1883
1884
1885
1886
1887
1888
1889
1890
1891
1892
1893
1894
1895
1896
1897
1898
1899
1900
1901
1902
1903
1904
1905
1906
1907
1908
1909
1910
1911
1912
1913
1914
1915
1916
1917
1918
1919
1920
1921
1922
1923
1924
1925
1926
1927
1928
1929
1930
1931
1932
1933
1934
1935
1936
1937
1938
1939
1940
1941
1942
1943
1944
1945
1946
1947
1948
1949
1950
1951
1952
1953
1954
1955
1956
1957
1958
1959
1960
1961
1962
1963
1964
1965
1966
1967
1968
1969
1970
1971
1972
1973
1974
1975
1976
1977
1978
1979
1980
1981
1982
1983
1984
1985
1986
1987
1988
1989
1990
1991
1992
1993
1994
1995
1996
1997
1998
1999
2000
2001
2002
2003
2004
2005
2006
2007
2008
2009
2010
2011
2012
2013
2014
2015
2016
2017
2018
2019
2020
2021
2022
2023
2024
2025
2026
2027
2028
2029
2030
2031
2032
2033
2034
2035
2036
2037
2038
2039
2040
2041
2042
2043
2044
2045
2046
2047
2048
2049
2050
2051
2052
2053
2054
2055
2056
2057
2058
2059
2060
2061
2062
2063
2064
2065
2066
2067
2068
2069
2070
2071
2072
2073
2074
2075
2076
2077
2078
2079
2080
2081
2082
2083
2084
2085
2086
2087
2088
2089
2090
2091
2092
2093
2094
2095
2096
2097
2098
2099
2100
2101
2102
2103
2104
2105
2106
2107
2108
2109
2110
2111
2112
2113
2114
2115
2116
2117
2118
2119
2120
2121
2122
2123
2124
2125
2126
2127
2128
2129
2130
2131
2132
2133
2134
2135
2136
2137
2138
2139
2140
2141
2142
2143
2144
2145
2146
2147
2148
2149
2150
2151
2152
2153
2154
2155
2156
2157
2158
2159
2160
2161
2162
2163
2164
2165
2166
2167
2168
2169
2170
2171
2172
2173
2174
2175
2176
2177
2178
2179
2180
2181
2182
2183
2184
2185
2186
2187
2188
2189
2190
2191
2192
2193
2194
2195
2196
2197
2198
2199
2200
2201
2202
2203
2204
2205
2206
2207
2208
2209
2210
2211
2212
2213
2214
2215
2216
2217
2218
2219
2220
2221
2222
2223
2224
2225
2226
2227
2228
2229
2230
2231
2232
2233
2234
2235
2236
2237
2238
2239
2240
2241
2242
2243
2244
2245
2246
2247
2248
2249
2250
2251
2252
2253
2254
2255
2256
2257
2258
2259
2260
2261
2262
2263
2264
2265
2266
2267
2268
2269
2270
2271
2272
2273
2274
2275
2276
2277
2278
2279
2280
2281
2282
2283
2284
2285
2286
2287
2288
2289
2290
2291
2292
2293
2294
2295
2296
2297
2298
2299
2300
2301
2302
2303
2304
2305
2306
2307
2308
2309
2310
2311
2312
2313
2314
2315
2316
2317
2318
2319
2320
2321
2322
2323
2324
2325
2326
2327
2328
2329
2330
2331
2332
2333
2334
2335
2336
2337
2338
2339
2340
2341
2342
2343
2344
2345
2346
2347
2348
2349
2350
2351
2352
2353
2354
2355
2356
2357
2358
2359
2360
2361
2362
2363
2364
2365
2366
2367
2368
2369
2370
2371
2372
2373
2374
2375
2376
2377
2378
2379
2380
2381
2382
2383
2384
2385
2386
2387
2388
2389
2390
2391
2392
2393
2394
2395
2396
2397
2398
2399
2400
2401
2402
2403
2404
2405
2406
2407
2408
2409
2410
2411
2412
2413
2414
2415
2416
2417
2418
2419
2420
2421
2422
2423
2424
2425
2426
2427
2428
2429
2430
2431
2432
2433
2434
2435
2436
2437
2438
2439
2440
2441
2442
2443
2444
2445
2446
2447
2448
2449
2450
2451
2452
2453
2454
2455
2456
2457
2458
2459
2460
2461
2462
2463
2464
2465
2466
2467
2468
2469
2470
2471
2472
2473
2474
2475
2476
2477
2478
2479
2480
2481
2482
2483
2484
2485
2486
2487
2488
2489
2490
2491
2492
2493
2494
2495
2496
2497
2498
2499
2500
2501
2502
2503
2504
2505
2506
2507
2508
2509
2510
2511
2512
2513
2514
2515
2516
2517
2518
2519
2520
2521
2522
2523
2524
2525
2526
2527
2528
2529
2530
2531
2532
2533
2534
2535
2536
2537
2538
2539
2540
2541
2542
2543
2544
2545
2546
2547
2548
2549
2550
2551
2552
2553
2554
2555
2556
2557
2558
2559
2560
2561
2562
2563
2564
2565
2566
2567
2568
2569
2570
2571
2572
2573
2574
2575
2576
2577
2578
2579
2580
2581
2582
2583
2584
2585
2586
2587
2588
2589
2590
2591
2592
2593
2594
2595
2596
2597
2598
2599
2600
2601
2602
2603
2604
2605
2606
2607
2608
2609
2610
2611
2612
2613
2614
2615
2616
2617
2618
2619
2620
2621
2622
2623
2624
2625
2626
2627
2628
2629
2630
2631
2632
2633
2634
2635
2636
2637
2638
2639
2640
2641
2642
2643
2644
2645
2646
2647
2648
2649
2650
2651
2652
2653
2654
2655
2656
2657
2658
2659
2660
2661
2662
2663
2664
2665
2666
2667
2668
2669
2670
2671
2672
2673
2674
2675
2676
2677
2678
2679
2680
2681
2682
2683
2684
2685
2686
2687
2688
2689
2690
2691
2692
2693
2694
2695
2696
2697
2698
2699
2700
2701
2702
2703
2704
2705
2706
2707
2708
2709
2710
2711
2712
2713
2714
2715
2716
2717
2718
2719
2720
2721
2722
2723
2724
2725
2726
2727
2728
2729
2730
2731
2732
2733
2734
2735
2736
2737
2738
2739
2740
2741
2742
2743
2744
2745
2746
2747
2748
2749
2750
2751
2752
2753
2754
2755
2756
2757
2758
2759
2760
2761
2762
2763
2764
2765
2766
2767
2768
2769
2770
2771
2772
2773
2774
2775
2776
2777
2778
2779
2780
2781
2782
2783
2784
2785
2786
2787
2788
2789
2790
2791
2792
2793
2794
2795
2796
2797
2798
2799
2800
2801
2802
2803
2804
2805
2806
2807
2808
2809
2810
2811
2812
2813
2814
2815
2816
2817
2818
2819
2820
2821
2822
2823
2824
2825
2826
2827
2828
2829
2830
2831
2832
2833
2834
2835
2836
2837
2838
2839
2840
2841
2842
2843
2844
2845
2846
2847
2848
2849
2850
2851
2852
2853
2854
2855
2856
2857
2858
2859
2860
2861
2862
2863
2864
2865
2866
2867
2868
2869
2870
2871
2872
2873
2874
2875
2876
2877
2878
2879
2880
2881
2882
2883
2884
2885
2886
2887
2888
2889
2890
2891
2892
2893
2894
2895
2896
2897
2898
2899
2900
2901
2902
2903
2904
2905
2906
2907
2908
2909
2910
2911
2912
2913
2914
2915
2916
2917
2918
2919
2920
2921
2922
2923
2924
2925
2926
2927
2928
2929
2930
2931
2932
2933
2934
2935
2936
2937
2938
2939
2940
2941
2942
2943
2944
2945
2946
2947
2948
2949
2950
2951
2952
2953
2954
2955
2956
2957
2958
2959
2960
2961
2962
2963
2964
2965
2966
2967
2968
2969
2970
2971
2972
2973
2974
2975
2976
2977
2978
2979
2980
2981
2982
2983
2984
2985
2986
2987
2988
2989
2990
2991
2992
2993
2994
2995
2996
2997
2998
2999
3000
3001
3002
3003
3004
3005
3006
3007
3008
3009
3010
3011
3012
3013
3014
3015
3016
3017
3018
3019
3020
3021
3022
3023
3024
3025
3026
3027
3028
3029
3030
3031
3032
3033
3034
3035
3036
3037
3038
3039
3040
3041
3042
3043
3044
3045
3046
3047
3048
3049
3050
3051
3052
3053
3054
3055
3056
3057
3058
3059
3060
3061
3062
3063
3064
3065
3066
3067
3068
3069
3070
3071
3072
3073
3074
3075
3076
3077
3078
3079
3080
3081
3082
3083
3084
3085
3086
3087
3088
3089
3090
3091
3092
3093
3094
3095
3096
3097
3098
3099
3100
3101
3102
3103
3104
3105
3106
3107
3108
3109
3110
3111
3112
3113
3114
3115
3116
3117
3118
3119
3120
3121
3122
3123
3124
3125
3126
3127
3128
3129
3130
3131
3132
3133
3134
3135
3136
3137
3138
3139
3140
3141
3142
3143
3144
3145
3146
3147
3148
3149
3150
3151
3152
3153
3154
3155
3156
3157
3158
3159
3160
3161
3162
3163
3164
3165
3166
3167
3168
3169
3170
3171
3172
3173
3174
3175
3176
3177
3178
3179
3180
3181
3182
3183
3184
3185
3186
3187
3188
3189
3190
3191
3192
3193
3194
3195
3196
3197
3198
3199
3200
3201
3202
3203
3204
3205
3206
3207
3208
3209
3210
3211
3212
3213
3214
3215
3216
3217
3218
3219
3220
3221
3222
3223
3224
3225
3226
3227
3228
3229
3230
3231
3232
3233
3234
3235
3236
3237
3238
3239
3240
3241
3242
3243
3244
3245
3246
3247
3248
3249
3250
3251
3252
3253
3254
3255
3256
3257
3258
3259
3260
3261
3262
3263
3264
3265
3266
3267
3268
3269
3270
3271
3272
3273
3274
3275
3276
3277
3278
3279
3280
3281
3282
3283
3284
3285
3286
3287
3288
3289
3290
3291
3292
3293
3294
3295
3296
3297
3298
3299
3300
3301
3302
3303
3304
3305
3306
3307
3308
3309
3310
3311
3312
3313
3314
3315
3316
3317
3318
3319
3320
3321
3322
3323
3324
3325
3326
3327
3328
3329
3330
3331
3332
3333
3334
3335
3336
3337
3338
3339
3340
3341
3342
3343
3344
3345
3346
3347
3348
3349
3350
3351
3352
3353
3354
3355
3356
3357
3358
3359
3360
3361
3362
3363
3364
3365
3366
3367
3368
3369
3370
3371
3372
3373
3374
3375
3376
```

LEVEL 1.1.1 (DEC 81) VS FORTRAN DATE: JUL 24, 1986 TIME: 13:15:51 NAME: TRAJEC PAGE: 24

.....1.....2.....3.....4.....5.....6.....7.....8.....9.....0.....

ISN	42	1114.	250	CONTINUE
		1115.	C	
ISN	43	1116.		RETURN
ISN	44	1117.		END

STATISTICS SOURCE STATEMENTS = 44, PROGRAM SIZE = 122570 BYTES, PROGRAM NAME = TRAJEC PAGE: 21.

STATISTICS NO DIAGNOSTICS GENERATED.

* END OF COMPILATION 6

OPTIONS IN EFFECT: NOLIST NOMAP NOXREF NOGOSTMT NODECK SOURCE TERM OBJECT FIXED
OPTIMIZE(O) LANGVL(77) NOFIPS FLAG(I) NAME(MAIN) LINECOUNT(60) NOTEST SEQ

1 2 3 4 5 6 7 8 9

```

1118. C
1119. C
1120. C * SUBROUTINE POFLO - Uses the method of Kennedy and
1121. C * Marsden (ref) to solve for the matrix of potential
1122. C * vorticities about the airfoil surface. A reduced
1123. C * number of points is used to define the surface for
1124. C * this subroutine than for the accretion section.
1125. C * Subroutine KCALC is called to calculate the matrix
1126. C * of K values.
1127. C
1128. C * INPUT VARIABLES :
1129. C * CHORD - airfoil chord length
1130. C * NPOINT - number of points defining
1131. C * airfoil surface
1132. C
1133. C * COMMON VARIABLES :
1134. C * CO,SI - vectors of cosines and sines
1135. C * DELTA - vector containing control
1136. C * element half lengths
1137. C * GAMMA - vector containing the
1138. C * potential vorticities on
1139. C * the airfoil surface
1140. C * XCON.. - vectors containing control
1141. C * YCON - point coordinates
1142. C * XFOIL - vectors of surface
1143. C * YFOIL - point coordinates
1144. C
1145. C * OTHER VARIABLES :
1146. C * IDGT. routine
1147. C * IER
1148. C * K - vector input to matrix
1149. C * solver subroutine LEOTIF
1150. C * N - NPOINT/15, the no. of surface
1151. C * points used to calculate
1152. C * the stream function
1153. C * WKAREA.. input required for LEOTIF
1154. C * XF,YF - reduced vectors of surface
1155. C * points (length NPOINT/15)
1156. C
1157. C
1158. C SUBROUTINE POFLO(NPOINT,CHORD)
1159. C
1160. C DOUBLE PRECISION GAMMA(41),XFOIL(600),YFOIL(600),
1161. C XCON(41),YCON(41),XF(41),YF(41),
1162. C K(41,41),WKAREA(41),DELTA(40),
1163. C CO(40),SI(40),CHORD
1164. C
1165. C INTEGER NPOINT,N,IDGT,IER
1166. C
1167. C COMMON /MN/ XFOIL,YFOIL,GAMMA/DRP/DELTA,CO,SI,XCON,YCON
1168. C
1169. C Construct new surface from every 15th point of old surface
1170. C non-dimensionalised to the current chord length

```

1 2 3 4 5 6 7 8 9

```

1171. C
1172. C
1173. C
1174. C
1175. C
1176. C
1177. C
1178. C
1179. C
1180. C
1181. C
1182. C
1183. C
1184. C
1185. C
1186. C
1187. C
1188. C
1189. C
1190. C
1191. C
1192. C
1193. C
1194. C
1195. C
1196. C
1197. C
1198. C
1199. C
1200. C
1201. C
1202. C
1203. C
1204. C
1205. C
1206. C
1207. C
1208. C
1209. C
1210. C
1211. C
1212. C
1213. C
1214. C
1215. C
1216. C
1217. C
1218. C
1219. C
1220. C
1221. C
1222. C
1223. C
1224. C
1225. C
1226. C

ISN 5
ISN 6
ISN 7
ISN 8
ISN 9
ISN 10
ISN 11
ISN 12
ISN 13

ISN 14
ISN 15
ISN 16
ISN 17

ISN 18
ISN 19

ISN 20
ISN 21

ISN 22
ISN 23
ISN 24
ISN 25

ISN 26
ISN 27

ISN 28
ISN 29

ISN 30
ISN 31

ISN 32
ISN 33
ISN 34

N = NPOINT / 15
XF(1) = XFOIL(1) / CHORD
YF(1) = YFOIL(1) / CHORD
XF(N+1) = XF(1)
YF(N+1) = YF(1)
DO 10 I=2, N
  XF(I) = XFOIL((15 * (I-1)) + 1) / CHORD
  YF(I) = YFOIL((15 * (I-1)) + 1) / CHORD
10 CONTINUE

C Form arrays of control points
C
DO 20 I = 1,N
  XCON(I) = (XF(I) + XF(I+1)) / 2.0
  YCON(I) = (YF(I) + YF(I+1)) / 2.0
20 CONTINUE

C Define the trailing point
C
XCON(N+1) = ((XF((N/2)+1) - XCON(N/2)) * 0.01) + XF((N/2)+1)
YCON(N+1) = 0.0

C Calculate R (as defined in Kennedy and Marsden) for each
C control point, store in GAMMA
C
DO 30 J = 1,N+1
  GAMMA(J) = YCON(J)

C Set last column of K(I,J) to 1.0
C
IF (J EQ N+1) THEN
  DO 35 I=1,N+1
    K(I,N+1) = 1.0
  35 CONTINUE

C For all other J, calculate the control element half lengths
C and functions of the angle to the x-axis.
C
ELSE
  DELTA(J) = DSORT(((XF(J+1) - XF(J)) ** 2) +
    ((YF(J+1) - YF(J)) ** 2)) / 2
  CO(J) = (XF(J+1) - XF(J)) / (2.0 * DELTA(J))
  SI(J) = (YF(J+1) - YF(J)) / (2.0 * DELTA(J))

C Calculate K for all remaining I,J
C
DO 40 I=1,N
  CALL KCALC(XCON(J),YCON(J),XCON(I),YCON(I),
    DELTA(J),CO(J),SI(J),K(I,J))
  40 CONTINUE
ENDIF
30 CONTINUE

C Call IMSLPLIB routine to solve matrix equation:
C output matrix of potential vorticities is in GAMMA.

```

LEVEL 1.1.1 (DEC 81) VS FORTRAN DATE: JUL 24, 1986 TIME: 13:15:52 NAME: POFLO PAGE: 27
1 2 3 4 5 6 7 8 9

```

1227. C
1228. IDGT = 8
1229. CALL _LEQT1F(K,1,N+1,N+1,GAMMA, IDGT, WKAREA, IER)
1230. WRITE (6,*) GAMMA
1231. C
1232. RETURN
1233. END

```

STATISTICS SOURCE STATEMENTS = 89, PROGRAM SIZE = 16358 BYTES, PROGRAM NAME = POFLO PAGE: 25

STATISTICS NO DIAGNOSTICS GENERATED.

***** END OF COMPILATION 7 *****

OPTIONS IN EFFECT: NOLIST NOMAP NOXREF NOGOSTMT NODECK SOURCE TERM OBJECT FIXED
OPTIMIZE(O) LANGVL(77) NOFIPS FLAG(I) NAME(MAIN) LINECOUNT(60)

1 2 3 4 5 6 7 8 9

```

1234. C .....
1235. C * SUBROUTINE FLOWXY - calculates for the current step:
1236. C * air speed components from matrix equation for
1237. C * potential flow streamline, using the output
1238. C * matrix GAMMA from POFLO, and KCALC to generate the
1239. C * matrix elements K. Droplet accelerations are then
1240. C * calculated according to the equations of motion
1241. C * from the air speed, droplet Reynolds number, and
1242. C * drag coefficient according to the formulation of
1243. C * Beard and Pruppacher.
1244. C *
1245. C * INPUT VARIABLES :
1246. C * CHORD - chord length
1247. C * DROPDI - droplet diameter
1248. C * NPOINT - no of airfoil surface points
1249. C * VEL - free stream air speed
1250. C * VX,VY - current droplet speeds
1251. C * X,Y - current droplet positions
1252. C *
1253. C * OUTPUT VARIABLES :
1254. C * DVX,DVY - current droplet accelerations
1255. C *
1256. C * COMMON VARIABLES :
1257. C * CO,SI,GAMMA,DELTA,XCON,YCON,FOIL,YFOIL
1258. C *
1259. C * OTHER VARIABLES :
1260. C * COEFF - combined coefficients of the
1261. C * equations of motion
1262. C * DRAGCO - drag coefficient
1263. C * DROPRE - droplet Reynolds number
1264. C * GRIDX - gridpoints used in the finite
1265. C * GRIDY - difference calculation of air
1266. C * speed from the stream function
1267. C * N - NPOINT/15, the no. of surface
1268. C * points used to calculate the
1269. C * stream function
1270. C * K, R - variables for the calculation
1271. C * of stream function of the air flow
1272. C * field
1273. C * PSI - stream function of the air flow
1274. C *
1275. C * SUMK - array containing the sum of K
1276. C * times GAMMA(J) for I gridpoints
1277. C *
1278. C * UX,UY - current air speed components
1279. C *
1280. C .....
1281. C * SUBROUTINE FLOWXY(X,Y,VX,VY,VEL,CHORD,DROPDI,NPOINT,
1282. C * DVX,DVY)
1283. C *
1284. C * DOUBLE PRECISION CO(40),DELTA(40),GAMMA(41),GRIDX(4),
1285. C * GRIDY(4),PSI(4),SI(40),SUMK(4),
1286. C * XCON(41),YCON(41),XFOIL(600).

```

```

1287.      +      YFOIL(600)
1288.      C      DOUBLE PRECISION COEFF,CHORD,DRAGCO,DROPDI,DROPRE,DX,
1289.      +      DVI,K,R,UX,UY,VEL,VX,VY,X,Y
1290.
1291.      C      INTEGER      N,NPOINT
1292.
1293.      C      COMMON /M/XFOIL,YFOIL,GAMMA/DRP/DELTA,CO,SI,XCON,YCON
1294.
1295.      C      Set up non-dimensional grid for finite difference calculation
1296.      C      of the streamfunction derivatives
1297.      C
1298.      GRIDX(1) = X / CHORD
1299.      GRIDX(2) = X / CHORD
1300.      GRIDX(3) = (X - (DROPDI / 2.0)) / CHORD
1301.      GRIDX(4) = (X + (DROPDI / 2.0)) / CHORD
1302.      GRIDY(1) = (Y + (DROPDI / 2.0)) / CHORD
1303.      GRIDY(2) = (Y - (DROPDI / 2.0)) / CHORD
1304.      GRIDY(3) = Y / CHORD
1305.      GRIDY(4) = Y / CHORD
1306.
1307.      C      Define N as in POFLO
1308.
1309.      C      N = NPOINT / 15
1310.
1311.      C      Calculate for each grid point, R and the sum of products
1312.      C      K times GAMMA(J), for J = 1, N
1313.      C
1314.      DO 10 I = 1,4
1315.      R = (GRIDY(I))
1316.      SUMK(I) = 0.0
1317.      DO 20 J = 1,N
1318.      CALL KCALQ(XCON(J),YCON(J),GRIDX(I),GRIDY(I),
1319.      +      DELTA(J),CO(J),SI(J),K)
1320.      SUMK(I) = SUMK(I) + (GAMMA(J) * K)
1321.
1322.      20 CONTINUE
1323.
1324.      C      Calculate stream functions
1325.
1326.      PSI(I) = -SUMK(I) + R - GAMMA(N+1)
1327.
1328.      10 CONTINUE
1329.
1330.      C      Calculate dimensional air speeds at point x,y from finite
1331.      C      difference derivatives of the stream functions
1332.      UX = VEL * CHORD * (PSI(1) - PSI(2)) / DROPDI
1333.      UY = VEL * CHORD * (PSI(3) - PSI(4)) / DROPDI
1334.
1335.      C      Calculate Reynolds number and drag coefficient
1336.
1337.      DROPRE = DROPDI * DSQRT(((VX - UX) ** 2) + ((VY - UY)
1338.      +      ** 2)) / 1.262E-5
1339.      IF (DROPRE .LT. 2.0) THEN
1340.      DRAGCO = (24.0 / DROPRE) + (2.45 / (DROPRE ** 0.045))
1341.      ELSE IF (DROPRE .LT. 21.0) THEN
1342.      DRAGCO = (24.0 / DROPRE) + (2.76 / (DROPRE ** 0.198))

```

1.....2.....3.....4.....5.....6.....7.....8.....9.....

ISN 31 1343
 ISN 32 1344
 ISN 33 1345
 ISN 34 1346
 ISN 35 1347
 ISN 36 1348
 ISN 37 1349
 ISN 38 1350
 ISN 39 1351
 ISN 40 1352
 ISN 41 1353
 ISN 42 1354
 ISN 43 1355
 ISN 44 1356
 ISN 45 1357
 ISN 46 1358
 ISN 47 1359

```

ELSE IF (DROPRE .GT. 200.0) THEN
  DRAGCO = (24.0 / DROPRE) + (4.73 / (DROPRE ** 0.37))
  + (6.24E-3 * (DROPRE ** 0.38))
ELSE
  DRAGCO = (24.0 / DROPRE) + (4.536 / (DROPRE ** 0.368))
ENDIF
C Calculate accelerations according to the equations of motion
C
COEFF = 9.9225E-4 * (DRAGCO / DROPDI)
DVX = COEFF * DSORT(((VX - UX) ** 2) + ((VY - UY) ** 2))
+ (VX - UX)
DVY = -COEFF * DSORT(((VX - UX) ** 2) + ((VY - UY) ** 2))
+ (VY - UY)
RETURN
END
    
```

STATISTICS SOURCE STATEMENTS = 40, PROGRAM SIZE = 2150 BYTES, PROGRAM NAME = FLOWXY PAGE: 28

STATISTICS NO DIAGNOSTICS GENERATED.

***** END OF COMPILATION 8 *****

OPTIONS IN EFFECT: NOLIST NOMAP NOXREF NOGOSTMT NMODECK SOURCE TERM OBJECT FIXED OPTIMIZE(O) [ANGLVL(77) NOFIPS FLAG(I) NAME(MAIN) LINECOUNT(60)

1 2 3 4 5 6 7 8 9

```

1360. C .....
1361. C .....
1362. C * SUBROUTINE KCALC - calculates a single element of the
1363. C * matrix K for the control points I
1364. C * and J
1365. C .....
1366. C * INPUT DATA :
1367. C * CO,SI - direction angles of the segment
1368. C * DELTA - half length of the control
1369. C * element J
1370. C * XCI,XCU - x-coordinates of control points
1371. C * I and J , or of grid point I
1372. C * and control point J
1373. C * YCI,YCU - y-coordinates of above
1374. C .....
1375. C * OUTPUT VARIABLES :
1376. C * K - matrix element
1377. C .....
1378. C * OTHER VARIABLES :
1379. C * A,B - geometrical quantities defined
1380. C * in Figure 2, Kennedy and Marsden
1381. C * R1SQ, - squares of R1 and R2, also
1382. C * R2SQ defined in Figure 2 of K&M
1383. C * TERM1, - individual terms of the
1384. C * TERM2, expression for K
1385. C * TERM3,
1386. C * DENOM
1387. C .....
1388. C .....
1389. C .....
1390. C SUBROUTINE KCALC(XCJ,YCJ,XCI,YCI,DELTA,CO,SI,K)
1391. C .....
1392. C DOUBLE PRECISION A,B,CO,DELTA,DENOM,K,R1SQ,R2SQ,
1393. C SI,TERM1,TERM2,TERM3,XCI,XCU,YCI,YCU
1394. C .....
1395. C PARAMETER (PI = 3.1415926535897932)
1396. C .....
1397. C Calculate K
1398. C .....
1399. C B = ((XCI-XCU) * CO) + ((YCI-YCU) * SI)
1400. C A = ((YCI-YCU) * CO) - ((XCI-XCU) * SI)
1401. C R1SQ = (A*A) + ((B+DELTA)*(B+DELTA))
1402. C R2SQ = (A*A) + ((B-DELTA)*(B-DELTA))
1403. C TERM1 = (B + DELTA) * DLOG(R1SQ)
1404. C TERM2 = (B - DELTA) * DLOG(R2SQ)
1405. C DENOM = (A*A) + (B*B) - (DELTA*DELTA)
1406. C IF (DENOM .LE. 1.00-30) THEN
1407. C IF (DABS(A) .LT. 1.00-30) THEN
1408. C TERM3 = 2.0 * A * PI
1409. C ELSE
1410. C TERM3 = 2.0 * A * (DATAN((B + DELTA) / A) -
1411. C DATAN((B - DELTA) / A))
1412. C .....
1413. C .....
1414. C .....
1415. C .....
1416. C .....
1417. C .....
1418. C .....
1419. C .....
1420. C .....
1421. C .....
1422. C .....
1423. C .....
1424. C .....
1425. C .....
1426. C .....
1427. C .....
1428. C .....
1429. C .....
1430. C .....
1431. C .....
1432. C .....
1433. C .....
1434. C .....
1435. C .....
1436. C .....
1437. C .....
1438. C .....
1439. C .....
1440. C .....
1441. C .....
1442. C .....
1443. C .....
1444. C .....
1445. C .....
1446. C .....
1447. C .....
1448. C .....
1449. C .....
1450. C .....
1451. C .....
1452. C .....
1453. C .....
1454. C .....
1455. C .....
1456. C .....
1457. C .....
1458. C .....
1459. C .....
1460. C .....
1461. C .....
1462. C .....
1463. C .....
1464. C .....
1465. C .....
1466. C .....
1467. C .....
1468. C .....
1469. C .....
1470. C .....
1471. C .....
1472. C .....
1473. C .....
1474. C .....
1475. C .....
1476. C .....
1477. C .....
1478. C .....
1479. C .....
1480. C .....
1481. C .....
1482. C .....
1483. C .....
1484. C .....
1485. C .....
1486. C .....
1487. C .....
1488. C .....
1489. C .....
1490. C .....
1491. C .....
1492. C .....
1493. C .....
1494. C .....
1495. C .....
1496. C .....
1497. C .....
1498. C .....
1499. C .....
1500. C .....
1501. C .....
1502. C .....
1503. C .....
1504. C .....
1505. C .....
1506. C .....
1507. C .....
1508. C .....
1509. C .....
1510. C .....
1511. C .....
1512. C .....
1513. C .....
1514. C .....
1515. C .....
1516. C .....
1517. C .....
1518. C .....
1519. C .....
1520. C .....
1521. C .....
1522. C .....
1523. C .....
1524. C .....
1525. C .....
1526. C .....
1527. C .....
1528. C .....
1529. C .....
1530. C .....
1531. C .....
1532. C .....
1533. C .....
1534. C .....
1535. C .....
1536. C .....
1537. C .....
1538. C .....
1539. C .....
1540. C .....
1541. C .....
1542. C .....
1543. C .....
1544. C .....
1545. C .....
1546. C .....
1547. C .....
1548. C .....
1549. C .....
1550. C .....
1551. C .....
1552. C .....
1553. C .....
1554. C .....
1555. C .....
1556. C .....
1557. C .....
1558. C .....
1559. C .....
1560. C .....
1561. C .....
1562. C .....
1563. C .....
1564. C .....
1565. C .....
1566. C .....
1567. C .....
1568. C .....
1569. C .....
1570. C .....
1571. C .....
1572. C .....
1573. C .....
1574. C .....
1575. C .....
1576. C .....
1577. C .....
1578. C .....
1579. C .....
1580. C .....
1581. C .....
1582. C .....
1583. C .....
1584. C .....
1585. C .....
1586. C .....
1587. C .....
1588. C .....
1589. C .....
1590. C .....
1591. C .....
1592. C .....
1593. C .....
1594. C .....
1595. C .....
1596. C .....
1597. C .....
1598. C .....
1599. C .....
1600. C .....
1601. C .....
1602. C .....
1603. C .....
1604. C .....
1605. C .....
1606. C .....
1607. C .....
1608. C .....
1609. C .....
1610. C .....
1611. C .....
1612. C .....
1613. C .....
1614. C .....
1615. C .....
1616. C .....
1617. C .....
1618. C .....
1619. C .....
1620. C .....
1621. C .....
1622. C .....
1623. C .....
1624. C .....
1625. C .....
1626. C .....
1627. C .....
1628. C .....
1629. C .....
1630. C .....
1631. C .....
1632. C .....
1633. C .....
1634. C .....
1635. C .....
1636. C .....
1637. C .....
1638. C .....
1639. C .....
1640. C .....
1641. C .....
1642. C .....
1643. C .....
1644. C .....
1645. C .....
1646. C .....
1647. C .....
1648. C .....
1649. C .....
1650. C .....
1651. C .....
1652. C .....
1653. C .....
1654. C .....
1655. C .....
1656. C .....
1657. C .....
1658. C .....
1659. C .....
1660. C .....
1661. C .....
1662. C .....
1663. C .....
1664. C .....
1665. C .....
1666. C .....
1667. C .....
1668. C .....
1669. C .....
1670. C .....
1671. C .....
1672. C .....
1673. C .....
1674. C .....
1675. C .....
1676. C .....
1677. C .....
1678. C .....
1679. C .....
1680. C .....
1681. C .....
1682. C .....
1683. C .....
1684. C .....
1685. C .....
1686. C .....
1687. C .....
1688. C .....
1689. C .....
1690. C .....
1691. C .....
1692. C .....
1693. C .....
1694. C .....
1695. C .....
1696. C .....
1697. C .....
1698. C .....
1699. C .....
1700. C .....
1701. C .....
1702. C .....
1703. C .....
1704. C .....
1705. C .....
1706. C .....
1707. C .....
1708. C .....
1709. C .....
1710. C .....
1711. C .....
1712. C .....
1713. C .....
1714. C .....
1715. C .....
1716. C .....
1717. C .....
1718. C .....
1719. C .....
1720. C .....
1721. C .....
1722. C .....
1723. C .....
1724. C .....
1725. C .....
1726. C .....
1727. C .....
1728. C .....
1729. C .....
1730. C .....
1731. C .....
1732. C .....
1733. C .....
1734. C .....
1735. C .....
1736. C .....
1737. C .....
1738. C .....
1739. C .....
1740. C .....
1741. C .....
1742. C .....
1743. C .....
1744. C .....
1745. C .....
1746. C .....
1747. C .....
1748. C .....
1749. C .....
1750. C .....
1751. C .....
1752. C .....
1753. C .....
1754. C .....
1755. C .....
1756. C .....
1757. C .....
1758. C .....
1759. C .....
1760. C .....
1761. C .....
1762. C .....
1763. C .....
1764. C .....
1765. C .....
1766. C .....
1767. C .....
1768. C .....
1769. C .....
1770. C .....
1771. C .....
1772. C .....
1773. C .....
1774. C .....
1775. C .....
1776. C .....
1777. C .....
1778. C .....
1779. C .....
1780. C .....
1781. C .....
1782. C .....
1783. C .....
1784. C .....
1785. C .....
1786. C .....
1787. C .....
1788. C .....
1789. C .....
1790. C .....
1791. C .....
1792. C .....
1793. C .....
1794. C .....
1795. C .....
1796. C .....
1797. C .....
1798. C .....
1799. C .....
1800. C .....
1801. C .....
1802. C .....
1803. C .....
1804. C .....
1805. C .....
1806. C .....
1807. C .....
1808. C .....
1809. C .....
1810. C .....
1811. C .....
1812. C .....
1813. C .....
1814. C .....
1815. C .....
1816. C .....
1817. C .....
1818. C .....
1819. C .....
1820. C .....
1821. C .....
1822. C .....
1823. C .....
1824. C .....
1825. C .....
1826. C .....
1827. C .....
1828. C .....
1829. C .....
1830. C .....
1831. C .....
1832. C .....
1833. C .....
1834. C .....
1835. C .....
1836. C .....
1837. C .....
1838. C .....
1839. C .....
1840. C .....
1841. C .....
1842. C .....
1843. C .....
1844. C .....
1845. C .....
1846. C .....
1847. C .....
1848. C .....
1849. C .....
1850. C .....
1851. C .....
1852. C .....
1853. C .....
1854. C .....
1855. C .....
1856. C .....
1857. C .....
1858. C .....
1859. C .....
1860. C .....
1861. C .....
1862. C .....
1863. C .....
1864. C .....
1865. C .....
1866. C .....
1867. C .....
1868. C .....
1869. C .....
1870. C .....
1871. C .....
1872. C .....
1873. C .....
1874. C .....
1875. C .....
1876. C .....
1877. C .....
1878. C .....
1879. C .....
1880. C .....
1881. C .....
1882. C .....
1883. C .....
1884. C .....
1885. C .....
1886. C .....
1887. C .....
1888. C .....
1889. C .....
1890. C .....
1891. C .....
1892. C .....
1893. C .....
1894. C .....
1895. C .....
1896. C .....
1897. C .....
1898. C .....
1899. C .....
1900. C .....
1901. C .....
1902. C .....
1903. C .....
1904. C .....
1905. C .....
1906. C .....
1907. C .....
1908. C .....
1909. C .....
1910. C .....
1911. C .....
1912. C .....
1913. C .....
1914. C .....
1915. C .....
1916. C .....
1917. C .....
1918. C .....
1919. C .....
1920. C .....
1921. C .....
1922. C .....
1923. C .....
1924. C .....
1925. C .....
1926. C .....
1927. C .....
1928. C .....
1929. C .....
1930. C .....
1931. C .....
1932. C .....
1933. C .....
1934. C .....
1935. C .....
1936. C .....
1937. C .....
1938. C .....
1939. C .....
1940. C .....
1941. C .....
1942. C .....
1943. C .....
1944. C .....
1945. C .....
1946. C .....
1947. C .....
1948. C .....
1949. C .....
1950. C .....
1951. C .....
1952. C .....
1953. C .....
1954. C .....
1955. C .....
1956. C .....
1957. C .....
1958. C .....
1959. C .....
1960. C .....
1961. C .....
1962. C .....
1963. C .....
1964. C .....
1965. C .....
1966. C .....
1967. C .....
1968. C .....
1969. C .....
1970. C .....
1971. C .....
1972. C .....
1973. C .....
1974. C .....
1975. C .....
1976. C .....
1977. C .....
1978. C .....
1979. C .....
1980. C .....
1981. C .....
1982. C .....
1983. C .....
1984. C .....
1985. C .....
1986. C .....
1987. C .....
1988. C .....
1989. C .....
1990. C .....
1991. C .....
1992. C .....
1993. C .....
1994. C .....
1995. C .....
1996. C .....
1997. C .....
1998. C .....
1999. C .....
2000. C .....

```

1 2 3 4 5 6 7 8 9

```

17 1413. ELSE
18 1414. TERM3 = 2.0 * A * DATAN(2.0 * A * DELTA / DENOM)
19 1415. ENDIF
20 1416. C
21 1417. K = (TERM1 - TERM2 + TERM3 - (4.0 * DELTA)) / (4.0 * PI)
22 1418. RETURN
1419. END
1420.

```

STATISTICS SOURCE STATEMENTS = 22, PROGRAM SIZE = 1060 BYTES, PROGRAM NAME = KCALC PAGE: 31

STATISTICS NO DIAGNOSTICS GENERATED.

***** END OF COMPILATION 9 *****

OPTIONS IN EFFECT: NOLIST NOMAP NOXREF NOGOSTMT NMODECK SOURCE TERM OBJECT FIXED
 OPTIMIZE(O) LANGVL(77) NOFIPS FLAG(I) NAME(MAIN) LINECOUNT(GO)

1 2 3 4 5 6 7 8 9

```

1421. C
1422. C SUBROUTINE COLLID - Calculates the x,y position
1423. C of impact on the airfoil surface
1424. C
1425. C INPUT VARIABLES:
1426. C XOUT, - last droplet position outside
1427. C YOUT the airfoil
1428. C XIN, - first droplet position inside
1429. C YIN the airfoil
1430. C XF1,XF2 - x and y coordinates of the end-
1431. C points of the surface segment
1432. C YF1,YF2 intercepted by the trajectory
1433. C
1434. C OUTPUT VARIABLES:
1435. C FINALX, - estimated coordinates of the
1436. C FINALY impact point on the surface
1437. C
1438. C OTHER VARIABLES:
1439. C SLOPTR - slope of the trajectory segment
1440. C which crosses the airfoil surface
1441. C SLOPSF - slope of the surface segment
1442. C intercepted by the trajectory
1443. C INT1, - intercepts for the linear
1444. C INT2 equations of the two segments
1445. C
1446. C
1447. C
1448. C
1449. C SUBROUTINE COLLID (XOUT,XIN,YOUT,YIN,XF1,YF1,XF2,YF2,
1450. C FINALX,FINALY)
1451. C
1452. C DOUBLE PRECISION XOUT,XIN,YOUT,YIN,XF1,XF2,YF1,YF2,
1453. C SLOPTR,SLOPSF,INT1,INT2,FINALX,FINALY
1454. C
1455. C Calculate slope of trajectory at impact point
1456. C SLOPTR = (YIN - YOUT) / (XIN - XOUT)
1457. C
1458. C Calculate slope of surface segment at impact point
1459. C SLOPSF = (YF2 - YF1) / (XF2 - XF1)
1460. C
1461. C Find intercepts of the two linear equations
1462. C
1463. C INT1 = YIN - (SLOPTR * XIN)
1464. C INT2 = YF2 - (SLOPSF * XF2)
1465. C
1466. C Find the impact point as the intersection point
1467. C of the two segments
1468. C FINALX = (INT2 - INT1) / (SLOPTR - SLOPSF)
1469. C FINALY = (SLOPTR * FINALX) + INT1
1470. C
1471. C
1472. C
1473. C
    
```

LEVEL 1.1.1 (DEC 81) VS FORTRAN DATE: JUL 24, 1986 TIME: 13:15:54 NAME: COLLID PAGE: 34

1 2 3 4 5 6 7 8 9

ISN 9 1474 RETURN
ISN 10 1475 END

STATISTICS SOURCE STATEMENTS = 10, PROGRAM SIZE = 512 BYTES, PROGRAM NAME = COLLID PAGE: 33

STATISTICS NO DIAGNOSTICS GENERATED.

***** END OF COMPILATION 10 *****

SUMMARY OF MESSAGES AND STATISTICS FOR ALL COMPILATIONS

- *STATISTICS* SOURCE STATEMENTS = 162, PROGRAM SIZE = 21362 BYTES, PROGRAM NAME = MAIN PAGE: 1
- *STATISTICS* NO DIAGNOSTICS GENERATED.
- ***** END OF COMPILATION 1 *****
- *STATISTICS* SOURCE STATEMENTS = 62, PROGRAM SIZE = 7298 BYTES, PROGRAM NAME = DRAW PAGE: 12
- *STATISTICS* NO DIAGNOSTICS GENERATED.
- ***** END OF COMPILATION 2 *****
- *STATISTICS* SOURCE STATEMENTS = 9, PROGRAM SIZE = 370 BYTES, PROGRAM NAME = DMEBET PAGE: 15
- *STATISTICS* NO DIAGNOSTICS GENERATED.
- ***** END OF COMPILATION 3 *****
- *STATISTICS* SOURCE STATEMENTS = 13, PROGRAM SIZE = 608 BYTES, PROGRAM NAME = SPCBET PAGE: 16
- *STATISTICS* NO DIAGNOSTICS GENERATED.
- ***** END OF COMPILATION 4 *****
- *STATISTICS* SOURCE STATEMENTS = 25, PROGRAM SIZE = 926 BYTES, PROGRAM NAME = DRDPPS PAGE: 17
- *STATISTICS* NO DIAGNOSTICS GENERATED.
- ***** END OF COMPILATION 5 *****
- *STATISTICS* SOURCE STATEMENTS = 44, PROGRAM SIZE = 122570 BYTES, PROGRAM NAME = TRAJEC PAGE: 21
- *STATISTICS* NO DIAGNOSTICS GENERATED.
- ***** END OF COMPILATION 6 *****
- *STATISTICS* SOURCE STATEMENTS = 39, PROGRAM SIZE = 16358 BYTES, PROGRAM NAME = POFLO PAGE: 25
- *STATISTICS* NO DIAGNOSTICS GENERATED.
- ***** END OF COMPILATION 7 *****
- *STATISTICS* SOURCE STATEMENTS = 40, PROGRAM SIZE = 2150 BYTES, PROGRAM NAME = FLOWXY PAGE: 28
- *STATISTICS* NO DIAGNOSTICS GENERATED.
- ***** END OF COMPILATION 8 *****
- *STATISTICS* SOURCE STATEMENTS = 22, PROGRAM SIZE = 1060 BYTES, PROGRAM NAME = KCALC PAGE: 31
- *STATISTICS* NO DIAGNOSTICS GENERATED.
- ***** END OF COMPILATION 9 *****
- *STATISTICS* SOURCE STATEMENTS = 10, PROGRAM SIZE = 512 BYTES, PROGRAM NAME = COLLID PAGE: 33

STATISTICS NO DIAGNOSTICS GENERATED.

***** END OF COMPILATION 10 *****

***** SUMMARY STATISTICS ***** 0 DIAGNOSTICS GENERATED. HIGHEST SEVERITY CODE IS 0.

Appendix VI

The MVD Approximation for Collision Efficiency

The task of computing volume-weighted averages of collision efficiencies for a droplet size spectrum is often simplified by substituting a monodisperse size spectrum, at the median volume diameter of the distribution. As discussed in Chapter III, this can lead, in some cases, to a significant underestimation of the maximum accretion angle. However, it has often been assumed that the weighted overall and stagnation line collision efficiencies are well approximated by the mvd values. In this Appendix the validity of that assumption is examined.

Table A.1 lists a variety of atmospheric and marine droplet size spectra, as relative numbers of droplets in 10 or $3\mu\text{m}$ wide size bins. These spectra were either measured in the field, or in icing wind tunnels, or estimated from empirical parameterized distributions, and cover a range of types and mvds.

They are derived from the following sources: Bain and Gayet (1984), Battan and Reitan (1957), Best (1951), Rhrigian-Mazin, as reported by Pruppacher and Klett (1980), McComber and Touzot (1981), Preobrazhenskii (1973), and Squires (1958). Those marked FROST were measured by the oil

relative number of drops per unit volume							
mid-band droplet diameter	Khrgian-Mazin 1	Khrgian-Mazin 2	Khrgian-azin 3	Khrgian-Mazin 4	Squires Hawaiian	Squires dark stratus	Squires Trade-wind cy
5 μ m	0.724	0.069	0.014	0.002	0.25	6.5	9
15	2.397	0.340	0.082	0.012	0.65	6.0	16
25	2.449	0.518	0.148	0.024	1.0	5.4	29
35	1.766	0.557	0.189	0.035	0.8	5.1	21
45	1.074	0.505	0.203	0.043	0.8	2.5	3.5
55	0.590	0.414	0.198	0.047	0.7	0.5	
65	0.303	0.317	0.180	0.049	0.35	0.2	
75	0.149	0.232	0.156	0.048	0.15	0.1	
85	0.070	0.164	0.131	0.046	0.10	0.05	
95	0.032	0.112	0.106	0.042	0.06		
105	0.014	0.075	0.085	0.038	0.05		
115	0.006	0.049	0.066	0.034	0.04		
125	0.003	0.032	0.051	0.030	0.03		
135	0.001	0.021	0.039	0.026	0.04		
145		0.013	0.029	0.022	0.01		
155		0.008	0.022	0.019			
165		0.005	0.016	0.016			
175		0.003	0.012	0.013			
185		0.002	0.009	0.011			
195		0.001	0.006	0.009			
205			0.004	0.007			
215			0.003	0.006			
225				0.005			
235				0.004			
245				0.003			

Table A.1 - Droplet size spectra from many different sources
(see text for references).

relative number of drops per unit volume

mid-band droplet diameter	Battan and Reitan fairweather cumulus	Battan and Reitan stratus	FROST 1	FROST 2	FROST 3	FROST 4	FROST 5	Preobrazhenskii
5 μ m	600	100	127	94	97	3	17	5180
15	70	15	327	167	213	37	68	1620
25	13	1.1	104	33	86	63	64	480
35	0.26	0.2	13	6	33	58	31	200
45			1	4	14	51	12	110
55					2	35	11	56
65					1	26	9	32
75						17	3	21
85						14	2	14
95						16	4	10
105						12	9	7
115						5	2	5
125						4	3	4
135						8	2	3
145						7	1	2
155						2	0	1
165						1	2	
175						2		
185						2		

Table A.1 - continued.

relative number of drops per unit volume

mid-band droplet diameter	McComber and Touzot	mid-band droplet diameter	Bain and Gayet 1	Bain and Gayet 2	Bain and Gayet 3
5.1 μ m	945	1.5	20	7	13.0
15.3	1093	4.5	41	12	15.5
25.5	481	7.5	30	23	15.5
35.7	211	10.5	7.5	33	18.0
45.9	74	13.5	2.5	18	15.5
56.1	38	16.5		5	12.5
66.3	30	19.5		2	6.0
76.5	13	22.5			2
86.7	19	25.5			2
96.9	11				
107.1	10				
117.3	3				
127.5	1				
137.7	1				

percent volume

mid-band droplet diameter	Best 1	Best 2	Best 3	Best 4	Best 5
5 μ m	63.2	22	4	3	36
15	36.8	41	24	31	47
25		26	39	53	15
35		9	26	13	2
45		2	6		
55			1		

Table A.1 - continued.

slide technique in the FROST icing wind-tunnel facility at The University of Alberta.

For each spectrum, the mvd was calculated following the method derived by Lozowski (1978). Assuming a uniform distribution of droplets within each bin, the partial volume of each is given by:

$$V_i = (n_i/24) \pi w^3 (i^4 - (i-1)^4), \quad \text{A.8}$$

where n_i is the number of drops in the i th bin, and w is the bin width, say 10 μm . Then, if V is the total volume of all droplets, let

$$u_i = (\Sigma V_i) / V. \quad \text{A.9}$$

Now find u_k such that $u_{k-1} < 0.5$, and $u_k > 0.5$. Finally,

$$\begin{aligned} \text{mvd} = w & \left(\left((0.5 - u_{k-1}) / (u_k - u_{k-1}) \right) (k^4 - (k-1)^4) \right. \\ & \left. + (k-1)^4 \right)^{0.25}, \end{aligned} \quad \text{A.10}$$

Overall and stagnation line collision efficiencies have been calculated for the mvd of each spectrum. For the complete spectrum, weighted average collision efficiencies are calculated using the fractional volume of each bin as the weighting factor for the collision efficiency of the mvd of that bin.

All of the collision efficiencies are calculated according to Table II.6, and for the same conditions, i.e. $U = 10$ m/sec and $D_c = 0.0254$ m. The results are shown in Table A.2 and Figures A.2 and A.3. For a different type of comparison, the conditions have been varied for a single spectrum (labelled as Bain and Gayet 2 in Table A.1) to give a complete range of collision efficiencies. These results are compared in Table A.3 and in Figures A.4 and A.5.

Also calculated are collision efficiencies for the droplet at the 42nd volume percentile (d_{42}), on a suggestion made by Lozowski and Makkonen (private communication, 1986), based on a theoretical analysis using Gaussian quadrature to estimate the overall collision efficiency for a droplet spectrum. These data are included in figures and tables listed above.

Comparison of Figure A.4 with Figure 1 of Makkonen (1984), which shows the same type of calculations for the same spectrum used here as well as two other spectra given by Bain and Gayet, (1982), reveals a major disagreement in the sign of $E_{\text{spec.}} - E_{\text{mvd}}$. The disagreement is due to a misinterpretation of the original droplet spectrum diagram in Bain and Gayet (1982) on the part of Makkonen (private communication, 1986). Figure A.4 reflects the correct interpretation.

Spectrum	β_{spec}	E_{spec}	mvd	β_{mvd}	E_{mvd}	d42	β_{d42}	ϵ_{d42}
Khrgian-Mazin 1	0.824	0.710	56.9 μ m	0.852	0.745	52.1 μ m	0.835	0.718
Khrgian-Mazin 2	0.906	0.836	93.6	0.924	0.862	86.1	0.914	0.846
Khrgian-Mazin 3	0.936	0.886	126.2	0.949	0.906	116.5	0.943	0.895
Khrgian-Mazin 4	0.955	0.919	165.9	0.964	0.933	154.5	0.960	0.927
Squires Hawaiian	0.886	0.804	81.4	0.908	0.835	70.9	0.889	0.804
Squires dark stratus	0.767	0.626	43.0	0.790	0.650	39.7	0.769	0.619
Squires Trade-wind Cu	0.702	0.532	34.9	0.730	0.565	33.2	0.714	0.543
Battan and Reitan Cu	0.393	0.224	18.0	0.459	0.249	16.6	0.419	0.211
Battan and Reitan stratus	0.364	0.199	17.2	0.434	0.225	15.9	0.396	0.191
FROST 1	0.555	0.362	24.7	0.603	0.402	22.6	0.565	0.357
FROST 2	0.583	0.402	26.2	0.628	0.432	23.4	0.580	0.375
FROST 3	0.680	0.516	35.0	0.731	0.566	31.2	0.694	0.515
FROST 4	0.928	0.873	127.7	0.949	0.907	111.3	0.939	0.889
FROST 5	0.919	0.859	112.3	0.940	0.890	107.1	0.936	0.883
Preobrazhenskii	0.838	0.745	78.5	0.903	0.827	67.9	0.883	0.793
McComber and Touzot	0.836	0.736	75.9	0.899	0.820	65.8	0.878	0.786
Bain and Gayet 1	0.108	0.036	8.8	0.088	0.010	8.4	0.065	0.003
Bain and Gayet 2	0.284	0.123	13.3	0.301	0.118	12.5	0.267	0.096
Bain and Gayet 3	0.421	0.232	17.5	0.444	0.233	16.6	0.418	0.210
Best 1	0.415	0.247	18.3	0.467	0.255	17.0	0.429	0.220
Best 2	0.582	0.401	26.9	0.639	0.445	25.0	0.610	0.409
Best 3	0.542	0.350	24.4	0.599	0.397	22.5	0.564	0.357
Best 4	0.313	0.160	15.3	0.375	0.173	13.1	0.291	0.111
Best 5	0.186	0.070	9.4	0.120	0.021	9.0	0.098	0.014

standard error 0.031 0.029 0.027 0.026

Table A.2 Overall and stagnation line collision efficiencies as plotted in Figures A.2 and A.3.

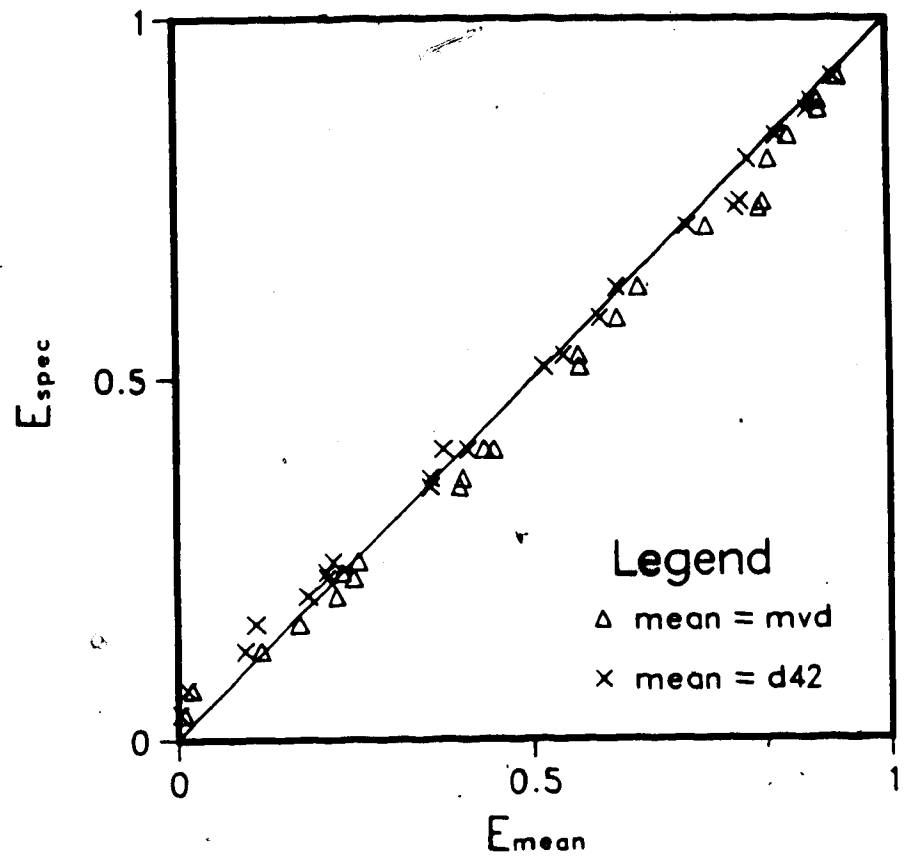


Figure A.2 - Overall collision efficiencies calculated for many different drop size spectra vs. E 's calculated for the mvd and d42 of each spectrum. In each case $U=10$ m/sec, $D_c=0.0254$ m.

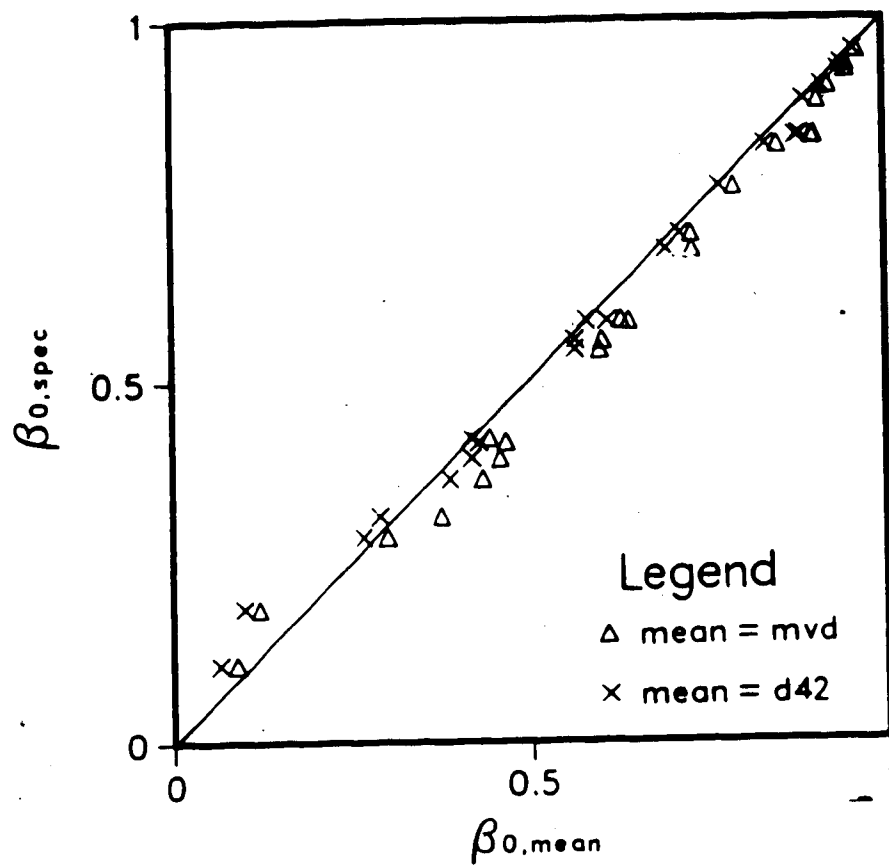


Figure A.3 - Stagnation line collision efficiencies calculated for many different drop size spectra vs. β_0 's calculated for the mvd and d42 of each spectrum. In each case $U=10$ m/sec, $D_c=0.0254$ m.

U	β_{o_spec}	E_{spec}	β_{o_mvd}	E_{mvd}	β_{o_d42}	E_{d42}
5m/sec	0.121	0.037	0.121	0.022	0.089	0.010
7	0.202	0.072	0.208	0.062	0.175	0.044
10	0.284	0.123	0.301	0.118	0.267	0.096
15	0.383	0.194	0.403	0.196	0.370	0.169
20	0.448	0.250	0.470	0.257	0.439	0.228
25	0.496	0.295	0.518	0.305	0.489	0.275
30	0.532	0.331	0.555	0.344	0.527	0.314
40	0.586	0.389	0.608	0.405	0.582	0.374
50	0.624	0.432	0.646	0.450	0.622	0.420
80	0.693	0.516	0.713	0.536	0.692	0.508
200	0.790	0.648	0.806	0.668	0.791	0.646
350	0.830	0.708	0.844	0.726	0.832	0.708
700	0.865	0.765	0.877	0.781	0.867	0.766
1500	0.892	0.811	0.901	0.825	0.894	0.812
standard error			0.012	0.013	0.011	0.011

Table A.3 - Overall and stagnation line collision efficiencies as plotted in Figures A.4 and A.5.

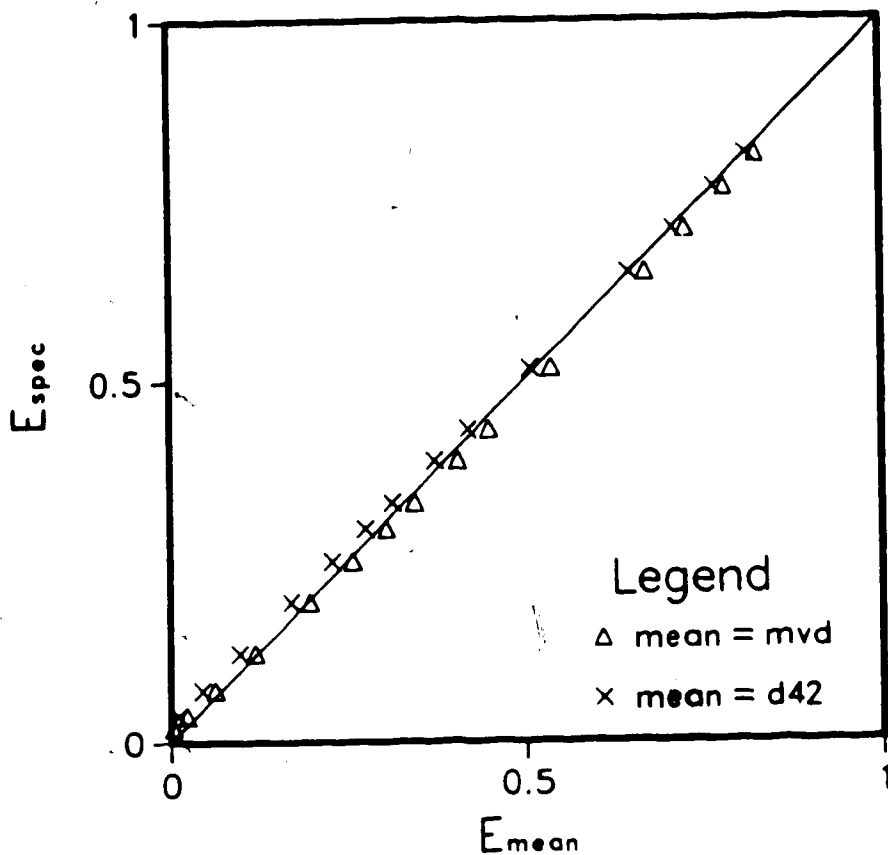


Figure A.4 - Overall collision efficiencies calculated for a single drop size spectrum (Bain and Gayet 2) at many different wind speeds, vs. E 's calculated for the mvd and d42 of the same spectrum for the same wind speeds. $D_c = 0.0254$ m.

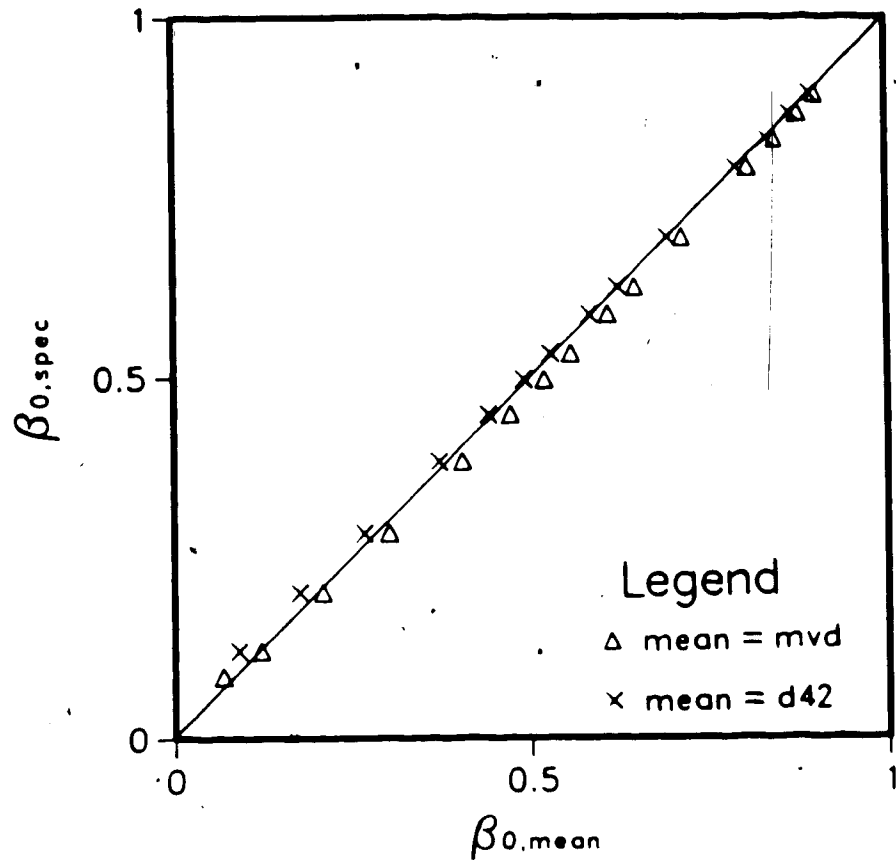


Figure A.5 - Stagnation line collision efficiencies calculated for a single drop size spectrum (Bain and Gayet 2) at many different wind speeds, vs. β_0 's calculated for the mvd and d42 of the same spectrum for the same wind speeds. $D_c = 0.0254$ m.

The conclusion which may be made from this exercise is that, although the standard errors are not significantly different over the entire range of collision efficiencies (see Tables A.2 and A.3), in the range of E or β_0 less than about 0.2 the mvd approximation is preferable. Above that range, for most types of spectra, the d42 approximation gives better agreement with the spectrum-weighted collision efficiencies. However, for certain types of spectra which depart significantly from a Gaussian distribution (e.g. the double peaked spectrum from McComber and Touzot) even the d42 value may be in error by more than 10 percent.

References

- Bain, M. and Gayet, J-F. 1982: Contribution to the Modelling of the Ice Accretion Process: Ice Density Variation with the Impacted Surface Angle. Proceedings, First International Workshop on Atmospheric Icing of Structures, Hanover, 13-20.
- Battan, L.J. and Reitan, C.H. 1957: Droplet Size Measurements in Convective Clouds. Artificial Stimulation of Rain, Weickmann and Smith, ed.s. London, Pergamon Press, p.184.
- Best, A.C. 1951: Drop-size Distribution in Cloud and Fog. *Quart. Jour. Roy. Meteor. Soc.* 77, 418-426.
- Lozowski, E.P. 1978: Stochastic Effects in Spray Droplet Sampling with Oiled Slides. National Research Council, Division of Mechanical Engineering, Laboratory Memorandum LT-172, 17 pp.
- Makkonen, L. 1984: Modeling of Ice Accretion on Wires. *J. Climate and App. Meteor.*, 23, 929-939.
- McComber, P. and Touzot, G. 1981: Calculation of the Impingement of Cloud Droplets in a Circular Cylinder by the Finite Element Method. *J. Atmos.*

Sci. 38, 1027-1036.

Preobrazhenskii, L.Yu. 1973: Estimate of the Content of
Spray Drops in the Near-Water Layer of the
Atmosphere. *Fluid Mechanics - Soviet Research*, 2,
95-100.

Pruppacher, H.R. and Klett, J.D. 1980: Microphysics of
Clouds and Precipitation. D. Reidel, p.11.

Squires, P. 1958: The Microstructure and Colloidal Stability
of Warm Clouds: I. The Relation between Structure
and Stability. *Tellus*, 10, 256-261.